Stability, Voltage Performance and Power Sharing Issues of Inverter-based Microgrids via LMI Optimization

vorgelegt von
M.Sc.
Truong Duc Trung
geb. in Quang Ninh

von der Fakultät IV - Elektrotechnik und Informatik
der Technischen Universität Berlin
zur Erlangung des akademischen Grades

Doktor der Ingenieurwissenschaften
- Dr.-Ing. -

genehmigte Dissertation

Promotionsausschuss:

Vorsitzender:	Prof. Dr.-Ing. Ronald Plath
Gutachter:	Prof. Dr.-Ing. Jörg Raisch
Gutachter:	Prof. Dr.-Ing. Kai Strunz
Gutachter:	Prof. Dr.-Ing. Johann Reger

Tag der wissenschaftlichen Aussprache: 02. Juli 2018

Berlin 2018

Abstract

Numerous small distributed energy resources (DERs) form a new generation of power systems - the microgrid. In general, a microgrid stands for a cluster of DERs, which can collectively operate as an individual low-voltage power system during islanded mode. A microgrid can also be operated in connected mode with a large power system. DERs are often interfaced to a microgrid through power electronic inverters, forming an inverter-based microgrid. As inverters obtain very different characteristics to conventional generation units (e.g. synchronous generators), characteristics of microgrids significantly differ from those of conventional power systems. As a result, popular stabilizing and power sharing approaches, which are applied to conventional power systems, are no longer effective for the control of islanded microgrids. For the case of islanded parallel-connected inverter-based microgrids, a novel power control approach together with a thorough stability analysis are developed in this thesis. Dynamics of lower control levels of inverters are relatively fast and can be neglected. For the stability analysis of microgrids at the power control level, inverters are considered to be ideal voltage sources with controllable voltage magnitudes and phase angles. In order to avoid fast communication and control interconnection between inverters, a decentralized power control approach is proposed. The control approach requires clock synchronization between inverters, which can be realized by the global positioning system. The main goal at the power control level is the control of power flows within a microgrid, where the closed-loop stability is an essential requirement. For a normal operation of loads, the performance of voltages and frequencies in the sense of magnitude deviations and higher-frequency harmonics is also important.

From a power system perspective the stability of microgrids is investigated in the sense of small-signal stability. In the thesis the stability of microgrids is analyzed by using control system techniques. For the nominal stability analysis, a linearized model of microgrids is derived. There are different uncertainties and disturbance sources to the stability of microgrids such as load dynamics, load and line uncertainties and changes of power references. Accordingly, stability of microgrids against the aforementioned uncertainties and disturbances is investigated. Load dynamics are considered by including load models in the stability analysis. With respect to load and line uncertainties, robust stability of a microgrid and robust performance of inverter output voltages are studied in the $\mathcal{H}_\infty$ control. With a proposed decentralized power control loop, inverter controllers are synthesized by using the linear matrix inequality (LMI) technique. Different LMI problems are proposed to design decentralized inverter controllers to guarantee the asymptotic stability of an overall microgrid. Furthermore, a droop-based power sharing control is proposed. Although a desired power sharing performance is not analytically proved, it will be shown via simulation that power sharing between inverters is achieved without causing stability and voltage performance problems. The effectiveness of proposed microgrid models and related controller design methods are validated via computer simulations.

Zusammenfassung

Zunehmende dezentrale Energiequellen leiten eine neue Generation von Stromsystemen ein - das Microgrid. Im allgemeinen Verständnis ist ein Microgrid ein Cluster von dezentralen Stromerzeugern, die kollektiv als ein individuelles Stromssystem im Inselbetrieb funktionieren können. Ein Microgrid kann auch im Verbundbetrieb mit einem großen Stromnetz betrieben werden. Dezentrale Stromerzeuger sind normalerweise mit einem Microgrid durch leistungselektronische Umrichter verbunden, dabei bildet sich ein Umrichter-basiertes Microgrid. Weil die Umrichter stark unterschiedliche Eigenschaften im Vergleich zu konventionellen Stromerzeugern (z.B. Synchrongeneratoren) haben, unterscheiden sich die Eigenschaften eines Microgrids deutlich von denen eines konventionellen Stromsystems. Daher sind die bekannten stabilisierenden und leistungsverteilenden Regelungsverfahren, die für große Stromnetze implementiert wurden, nicht effektiv für die Regelung eines Microgrids im Inselbetrieb. In dieser Arbeit wird für den Inselbetrieb eines Umrichter-basierten Microgrids, in dem die Umrichter in parallel zu einander verbunden sind, ein neues Leistungsregelungsverfahren zusammen mit einer ausführlichen Stabilitätsanalyse entwickelt. Die Dynamiken der untergeordneten Regelkreise eines Umrichters werden vernachlässigt. Für die Stabilitätsanalyse eines Microgrids auf dem Leistungsregelungsniveau werden die Umrichter als ideale Spannungsquellen mit steuerbaren Spannungsmagnituden und Phasenwinkeln betrachtet. Um auf eine schnelle Kommunikation und Regelkopplung zwischen den Umrichtern zu verzichten, wird ein dezentraler Leistungsregelkreis für die Umrichter-basierten Microgrids vorgeschlagen. Das Leistungsregelungsverfahren benötigt lediglich eine Uhrensynchronisation für die Umrichter, die durch das Globale Positionsbestimmungssystem realisiert werden kann. Das Hauptziel der Leistungsregelung ist die Regelung des Energieflusses innerhalb eines Microgrids, wobei die Stabilität des geschlossenen Microgrids eine wichtige Voraussetzung ist. Für einen sicheren Betrieb der verbundenen Lasten ist darüber hinaus die Regelgüte der Spannungen und Frequenzen im Sinne von Magnitudenabweichungen und Oberschwingungen wichtig.

Aus Sicht der Energiesystemtheorie wird die Stabilität eines Microgrids hinsichtlich der Kleinsignalstabilität untersucht. In dieser Arbeit wird die Stabilitätsanalyse eines Microgrids mit Hilfe der Regelungstheorie durchgeführt. Für die nominale Stabilitätsanalyse wird ein linearisiertes Modell eines Microgrids vorgestellt. Allerdings gibt es verschiedene Unsicherheits- und Störungsquellen für die Stabilität eines Microgrids, z.B. Lastdynamiken, Lastunsicherheiten, Leitungsunsicherheiten sowie Änderungen von Leistungssollwerten. Demzufolge wird die Stabilitätsanalyse eines Microgrids gegenüber den obengenannten Unsicherheiten und Störungen durchgeführt. Die Lastdynamiken werden mit Hilfe von Lastmodellen in der Stabilitätsanalyse betrachtet. In Bezug auf die Last- und Leitungsunsicherheiten werden die robuste Stabilität eines Microgrids und die robuste Performance der Umrichterausgangsspannungen im Rahmen

der $\mathcal{H}_\infty$-Regelung untersucht. Anhand eines vorgeschlagenen dezentralen Leistungsregelkreises werden die Leistungsregler für die Umrichter mit Hilfe der Linear Matrix Inequality (LMI) Technik entworfen. Verschiedene LMI-Optimierungsprobleme werden für den Entwurf von den dezentralen Leistungsreglern vorgestellt, die die asymptotische Stabilität eines gesamten Microgrids gewährleisten sollen. Außerdem wird ein droop-basierter Regelungsansatz für die Leistungsverteilung innerhalb eines Microgrids vorgestellt. Obwohl eine genaue Leistungsverteilung zwischen den Umrichtern nicht hergestellt worden ist, zeigt die Simulation, dass eine Wirkleistungsverteilung zwischen den Umrichtern dem eingestellten Verteilungsverhältnis annähernd entspricht, ohne Stabilitäts- und Spannungsperformanceprobleme auszulösen. Die Wirksamkeit der vorgeschlagenen Reglerentwurfsmethoden wird durch die Simulationen validiert.

Acknowledgements

Dear reader, although I am the responsible author of this thesis, it is a far cry from meaning that I could finish it without support, inspiration, patience and love of many people around me through these years. Since the beginning my promotion has always had two parallel developing aspects: the scientific aspect and the personal-developing one. I would like to take this occasion to thank all people, who have accompanied me during my promotion years, in which I have gained a lot of developments in both of these aspects. There are people, who have been there with me since the beginning of the journey. There are also people, who have accompanied me for some parts of it and drawn a lot of inspiration and thankful feelings in me. From the bottom of my heart, I would like to express my most sincere gratitude and appreciation to all of them.

I would like to dedicate my sincere thanks to my supervisor, Professor Jörg Raisch. There are so many reasons for me to thank Professor Raisch. First of all is certainly for giving me a chance to work on my PhD thesis at TU Berlin. Dear Professor Raisch, dear reader, I would like you to know how life-changing does it mean for me as a foreign student from Vietnam to do a PhD in Germany. For myself, it does not only mean working on a future-sustaining topic like the Microgrid, or having an access to invaluable scientific resources, but also means living in a scientific environment, meeting and talking to inspiring scientists and colleagues. I would like to thank Professor Raisch for this door-opening opportunity to enter the scientific world. I would like to thank him also for teaching me how to work and think like a scientist, for his time, support, guides and advices during these years.

My great thanks and acknowledgements to Professor Kai Strunz and Professor Johann Reger for accepting to be my dissertation reviewers. I am furthermore indebted to Dr. Johannes Schiffer, Dr. Adolfo Anta and Dr. Tevfik Sezi, who guided me into the Microgrid field in the beginning of my promotion. I am also grateful for many helpful discussions with my colleagues Steffen Hofmann, Yashar Kouhi and Miguel Parada Contzen. Steffen Hofmann, Miguel Parada Contzen, Yashar Kouhi, Thomas Seel and Ulf Schaper are the proofreaders of this thesis, many thanks for their helpful comments and support.

I would like to express my great appreciation to the Ministry of Education and Training of Vietnam, which financially supported me in the first three years of my promotion. My great appreciation also goes to my current company Enercon, for giving me an opportunity to continue working in the renewable energy field, where I have gained a lot of working experience and understanding about power electronics, real-time simulations, etc.

Dear reader, it would be impossible for me to stand where I am today without my little family. My deep appreciation goes to my partner Anja Ostrowski for her patience and taking care of me all these years, for her continuous inspiration and mental support during my doctoral life-span. All the support Anja has given me through these years is the greatest gift I have ever received. I would like to thank my parents for their continuous support, inspiration and their belief in me as well as in my decisions.

I would like to thank all my colleagues in Control Systems Group at TU Berlin for the scientific life they created in the university, and for our coffee breaks in the library, through which I have improved my German and understood more about life in Germany. The way from my dormitory to TU Berlin through the Tiergarten-Park is, in my opinion, one of the most beautiful city-cycling routes of the world. Thanks Berlin for making that my everyday route to university.

Last but not least, my dear reader, whoever you are, spending your time reading these lines, I would like to thank you for your interest in what I write here. I wish you and your family all the best, happiness, good health and a lot of motivations and creativities in your activities.

Aurich, 27th November, 2017.

Contents

List of Figures

List of Tables

Abbreviations

AC	**A**lternative **C**urrent
CHP	**C**ombined **H**eat and **P**ower
COI	**C**enter **O**f **I**nertia
DC	**D**irect **C**urrent
DER	**D**istributed **E**nergy **R**esource
FACTS	**F**lexible **AC** **T**ransmission **S**ystem
GPS	**G**lobal **P**ositioning **S**ystem
IGBT	**I**nsulated-**G**ate **B**ipolar **T**ransistor
LMI	**L**inear **M**atrix **I**nequality
LTI	**L**inear **T**ime **I**nvariant
MIMO	**M**ultiple-**I**nput **M**ultiple-**O**utput
MPPT	**M**aximum **P**ower **P**oint **T**racking
NLCF	**N**ormalized **L**eft **C**oprime **F**actorization
ODE	**O**rdinary **D**ifferential **E**quation
PCC	**P**oint of **C**ommon **C**oupling
PWM	**P**ulse-**W**idth **M**odulation
SG	**S**ynchronous **G**enerator
THD	**T**otal **H**armonic **D**istortion
VSI	**V**oltage **S**ource **I**nverter

Symbols

B	susceptance	Ω^{-1}
δ_i	phase angle of the output voltage of an inverter node i	rad
δ_{i_0}	voltage phase angle of an inverter node i at an equilibrium	rad
$\tilde{\Delta}$	model uncertainty caused by uncertain admittances	
f	frequency	Hz
G	conductance	Ω^{-1}
H_i	inertia constant of an inverter i	
ϕ_{ik}	angle of an admittance Y_{ik}	rad
I_i	magnitude of the output current of a node i	A
Im	imaginary part of a complex number	
j	imaginary unit	
λ	eigenvalue	
n	number of inverters in a microgrid	
ω	frequency	rad/s
ω_{nom}	nominal frequency	rad/s
ω_s	frequency of the stator voltage of an induction machine	rad/s
P_i	active power exchange at an inverter node i	W
$\tilde{P}_i$	measured active power exchange at an inverter node i	W
$\tilde{P}_{i_0}$	active power exchange at an inverter node i at an equilibrium	W
Q_i	reactive power exchange at an inverter node i	Var
$\tilde{Q}_i$	measured reactive power exchange at an inverter node i	Var
$\tilde{Q}_{i_0}$	reactive power exchange at an inverter node i at an equilibrium	Var
R	resistance	Ω
$r_{0_e}^{\delta_i}$, $r_{0_e}^{\tilde{P}_i}$, $r_{0_e}^{\tilde{Q}_i}$	low-frequency gains of the weight function $W_{e_{ik}}(s)$, $k = 1,2,3$	
$r_{\infty_e}^{\delta_i}$, $r_{\infty_e}^{\tilde{P}_i}$, $r_{\infty_e}^{\tilde{Q}_i}$	high-frequency gains of the weight function $W_{e_{ik}}(s)$, $k = 1,2,3$	

$r_0^t,\ r_\infty^t$	gains of the weight function $W_T(s)$	
$r_{0_i}^V,\ r_{\infty_i}^V, r_{0_i}^\omega,\ r_{\infty_i}^\omega$	gains of the weight functions $W_{u_{i1}}(s)$ and $W_{u_{i2}}(s)$	
$\mathbb{R}$	set of real numbers	
Re	real part of a complex number	
σ	singular value	
$\bar{\sigma}$	maximum singular value	
θ_r	electrical angular difference between the rotor	
	and the stator of an induction machine	rad
$\mathcal{T}_s$	electrical torque of an induction machine	N.m
$\mathcal{T}_m$	mechanical torque of an induction machine	N.m
τ_i	time constant of a measuring low-pass filter of an inverter i	second
$\tau_e^{\delta_i},\ \tau_e^{\tilde{P}_i},\ \tau_e^{\tilde{Q}_i}$	time constants of the weight functions $W_{e_{ik}}(s),\ k = 1,2,3$	second
τ^t	time constant of the weight function $W_T(s)$ of a model uncertainty	second
$\tau_i^V,\ \tau_i^\omega$	time constants of the weight functions $W_{u_{i1}}(s)$ and $W_{u_{i2}}(s)$	second
	of inverter output voltage and frequency	
V_i	magnitude of an inverter output voltage	volt
V_{i_0}	magnitude of an inverter output voltage at an equilibrium	volt
X	reactance	Ω
Y	admittance	Ω^{-1}
Z	impedance	Ω
$\|\|\cdot\|\|_\infty$	$\mathcal{H}_\infty$ norm	
$\|\cdot\|$	absolute value	

to Anja and Anton

Chapter 1

Introduction

1.1 Motivation of microgrids

Power system engineers, researchers and power customers everywhere are concerned with problems of fossil fuel resource depletion, poor energy efficiency and environmental pollution. As part of the Kyoto Protocol [3], many countries plan to cut down greenhouse gas emissions to counter climate change and global warming. Therefore, the interest in alternative energy resources, such as biogas, wind power, solar energy, fuel cells, etc., has increased significantly in the last decades. The widespread implementation of renewable energy sources leads to an increasing amount of small grid-connected generation units (100's of [kVA] [4]) at *low-voltage* levels, such as windturbines, solar photovoltaics, microturbines, among others. Those power generation units are often called distributed energy resources (DERs) and are usually placed next to consumption points. Most DERs are naturally direct current (DC) or unregulated alternative current (AC) sources, while conventional power networks are normalized AC systems. Thus, DERs are interfaced to power networks via power electronic devices called *inverters*. In order to take control over those small generation units, the concept of microgrids has been introduced [5–7]. A microgrid formed by a combination of DERs with inverter interfaces is called an inverter-based microgrid [8–11]. In Figure 1.1, a schematic representation of a microgrid is shown.

Microgrid is a relatively new concept for both power system and control system communities. It was first formulated in the Consortium for Electric Reliability Technology Solutions program (CERTS) in 1999 as a cluster of micro-generators and storages with an ability to separate and isolate itself from the utility seamlessly with little or no disruption to connected loads [12, 13]. A definition of an AC microgrid is made in [14], providing a common understanding of microgrids among the research community. A microgrid can operate in connected mode with a high-voltage transmission network and execute power exchange with it. In connected mode, the transmission

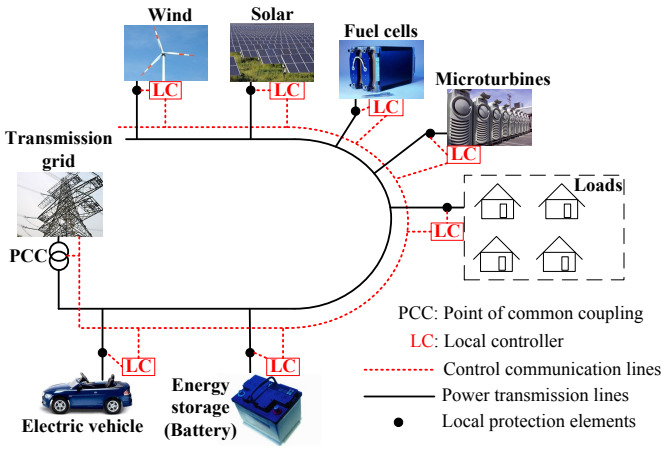

FIGURE 1.1: Schematic representation of a microgrid.

network is dominant and the microgrid is considered as a single load or a single generation unit. Another valuable motivation of microgrids is their possibility to automatically separate themselves and start operating in isolated mode in case of detected faults in the transmission network [12]. Thus, a microgrid can isolate its loads from faults and thereby maintain its service without harming the transmission network's integrity. A microgrid then operates autonomously and supplies power due to load priorities [15]. A microgrid can be reconnected to a transmission network when all faults are cleared [5, 16].

1.2 Challenges and contributions

One of the most meaningful contributions of microgrids is the possibility of constructing small autonomous power systems. It will enable a big step forward in changing from centralized to decentralized power generation. In addition, stand-alone microgrids can supply electrical power to off-grid areas without long power lines to large power plants. However, researchers have identified many technical challenges concerned with stability and performance in the sense of voltage and frequency as well as power balance and synchronous operation between inverters in microgrids while operating in isolated mode [5, 8, 10, 17–21]. Hence, the case of isolated inverter-based microgrids is investigated in this thesis.

Being mainly formed by DERs with low inertia and capacity, microgrids are highly sensitive to uncertainties. Moreover, due to the intermittent nature of renewable sources, i.e., inconsistent sunshine or wind, some DERs can be unavailable during operation. Hence, it is a *control challenge* to maintain service of microgrids with a sufficient performance of frequencies and voltages in the presence of disturbances from natural sources and load uncertainties. Sufficient performance of voltage and frequency refers to their acceptable (small) variations around nominal values. The difficult task is to achieve this functionality without extensive custom engineering while still ensuring high system reliability and generation placement flexibility [22].

Another important challenge associated to the operation of microgrids is the power flow strategy, which announces that all generation units in a microgrid should collectively perform a power exchange strategy for an optimal and economic operation. A common power flow strategy within a microgrid is the power sharing between inverters [5, 6, 21]. The power sharing concept indicates an ability of generation units in a microgrid, which should share any increase in system load by predefined ratios [6, 19–21, 23–26]. Power sharing ratios between inverters can also be adjusted during operation of microgrids due to different system conditions.

Dealing with inverter-based microgrids, whose physical characteristics are significantly different from characteristics of large power systems, the classical control approaches applied to large power systems are no longer adequate. Hence, it is necessary to investigate novel control approaches together with a thorough stability analysis for microgrids.

The thesis presents a combination of several fields: the LMI-based optimization, control of microgrids and $\mathcal{H}_\infty$ control. The contributions of this thesis are summarized as follows. (i) Stability of microgrids at the power control level is considered. A power control loop of an inverter is mainly characterized by a power control law and dynamics of a low-pass filter, which is required for the measurement of inverter output power. Dynamics of lower control levels as well as dynamics of physical output filters of inverters are neglected. A linear state-space model of microgrids is derived for stability analysis and controller design purpose. A decentralized control approach together with an LMI stability condition is proposed to asymptotically stabilize microgrids, while simultaneously guaranteeing zero steady-state deviations of inverter output frequencies. (ii) Load models are presented to outline an influence of loads on the microgrid stability. Accordingly, controller design methods based on the LMI technique, the Lyapunov stability theorem and the small-gain theorem are proposed to guarantee the asymptotic stability of microgrids despite load dynamics. (iii) With the proposed power control loop, magnitudes of inverter output voltages should vary around their nominal values to manage output active and reactive power. Therefore, if a microgrid is subjected to load and line changes (uncertainties), voltage magnitudes can violate acceptable limits and cause functionality problems to connected loads. Regarding this issue, the robust stability of microgrids and the robust performance with respect to output voltages of inverters are investigated in an $\mathcal{H}_\infty$ control framework. As the $\mathcal{H}_\infty$ control framework employed in the thesis requires asymptotically stable model uncertainties, a modification of the power control loop is proposed. As a result, load and line uncertainties in a microgrid are represented by an asymptotically stable model uncertainty. A generalized system model with possible uncertainties and weight functions is then introduced. (iv) Furthermore, based on an $\mathcal{H}_\infty$ norm condition for robust performance, an LMI optimization problem is proposed for controller synthesis. Feasible inverter controllers guarantee the robust stability of microgrids and the robust performance with respect to voltages under considered uncertainties (e.g., load uncertainties, reference changes). (v) Based on the LMI problem mentioned in (iv), a droop-based power sharing control is proposed to improve power sharing performance

between inverters without causing stability and voltage performance problems. This is achieved by adding variable constraints to the LMI problem.

1.3 Outline

The thesis is organized as follows:

Chapter 2 recalls some preliminaries from power system theory and control theory, which are used in the thesis. An introduction of several considered control issues and the case study description are given. A review of existing control approaches to microgrids is provided.

Chapter 3 gives a model of inverter-based microgrids. A power control loop for each inverter is proposed. Then, based on the LMI technique, a stability condition is presented to design decentralized stabilizing controllers for inverters in a microgrid.

Chapter 4 outlines the importance of load modeling in microgrids. Accordingly, a combination of a polynomial load model and an induction machine model is proposed as a dynamic load model for microgrids. The load model is combined with the inverter model derived in Chapter 3 to form an overall microgrid model. Based on the Lyapunov stability theorem, the small-gain theorem and Bounded Real Lemma, two separate LMI stability conditions are proposed to guarantee the asymptotic stability of microgrids under load dynamics.

Chapter 5 investigates the robust stability of microgrids and the robust performance of inverter output voltages against uncertainties, using the $\mathcal{H}_\infty$ control technique. In order to derive an asymptotically stable model uncertainty, which is caused by load and line uncertainties, a modification of the power control loop proposed in Chapter 3 is presented. A generalized model of a microgrid is obtained, which consists of a nominal model of interconnected inverters, an additive model uncertainty and weight functions. Within the $\mathcal{H}_\infty$ control, weight functions reflect knowledge of model uncertainties and performance requirements for voltages. For a derived system model, an LMI optimization problem is introduced to guarantee the robust stability of a microgrid and the robust performance of inverter output voltages.

Chapter 6 investigates the power sharing between inverters in a microgrid. Based on the power control loop proposed in Chapter 5, droop gains in each inverter controller are defined. By introducing additional variable constraints to the LMI problem derived in Chapter 5, droop-based controllers for inverters can be designed, which improve the power sharing performance between inverters without causing stability and voltage performance problem.

Chapter 7 concludes the thesis and gives an outlook for future research.

Chapter 2

Control problem formulation and state of the art

This chapter gives an overview of the considered class of microgrids, introducing a general system setup, assumptions and related control issues, which serve as a framework of contributions achieved in the thesis. A review of existing control approaches to inverter-based microgrids is presented. Moreover, some general requirements for control strategies at the power control level of microgrids are recast in this chapter, serving as a guideline for the controller synthesis proposed in the following chapters.

2.1 System setup and general assumptions

The most common architecture of microgrids is the one in which inverters are connected to each other in parallel. Microgrids with parallel structures attract most attention from microgrid research communities. This is confirmed by numerous publications such as [10, 21, 25, 27–29] as well as by most real-world microgrid prototypes, which are recast in [11, 30]. Such a microgrid can contain an arbitrary number of generation units and loads. Generation units are interfaced to the network via inverters. A parallel structure means that all the inverters in a microgrid are connected to a common bus. The common bus in turn is connected to a point of common coupling, which is a connection point between a microgrid and a transmission network.

This thesis investigates only the case of microgrids with parallel-connected inverters. Loads are modelled as constant impedances for all stability studies, except in Chapter 4, where a more detailed load modeling is addressed. A structure of a microgrid consisting of n inverters and $(n+m)$ loads is shown in Figure 2.1, where Z_i denotes constant impedance loads, and Z_{Li} are

impedances of connecting power lines, $i = 1, \ldots, (n+m)$. In Figure 2.1, there are n loads, which are directly connected at inverter outputs, and m independent loads.

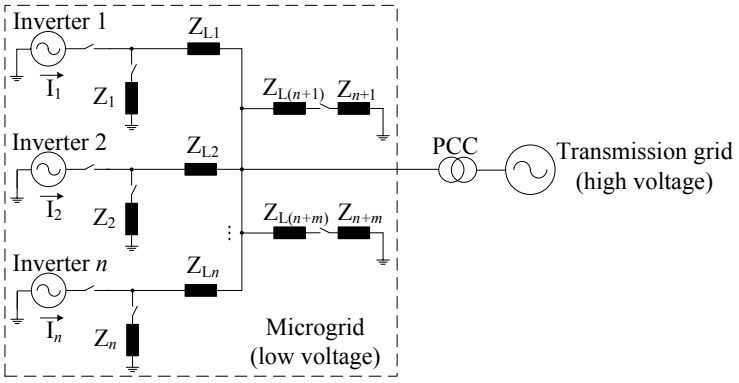

FIGURE 2.1: A microgrid network.

Inverters inject energy into the network and are therefore called *active* nodes. Constant impedance loads Z_i, $i = 1, \ldots, (n+m)$, simply consume electrical energy and are called *passive* nodes. The definitions of active and passive nodes are taken from the electrical network theory and passivity theory. Active nodes generate power and may cause system instability [31], whereas passive loads absorb power, keeping a power balance condition in the system.

An impedance Z can be represented in Cartesian form and in phasor form as follows:

$$Z = R + jX = |Z|e^{j\phi_Z}, \tag{2.1}$$

where R is the resistance, X is the reactance, $|Z| = \sqrt{R^2 + X^2}$ and $\phi_Z = \arctan \frac{X}{R}$ are the magnitude and angle of the impedance, and j is the imaginary unit.

In order to derive a network equation, the definition of an admittance Y is introduced as follows:

$$Y = \frac{1}{Z} = \frac{1}{R+jX} = \frac{R}{R^2+X^2} - j\frac{X}{R^2+X^2} = G + jB, \tag{2.2}$$

where G is a conductance, and B is a susceptance [32].

The network equations in terms of the node admittance matrix can be written as follows [33]:

$$\begin{bmatrix} \vec{I}_1 \\ \vec{I}_2 \\ \vdots \\ \vec{I}_n \\ 0 \\ \vdots \\ 0 \end{bmatrix} = \begin{bmatrix} Y_{11} & Y_{12} & \cdots & Y_{1n} & Y_{1(n+1)} & \cdots & Y_{1(n+m)} \\ Y_{21} & Y_{22} & \cdots & Y_{2n} & Y_{2(n+1)} & \cdots & Y_{2(n+m)} \\ \vdots & \vdots & \ddots & \vdots & \vdots & \ddots & \vdots \\ Y_{n1} & Y_{n2} & \cdots & Y_{nn} & Y_{n(n+1)} & \cdots & Y_{n(n+m)} \\ Y_{(n+1)1} & Y_{(n+1)2} & \cdots & Y_{(n+1)n} & Y_{(n+1)(n+1)} & \cdots & Y_{(n+1)(n+m)} \\ \vdots & \vdots & \ddots & \vdots & \vdots & \ddots & \vdots \\ Y_{(n+m)1} & Y_{(n+m)2} & \cdots & Y_{(n+m)n} & Y_{(n+m)(n+1)} & \cdots & Y_{(n+m)(n+m)} \end{bmatrix} \begin{bmatrix} \vec{V}_1 \\ \vec{V}_2 \\ \vdots \\ \vec{V}_n \\ \vec{V}_{n+1} \\ \vdots \\ \vec{V}_{n+m} \end{bmatrix}, \tag{2.3}$$

where

n number of inverter nodes in the system,
m number of load nodes in the system,
Y_{ii} self admittance at node i, $i = 1,\dots,(n+m)$,
Y_{ik} mutual admittance between node i and node k, $i \neq k$, $i,k = 1,\dots,(n+m)$,
$\vec{I}_i$ output current of node i, i.e., current provided by an inverter i, $i = 1,\dots,n$,
$\vec{V}_i$ voltage to the ground of node i, $i = 1,\dots,(n+m)$.

A self admittance Y_{ii} is equal to the sum of all admittances terminating at node i, whereas a mutual admittance Y_{ik} is equal to the negative sum of the two admittances between node i and node k [33]. From the Figure 2.1, the following is obtained:

$$Y_{ii} = \frac{1}{Z_i} + \frac{1}{Z_{Li}} = G_{ii} + jB_{ii}, \quad i = 1,\dots,(n+m), \tag{2.4a}$$

$$Y_{ik} = -\frac{1}{Z_{Li}} - \frac{1}{Z_{Lk}} = G_{ik} + jB_{ik}, \quad i \neq k,\ i,k = 1,\dots,(n+m). \tag{2.4b}$$

As seen in (2.3), passive nodes, i.e., constant impedance loads, do not inject electrical current into the network, i.e., $\vec{I}_i = 0$, $i = (n+1),\dots,(n+m)$. Thus, a microgrid can be represented equivalently by using the standard *Kron-reduction* technique to eliminate passive nodes in the system [32, 34]. For the stability analysis conducted in the thesis, instead of working with the node admittance matrix (2.3), it is more convenient to consider a lower dimensional Kron-reduced admittance matrix of the microgrid, which only contains active nodes [19, 20, 32–34].

The Kron-reduction technique is illustrated by the following example. Consider a simple electrical network with two active nodes and one passive node. Assume that node 1 and node 2 are active, while node 3 is passive, i.e., $\vec{I}_3 = 0$. Then, the network equations in terms of the node admittance matrix can be written as follows:

$$\begin{bmatrix} \vec{I}_1 \\ \vec{I}_2 \\ 0 \end{bmatrix} = \begin{bmatrix} Y_{11} & Y_{12} & Y_{13} \\ Y_{21} & Y_{22} & Y_{23} \\ Y_{31} & Y_{32} & Y_{33} \end{bmatrix} \begin{bmatrix} \vec{V}_1 \\ \vec{V}_2 \\ \vec{V}_3 \end{bmatrix}. \tag{2.5}$$

From the equation above, the following is obtained:

$$\begin{cases} \vec{I}_1 &= Y_{11}\vec{V}_1 + Y_{12}\vec{V}_2 + Y_{13}\vec{V}_3, \\ \vec{I}_2 &= Y_{21}\vec{V}_1 + Y_{22}\vec{V}_2 + Y_{23}\vec{V}_3, \\ 0 &= Y_{31}\vec{V}_1 + Y_{32}\vec{V}_2 + Y_{33}\vec{V}_3. \end{cases} \tag{2.6}$$

The last equation in (2.6) yields $\vec{V}_3 = -\frac{Y_{31}\vec{V}_1 + Y_{32}\vec{V}_2}{Y_{33}}$. By substituting $\vec{V}_3$ into equations of $\vec{I}_1$ and $\vec{I}_2$, the following is obtained:

$$\begin{cases} \vec{I}_1 &= \underbrace{\left(Y_{11} - \frac{Y_{13}Y_{31}}{Y_{33}}\right)}_{:= Y_{11}^{\text{Kron}}} \vec{V}_1 + \underbrace{\left(Y_{12} - \frac{Y_{13}Y_{32}}{Y_{33}}\right)}_{:= Y_{12}^{\text{Kron}}} \vec{V}_2, \\ \vec{I}_2 &= \underbrace{\left(Y_{21} - \frac{Y_{23}Y_{31}}{Y_{33}}\right)}_{:= Y_{21}^{\text{Kron}}} \vec{V}_1 + \underbrace{\left(Y_{22} - \frac{Y_{23}Y_{32}}{Y_{33}}\right)}_{:= Y_{22}^{\text{Kron}}} \vec{V}_2, \end{cases} \Leftrightarrow \begin{bmatrix} \vec{I}_1 \\ \vec{I}_2 \end{bmatrix} = \begin{bmatrix} Y_{11}^{\text{Kron}} & Y_{12}^{\text{Kron}} \\ Y_{21}^{\text{Kron}} & Y_{22}^{\text{Kron}} \end{bmatrix} \begin{bmatrix} \vec{V}_1 \\ \vec{V}_2 \end{bmatrix}. \quad (2.7)$$

Thus, the network with the admittance matrix in (2.5) can be represented equivalently by a Kron-reduced network with the admittance matrix in (2.7). For the ease of notation, the index "Kron" is eliminated. Instead of Y_{ii}^{Kron} and Y_{ik}^{Kron}, self and mutual admittances of Kron-reduced microgrid networks are denoted by Y_{ii} and Y_{ik} throughout the thesis, respectively. Then, the Kron-reduced network of a microgrid with n inverters is represented by the following equation:

$$\begin{bmatrix} \vec{I}_1 \\ \vec{I}_2 \\ \vdots \\ \vec{I}_n \end{bmatrix} = \begin{bmatrix} Y_{11} & Y_{12} & \dots & Y_{1n} \\ Y_{21} & Y_{22} & \dots & Y_{2n} \\ \vdots & \vdots & \ddots & \vdots \\ Y_{n1} & Y_{n2} & \dots & Y_{nn} \end{bmatrix} \begin{bmatrix} \vec{V}_1 \\ \vec{V}_2 \\ \vdots \\ \vec{V}_n \end{bmatrix}. \quad (2.8)$$

A Kron-reduced structure of a simple microgrid with three inverters is illustrated in Figure 2.2. The Kron-reduced structure of a microgrid with n inverters can be represented in the same manner as in Figure 2.2.

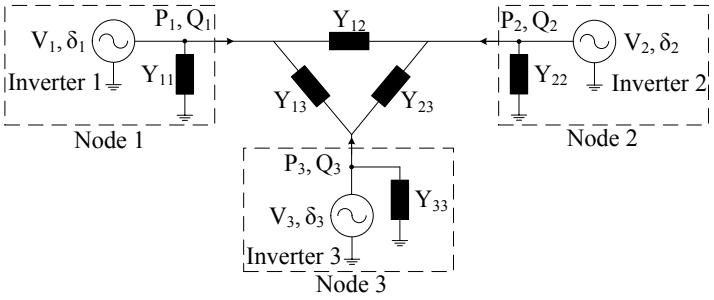

FIGURE 2.2: A Kron-reduced microgrid network.

Based on the admittance matrix in (2.8), the active and reactive power exchange at each active node i of a microgrid, i.e., P_i and Q_i, respectively, is computed by the following standard power flow equations [33]:

$$P_i = \sum_{k=1}^{n} V_i V_k |Y_{ik}| \cos(\delta_i - \delta_k - \phi_{ik}), \quad (2.9a)$$

$$Q_i = \sum_{k=1}^{n} V_i V_k |Y_{ik}| \sin(\delta_i - \delta_k - \phi_{ik}), \quad (2.9b)$$

where V_i, V_k are voltage magnitudes, δ_i, δ_k are phase angles of the related voltages, $|Y_{ik}|$ and ϕ_{ik}, where $i \neq k$, are the absolute value and the angle of the admittance Y_{ik} between node i and node k, whereas $|Y_{ii}|$ and ϕ_{ii} are the absolute value and the angle of a self admittance Y_{ii} of each node i, and n is the number of inverters in the system. A standard procedure to derive the power flow equations above is given in Appendix A.1.

Throughout the thesis, it is assumed that all the phase angles of inverter output voltages are expressed relative to a common rotating reference frame with a *constant* angular velocity ω_{nom}, which is equal to the rated frequency of the system, e.g., $2\pi 50$ [rad/s]. This assumption allows to correctly calculate the power exchange P_i and Q_i in (2.9).

The power flow equations (2.9) show that the mutual admittance Y_{ik} characterizes the interconnection between node i and node k. Moreover, Equations in (2.9) also show that in order to manage power exchange at each node i, it is necessary and sufficient to take control over voltage magnitudes V_i and phase angles δ_i, $i = 1, \ldots, n$.

Regarding the inverter interface, throughout the thesis, it is considered that generation units are connected to a microgrid via voltage source inverters, which are also called network-forming inverters [27, 35, 36]. It is well known that the control system of a voltage source inverter consists of a three-level structure as presented in Figure 2.3 [8, 10, 27, 35, 37–39]. The PWM modulator forms the innermost control level, which directly controls the inverter switching. The current control loop[1] regulates the current supplied by the inverter. Setpoint for the current control loop is provided by the voltage control loop, which controls the output voltage of the inverter to match its reference.

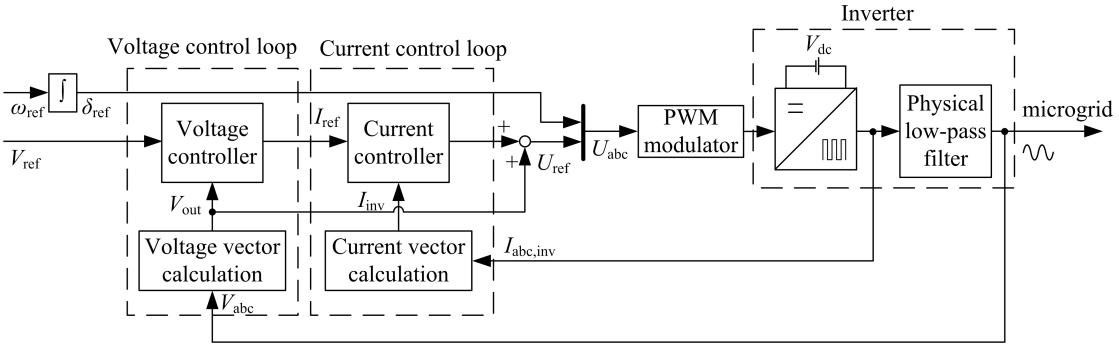

FIGURE 2.3: Three-level control structure of a voltage source inverter.

As seen in Figure 2.3, an inverter consists of a DC voltage source, a power electronic device and a physical output filter. One of the commonly used power electronics to convert a DC voltage to an AC voltage is the insulated-gate bipolar transistor (IGBT). The output voltage of the power electronic is not sinusoidal. Therefore, a physical low-pass filter is connected in series with the power electronic to obtain a near sinusoidal AC voltage at the output of the inverter.

[1]The current controller is the fastest closed-loop controller, which operates as well as a current limiter to prevent inverter overcurrents, which can occur for several periods due to sudden load changes at inverter output.

The fact is that inverters are relatively stiff sources with unique values of voltage magnitude and frequency (if there is no higher control level, which adjusts setpoints for voltage magnitude and phase angle). When inverters are connected in parallel, due to component and measuring tolerances, large circulating currents[2] between inverters would result if no additional control is taken [17, 40, 41]. In order to regulate power exchange at each inverter node i, which are directly related to the current generated by that inverter (i.e. current flow direction, current magnitude, relative angle between current and voltage, etc.), a power control loop is introduced. As seen in Figure 2.4, the power control loop generates magnitude and phase angle setpoints for the inverter output voltage.

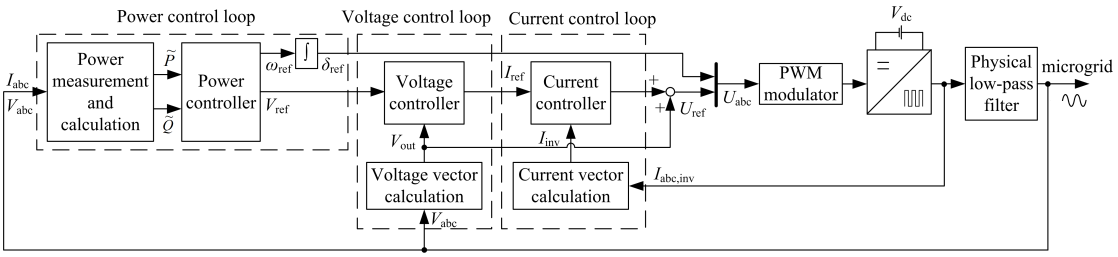

FIGURE 2.4: Control loops of a voltage source inverter.

The switching frequency of inverters is in the range of about 2-20 [kHz] [14], which is much faster than the rated frequency of power systems, e.g., 50 [Hz]. Voltage and current control loops of inverters normally consist of very fast proportional-integral controllers to track their references [35]. Moreover, inverter output power is required to drive the power control loop. Usually, inverter output power is measured through a low-pass filter, which makes the bandwidth of the power control loop much smaller than the bandwidth of the lower-level control loops. Hence, dynamics of the pulse-width modulation (PWM) and the middle control loops are much faster than dynamics of the power control loop, which is strongly influenced by the measuring low-pass filter.

Based on the facts above, for the stability analysis of inverter-based microgrids the following assumptions are made. Suppose that there is an ideal voltage source on the DC-side of each inverter. All inverters are equally treated as voltage source inverters with controllable magnitudes V_i and phase angles δ_i of their output voltages. Moreover, the case of *ideal* voltage source inverters (VSIs) is assumed, i.e., only the power control loop of inverters is explicitly considered, while the dynamics of lower control levels are assumed to be exceedingly fast and can be neglected [8, 27, 37, 38, 42, 43]. This assumption is made to simplify the inverter modelling task, while performing stability analysis of microgrids at the power control level. An inverter model includes merely dynamics of the power control loop, which causes most stability problems

[2] A circulating current between two parallel-connected inverters is a current, which is generated by one inverter and absorbed by the other. A circulating current between two inverters happens due to (small) differences between inverter output voltages, which is mainly a consequence of parameter mismatch [40]. Large circulating currents between inverters can lead to overcurrent or overvoltage for IGBTs and components on the DC-side of inverters, e.g. capacitors. Circulating currents can result in permanent damage of hardware components and should be avoided.

[1, 8, 9, 42]. The lower-level control loops are assumed to perfectly and rapidly track their references [8].

It should be clear that each VSI with the power control loop in Figure 2.4 includes two low-pass filters: the measuring low-pass filter and the physical output filter. The measuring low-pass filter is realized digitally, whereas the physical output filter is often an LCL low-pass filter. Usually, the time constant of the physical output filter is negligible, compared to the time constant of the measuring low-pass filter [10, 36]. Hence, with negligible dynamics of lower-level control loops as well as a negligible time constant of the physical filter, Figure 2.5 presents an ideal voltage source inverter with a power control loop.

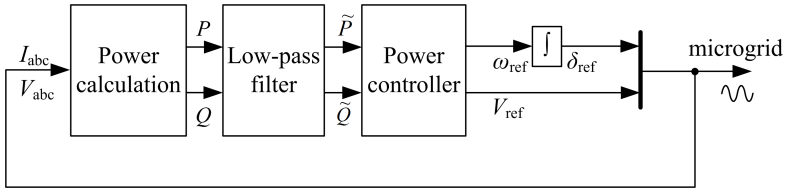

FIGURE 2.5: Voltage source inverter with a power control loop.

Remark 2.1.1. In the thesis, the power control loop represents the outermost control loop of a voltage source inverter (see Figure 2.4). There exist higher (supervisory) control levels of inverters. For instance, a power management level provides power setpoints for the power control loop, assuming stability of microgrids at the power control level [7, 15, 44–46]. Higher supervisory control levels obtain even slower dynamics than the power control loop, and are not considered in this thesis.

Remark 2.1.2. The realization of the voltage and current control loops in Figure 2.4 is usually done using the $abc/dq0$ transformation (Park transformation), which refers 3-phase AC voltages or currents to a $d-q$ rotating reference frame [35, 47]. The resulting 0-component of a symmetric 3-phase AC value is zero. Rotating angular velocity of the $d-q$ reference frame can be arbitrarily assigned. In this thesis, all inverters in a microgrid obtain a *common* rotating reference frame with a *constant* angular velocity ω_{nom}. $dq0/abc$ is an inverse transformation of $abc/dq0$. $dq0/abc$ transformation is implemented to transform outputs of inverter control loops to 3-phase AC values, providing references for the PWM modulation procedure. As the voltage and current control loops of an inverter are not in the focus of this thesis, the $abc/dq0$ and $dq0/abc$ transformations of three-phase voltages and currents are not explicitly presented in Figure 2.4. More details on the control of an inverter as a voltage source can be easily found in literature [8, 27, 35, 36].

Remark 2.1.3. Different from generators, inverters are power electronic devices which do not contain any rotating mass and therefore, do not obtain any mechanical inertia [27, 48, 49]. Generators obtain a possibility to instantly change their generated output power to supply load

changes, i.e., inertial response [50–52]. As will be shown in Chapter 3, with negligible dynamics of lower-level control loops, a power control loop for each inverter is proposed so that inverters in a microgrid operate and react inertially to load changes. As seen in Figure 2.5, inverter output power is measured through a low-pass filter to drive the power control loop. In addition, the power control loop contains an integrator, which is needed to generate a phase angle reference for inverter output voltage. Dynamics of the low-pass filter and the integrator result in delayed response of inverters to load changes, i.e., providing an artificial inertia to inverters. In Chapter 3 it will be shown that dynamic model of an inverter is associated to the integrator and the measuring low-pass filter. The stability of a microgrid therefore depends explicitly on parameters of the low-pass filters, on control laws for the power control loop of inverters as well as on the network structure, which is described by the admittance matrix.

In Figure 2.6, a line-to-neutral output voltage of a three-phase inverter with different PWM switching frequencies is presented. For this example, a three-phase sinusoidal reference input is compared with a triangle carrier signal, generating logic commands for the inverter to switch on/off. The inverter output voltage has a switching form. This three-phase PWM voltage is filtered by a physical low-pass filter, resulting in a near sinusoidal inverter output voltage. It is seen in Figure 2.6 that with a low PWM switching frequency (2.5 kHz), the output voltage is not ideal sinusoidal. With higher PWM switching frequencies (5 kHz and 10 kHz), the sinusoidal wave form of the output voltage is significantly improved. Today's inverter technologies possess high switching frequencies, which allow voltage source inverters (with physical low-pass filters) to generate almost ideal sinusoidal output voltages.

The motivation of the system setup and assumptions above will be further elaborated in the next section, where the control issues of microgrids are introduced. Additional assumptions are also presented during the thesis depending on particular problem settings.

2.2 Stability and performance aspects of microgrids

Stability is essential for the operation of microgrids and therefore, it is the main objective of the thesis. However, there exist different stability definitions in control theory and power system theory. Stability of microgrids will be first discussed from both perspectives to specify stability issues of microgrids, which are considered in the thesis. Afterwards, several stability definitions from control theory will be introduced for their implementation throughout the thesis. Several performance requirements for microgrids will also be mentioned in this section.

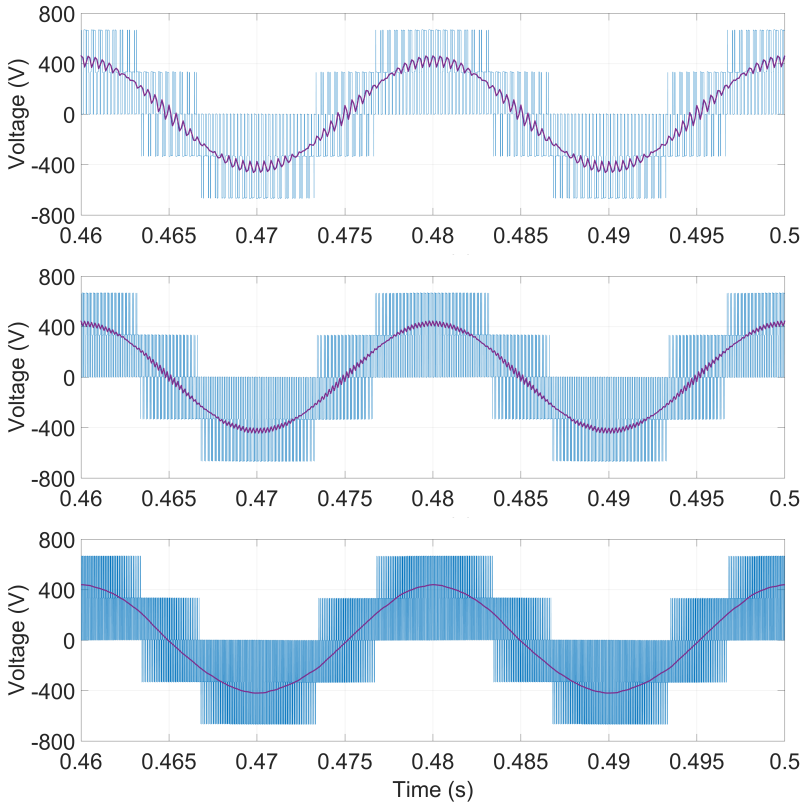

FIGURE 2.6: Output voltage of an inverter with different PWM switching frequencies: upper figure 2.5 kHz; middle figure 5 kHz; lower figure 10 kHz.

2.2.1 Stability of microgrids from a power system perspective

Definition 2.1. [33] Microgrid stability in particular, and power system stability in general can be broadly defined as a property of a power system to remain in a state of operating equilibrium under normal operating conditions and to regain an acceptable state of equilibrium after being subjected to a disturbance. □

Similar to large power systems, different stability issues of inverter-based microgrids are classified as illustrated in Figure 2.7 [1, 12, 33, 53]. It is seen that, with respect to Definition 2.1, power system theory introduces different stability definitions based on different reasons, which affect the state of operating equilibrium of a microgrid.

In this thesis, stability analysis will be studied explicitly in the sense of *small-signal stability*. Small-signal stability is also called small-disturbance rotor angle stability [53]. In power system theory, the rotor angle stability refers to an ability of synchronous machines of an interconnected power system to remain in synchronism after being subjected to a disturbance [33, 53]. As most generation units in today's power systems are synchronous machines, the rotor angle stability definition was introduced for them. In the case of microgrids, VSIs are operated as network-forming generation units to replace synchronous generators. VSIs can be seen as power

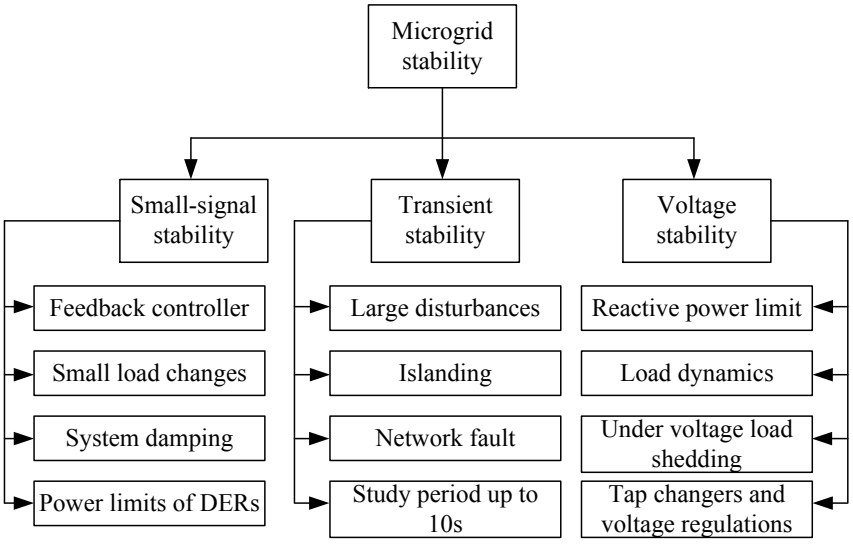

FIGURE 2.7: Microgrid stability issues from power system perspective [1].

electronic devices, which mimic synchronous generators. Therefore, it is a common practice to analyze stability of microgrids based on the classical stability definitions of large power systems. As inverters do not contain any rotor, rotor angles in this case should be understood as voltage phase angles of inverters, and the term *phase angle stability* will be used instead of rotor angle stability.

In the small-signal stability analysis, state variables of a microgrid are expressed as deviations of system values from their equilibriums. Small-signal stability is defined as an ability of a system to maintain synchronism among generation units when subjected to small disturbances [53]. In power system analysis, small disturbances are considered to be small enough so that by considering a linear model of a nonlinear power system, the state of the system can be inferred [33]. As illustrated in Figure 2.7, the focus of small-signal analysis lies on feedback power controller, small load changes, system damping and power limits of DERs.

Microgrids can also be subjected to larger disturbances, e.g., large changes of system loads. As will be shown in Chapter 5, impedance uncertainties of a microgrid will be formulated as a model uncertainty for stability analysis.

Remark 2.2.1. It should be noted that there is no clear difference between *disturbance* and *uncertainty* in power system theory. In power system literature, these two terms are used interchangeably. However, *disturbance* and *uncertainty* are two different definitions in control system theory. For instance, in power system literature a disturbance can refer to a connection of a load to a power system. From the control system point of view, a connection of a load creates a model uncertainty, where *model uncertainty* refers to the difference or errors between models and reality [54–56]. *Disturbance* is also called *signal uncertainty* in control system theory and refers to measurement noise, process noise, etc. [54, 56].

Given an initial stable operating condition of a microgrid, there is a power balance in the system and the power flow equations (2.9) hold. If the system is perturbed, this stable condition is upset, resulting in oscillations of system variables (e.g., inverter phase angles, voltage magnitudes, output power of inverters). Instability may occur if inverter phase angles and voltage magnitudes are not properly controlled to maintain a synchronous operation. It is a fact that most stability problems of microgrids appear from the most outer control loop of inverters, i.e., the power control loop [1, 18]. Inverter output power is directly dependent on phase angles (and voltage magnitudes). Hence, by addressing the power control loop of a microgrid, it is dealt with the phase angle stability of the system, and vice versa. Especially small-signal analysis can give useful information about the system state and therefore is a powerful tool widely used in controller design for microgrids [8, 9, 15, 28, 39].

Moreover, disturbances from loads can be in form of a feedback influence of load dynamics on the system stability. In power system studies, load dynamics create most *voltage stability* problems (see Figure 2.7). Voltage stability refers to the ability of a power system to maintain steady voltages at all buses in the system after being subjected to a disturbance from a given initial operating condition [53]. Dealing with load dynamics, load modeling must be investigated to achieve a more precise insight into load influences on the system stability. A suitable controller design can then be proposed to stabilize a microgrid under an influence of load dynamics.

Remark 2.2.2. The term *voltage stability* does not mean that in a power system, voltages can be stable, while other system variables can be unstable, and vice versa. As will be shown in Chapter 4, measurements of real power systems show that load variations cause variations of voltages. Consequently, voltage variations induce via load dynamics power demand variations, which can further cause oscillations of other system variables. Strong oscillations of system variables may cause system instability. Thus, voltage variations and load dynamics represent a reason of oscillations of other system variables, rather than a result of it. Therefore, the term *voltage stability* is used in literature and load dynamics are specified as a voltage stability problem [33].

2.2.2 Stability of microgrids from a control system perspective

In control system theory, the system stability in the sense of Lyapunov is defined as follows. Consider an autonomous system, which satisfies the Lipschitz condition on the uniqueness of solution [57]

$$\dot{x} = f(x), \tag{2.10}$$

where $f : \mathcal{D} \to \mathbb{R}^n$ is a locally Lipschitz map from a domain $\mathcal{D} \subset \mathbb{R}^n$ into $\mathbb{R}^n$.

Assume that $f(x)$ in (2.10) satisfies $f(0) = 0$.

Definition 2.2. [57] The equilibrium point $x = 0$ of (2.10) is

- stable if, for each $\epsilon > 0$, there is $\eta = \eta(\epsilon) > 0$ such that:

$$\|x(0)\| < \eta \;\Rightarrow\; \|x(t)\| < \epsilon,\ \forall t \geq 0, \tag{2.11}$$

- unstable if not stable,
- asymptotically stable if it is stable and η can be chosen such that:

$$\|x(0)\| < \eta \;\Rightarrow\; \lim_{t\to\infty} x(t) = 0. \tag{2.12}$$

□

With respect to Stability Definition 2.2, the Lyapunov's stability theorem is presented in the following.

Theorem 2.3. *[57] Let $x = 0$ be an equilibrium point for (2.10) and $\mathcal{D} \subset \mathbb{R}^n$ be a domain containing $x = 0$. Let $\mathcal{V} : \mathcal{D} \to \mathbb{R}$ be a continuously differentiable function such that:*

$$\mathcal{V}(0) = 0 \text{ and } \mathcal{V}(x) > 0 \text{ in } \mathcal{D} - \{0\}, \tag{2.13}$$

$$\dot{\mathcal{V}}(x) \leq 0 \text{ in } \mathcal{D}. \tag{2.14}$$

Then, $x = 0$ is stable. Moreover, if

$$\dot{\mathcal{V}}(x) < 0 \text{ in } \mathcal{D} - \{0\}, \tag{2.15}$$

then $x = 0$ is asymptotically stable.

In this thesis, the control system approach is used to formulate stability conditions for microgrids. Throughout the thesis, Stability Definition 2.2 and Theorem 2.3 will be used to state, whether a system is (asymptotically) stable.

Furthermore, for stability and performance analysis in the thesis, the following definitions are introduced.

Definition 2.4. [56]

- Nominal stability - a system is stable without model uncertainty.
- Nominal performance - a system satisfies some performance specifications without model uncertainties.

- Robust stability - a system is stable for all perturbed plants about the nominal model up to the worst-case model uncertainty.
- Robust performance - a system satisfies some performance specifications for all perturbed plants about the nominal model up to the worst-case model uncertainty. □

As mentioned in Subsection 2.2.1, the small-signal stability (in the power system sense) of microgrids will be studied in the thesis. A common approach for small-signal analysis of a power system is to study a linearized system model around an equilibrium point [9, 39, 58]. Variables of the linearized model are defined as deviations of system values from their equilibriums. From the control system theory, by analyzing the stability of a nonlinear system based on a linearized model of that system around an equilibrium point, the *local stability* of the system around this equilibrium point can be stated (if the linearized model does not have eigenvalues on the imaginary axis (see Remark 2.2.3)).

Note that the nominal stability of a microgrid (defined in control system sense) can be compared with its small-signal stability (defined in power system sense). However, these two stability definitions should be clearly separated. The small-signal stability in power system theory refers to the system stability despite small uncertainties such as small load changes, i.e., small model uncertainties. In comparison to that, the nominal stability in control system theory defines system stability without model uncertainties [56].

Furthermore, load and line changes/uncertainties in a power system can be large enough to cause large oscillations of system variables, which may result in system instability. In this case, stability analysis of a microgrid based on its nominal model is not sufficient, but stability analysis must consider also model uncertainties, which are caused by load and line uncertainties. According to Definition 2.4, the stability analysis concerning a nominal system model and model uncertainties refers to the *robust stability* of the system. Note that local robust stability of microgrids will be studied as it is based on a linearized system model at an equilibrium and a model uncertainty.

For studying a linearized system model of a microgrid, the following theorem and definition are also useful.

Theorem 2.5. *[57] Consider a linear time-invariant system:*

$$\dot{x} = Ax, \tag{2.16}$$

the equilibrium point $x = 0$ is asymptotically stable if and only if all eigenvalues of A have negative real parts.

Definition 2.6. [57] When all eigenvalues of A in (2.16) have negative real parts, A is called a Hurwitz matrix. □

Thus, the equilibrium point $x = 0$ of (2.16) is asymptotically stable if and only if A is Hurwitz. In this case, $x = 0$ is also the unique equilibrium point.

The following theorem is known as Lyapunov's indirect method, which is used for the case when stability of a nonlinear system at the origin is analyzed on the basis of a linearized system model.

Theorem 2.7. *[57] Let $x = 0$ be an equilibrium point for the nonlinear system:*

$$\dot{x} = f(x), \tag{2.17}$$

where $f : \mathcal{D} \to \mathbb{R}^n$ is continuously differentiable and $\mathcal{D}$ is a neighborhood of the origin. Let

$$A = \frac{\partial f}{\partial x}(x)\bigg|_0. \tag{2.18}$$

Then,

1. *The origin is asymptotically stable if $Re\lambda_i < 0$ for all eigenvalues λ_i of A.*
2. *The origin is unstable if $Re\lambda_i > 0$ for one or more of the eigenvalues λ_i of A.*

Remark 2.2.3. [57] Regarding Theorem 2.7, if A has some eigenvalues with zero real parts with the rest of the eigenvalues having negative real parts, then linearization fails to determine the stability properties of the origin of the nonlinear system. In Chapter 3, a multi-input multi-output (MIMO) state-space model for each inverter in a microgrid will be proposed, which contains P_i and Q_i from the power flow equations (2.9). As seen in (2.9), P_i and Q_i are nonlinear algebraic equations, making each inverter a nonlinear system. As a result, a microgrid is a MIMO nonlinear system. Therefore, in order to state the asymptotic stability of a nonlinear microgrid at an equilibrium based on a linearized system model, the linearized system must be asymptotically stable.

2.2.3 Voltage and frequency performance

Analyzing stability of microgrids under different uncertainties such as load and line changes, loss of generation units, etc., one realizes that uncertainties have a potential to deteriorate the system stability margin as well as the performance of inverter output voltages and frequencies. According to grid-code requirements [59, 60], deviations of voltage magnitudes and frequencies

must be kept within acceptable ranges around their nominal values, e.g., $\pm 1\%$ around nominal value for frequencies, and $\pm 5\%$ around nominal value for voltages [61]. Additionally, inverter output voltages should not contain a large amount of the total harmonic distortion (THD), which is a measurement of higher harmonic components in voltages [62]. For low-voltage power systems (whose nominal voltage is less than 1 [kV] [63]), an acceptable range for THD is normally around 8% [61, 64]. These requirements are included in power system design to ensure safe functionality of system loads. Therefore, beside the stability analysis, this thesis also partly considers the voltage and frequency performance, which is often referred to power quality problems in literature [33, 65–67]. A detailed review of power quality issues of microgrids can be found in [68–70].

2.2.4 Power flow strategy

For a safe, reliable and beneficial operation of microgrids, beside the stability issues and the performance with respect to voltages and frequencies, power flow strategies should also be studied. Within a power system with a large amount of generation units, a power flow strategy is often interpreted as a possibility of the system to regulate the portions of electrical power, which are generated by individual generation units to supply the total system load demand [15, 22, 33]. With the possibility to control the power flow within microgrids, system operators can apply different power management strategies with respect to different conditions of weather, time, load demand, etc., to provide the most beneficial system operation. Among different power flow strategies, the most popular is the *power sharing*.

Power sharing is a classical definition in the power system field, which means that all the generation units in a power system should share the total system load demand in a desired way, which is predefined by power sharing ratios [19, 20, 33, 38]. A popular power sharing approach is the classical droop control, which will be reviewed in detail in Section 2.4. The thesis will explicitly consider the power sharing strategy as an attempt to operate inverter-based microgrids similarly to conventional power systems. Technically, power sharing between inverters will reduce current and loading stress, e.g. overcurrent, thermal stress, on particular inverters. Consequently, less stressful operation of inverters will reduce faults during operation and prolong life of power electronics.

Remark 2.2.4. It is noteworthy that the main *goal* at the power control level is the control of power flows within a microgrid. However, once a (power) control loop is added to each inverter, the closed-loop stability of microgrids and the performance of voltages and frequencies become the most important *requirements*. Different power flow strategies can be accomplished only when the stability of microgrids and a sufficient performance of voltages and frequencies are guaranteed. Power flow strategy is a performance criterion of the power control loop,

whereas the stability of microgrids and the performance of voltages and frequencies are essential requirements. This point of view will also be reflected in the thesis. The stability of microgrids and the performance of voltages and frequencies against uncertainties and disturbances will be considered first. The power sharing control will be investigated in Chapter 6.

2.3 Requirements for power control strategy

At the power control level, inverter control approaches must be definitely decentralized for microgrids to be largely independent of communication [5, 71]. Following the common acceptance of the microgrid research community while searching for requirements for stabilizing and power flow controllers of microgrids, the following specifications are summarized [5, 8, 10, 42]:

1. A power controller of each inverter in a microgrid is decentralized.
2. Inverter controllers must guarantee the overall system stability.
3. Deviations of inverter output voltages and frequencies should not violate acceptable limits defined by grid-code documents to maintain a smooth functionality of system loads.
4. Controllers must allow all the inverters to work in plug-and-play and peer-to-peer manner.
5. Despite the intermittent nature of renewable energy sources, the power balance in microgrids must be guaranteed.
6. Controllers should be able to allow all the generation units in a microgrid to establish a desired power flow strategy.

The first two requirements are necessary for microgrids to operate independently from a communication infrastructure, i.e., there is no control interconnection between inverters. Communication can be added to improve system performance and robustness. However, these requirements are essential for a secure and reliable power supply of a microgrid, i.e., the system should continue to operate and supply load demand even in case of loss of communication.

The third requirement was explained in Subsection 2.2.3, whereas the fourth is complementary to the first two requirements, addressing the structural flexibility of microgrids. That is, the peer-to-peer and plug-and-play concepts must be promoted in each component of microgrids [5, 72]. The peer-to-peer concept implies that there are no components like a main generation unit or a large storage, which are critical for the operation of microgrids. The system must continue operating in case of loss of any unit. Meanwhile, the plug-and-play means that a generation unit can be arbitrarily added to a microgrid without causing control and protection problems to already existing units of the system [6].

The last two requirements, in other words, express that a stable operation of microgrids is achieved only in the case generated power is equal to system load demand, and for a beneficial system operation, inverter controllers should be able to form a desired power flow strategy. As mentioned above, power flow strategy will be investigated in the sense of power sharing between inverters. The power sharing control proposed in this thesis is decentralized and does not require any communication.

2.4 Review of existing control approaches

Regarding the aforementioned control issues of microgrids, researchers have published different solutions to answer the question: How to make microgrids work? This section gives a review of several popular methods. An important decentralized control approach to provide power sharing to microgrids and maintain output frequencies and voltages of inverters around nominal values is the classical *droop control*, which is commonly applied to synchronous generators in large power systems [33]. The idea of the classical droop control is explained as follows. Consider a power system with n generation units attached with the following assumptions:

- The connecting lines between generation units are inductive ($R_{ik} \ll X_{ik},\ i \neq k,\ i,k = 1,\ldots,n$), i.e., line resistances can be neglected ($R_{ik} \approx 0,\ G_{ik} \approx 0$).
- Differences between phase angles of different generation units are assumed to be small, then $\sin(\delta_i - \delta_k) \approx (\delta_i - \delta_k)$, $\cos(\delta_i - \delta_k) \approx 1$.

Based on the assumptions above, the following is derived from the power flow equations (2.9) (see Appendix A.2 for more detail):

$$P_i \approx V_i^2 G_{ii} - \sum_{k=1,\ k\neq i}^{n} V_i V_k (\delta_i - \delta_k) B_{ik}, \quad Q_i \approx V_i^2 B_{ii} + \sum_{k=1,\ k\neq i}^{n} V_i V_k B_{ik}. \tag{2.19}$$

It can be seen from (2.19) that P_i can be influenced through the phase angles and the voltage magnitudes, whereas Q_i can be controlled by the voltage magnitudes. In order to establish a decentralized power control law, the droop control feeds back Q_i to V_i, and P_i to δ_i, or explicitly to its derivative ω_i. The droop control is represented by the following (known as f/P and V/Q control loops) [8, 10, 33]:

$$\begin{aligned} \omega_i &= \omega_{i_0} - k_{\mathrm{p}_i}(P_i - P_{i_0}), \\ V_i &= V_{i_0} - k_{\mathrm{q}_i}(Q_i - Q_{i_0}), \end{aligned} \tag{2.20}$$

where k_{p_i} and k_{q_i} are the droop gains, ω_i and V_i are the frequency and the voltage magnitude, P_i and Q_i are the output active and reactive power, and $\omega_{i_0}, V_{i_0}, P_{i_0}, Q_{i_0}$ are the nominal values of the frequency, voltage, active and reactive power, respectively.

From the control point of view, the droop control law refers to a relatively simple proportional controller, which defines a ratio of power portions shared between generation units by the droop gains. Furthermore, the frequency is assumed to be identical everywhere in a power system and serves implicitly as a communication channel to inform each generation unit about the active power demand in the system. The voltage deviations command the generation units to adjust their reactive power outputs, although voltage and reactive power compensation have a more local characteristic in power systems [33, 73].

Using the classical droop control, Coelho, Katiraei, Brabandere, Filho, Pogaku, Doerfler *et al.* have investigated the power sharing and stability issues of inverter-based microgrids in the sense of small-signal stability [8, 15, 26, 39, 42, 72, 74]. Although being a successful control method in large power systems, the droop control experiences many drawbacks when being theoretically and practically applied to microgrids. The reasons are recast as follows. The physical characteristics of inverter-based microgrids differ significantly from the characteristics of large power systems. Microgrids normally operate at low-voltage levels, where the ratios between line resistances and reactances (known as R/X ratio) are considerable, making the above assumption of the droop control approach on purely inductive connecting lines between generation units no longer correct. Besides, dealing with power electronic devices like inverters, there is no inherent physical relation between power balance and network frequency as in power systems with synchronous generators. Therefore, the classical droop control method exhibits limitations in low-voltage inverter-based microgrids, resulting in poor power sharing performance and lack of system robustness [19, 20, 38, 75].

As the connecting lines between generation units in low-voltage microgrids are no longer purely inductive, there exist strong linkages between the active power and the output voltage as well as between the reactive power and the output frequency of a generation unit. This fact has been reported in a number of publications as a main reason to cause drawbacks of the droop control to stabilize microgrids and achieve a desired power sharing [10, 29, 76, 77]. Guerrero, Filho, Brabandere, Lee *et al.* have tried to overcome the coupling problem by including line resistances in the controller design procedure [10, 21, 28, 37, 38]. Brabandere and Filho *et al.* have developed alternative droop control methods in order to include the couplings between f/P and V/Q in the controller design. In their approaches, the active and reactive power are modified by both frequency and voltage variations. This can be done by adding V/P and f/Q control loops to the classical droop control.

Guerrero, Matas *et al.* proposed a technique called virtual output impedance to virtually reduce the R/X ratio of connecting lines [21, 38]. The virtual output impedance is an additional control

loop, which is placed at the output of the droop control loop. It is known that the droop control loop provides a voltage reference input for the voltage control loop (see Figure 2.4). By deducting an appropriate portion of the inverter output current I_i from the voltage reference input, this technique is able to virtually modify the output impedance of an inverter. That is:

$$V_{\text{virtual Z}_i} = V_{\text{ref}_i} - \mathcal{Z}_i(s)I_i, \tag{2.21}$$

where V_{ref_i} is delivered by the droop control loop, $V_{\text{virtual Z}_i}$ is the modified voltage reference, and $\mathcal{Z}_i(s)$ is the virtual output impedance, where s is the Laplace variable. Based on this principle, different designs of the virtual output impedance $\mathcal{Z}_i(s)$ have been proposed in order to improve the stability margin and the power sharing performance in microgrids [21, 24, 38].

The methods above perform better power sharing and partially reduce the coupling between active and reactive power control loops in particular cases of microgrids with a small number of generation units. However, a desired power sharing is not achieved, and it is still impossible to derive an analytical solution to guarantee the stability for the general case of microgrids.

To overcome the stability drawback of the droop-based control approaches, several alternative stabilizing control strategies have been published. Zhu, Dasgupta, Yang, Gustavo *et al*. proposed a master/slave operational approach of microgrids [44, 78–80]. The main idea of the master/slave operational approach is that there exist master generation units, which form a power network and assure the voltage and frequency stability of the system. Those master generation units can be a diesel generator, a large storage device or a microturbine, which operate uninterruptedly and mainly provide electrical power to sensitive loads of the system. Other generation units such as, wind turbines, photovoltaics, etc., operate like current sources, which simply attempt to maximally inject their harvested electrical energy into the system, but do not act as network-forming units. This concept can guarantee stability of autonomous microgrids, and is therefore preferred in industry. This approach is also implemented in several real-world microgrids as a first step of the microgrid realization [30]. Nevertheless, the main disadvantage of the master/slave approach is that the system stability depends on the master generation units. In case master units are lost, the other generation units do not guarantee the system stability.

Hesse, Zhong, Beck *et al*. have reported the instability of microgrids due to the low-inertia nature of distributed energy resources with inverter interfaces, in contrast to synchronous generators with rotating masses. To overcome this problem, the concepts of virtual synchronous machine and synchronverter to combine inverter technology with properties of synchronous generators were introduced [50, 51, 81, 82]. The main idea of those methods is to provide a larger inertia to distributed energy resources by letting inverters mimic the operating principle of synchronous generators. The synchronverter concept proposed in [50, 83] by Zhong *et al*. is a very promising approach to control voltage source inverters. In this approach, an inverter model is proposed, which is similar to a model of an synchronous generator. The control of a synchronverter

is also similar to the control of a synchronous generator with virtual excitation voltage and virtual mechanical torque. However, there is still a lack of a mathematical stability proof for an implementation of synchronverters in a microgrid. In addition, the model of a synchronverter with its complexity makes the stability analysis of a synchronverter network a nontrivial task.

The aforementioned approaches were developed mainly by researchers from the power system community. Since it concerns control issues, the microgrid topic has also become a research interest of the control community. Using powerful tools from the control system theory, several authors have investigated the stability aspects of microgrids with respect to line and load uncertainties and disturbances. Several contributions on the synchronization, robust plug-and-play operation of microgrids as well as a desired power sharing control based on the droop control idea were proposed [26, 36, 72, 74, 75, 84–86]. Though proposing several encouraging control approaches which guarantee the local exponential stability of inverter-based microgrids, these methods face implementation challenges. An example among other challenges is that different assumptions of different classes of microgrids were made for stability analysis. The reason originates from the definition and lack of established standards for microgrids [87]. A guideline for design and implementation of microgrids has been made by IEEE in [7]. However, being a new engineering topic, different classes of microgrids were defined by research interests of authors. A review of different types of real-world microgrids can be found in [30]. As a consequence, a stability analysis proposed for one class of microgrids may not be relevant for the others. For instance, stability analysis and reactive power sharing of inductive microgrids were investigated in [26, 85]. However, the assumption on inductive microgrids is not always appropriate. At the same time, the case of resistive microgrids is studied in [24, 88]. Another example can be the communication-based distributed control approach proposed in [68]. The control approach considers the load nonlinearity and transient disturbances in microgrids. Then, a distributed current controller for each inverter subsystem is introduced. The power sharing and power quality performances depend on the bandwidth of the communication link. However, in case of a collapse of the communication channel, distributed inverter controllers do neither guarantee a good power sharing ratio, high-quality of output power nor the system stability.

The above discussion has just briefly reviewed some research activities in the microgrid field. Being a relatively new concept, microgrid attracts more and more attention from researchers all over the world. Although there are various published contributions on control and stability analysis of microgrids, none of those approaches truly guarantees the system stability as well as sufficient power flow performance with respect to the decentralized control requirements recast in Section 2.3. Often, stability issues are either ignored or lack mathematical proof. The main reason is the lack of a suitable system modeling to enable an application of strong controller design approaches. Therefore, many issues on the stability analysis, control approach, voltage and frequency performance, power flow strategy, etc., in the microgrid field are still open.

With respect to the presented material, a new model of inverter-based microgrids, a new power control loop for each inverter as well as suitable controller designs need to be investigated to satisfy the control requirements recast in Section 2.3. As stability of inverter-based microgrids is claimed to be difficult to achieve, a thorough stability analysis is required. Decentralized controllers of inverters must target several control goals simultaneously: robust stability against load and line uncertainties, sufficient voltage and frequency performance, and power flow strategy. It is worth mentioning that these control goals are separated into different categories. Since a power control loop is added to each inverter, the stability and the performance of voltage and frequency are the essential requirements for a normal operation of microgrids. The power flow issue remains the main goal at the power control level. However, different power flow strategies can be accomplished only when the stability of microgrids is assured.

2.5 Summary

General assumptions and the considered class of microgrids were introduced. The considered stability aspects of microgrids have been reviewed from both power system and control system perspectives. From a power system perspective, the small-signal stability of microgrids against small load and line uncertainties was discussed. In addition, load dynamics represent a reason, which can cause voltage stability problems for microgrids. Consequently, stability of microgrids against influences of load dynamics should be studied via load modeling. Furthermore, as stability of microgrids will be analyzed based on control theory in the following chapters, several stability definitions from the control theory were introduced. Moreover, a sufficient performance of voltages and frequencies is also essential for a normal operation of microgrids. The control goal at the power control level is the control of power flows within a microgrid. However, the essential requirements for the power control level have been defined as: the (robust) stability of microgrids, sufficient voltage and frequency performance. Further, general requirements for the realization and design of the power control level of microgrids have been listed. Some research activities in the field of control of microgrids have been reviewed. In the following, the contributions of the thesis announced in Section 1.2 will be presented with respect to the framework described above.

Chapter 3

Modeling of inverter-based microgrids and decentralized control approach

The main goal at the power control level involves the control of power flows within a microgrid. However, since a control loop is added, the (closed-loop) stability of microgrids becomes an essential requirement. Hence, priority is given to the stability of microgrids. In this chapter, a state-space model of inverter-based microgrids is presented. Then, a power control loop for each inverter is proposed, which requires a global time receiver for the clock synchronization purpose. All inverters in a microgrid receive the same timing information, e.g. via GPS, for local clocks of inverters to synchronize. This will assure that phase angles of all inverters in a microgrid are expressed relative to the same rotating reference frame. In order to construct a complete control approach for microgrids, an LMI stability condition is proposed to synthesize decentralized inverter controllers. The control approach will be validated via simulation.

3.1 Modeling of inverter-based microgrids

Based on the assumptions of the considered microgrids presented in Chapter 2, the active and reactive power exchange at each node i of a microgrid is expressed by the standard power flow equations (2.9). The active and reactive power are measured through a low-pass filter with time constant τ_i and unity gain as follows:

$$\tilde{P}_i = \frac{P_i}{\tau_i s + 1}, \quad \tilde{Q}_i = \frac{Q_i}{\tau_i s + 1}, \tag{3.1}$$

where P_i, Q_i are the Laplace transforms of the active and reactive power, while $\tilde{P}_i$ and $\tilde{Q}_i$ are the Laplace transforms of the measured active and reactive power, and s is the Laplace variable.

Note that by a slight abuse of notation, $P_i, Q_i, \tilde{P}_i, \tilde{Q}_i$ are used to denote active power, reactive power and their measured values in both time and Laplace domains throughout the thesis, respectively.

As mentioned in Chapter 2, voltage phase angles $\delta_i,\ i = 1,\ldots,n$, are expressed relative to a common rotating reference frame with a constant angular velocity ω_{nom}, where ω_{nom} is chosen to be equal to desired network frequency, e.g., $2\pi 50$ [rad/s]. Relative to this reference frame, a voltage phase angle $\delta_i(t)$ is computed as follows:

$$\delta_i(t) = (\omega_i - \omega_{\text{nom}})t + \delta_{i_0}, \tag{3.2}$$

where ω_i is an inverter output frequency, δ_{i_0} is an initial value of δ_i.

Throughout the thesis, $(\omega_i - \omega_{\text{nom}})$ is denoted by $\Delta\omega_i$. Thus, $\Delta\omega_i$ stands for the deviation of an inverter output frequency from its (nominal) desired value.

Hence, a state-space model of an inverter i is represented by the following ordinary differential equations (ODEs):

$$\begin{cases} \dot{\delta}_i &= \Delta\omega_i, \\ \dot{\tilde{P}}_i &= \dfrac{-\tilde{P}_i + P_i(V_1,\ldots,V_n,\delta_1,\ldots,\delta_n)}{\tau_i}, \\ \dot{\tilde{Q}}_i &= \dfrac{-\tilde{Q}_i + Q_i(V_1,\ldots,V_n,\delta_1,\ldots,\delta_n)}{\tau_i}, \end{cases} \tag{3.3}$$

where $\Delta\omega_i$ denotes deviation of inverter output frequency from its desired value ω_{nom}, V_i is the magnitude of the output voltage of an inverter i, P_i and Q_i are given in (2.9) and $i = 1,\ldots,n$.

It is noteworthy that the inverter model above is nonlinear as P_i and Q_i are nonlinear functions of $V_i,\ \delta_i,\ i = 1,\ldots,n$. The network structure and the interconnection between inverters are represented by network admittances, which are involved in P_i and Q_i (see (2.9)).

In order to investigate the stability of a microgrid around an equilibrium point, a linearized state-space model of a microgrid is considered. The microgrid model obtains a state variable $x(t)$, a control input $u(t)$ and a system output $y(t)$ defined in time domain as follows:

$$x_i(t) = \begin{bmatrix} \delta_i - \delta_{i_0} \\ \tilde{P}_i - \tilde{P}_{i_0} \\ \tilde{Q}_i - \tilde{Q}_{i_0} \end{bmatrix},\ u_i(t) = \begin{bmatrix} \Delta\omega_i \\ V_i - V_{i_0} \end{bmatrix},\ x(t) = y(t) = \begin{bmatrix} x_1(t) \\ \vdots \\ x_n(t) \end{bmatrix},\ u(t) = \begin{bmatrix} u_1(t) \\ \vdots \\ u_n(t) \end{bmatrix}, \tag{3.4}$$

where $x_i(t), u_i(t)$ are the state variable and the control input of an inverter i, which are defined with respect to a nominal equilibrium point:

$$x_{i_0} = \begin{bmatrix} \delta_{i_0} & \tilde{P}_{i_0} & \tilde{Q}_{i_0} \end{bmatrix}^T,\ u_{i_0} = \begin{bmatrix} 0 & V_{i_0} \end{bmatrix}^T. \tag{3.5}$$

As seen in (2.9), P_i, Q_i can be varied by adjusting phase angles and voltage magnitudes. However, by applying the idea of the droop control, the frequency deviation $\Delta\omega_i$ is controlled instead of a direct modification of the phase angle δ_i. A power control loop for each inverter with the chosen variables as in (3.4) will be presented in the next section. It will be shown that under this power control loop inverter output frequencies will always converge to a common rated value, i.e., $\Delta\omega_i = 0$ in steady-state. Thus, the selected system variables refer to an *angle droop control* and a *voltage droop control*.

Remark 3.1.1. Based on the control input $u_i(t)$ and the output $y_i(t) = x_i(t)$ defined in (3.4), a decentralized power control loop for each inverter will be presented in the next section. The stability of a closed-loop microgrid with respect to the variables (3.4) and the nominal equilibrium point (3.5) indicates the system nominal stability. However, an equilibrium point of a power system is often not completely known in advance and changes during operation, depending on the system topology and load conditions. This results in new equilibrium points, and invalidates the variables (3.4). Regarding this matter, load uncertainties will be considered as model uncertainty to a linear time-invariant (LTI) system model in the $\mathcal{H}_\infty$ control in Chapter 5. Load uncertainties will be represented by an additive uncertainty $\tilde{\Delta}$. The stability of the closed-loop system with respect to the state variables in (3.4) and the load uncertainty $\tilde{\Delta}$ implies the robust stability of the system. The system stability will then be guaranteed within a region around the nominal equilibrium point (3.5).

Based on the inverter model (3.3), by linearizing the power flow equations (2.9) around the interesting operating point (3.5), an LTI state-space model of a microgrid with n inverters is derived as follows:

$$\begin{cases} \dot{x}(t) &= Ax(t) + Bu(t), \\ y(t) &= Cx(t) = x(t), \end{cases} \tag{3.6}$$

and an inverter i is associated to one subsystem of (3.6) with the following state-space model:

$$\dot{x}_i(t) = A_{ii}x_i(t) + B_{ii}u_i(t) + \sum_{\substack{k=1 \\ k\neq i}}^{n} \Big(A_{ik}x_k(t) + B_{ik}u_k(t)\Big), \quad i = 1,\ldots,n, \tag{3.7}$$

where $A \in \mathbb{R}^{3n\times 3n}, B \in \mathbb{R}^{3n\times 2n}, C = I_{3n\times 3n}$ is an identity matrix, and

$$A_{ii} = \begin{bmatrix} 0 & 0 & 0 \\ \frac{\partial P_i}{\tau_i \partial \delta_i}\Big|_0 & \frac{-1}{\tau_i} & 0 \\ \frac{\partial Q_i}{\tau_i \partial \delta_i}\Big|_0 & 0 & \frac{-1}{\tau_i} \end{bmatrix}, \; B_{ii} = \begin{bmatrix} 1 & 0 \\ 0 & \frac{\partial P_i}{\tau_i \partial V_i}\Big|_0 \\ 0 & \frac{\partial Q_i}{\tau_i \partial V_i}\Big|_0 \end{bmatrix}, \; A_{ik} = \begin{bmatrix} 0 & 0 & 0 \\ \frac{\partial P_i}{\tau_i \partial \delta_k}\Big|_0 & 0 & 0 \\ \frac{\partial Q_i}{\tau_i \partial \delta_k}\Big|_0 & 0 & 0 \end{bmatrix}, \; B_{ik} = \begin{bmatrix} 0 & 0 \\ 0 & \frac{\partial P_i}{\tau_i \partial V_k}\Big|_0 \\ 0 & \frac{\partial Q_i}{\tau_i \partial V_k}\Big|_0 \end{bmatrix}. \tag{3.8}$$

The linearization of the power flow equations (2.9) around the equilibrium point (3.5) can be found in Appendix A.3. It can be seen from (3.7) that inverters are interconnected with each

other through their state variables and control inputs, which are specified by the matrices A_{ik} and B_{ik}. A_{ii} and B_{ii} are system matrices of each inverter i.

Remark 3.1.2. The interconnection term $\sum_{\substack{k=1\\k\neq i}}^{n}\Big(A_{ik}x_k(t)+B_{ik}u_k(t)\Big)$ in (3.7) can be considered as a disturbance source to an inverter subsystem i. Thus, the interconnection between inverters is a disturbance source to the stability of inverters as well as to the stability of an overall microgrid.

Matrix A in (3.6) has $3n$ eigenvalues, which are the roots of its characteristic equation:

$$\det(\lambda I - A) = 0. \tag{3.9}$$

Denote the $3n$ eigenvalues of the matrix A by $\lambda_{1_1},\lambda_{1_2},\lambda_{1_3},\ldots,\lambda_{n_1},\lambda_{n_2},\lambda_{n_3}$. As seen in (3.8), the first row of matrix A contains only zero elements. The characteristic equation (3.9) is equivalent to the following:

$$\begin{aligned}&\lambda_{1_1}\cdot\big(\lambda_{1_2}-A_{11}(2,2)\big)\cdot\big(\lambda_{1_3}-A_{11}(3,3)\big)\cdots\lambda_{n_1}\cdot\big(\lambda_{n_2}-A_{nn}(2,2)\big)\cdot\big(\lambda_{n_3}-A_{nn}(3,3)\big)=0\\ \Leftrightarrow\quad&\lambda_{1_1}\cdot\Big(\lambda_{1_2}+\tfrac{1}{\tau_1}\Big)\cdot\Big(\lambda_{1_3}+\tfrac{1}{\tau_1}\Big)\cdots\lambda_{n_1}\cdot\Big(\lambda_{n_2}+\tfrac{1}{\tau_n}\Big)\cdot\Big(\lambda_{n_3}+\tfrac{1}{\tau_n}\Big)=0.\end{aligned} \tag{3.10}$$

It is seen from (3.10) that matrix A has n zero eigenvalues, i.e., $\lambda_{i_1}=0,\ i=1,\ldots,n$. The other $2n$ eigenvalues are negative real, which are determined by the time constants τ_i of the measuring low-pass filters, i.e., $\lambda_{i_2}=\lambda_{i_3}=-\frac{1}{\tau_i},\ i=1,\ldots,n$. The eigenvalues imply that dynamic behaviour of an open-loop microgrid depends on the time constants of the employed low-pass filters.

Remark 3.1.3. The fact that eigenvalues of matrix A in (3.6) do not depend on the interconnection between inverters should be explained at this point. As seen in Figure 2.3, with negligible dynamics of lower control levels as well as dynamics of the physical low-pass filter, an inverter is considered as an ideal voltage source, generating a voltage with constant magnitude and frequency. Therefore, when low-pass filters are added to measure output power of inverters, dynamics of the open-loop microgrid are caused only by these measuring filters. This explains why the nonzero eigenvalues of the system matrix A in (3.6) only depend on the time constants of the measuring filters. It is a contrast to synchronous generators with internal dynamics of frequency, which are often described by the classical *swing equation* [33, 47].

As mentioned in Remark 2.2.3, the zero eigenvalues of matrix A make the system (3.6) fail to determine the stability properties of the nonlinear microgrid. Hence, a controller shall be designed to asymptotically stabilize the system (3.6).

The definition of stabilizability of the system (3.6) with the chosen variables should be mentioned here.

Definition 3.1. [54] A dynamic system of Equation (3.6) or a pair (A,B) is stabilizable if there exists a state-feedback controller K such that the closed-loop system is asymptotically stable, i.e., all the eigenvalues of matrix $(A+BK)$ are in the open left-half plane. □

The system stabilizability can be mathematically checked by the Popov-Belevitch-Hautus (PBH) rank test [54, 89]. The system (3.6) is stabilizable if and only if the matrix $[A-\lambda I, B]$ has full-row rank for all eigenvalues λ of A with $Re\lambda \geq 0$. As shown in (3.10), matrix A has n zero eigenvalues and $2n$ negative real eigenvalues. Thus, in order to check the stabilizability of the system (3.6), it is necessary and sufficient to check whether the matrix $[A,B]$ has full-row rank.

By investigating the $3n \times 5n$ matrix $[A,B]$, it becomes apparent that it has $3n$ columns, which contain precisely one nonzero element. All these elements appear in different positions of the respective columns, indicating the linear independence of these columns. Hence, column (and therefore row) rank of the matrix $[A,B]$ is always $3n$, which implies the system stabilizability.

Problem 3.1.1. *Design local state-feedback controllers* $K_i : u_i(t) = K_i x_i(t),\ i = 1,\ldots,n$, *for each subsystem (3.7) so that the overall interconnected system consisting of (3.6) and the state-feedback control law:*

$$u(t) = Kx(t), \quad K = diag(K_1,\ldots,K_n) \tag{3.11}$$

is asymptotically stable in the sense of Lyapunov.

In order to derive an LMI stability condition to design the controller K in the next section, the system matrices A,B in (3.6), which are given according to (3.7) and (3.8), are decomposed into block-diagonal A_d, B_d and block off-diagonal parts A_H, B_H as:

$$\begin{aligned} A_d &= \text{diag}(A_{11},\ldots,A_{nn}), \quad A_H = A - A_d, \\ B_d &= \text{diag}(B_{11},\ldots,B_{nn}), \quad B_H = B - B_d. \end{aligned} \tag{3.12}$$

Define the block-diagonal closed-loop system as $A_{\text{cl}_d} := A_d + B_d K$; then the state-space model of the closed-loop system with the controller K can be written as follows:

$$\begin{cases} \dot{x}(t) &= A_{\text{cl}_d} x(t) + (A_H + B_H K)x(t) = (A+BK)x(t) = A_{\text{cl}} x(t), \\ y(t) &= x(t). \end{cases} \tag{3.13}$$

3.2 Decentralized state-feedback stabilizing controller design

In this section, a decentralized controller design based on the LMI technique is proposed, which guarantees the asymptotic stability of the system (3.13). The control loop of a single inverter is shown in Figure 3.1. Inverter output current I_i and voltage V_i are measured in order to calculate

the active and reactive power. The phase angles δ_i of all inverters are expressed relative to a common rotating reference frame with a constant angular velocity ω_{nom}. The common rotating reference frame for all inverters is created by local clocks of inverters, which are synchronized by a global time signal, e.g. via GPS signal or Ethernet network. Therefore, a global time receiver, e.g. a GPS receiver or an Ethernet device, is required for each inverter, but no other communication link between inverters is needed [90–92]. This procedure is referred to as *clock synchronization*. In case the global time input of an inverter is lost for several seconds, the local clock is still able to create a sufficiently accurate rotating reference frame for the inverter [92].

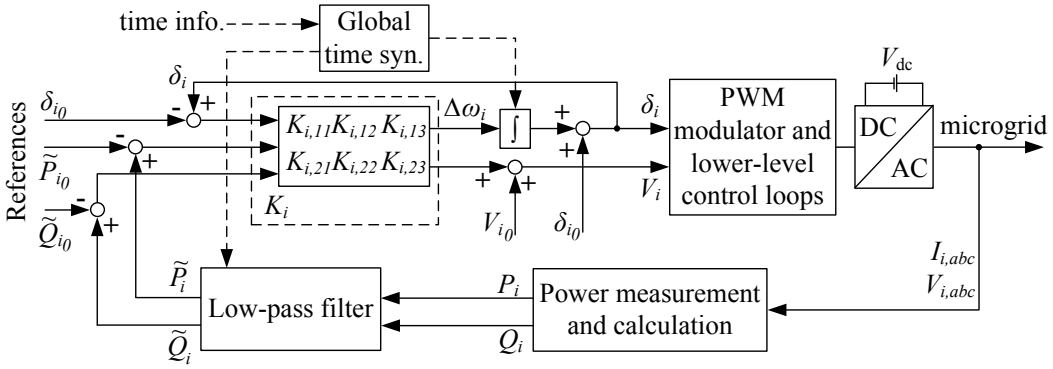

FIGURE 3.1: Power control loop of an inverter.

Note that in the proposed system model (3.6), the deviation of the phase angle $(\delta_i - \delta_{i_0})$ is defined as a state of an inverter subsystem. Therefore, if the controller K in (3.11) stabilizes the microgrid, the steady-state deviations of the inverter phase angles $\delta_i(t),\ i = 1,\ldots,n$, will be constant. In case the system operates exactly at the interesting equilibrium point (3.5), it follows that $\lim_{t\to\infty}(\delta_i(t) - \delta_{i_0}) = 0$. This infers zero steady-state deviations of inverter output frequencies as $\Delta\omega_i = \dot{\delta}_i = 0$.

The zero steady-state deviation of inverter output frequencies is consistent with the nature of microgrids with power electronic interfaces, where there is no inherent relation between network frequency and power balance in the system. Instead, according to the power flow equations (2.9) the power balance is obtained by drooping phase angles and magnitudes of voltages with respect to their nominal values.

A note on steady-state magnitude deviations of voltages is made here. With the variables defined in (3.4), the state-feedback controller $u_i(t) = K_i x_i(t)$ is as follows:

$$\begin{bmatrix} \Delta\omega_i \\ V_i - V_{i_0} \end{bmatrix} = \begin{bmatrix} K_{i,11} & K_{i,12} & K_{i,13} \\ K_{i,21} & K_{i,22} & K_{i,23} \end{bmatrix} \begin{bmatrix} \delta_i - \delta_{i_0} \\ \tilde{P}_i - \tilde{P}_{i_0} \\ \tilde{Q}_i - \tilde{Q}_{i_0} \end{bmatrix}, \tag{3.14}$$

which infers the following:

$$V_i - V_{i_0} = K_{i,21}(\delta_i - \delta_{i_0}) + K_{i,22}(\tilde{P}_i - \tilde{P}_{i_0}) + K_{i,23}(\tilde{Q}_i - \tilde{Q}_{i_0}). \tag{3.15}$$

In steady-state, it can be inferred from (3.3) that $\tilde{P}_i = P_i$ and $\tilde{Q}_i = Q_i$. Consider the equation above in steady-state. Assume that the controller gains are nonzero. Then, $(V_i - V_{i_0})$ is equal to zero in two cases. First, $(V_i - V_{i_0}) = 0$ if $(\delta_i - \delta_{i_0}) = (\tilde{P}_i - \tilde{P}_{i_0}) = (\tilde{Q}_i - \tilde{Q}_{i_0}) = 0$, which means that the inverter i operates exactly at the interesting equilibrium point (3.5). Second, in case the inverter i does not operate exactly at the interesting equilibrium, $(V_i - V_{i_0}) = 0$ happens for particular load conditions so that the elements on the right-hand side of (3.15) are not simultaneously zero, but the sum is zero.

However, in most cases with arbitrary load conditions there are steady-state deviations of voltage magnitudes from their nominal values. Although the voltage restoration is not in the scope of this thesis, in Chapter 5 the performance controller design will be proposed to reduce deviations of voltage magnitudes from their nominal values, i.e., reduce the control effort.

Remark 3.2.1. The power sharing issue is considered to be the main task of the power control loop (see Remark 2.2.4). It will be demonstrated via simulation that the load demand of a microgrid is shared among inverters. That is, when a load demand at node i of a microgrid is increased during operation, other inverters also react to the load change and there is power exchange between system nodes, namely, the power sharing. As will be shown in Chapter 6, by adjusting controller gains without causing system instability, the power sharing performance can be improved. However, an exact power sharing is not achieved. None of the up-to-date proposed (communicationless) control methods gives an analytical solution to ensure a desired power sharing in microgrids with arbitrary R/X ratios of power connecting lines, especially in the case of reactive power sharing. For the case of microgrids with negligible resistive effects of connecting power lines between inverters, a consensus-based distributed voltage control is proposed in [85, 86], which guarantees a desired reactive power distribution in steady-state, while only requiring distributed communication among inverters.

Theorem 3.2. *Consider the closed-loop system (3.13). Let $P_{ii} \in \mathbb{R}^{3\times 3}$, $i = 1,\ldots,n$, be symmetric positive definite matrices and define $P = diag(P_{11},\ldots,P_{nn}) \in \mathbb{R}^{3n\times 3n}$, where n is the number of inverters in the system. Define the following variables:*

$$\mathbf{X} = diag(\mathbf{X}_{11},\ldots,\mathbf{X}_{nn}) = P^{-1}, \quad \mathbf{Y} = diag(\mathbf{Y}_{11},\ldots,\mathbf{Y}_{nn}) = KP^{-1}, \tag{3.16}$$

where $\mathbf{X}_{ii} \in \mathbb{R}^{3\times 3}$, $\mathbf{Y}_{ii} \in \mathbb{R}^{2\times 3}$, $i = 1,\ldots,n$. The block-diagonal controller $K = \mathbf{Y}\mathbf{X}^{-1} \in \mathbb{R}^{2n\times 3n}$ guarantees the asymptotic stability of the closed-loop system (3.13) if the following LMI is

feasible with $0 < \gamma \leq 1$*:*

$$\begin{bmatrix} A_d\mathbf{X} + B_d\mathbf{Y} + (A_d\mathbf{X} + B_d\mathbf{Y})^T & A_H & B_H & \mathbf{X} & \mathbf{Y}^T \\ A_H^T & -\gamma I & 0 & 0 & 0 \\ B_H^T & 0 & -\gamma I & 0 & 0 \\ \mathbf{X} & 0 & 0 & -\gamma I & 0 \\ \mathbf{Y} & 0 & 0 & 0 & -\gamma I \end{bmatrix} < 0. \tag{3.17}$$

Proof. The proof of Theorem 3.2 uses Lyapunov's stability theorem [93] and is inspired by [94]. Let the selected Lyapunov function associated to the closed-loop system (3.13) be given in the form $\mathcal{V}(x) = x^T P x$, with a symmetric positive definite block-diagonal matrix P. Then, with (3.13), the derivative of the Lyapunov function $\mathcal{V}(x)$ with respect to time is obtained as follows:

$$\dot{\mathcal{V}}(x) = \dot{x}^T P x + x^T P \dot{x} = x^T \left(A_{\mathrm{cl}_d}^T P + P A_{\mathrm{cl}_d} + A_H^T P + P A_H + K^T B_H^T P + P B_H K\right) x. \tag{3.18}$$

The product of a matrix and its transpose is a positive semidefinite matrix. Then, the following is derived:

$$(P A_H - I)(A_H^T P - I) = P A_H A_H^T P + I - A_H^T P - P A_H \geq 0, \tag{3.19a}$$

$$(K^T - P B_H)(K - B_H^T P) = K^T K + P B_H B_H^T P - K^T B_H^T P - P B_H K \geq 0. \tag{3.19b}$$

The above matrix inequalities can be rewritten as follows:

$$P A_H A_H^T P + I \geq A_H^T P + P A_H, \tag{3.20a}$$

$$K^T K + P B_H B_H^T P \geq K^T B_H^T P + P B_H K. \tag{3.20b}$$

where $P A_H A_H^T P + I > 0$, $K^T K + P B_H B_H^T P \geq 0$.

With $0 < \gamma \leq 1$,

$$\frac{1}{\gamma}(P A_H A_H^T P + I) \geq P A_H A_H^T P + I \geq A_H^T P + P A_H, \tag{3.21a}$$

$$\frac{1}{\gamma}(K^T K + P B_H B_H^T P) \geq K^T K + P B_H B_H^T P \geq K^T B_H^T P + P B_H K. \tag{3.21b}$$

Substituting (3.21) into (3.18) yields the following upper bound for $\dot{\mathcal{V}}(x)$:

$$\dot{\mathcal{V}}(x) \leq x^T \left(A_{\mathrm{cl}_d}^T P + P A_{\mathrm{cl}_d} + \frac{1}{\gamma} P A_H A_H^T P + \frac{1}{\gamma} I + \frac{1}{\gamma} K^T K + \frac{1}{\gamma} P B_H B_H^T P\right) x. \tag{3.22}$$

Forcing the above upper bound of $\dot{\mathcal{V}}(x)$ to be negative for all $x \neq 0$, which is equivalent to the following:

$$A_{\mathrm{cl}_d}^T P + P A_{\mathrm{cl}_d} + \frac{1}{\gamma} P A_H A_H^T P + \frac{1}{\gamma} I + \frac{1}{\gamma} K^T K + \frac{1}{\gamma} P B_H B_H^T P < 0, \tag{3.23}$$

is a *sufficient* condition for the asymptotic stability of the system (3.13) to be achieved.

For the following part of the proof, the Schur complement formula is recalled, which states the following equivalent conditions [95]:

$$M = \begin{bmatrix} M_{11} & M_{12} \\ M_{12}^T & M_{22} \end{bmatrix} < 0 \;\Leftrightarrow\; \begin{cases} M_{22} < 0, \\ M_{11} - M_{12} M_{22}^{-1} M_{12}^T < 0. \end{cases} \tag{3.24}$$

According to the Schur complement formula, Inequality (3.23) is equivalent to the following matrix inequality:

$$\begin{bmatrix} A_{\mathrm{cl}_d}^T P + P A_{\mathrm{cl}_d} & P A_H & P B_H & I & K^T \\ A_H^T P & -\gamma I & 0 & 0 & 0 \\ B_H^T P & 0 & -\gamma I & 0 & 0 \\ I & 0 & 0 & -\gamma I & 0 \\ K & 0 & 0 & 0 & -\gamma I \end{bmatrix} < 0. \tag{3.25}$$

The matrix inequality above cannot be directly solved by the available LMI tools because of the product of variables in $(A_{\mathrm{cl}_d}^T P + P A_{\mathrm{cl}_d})$. However, by taking the standard change of variables as in (3.16), Inequality (3.25) can be turned into an LMI, which can be solved by LMI tools [95]. By pre- and post-multiplying (3.25) by the symmetric positive definite matrix $\mathrm{diag}(P^{-1}, I, I, I, I)$, where P is a block-diagonal matrix, the LMI (3.17) with two variables $\mathbf{X} > 0, \mathbf{Y}$ is derived, where both $\mathbf{X}$ and $\mathbf{Y}$ are block-diagonal. Note that the standard variable transformation (3.16) to synthesize state-feedback controllers does not introduce conservatism [95].

The structure constraints of the variables $\mathbf{X}$ and $\mathbf{Y}$ in (3.16) are introduced in order to derive a block-diagonal controller for the overall system. A decentralized power controller of each inverter i is calculated by $K_i = \mathbf{Y_{ii}} \mathbf{X_{ii}}^{-1}$. This note completes the proof. □

Based on the matrix inequality (3.23), a note on the introduction of γ in (3.21) can be made. Denote the derivative of the Lyapunov function in (3.18) by $\dot{\mathcal{V}}(x) = x^T \mathcal{P} x$, where $\mathcal{P} = \big(A_{\mathrm{cl}_d}^T P + P A_{\mathrm{cl}_d} + A_H^T P + P A_H + K^T B_H^T P + P B_H K\big)$. The condition (3.23) is equivalent to the following:

$$\underbrace{\mathcal{P} + \frac{1}{\gamma}(P A_H A_H^T P + I + K^T K + P B_H B_H^T P) - (A_H^T P + P A_H) - (K^T B_H^T P + P B_H K)}_{:= \mathcal{Q}} < 0, \tag{3.26}$$

where $\gamma \in (0,1]$ and $\mathcal{Q}$ is a symmetric positive semidefinite matrix as shown in (3.21). The singularity of $\mathcal{Q}$ happens if $\gamma = 1$ and equality holds in (3.20).

By decreasing $\gamma \in (0,1]$, $\mathcal{Q}$ is forced to be "more" positive semidefinite[1]. Therefore, $\mathcal{P}$ must be "more" negative definite so that the condition (3.26) is satisfied. Hence, by decreasing $\gamma \in (0,1]$, $\mathcal{P}$ is forced to be "more" negative definite and $\dot{\mathcal{V}}(x)$ is more negative. This indicates faster settling time of the closed-loop system (3.13) with a resulting controller K. Therefore, the decrease of γ can be implemented as an optimization objective, while solving the LMI (3.17). Decreasing γ makes the upper bound in (3.22) more conservative. Consequently, smaller γ yields more conservatism of the LMI (3.17).

The LMI optimization problem is formulated as follows:

$$\texttt{minimize } \gamma \texttt{ such that } \begin{cases} \texttt{LMI } (3.17) \texttt{ is feasible over } \mathbf{X} \texttt{ and } \mathbf{Y}, \\ \mathbf{X} \texttt{ and } \mathbf{Y} \texttt{ are block-diagonal as defined in } (3.16), \\ \mathbf{X} > 0, \\ 0 < \gamma \leq 1. \end{cases} \tag{3.27}$$

Remark 3.2.2. It is clear that the decentralized control approach with an overall block-diagonal controller is generally more conservative than the case with full-matrix controller, where no structure constraint on the LMI variables is needed. However, a full-matrix controller would indicate control interconnection between inverters, which is not desired as it relies on a communication network. The feasibility of the LMI (3.17) depends on the inevitable interconnection between inverters. Meanwhile, the LMI achieves the highest feasibility chance in the case of no or a slight interconnection. In addition, the conservatism of Theorem 3.2 arises also from the inequalities in (3.21), i.e., the chance of feasibility of the LMI (3.17) reduces when γ moves toward zero.

Remark 3.2.3. The upper bounds of the matrix inequalities in (3.21) could be chosen with four different optimization variables as $\left(\frac{1}{\gamma_1} PA_H A_H^T P + \frac{1}{\gamma_2} I\right)$ and $\left(\frac{1}{\gamma_3} K^T K + \frac{1}{\gamma_4} PB_H B_H^T P\right)$, where $\gamma_1, \gamma_2, \gamma_3, \gamma_4 \in (0,1]$. As a result, these four different optimization variables can appear in the diagonal elements of the LMI (3.17), instead of a single optimization variable γ. However, for the sake of simplicity and later implementation of Theorem 3.2 in the thesis, only one optimization variable γ is suggested. Note that this simplification also introduces some conservatism to the LMI (3.17).

[1] A matrix A is said to be "more" positive (semi)definite than a matrix B if $(A - B)$ is a positive (semi)definite matrix. Similarly, a matrix A is "more" negative (semi)definite than a matrix B if $(A - B)$ is a negative (semi)definite matrix.

3.3 Simulation study

In this section, an academic example is provided to show the effectiveness of the proposed control loop in Figure 3.1 and the stability condition presented in Theorem 3.2. Consider a simple system shown in Figure 3.2, which consists of two inverters with constant impedance loads. The structure and parameters of the test system are similar to the test microgrid with two inverters in [42]. However, the output power of inverters in the example in [42] is relatively small ($< 1[\text{kVA}]$). In order to derive more realistic simulation results, compared to one of the first real-world microgrids presented in [96], parameters of loads in this example are selected so that the output power of inverters is in the range of 10's of $[\text{kVA}]$. Parameters of the test system are provided in Table 3.1.

As the stability condition derived in Theorem 3.2 refers to the system nominal stability, the simulation goal is to validate the nominal stability of the system around an equilibrium point. From the power system point of view, small load changes are applied to the system during operation in order to verify the small-signal stability of the system.

Remark 3.3.1. Note that there is a difference between the nominal stability (defined in control system theory) and the small-signal stability (defined in power system theory). The nominal stability means that the system is asymptotically stable without model uncertainty [56]. However, small-signal stability implies an ability of a system to maintain synchronism among generation units when subjected to small uncertainties [33, 53] (see Subsection 2.2.1). Small uncertainties in this case are small load changes, which refer to small model uncertainties of the system.

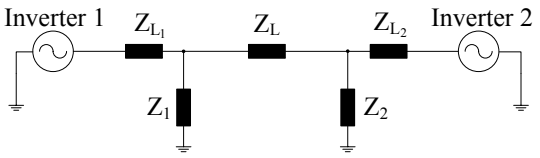

FIGURE 3.2: Test system with two inverters and impedance loads.

A controller K is designed by solving the LMI optimization problem (3.27). As shown in the proof of Theorem 3.2, a resulting controller K guarantees the asymptotic stability of the microgrid in a small region around the equilibrium point, where dynamic behaviour of the microgrid can be described by the linearized model (3.6). Simultaneously, by decreasing $\gamma \in (0,1]$, the settling time of the closed-loop system can be expected to decrease.

Simulation is conducted in Matlab. Note that a Matlab Simulink model of the system in Figure 3.2 is simulated, but not the linearized system model (3.6). The linearized model is constructed for the controller design purpose. The equilibriums of active and reactive power are calculated by solving the power flow equations (2.9) using the admittance matrix Y of the system at nominal operating frequency ω_{nom}. Small load changes are applied at $t = 5[s]$ ($Z_1 := Z_1 + \Delta Z_1$) and $t = 10[s]$ ($Z_2 := Z_2 + \Delta Z_2$).

TABLE 3.1: Test system parameters

Voltages and phase angles	$V_{1_0} = 1029[\text{V}]$ $V_{2_0} = 1030 + 1.3i[\text{V}]$	$\delta_{1_0} = 0.000[\text{rad}]$ $\delta_{2_0} = 0.0013[\text{rad}]$
Active and reactive powers	$\tilde{P}_{1_0} = 10.75[\text{kW}]$ $\tilde{Q}_{1_0} = 3.56[\text{kVar}]$	$\tilde{P}_{2_0} = 15.62[\text{kW}]$ $\tilde{Q}_{2_0} = 8.06[\text{kVar}]$
Base values	$S_{\text{base}} = 40[\text{MVA}]$ $Z_{\text{base}} = 0.0265[\Omega]$	$V_{\text{base}} = 1030[\text{V}]$ $\delta_{\text{base}} = 1[\text{rad}]$
Load impedances	$Z_1 = 108 + i10.8[\Omega]$ $\Delta Z_1 = -18.8 - i0.166[\Omega]$	$Z_2 = 45 + i28[\Omega]$ $\Delta Z_2 = -4.05 - i4.35[\Omega]$
Line impedances	$Z_{\text{L}_1} = 0.4 + i0.4[\Omega]$ $Z_{\text{L}_2} = 0.4 + i0.3[\Omega]$	$Z_{\text{L}} = 0.8 + i0.42[\Omega]$
Nominal frequency	$f_{\text{base}} = 50[Hz]$	$\omega_{\text{nom}} = 2\pi f_{\text{base}}[\text{rad/s}]$
Filter parameter	$\tau_1 = 0.0265[\text{s}]$	$\tau_2 = 0.0265[\text{s}]$

In the controller design procedure, the system variables are converted into per unit values for computational simplicity by eliminating units and expressing system quantities as dimensionless ratios [33]. Thus,

$$\text{quantity in per unit} = \frac{\text{actual quantity}}{\text{base value of quantity}}. \tag{3.28}$$

Generally, the base values of power and voltage, and the nominal rated system frequency f_{base} are selected. In case the stability of power systems is analyzed, the base power S_{base} can be chosen as an arbitrary large number [33]. In this simulation study, the base power is chosen to be high enough to increase numerical efficiency when solving the LMI problem. The base voltage V_{base} is normally chosen to be equal to the rated voltage of the system. The base values of other system quantities are automatically set and depend on the base power and the base voltage, for instance:

$$Z_{\text{base}} = \frac{V_{\text{base}}^2}{S_{\text{base}}}[\Omega]. \tag{3.29}$$

The LTI state-space model (3.6) and the LMI problem (3.27) are formulated for the system in Figure 3.2 with parameters presented in Table 3.1. The LTI state-space model can be derived by using Matlab Simulink as shown in Appendix A.4. The LMI optimization problem (3.27) is solved by using Yalmip toolbox [97] and SeDuMi solver [98] in Matlab. The LMI variables $\mathbf{X}, \mathbf{Y}$ are defined in advance to obtain the block-diagonal structures as in (3.16).

The LMI solver stops when the least possible value of γ is reached. In this particular example, an optimum $\gamma = 0.18978$ is achieved after 12 iterations. As the LTI state-space model of the system in Figure 3.2 and the associated LMI problem are constructed with per unit values, the

resulting inverter controllers are also given in per unit as follows:

$$K_1 = \begin{bmatrix} -1.9762 & -0.0191 & 0.0148 \\ 0.0008 & -0.3696 & -0.5071 \end{bmatrix}, \quad K_2 = \begin{bmatrix} -1.9726 & -0.0185 & 0.0162 \\ 0.0126 & -0.4763 & -0.4657 \end{bmatrix}. \tag{3.30}$$

The equivalences of the controllers above in actual quantities are as follows:

$$K_1 = \begin{bmatrix} -2.0[\frac{1}{s}] & -5.0\cdot10^{-7}[\frac{\text{rad}}{\text{skW}}] & 3.7\cdot10^{-7}[\frac{\text{rad}}{\text{skVar}}] \\ 0.86[\frac{\text{V}}{\text{rad}}] & -0.01[\frac{\text{V}}{\text{kW}}] & -0.013[\frac{\text{V}}{\text{kVar}}] \end{bmatrix}, K_2 = \begin{bmatrix} -2.0[\frac{1}{s}] & -5.0\cdot10^{-7}[\frac{\text{rad}}{\text{skW}}] & 4.1\cdot10^{-7}[\frac{\text{rad}}{\text{skVar}}] \\ 13.01[\frac{\text{V}}{\text{rad}}] & -0.013[\frac{\text{V}}{\text{kW}}] & -0.012[\frac{\text{V}}{\text{kVar}}] \end{bmatrix}. \tag{3.31}$$

Remark 3.3.2. It is seen in (3.30) and (3.31) that the controller gains $K_1(1,2)$, $K_2(1,2)$ from active power to frequency deviations are relatively small. However, this is comparable to the typical droop gains provided in [8, 27, 45, 92, 99].

Remark 3.3.3. An empirical experience was achieved, while solving the LMI problem (3.27). If γ is decreased to be close to zero, the resulting matrix P and the LMI (3.17) also become closer to singularity. Therefore, it is useful to set a small positive lower bound for γ, while solving the LMI problem (3.27), to avoid numerical problems.

Remark 3.3.4. Making the closed-loop system "as fast as possible" by minimizing $\gamma \in (0,1]$, one may also make the system nonresistant with respect to modelling errors. This is already explained by the fact mentioned in Remark 3.3.3. Therefore, the issue with modelling errors, also called model uncertainties, should be addressed. Chapter 5 is dedicated to this issue.

The controllers (3.30) result in stable real eigenvalues of the closed-loop system matrix $(A+BK)$ in a range $[-61.9349, -1.9654]$ [2].

The transfer function matrix from reference input to system output of the closed-loop system is as follows:

$$G_{\text{cl}}(s) = -(sI - A - BK)^{-1}BK. \tag{3.32}$$

A plot of singular values of the closed-loop system as functions of frequency is presented in Figure 3.3. The singular values give information about the gains of the system [56]. It is seen in Figure 3.3 that the system gains are relatively small at high frequencies. Moreover, uncertainties of power systems often occur at high frequencies [100, 101]. Therefore, the relatively small gains of the closed-loop system at high frequencies should reduce effects of uncertain perturbations on the system stability.

[2] With a larger $\gamma = 0.5$, the LMI (3.17) is still feasible and yields closed-loop eigenvalues in the range $[-37.7323, -1.7975]$. Thus, $\gamma = 0.5$ results in a slower settling time of the closed-loop system, compared to the optimal case.

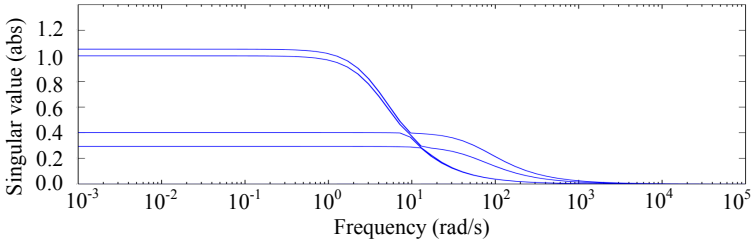

FIGURE 3.3: Singular values of the frequency response $G_{\mathrm{cl}}(j\omega)$.

The simulation is carried out in Matlab Simulink with a nonlinear microgrid, whose parameters are given in Table 3.1. Each inverter is modelled as an ideal voltage source with controllable voltage magnitude and phase angle. Power electronic IGBT and lower inverter control levels are not simulated.

Simulation results are displayed in Figure 3.4. The transfer processes in Figure 3.4 show that the system is stabilized around the equilibrium point presented in Table 3.1. When load changes are applied, both inverters have to generate more power to supply the load demand. As stated in Section 3.2, with the proposed control scheme in Figure 3.1 deviations of inverter output frequencies always converge to zero. As shown in Equation (3.15), there exist steady-state deviations of voltages in most cases. In this particular example, the voltage deviations are relatively small under small load changes. However, when the load demand is increased, a tendency of increasing deviations of voltage magnitudes from their nominal values is observed. Thus, there must be a guarantee that under large uncertainties, magnitude deviations of voltages do not violate acceptable limits. This control issue concerning the performance of inverter output voltages will be discussed in Chapter 5.

3.4 Summary

An LTI state-space model of inverter-based microgrids was introduced in this chapter. The model includes the coupling between inverters as well as the arbitrary R/X ratios of connecting lines between them. A power control loop with a decentralized controller for each inverter was proposed. In the proposed control loop, a global time signal is required to synchronize the clocks of all inverters in a microgrid, but no other communication link between inverters is required. Then, an LMI stability condition for the linearized system model of microgrids was presented. The derived LMI is a sufficient stability condition and was formulated as a theorem. Based on the derived LMI optimization problem, a state-feedback controller for a microgrid can be designed. By forcing LMI variables to obtain block-diagonal structures, a resulting controller is also block-diagonal. Each diagonal block of the resulting controller is a decentralized controller of a single inverter. By forcing block-diagonal structures of the LMI variables, a conservatism is also introduced to the LMI problem.

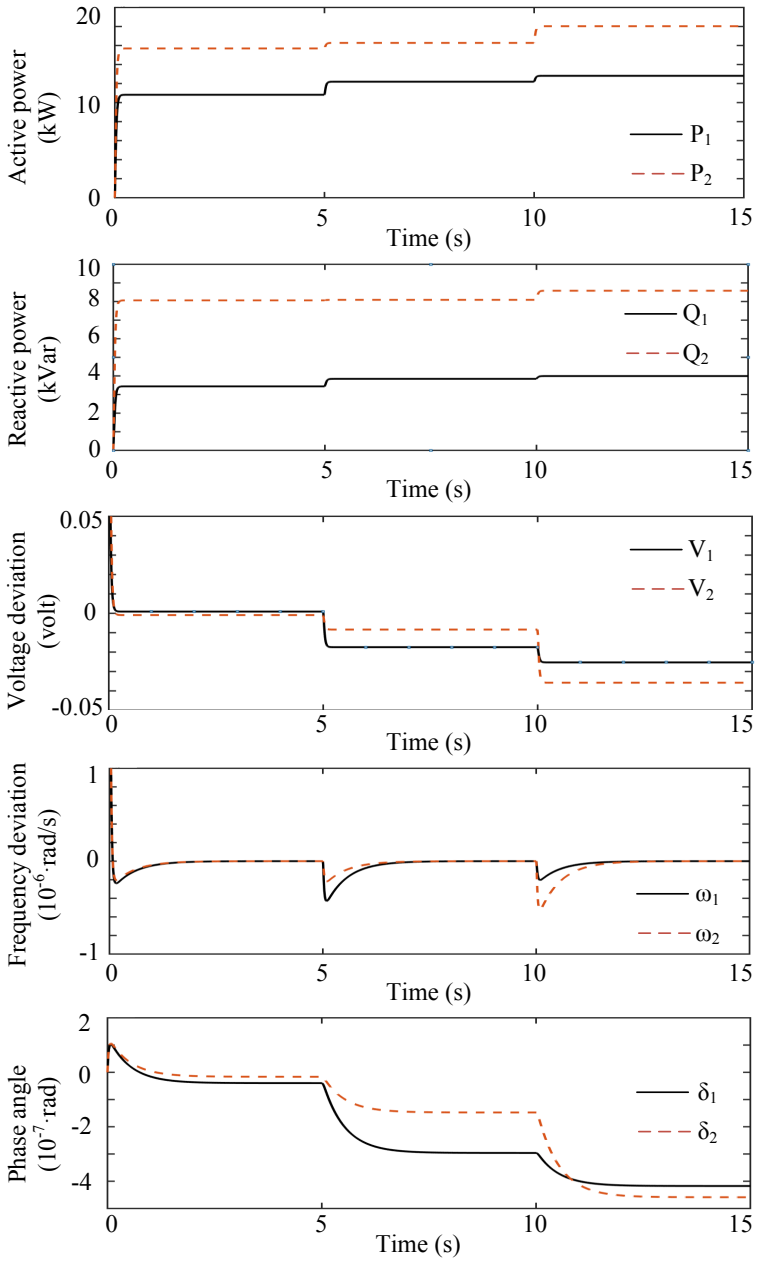

FIGURE 3.4: Transfer processes of the test system with decentralized stabilizing controllers.

The simulation of a simple microgrid was conducted to validate the effectiveness of the proposed control approach. For this particular example, it was shown that the microgrid still remains stable in spite of small load changes. Simultaneously, inverter output frequencies always return to a nominal value ω_{nom}. Voltage deviations are relatively small against small load changes. However, zero-steady state deviations of inverter output voltages are not guaranteed when load changes are applied. Voltage magnitudes should vary around their nominal values to modify inverter output power.

It should be mentioned that by conducting a computer simulation of a microgrid, all inverters are synchronized. A global time signal is required in the proposed decentralized control approach

to provide the synchronization to all inverters in real microgrids. The synchronization between inverters is often reflected by the Precision Time Protocol, which is defined in the IEEE Standard 1588-2008 [102]. A promising solution for the global time synchronization between inverters is the GPS time synchronization, which was presented at the start of the 1990s [90], after the GPS technology was available for civil applications. Nowadays, GPS clock signal for inverter synchronization is more and more accepted in the microgrid world to be a potential implementation of the IEEE Precision Time Protocol. Several independent references on the use of GPS for inverter synchronization are [91, 92, 99, 103–106].

Based on the contributions presented in this chapter, several control issues concerning voltage performance, robust stability of microgrids under load changes and power sharing between inverters will be investigated in the following chapters.

Chapter 4

Load modeling and system stability under load dynamics

In large power systems, where dynamics of generation units are dominant, dynamics of loads are negligible and were often ignored in the past. However, the amount of loads in power systems quickly increases, which leads to the fact that power systems are often heavily loaded[1]. Consequently, dynamics of loads in modern power systems demonstrate a significant influence on system stability [2, 33, 107–111]. Interconnection between loads and generation units in power systems (also called load responses) has been reviewed in details in literature, see [2, 108, 109] for instance.

In the case of inverter-based microgrids, distributed generation units mostly formed by renewable energy sources obtain smaller inertia and capacity than synchronous generators in traditional large power systems. Therefore, microgrids are highly sensitive to load dynamics, compared to large power systems [112]. Load dynamics and the interconnection between loads and generation units in microgrids should be studied in order to propose an effective control law for inverters to compensate disturbances from load dynamics.

In this chapter, the interaction between loads and inverters in microgrids is studied. A load modeling is introduced for stability analysis of microgrids. Then, a system model consisting of interconnected inverters and a dynamic load is proposed. Based on the power control loop proposed in Chapter 3, two separate LMI stability conditions will be presented to guarantee the robust stability of microgrids under influences of load dynamics.

[1] It is mentioned in [107] that voltage instabilities, e.g. voltage collapse, are always related to heavily loaded power systems, where voltage collapse is a dynamic phenomenon.

4.1 Interaction between loads and generation units

Classical power system studies used to neglect load dynamics, using static load models. However, loads not only statically depend on voltages and frequencies, but also demonstrate dynamic characteristics. As reported in a number of publications [2, 107, 110, 111, 113], measurement results of actual power systems indicate that the typical response of loads to a step change in voltage has a general form presented in Figure 4.1. Active and reactive power have qualitatively similar responses [2]. It can be seen that the step change in voltage V causes an immediate step change in power demand P. Following this, the power demand converges to a steady-state value. As seen in Figure 4.1, the recovery of the power demand has an exponential form. This transient recovery of power demand describes the dynamic behavior of loads. When the load response settles at a new equilibrium point and the transient processes complete, the steady-state power demand is a function of the steady-state voltage. The power mismatch, the rate of the recovery and the initial power step greatly depend on load conditions [109].

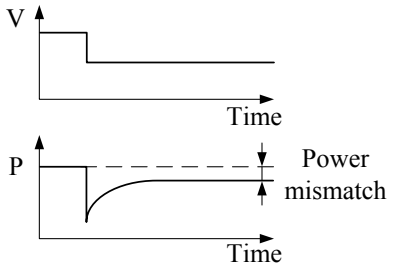

FIGURE 4.1: Typical load response to a voltage step change of a power system [2].

Researchers from power system communities often analyze a load-system interaction by decomposing a power system into a feedback system as shown in Figure 4.2 [108, 109]. The *Power System* block in Figure 4.2 stands for generators, their controllers, connecting lines, FACTS devices, etc. A power system normally has many loads. A single load, whose dynamics are of interest, is presented by the *Dynamic Load* block in Figure 4.2. Other loads, which are not of immediate interest, are treated as part of the *Power System*. See [108, 109] for more details on this decomposition approach. Depending on load and system parameters, the feedback from *Dynamic Load* may improve or deteriorate overall system damping [2, 108, 109, 113, 114].

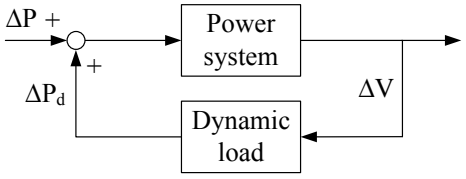

FIGURE 4.2: Load - power system interaction.

Consider some sinusoidal variation in bus power ΔP (power disturbance). A voltage variation ΔV in power system buses will appear, whose magnitude and phase relative to ΔP depend on

dynamic behaviour of the *Power System*. Via the *Dynamic Load* ΔV will induce some power demand variation ΔP_d. Magnitude of ΔP_d and its phase relative to ΔV depend on dynamic behaviour of the *Dynamic Load*. If ΔP_d happens against the phase of ΔP, overall power system damping will be improved. However, if ΔP_d happens to be in phase with ΔP, oscillations in the system will be reinforced. Especially for the case of weak power systems a feedback due to *Dynamic Load* could reduce system damping and cause system instability [108, 109, 115, 116].

Because of small capacity and low inertia of distributed energy resources, it is expected that load dynamics have an even more significant impact on stability of microgrids, compared to conventional power systems. In order to accurately investigate the stability and performance of inverter-based microgrids, load dynamics should be studied via load modeling. Furthermore, the same feedback influence of dynamic load in Figure 4.1 and Figure 4.2 is adopted for the case of inverter-based microgrids. It will be clear in the next section that the *Power System* block stands for inverters, their controllers and constant impedance loads. The *Dynamic Load* block stands for an aggregate load, which is modelled by an induction machine model.

4.2 Load modeling

The importance and complexity of load modeling are discussed in detail in literature [2, 33, 109, 113, 117]. Load modeling is a nontrivial task in power system studies because of the complicated composition of a large number of individual loads in power systems, e.g., TVs, lamps, motors, heaters, etc., which can vary depending on many factors, e.g., weather, time, system operation.

Even if the load composition were known, it would be impractical to present a model for each individual load due to their large number in power systems, resulting in highly complex system models. Hence, a load representation for power system stability studies is based on a number of simplifications [33]. The common practice is to represent the composite load characteristics as seen from a generation point by composite load models [2, 33, 107, 118].

Load models should describe load dynamics accurately enough and at the same time be relatively simple for stability analysis. By searching for a suitable load model for microgrids, the common acceptance of power system communities is considered. As common practice, a combination of a polynomial load model and an induction machine model is implemented to describe the composite load characteristics of a microgrid. The load models will be presented in the following subsections, whereas an explanation to their implementation is given hereafter.

Typically, induction machines are extensively employed in today's power systems and consume about 60% up to 70% of the total system load demand [33, 119–121]. Thus, dynamics attributable to induction machines are usually considered to exhibit the most significant aspects of composite load dynamics. By applying this common assumption in power system studies

to the case of microgrids, a model of an induction machine for transient stability analysis is implemented to describe the dynamic behavior of the aggregate load of a microgrid. This aggregate induction machine is considered to be connected to a *common bus* between inverters. Accordingly, the induction machine model represents the most important influence of the feedback path from loads. The aggregate load modelled by an induction machine is a dynamic load and should therefore be seen as an active node in a microgrid. It is consistent with the representation of network equations in terms of the node admittance matrix (2.3), where effects of generation units and active elements in a power system are reflected in node currents [33, page 257]. It is different from constant impedance loads, which are included in node admittance matrix.

A representation of a microgrid with n inverters and an induction machine is shown in Figure 4.3, where the induction machine is denoted by a node S (S stands for *stator* as the stator is connected to a power source).

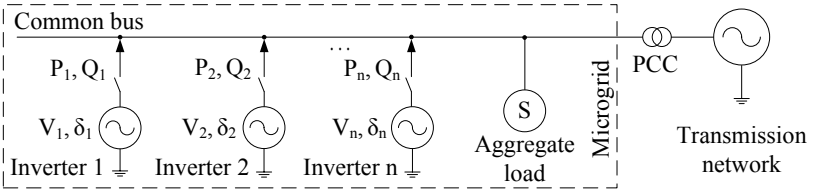

FIGURE 4.3: Representation of a microgrid with n inverters and an aggregate load S.

It was shown in Chapter 3 that under the power control loop proposed in Figure 3.1, if a microgrid is stabilized, inverter output frequencies always return to a common nominal value. However, in most cases with arbitrary load conditions, steady-state deviations of voltage magnitudes from their nominal values exist (see Equation (3.15)).

Characteristics of loads depend on magnitudes and frequencies of their supplied voltages [33]. As inverter output frequencies always converge to a nominal value, frequency dependent characteristics of loads are neglected[2]. However, because of steady-state magnitude deviations of inverter output voltages, the dependence of loads on voltage magnitudes should be considered. As reported in literature, voltage magnitudes have a relatively local behavior [6, 17, 33, 36]. Thus, loads connected close to an inverter i are more dependent on the voltage magnitude of that particular inverter. Stemming from the local behavior of voltage magnitudes as well as their influence on loads, the voltage magnitude dependence of loads connected to each inverter node should be locally described by a local voltage dependent load model.

[2]During transients in a microgrid, inverter output frequencies also vary and can effect load characteristics. However, the frequency dependence of loads during transients is also neglected. This is encouraged by the facts that (i) an inverter can change the frequency of its output voltage very fast, independently of its injected power, and (ii) relatively large deviations of inverter output frequencies from a nominal value (100's of [mHz]) normally happen during transients, which are caused by sudden changes, such as loss of a generation unit, (large) sudden load changes, etc. These kinds of changes have a switching behavior, which is not analytically considered in the thesis.

In order to include the voltage dependent nature of loads in stability analysis of microgrids, a polynomial load model is implemented for loads, which are locally connected to each inverter. The polynomial model is individual for each inverter. As will be shown in Subsection 4.2.1, the polynomial model is a static load model, which expresses the voltage dependence of the output power of an inverter at any instant of time as algebraic functions of a local voltage magnitude at that instant [33].

Remark 4.2.1. By applying a polynomial static load model for the local load of each inverter, it is assumed that local load dynamics associated to each inverter are negligible, compared to dynamics of the common aggregate load, i.e., the aggregate induction machine. For local loads of inverters, power mismatches are concerned, when local voltage magnitudes vary around their nominal values during operation of microgrids (see Figure 4.1).

Remark 4.2.2. Assuming that the structures of the load models are known, the task of load modeling is in fact a system identification procedure [122], i.e., finding coefficients of the induction machine model and the polynomial load model. Load identification methods are widely documented in literature [118, 122–126], where the two most popular approaches to load modeling are the component-based approach [127] and the measurement-based approach [118, 122, 128, 129]. The component-based approach develops load models, using information of dynamic behaviors of all individual loads in a power system. The measurement-based approach is possible by placing sensors at system buses to determine parameters of load models. Therefore, for the load modeling task, it is necessary to obtain either sensor measurements or information of load compositions, which is the case assumed in this thesis. Consider a particular microgrid, system designer should decide which method is more suitable. The thesis does not investigate the identification task, but rather focuses on general stability analysis of microgrids, assuming that parameters of load models are known.

4.2.1 Polynomial model

In a microgrid with n inverters and an induction machine S presented in Figure 4.3, the active and reactive power P_i, Q_i exchange at each inverter node i is computed similarly to the power flow equations (2.9) as follows:

$$\begin{aligned} P_i &= \sum_{k=1}^{n} V_i V_k |Y_{ik}| \cos(\delta_i - \delta_k - \phi_{ik}) + V_i V_s' |Y_{is}| \cos(\delta_i - \tilde{\delta}_s' - \phi_{is}), \\ Q_i &= \sum_{k=1}^{n} V_i V_k |Y_{ik}| \sin(\delta_i - \delta_k - \phi_{ik}) + V_i V_s' |Y_{is}| \sin(\delta_i - \tilde{\delta}_s' - \phi_{is}), \end{aligned} \tag{4.1}$$

where $\tilde{\delta}'_s$ and V'_s are the phase angle and the voltage magnitude of the aggregate load S. Note that $\tilde{\delta}'_s$ is expressed in the same reference frame as $\delta_i, i = 1,\ldots,n$. $|Y_{is}|$ and ϕ_{is} are the absolute value and the phase angle of the admittance Y_{is} between node i and the load S.

The polynomial load model to investigate the voltage dependent behavior of local loads of an inverter i is given as follows [33, 107]:

$$\begin{aligned} P_i^p &= P_i\left(p_{i_1}\left(\frac{V_i}{V_{i_0}}\right)^2 + p_{i_2}\frac{V_i}{V_{i_0}} + p_{i_3}\right), \\ Q_i^p &= Q_i\left(q_{i_1}\left(\frac{V_i}{V_{i_0}}\right)^2 + q_{i_2}\frac{V_i}{V_{i_0}} + q_{i_3}\right), \end{aligned} \tag{4.2}$$

where P_i^p, Q_i^p denote the actual active and reactive power exchange at node i, P_i, Q_i are calculated by Equations (4.1). p_{i_1} to p_{i_3} and q_{i_1} to q_{i_3} are coefficients of the model, where $p_{i_1}+p_{i_2}+p_{i_3} = 1$, $q_{i_1}+q_{i_2}+q_{i_3} = 1$, $i = 1,\ldots,n$, V_i and V_{i_0} are the magnitude of an inverter output voltage and its nominal value, respectively.

As shown in (3.2), inverter phase angles $\delta_i(t), i = 1,\ldots,n$, are expressed relative to the same rotating reference frame with a constant angular velocity ω_{nom}. It is seen from (4.1) that power exchange between an inverter node i and the induction machine node S depends not only on the voltage magnitudes V'_s and V_i, but also on the angular difference between these voltages. Therefore, in order to calculate P_i, Q_i in (4.1), it is necessary to represent inverter phase angles $\delta_i(t)$ and the phase angle $\tilde{\delta}'_s(t)$ of the induction machine in the same rotating reference frame. This issue is introduced in the next subsection.

4.2.2 Induction machine model

An induction machine contains a rotor, a stator and a flux linkage between them. An external AC current is applied to the stator but the rotor is not supplied by any external source. Following Faraday's law, there appears an induction and AC currents in the rotor, which enable the rotor to rotate. More details on the physical description of induction machines can be found in [33, 130].

A representation of an induction machine can be obtained by taking effects of mechanical transients and rotor electrical transients into account. Effects of stator electrical transients can usually be neglected [33, 119]. Rotor voltage is assumed to be equal to zero [33]. These simplifications are normally taken to ensure compatibility of the induction machine model with models of other system components, e.g., inverter model in this case. It will be shown that a suitable dynamic model of an induction machine for stability analysis is derived by eliminating rotor currents and expressing a relationship between stator current and voltage behind the transient reactance.

Mathematically, the model of an induction machine is derived by the following procedure. First, a standard induction machine model in a $d-q$ rotating reference frame is introduced, which can be easily found in literature [33, 47, 131, 132]. Note that the standard model of an induction machine is derived in per unit. Based on the *Center of inertia* (COI) principle[3], the angular velocity of the $d-q$ rotating reference frame of the standard induction machine model will be defined by the output frequencies of inverters, i.e., generation units in the system. In addition, stator currents of the induction machine will be replaced by expressions with voltages and phase angles of inverters and the induction machine. This will enable a modification of the standard induction machine model. A modified induction machine model can be then combined with the inverter model (3.3) to form an overall microgrid model.

Induction machines can obtain one or more pairs of poles. However, without loss of generality and for convenience in analysis, only one pair of poles is considered. The basic equations of an induction machine are associated to its stator, rotor circuits, and the linkage between stator and rotor, which are AC quantities and contain electrical angles, which in turn vary in time. This introduces considerable mathematical complexity in deriving induction machine models. Regarding this issue, the standard equations of an induction machine are usually represented in a $d-q$ rotating reference frame. Thus, the $d-q$ transformation simplifies the basic equations of an induction machine, replacing its AC quantities by DC quantities.

Usually, the preferred $d-q$ reference frame for an induction machine is selected to have the axes rotating at the frequency of the stator voltage [33, 132]. In this case, the frequency of the stator voltage is the network frequency, namely, the synchronous speed of a microgrid, which can vary during transient processes in the system.

As shown in Figure 4.3, the considered induction machine is connected to the common bus of the microgrid. Therefore, it is assumed that the synchronous speed (i.e., generalized network frequency) denoted by ω_s can be calculated by the Center of inertia principle [33, 133, 134] to form a COI $d-q$ reference frame for the induction machine model. The axes of the COI $d-q$ reference frame rotate at the frequency of the common bus of the microgrid, which is influenced by all inverters. Hence, ω_s can vary during transients in the system. Additionally, ω_s is also the frequency of the AC voltage provided to the stator of the induction machine. At a steady-state, the microgrid is synchronously stable, i.e., the frequencies ω_s and ω_i, $i=1,\ldots,n$, are equal to each other, converging to a fixed nominal value of the system frequency ω_{nom}, e.g., $2\pi 50$ [rad/s].

The COI principle for calculating ω_s in dependence on ω_i, $i=1,\ldots,n$, will be introduced thereafter. Thus, for the microgrid in Figure 4.3, there are the COI reference frame for the induction machine and the reference frame of inverter phase angles with a constant angular

[3]For convenience in describing transient behavior of a power system with multiple synchronous generators, generator rotor angles are expressed relative to an inertial center of all generators. The position of the center of inertia is defined by the COI principle.

velocity ω_{nom}. The angular difference between the two rotating reference frames will also appear in the modified induction machine model.

The standard per unit model of an induction machine in the COI $d-q$ reference frame. The basic equations of an induction machine are associated to voltages, currents and flux linkages of a stator and a rotor. The stator and rotor flux linkages are [33, 132]:

$$\Psi_{ds} = L_{ss} i_{ds} + L_m i_{dr}, \tag{4.3a}$$

$$\Psi_{qs} = L_{ss} i_{qs} + L_m i_{qr}, \tag{4.3b}$$

$$\Psi_{dr} = L_{rr} i_{dr} + L_m i_{ds}, \tag{4.3c}$$

$$\Psi_{qr} = L_{rr} i_{qr} + L_m i_{qs}, \tag{4.3d}$$

where Ψ_{ds}, Ψ_{qs} are correspondingly the $d-q$ components of the stator flux, Ψ_{dr}, Ψ_{qr} are the $d-q$ components of the rotor flux. i_{dr}, i_{qr}, i_{ds} and i_{qs} are the $d-q$ components of the rotor and stator currents. L_s, L_r are the stator and rotor leakage inductances, respectively. L_m is the magnetizing inductance. Finally, L_{ss} and L_{rr} are the stator and rotor inductances defined as:

$$L_{ss} = L_s + L_m, \quad L_{rr} = L_r + L_m. \tag{4.4}$$

The stator and rotor voltages in the $d-q$ reference frame are [33, 132]:

$$v_{ds} = R_s i_{ds} - \omega_s \Psi_{qs} + \frac{\mathrm{d}\Psi_{ds}}{\mathrm{d}t}, \tag{4.5a}$$

$$v_{qs} = R_s i_{qs} + \omega_s \Psi_{ds} + \frac{\mathrm{d}\Psi_{qs}}{\mathrm{d}t}, \tag{4.5b}$$

$$v_{dr} = R_r i_{dr} - \frac{\mathrm{d}\theta_r}{\mathrm{d}t} \Psi_{qr} + \frac{\mathrm{d}\Psi_{dr}}{\mathrm{d}t}, \tag{4.5c}$$

$$v_{qr} = R_r i_{qr} + \frac{\mathrm{d}\theta_r}{\mathrm{d}t} \Psi_{dr} + \frac{\mathrm{d}\Psi_{qr}}{\mathrm{d}t}, \tag{4.5d}$$

where v_{ds}, v_{qs}, v_{dr} and v_{qr} are the $d-q$ components of the stator voltage and rotor voltage, respectively. R_s and R_r are the resistances of stator and rotor. ω_s is the frequency of the stator field. The corresponding transformations of the rotor quantities in relation to the synchronous COI rotating $d-q$ reference frame are defined by an angle θ_r, by which the stator phase angle leads the rotor phase angle. The rotor slip defined by $\frac{\mathrm{d}\theta_r}{\mathrm{d}t}$ characterizes the difference between the rotor speed ω_r and the speed of stator field. The rotor slip is computed in per unit as follows:

$$\frac{\mathrm{d}\theta_r}{\mathrm{d}t} = \frac{\omega_s - \omega_r}{\omega_s}. \tag{4.6}$$

For stability analysis, stator transients caused by DC components in stator transient currents are neglected, then the terms $\frac{\mathrm{d}\Psi_{ds}}{\mathrm{d}t}$ and $\frac{\mathrm{d}\Psi_{qs}}{\mathrm{d}t}$ in (4.5) can be eliminated [33]. Moreover, there are several types of rotor structure, e.g., wound rotor, squirrel-cage rotor. It is a common practice

in power system analysis to consider the squirrel-cage rotor, whose rotor voltages are zero, i.e., $v_{dr} = v_{qr} = 0$ [33]. Based on these assumptions, the equations of stator and rotor voltages (4.5) become the following:

$$v_{ds} = R_s i_{ds} - \omega_s \Psi_{qs}, \tag{4.7a}$$

$$v_{qs} = R_s i_{qs} + \omega_s \Psi_{ds}, \tag{4.7b}$$

$$v_{dr} = R_r i_{dr} - \frac{\mathrm{d}\theta_r}{\mathrm{d}t}\Psi_{qr} + \frac{\mathrm{d}\Psi_{dr}}{\mathrm{d}t} = 0, \tag{4.7c}$$

$$v_{qr} = R_r i_{qr} + \frac{\mathrm{d}\theta_r}{\mathrm{d}t}\Psi_{dr} + \frac{\mathrm{d}\Psi_{qr}}{\mathrm{d}t} = 0. \tag{4.7d}$$

From (4.3c) and (4.3d), the following is achieved:

$$i_{dr} = \frac{\Psi_{dr} - L_m i_{ds}}{L_{rr}}, \quad i_{qr} = \frac{\Psi_{qr} - L_m i_{qs}}{L_{rr}}. \tag{4.8}$$

Substituting the equations above into (4.3a) and (4.3b) yields the following:

$$\Psi_{ds} = L_{ss} i_{ds} + L_m \frac{\Psi_{dr} - L_m i_{ds}}{L_{rr}} = \frac{L_m}{L_{rr}}\Psi_{dr} + \Big(L_{ss} - \frac{L_m^2}{L_{rr}}\Big) i_{ds}, \tag{4.9a}$$

$$\Psi_{qs} = L_{ss} i_{qs} + L_m \frac{\Psi_{qr} - L_m i_{qs}}{L_{rr}} = \frac{L_m}{L_{rr}}\Psi_{qr} + \Big(L_{ss} - \frac{L_m^2}{L_{rr}}\Big) i_{qs}. \tag{4.9b}$$

With Ψ_{ds} and Ψ_{qs} in (4.9), the equations for stator voltages (4.7a) and (4.7b) can be written as follows:

$$v_{ds} = R_s i_{ds} - \omega_s \Psi_{qs} = R_s i_{ds} + \underbrace{\omega_s \frac{-L_m}{L_{rr}}\Psi_{qr}}_{:= v'_{ds}} - \underbrace{\omega_s \Big(L_{ss} - \frac{L_m^2}{L_{rr}}\Big)}_{:= X'_s} i_{qs}, \tag{4.10a}$$

$$v_{qs} = R_s i_{qs} + \omega_s \Psi_{ds} = R_s i_{qs} + \underbrace{\omega_s \frac{L_m}{L_{rr}}\Psi_{dr}}_{:= v'_{qs}} + \omega_s \Big(L_{ss} - \frac{L_m^2}{L_{rr}}\Big) i_{ds}. \tag{4.10b}$$

In the equations above, X'_s is called the transient reactance of the induction machine. The stator voltage in the complex number form can be expressed as follows:

$$\vec{V}_s = v_{ds} + j v_{qs} = R_s \underbrace{(i_{ds} + j i_{qs})}_{:= \vec{I}_s} + j X'_s (i_{ds} + j i_{qs}) + \underbrace{v'_{ds} + j v'_{qs}}_{:= \vec{V}'_s}, \tag{4.11}$$

where $\vec{V}_s$ is the stator voltage vector, $\vec{I}_s$ is the stator current vector, and $\vec{V}'_s$ is called the *voltage behind transient impedance* $(R_s + jX'_s)$.

Equation (4.11) implies that for stability studies, an induction machine can be replaced by a simpler electrical circuit as displayed in Figure 4.4 with the following relation [33]:

$$\vec{V}_s = (R_s + jX'_s)\vec{I}_s + \vec{V}'_s. \tag{4.12}$$

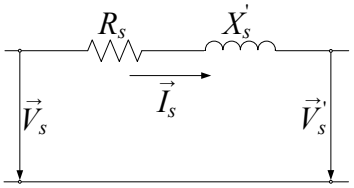

FIGURE 4.4: Equivalent circuit of an induction machine for stability studies.

As defined in (4.10), Ψ_{dr} and Ψ_{qr} can be expressed by v'_{ds} and v'_{qs}. Then, by plugging the derived expressions with v'_{ds} and v'_{qs} into (4.7c) and (4.7d), the following ODEs are derived:

$$\frac{\mathrm{d}v'_{ds}}{\mathrm{d}t} = -\frac{R_r}{L_{rr}}\left(v'_{ds} + \frac{\omega_s L_m^2}{L_{rr}} i_{qs}\right) + \frac{\mathrm{d}\theta_r}{\mathrm{d}t} v'_{qs}, \tag{4.13a}$$

$$\frac{\mathrm{d}v'_{qs}}{\mathrm{d}t} = -\frac{R_r}{L_{rr}}\left(v'_{qs} - \frac{\omega_s L_m^2}{L_{rr}} i_{ds}\right) - \frac{\mathrm{d}\theta_r}{\mathrm{d}t} v'_{ds}. \tag{4.13b}$$

Denote

$$X_s = \omega_s L_{ss}\ , \quad \frac{L_{rr}}{R_r} = T'_0\ , \quad \frac{\mathrm{d}\theta_r}{\mathrm{d}t} = \frac{\omega_s - \omega_r}{\omega_s}, \tag{4.14}$$

then the ODEs (4.13) and an acceleration equation of the rotor build a state-space model of an induction machine as follows:

$$\begin{cases} \dfrac{\mathrm{d}v'_{ds}}{\mathrm{d}t} &= -\dfrac{1}{T'_0}\left(v'_{ds} + (X_s - X'_s) i_{qs}\right) + \dfrac{\mathrm{d}\theta_r}{\mathrm{d}t} v'_{qs}, \\ \dfrac{\mathrm{d}v'_{qs}}{\mathrm{d}t} &= -\dfrac{1}{T'_0}\left(v'_{qs} - (X_s - X'_s) i_{ds}\right) - \dfrac{\mathrm{d}\theta_r}{\mathrm{d}t} v'_{ds}, \\ \dfrac{\mathrm{d}\omega_r}{\mathrm{d}t} &= \dfrac{\omega_s}{2H_s}(\mathcal{T}_s - \mathcal{T}_m), \end{cases} \tag{4.15}$$

where X'_s and X_s are defined in (4.10) and (4.14), respectively. The acceleration equation of the rotor describes the relation between the input electrical torque $\mathcal{T}_s$, the output mechanical torque $\mathcal{T}_m$ of an induction machine and the rotor speed ω_r. H_s is the inertia constant of the induction machine.

A common representation of the mechanical torque $\mathcal{T}_m$ is as follows:

$$\mathcal{T}_m = \mathcal{T}_{m_0}\left(a_r\left(\frac{\omega_r}{\omega_s}\right)^2 + b_r\frac{\omega_r}{\omega_s} + c_r\right), \quad a_r + b_r + c_r = 1, \tag{4.16}$$

where a_r, b_r, c_r are torque coefficients, and $\mathcal{T}_{m_0}$ is the torque at rated rotating speed [33].

Equations in (4.15) form the classical model of an induction machine, which is commonly used in stability studies [33, 47, 132].

It is seen that the induction model (4.15) depends on i_{ds}, i_{qs} and ω_s. In the following, based on power flow equations between inverters and the induction machine, i_{ds}, i_{qs} will be replaced by other variables of inverters and the induction machine. Moreover, by applying the Center of inertia principle, the phase angle and the frequency of the stator voltage of the induction machine will be described by inverter phase angles δ_i and inverter output frequencies $\omega_i,\ i = 1,\dots,n$. Following these replacements of variables, a modified induction machine model will be derived, which can be combined with the inverter model (3.3) to form an overall microgrid model. The stability analysis and controller design will be provided based on a derived overall microgrid model in the next section.

The relation between the two rotating reference frames.
Let δ'_s be an angle of the voltage $\vec{V}'_s$ in (4.12). As the standard induction machine model (4.15) is defined in the COI $d-q$ rotating reference frame with an angular velocity ω_s, δ'_s is also defined in this COI $d-q$ rotating reference frame.

Let $\tilde{\delta}'_s$ denote an equivalence of δ'_s in the rotating reference frame with a constant angular velocity ω_{nom} of the inverters. Thus, $\tilde{\delta}'_s$ and δ_i are represented in the same rotating reference frame. By using the COI principle, it is assumed that the phase angle $\tilde{\delta}'_s$ of the induction machine can be calculated by the phase angles $\delta_i,\ i = 1,\dots,n$, of all generation units in the system as follows:

$$\tilde{\delta}'_s := \frac{1}{H_T}\sum_{i=1}^{n} H_i\delta_i, \tag{4.17}$$

where H_i is the inertia constant of each inverter i, and $H_T := \sum_{i=1}^{n} H_i$ [33].

The equation above is often applied for power systems with synchronous generators. Each generator obtains mechanical and electrical inertia, which is quantitatively represented by an inertia constant. As mentioned in Remark 2.1.3, an inverter itself does not obtain any inertia. However, with an additional power control loop presented in Figure 3.1, an artificial inertia is created by the measuring low-pass filter and the integrator. Therefore, an inertia constant H_i of an inverter i can be determined by time constant of its power control loop.

As the phase angle $\tilde{\delta}'_s$ is expressed relative to the common rotating reference frame of inverters with an angular velocity ω_{nom}, $\tilde{\delta}'_s$ is computed similarly to (3.2) as follows:

$$\tilde{\delta}'_s(t) = (\omega_s - \omega_{\text{nom}})t + \tilde{\delta}'_{s_0}, \tag{4.18}$$

where $\tilde{\delta}'_{s_0}$ is an initial value of $\tilde{\delta}'_s$ in the rotating reference frame of inverters.

Based on the equation above and Equation (4.17), the frequency ω_s of the stator voltage $\vec{V}'_s$ of the induction machine S is calculated as follows:

$$\omega_s - \omega_{\text{nom}} = \dot{\tilde{\delta}}'_s = \frac{1}{H_T}\sum_{i=1}^{n} H_i(\omega_i - \omega_{\text{nom}}) = \frac{1}{H_T}\sum_{i=1}^{n} H_i \Delta\omega_i, \tag{4.19}$$

where ω_i is an output frequency of an inverter i, $i = 1,\ldots,n$, and $\Delta\omega_i = \omega_i - \omega_{\text{nom}}$.

Equations (4.17) and (4.19) imply that the phase angle $\tilde{\delta}'_s$ and the frequency ω_s of the stator voltage $\vec{V}'_s$ of the induction machine are influenced by all generation units in a microgrid. The influential strength of each inverter (with the power control loop in Figure 3.1) is defined by its inertia constant H_i.

In Figure 4.5 the relation between the COI $d-q$ reference frame and the rotating reference frame of inverter phase angles is explained, where θ_0 is an initial angular difference between the two rotating reference frames θ.

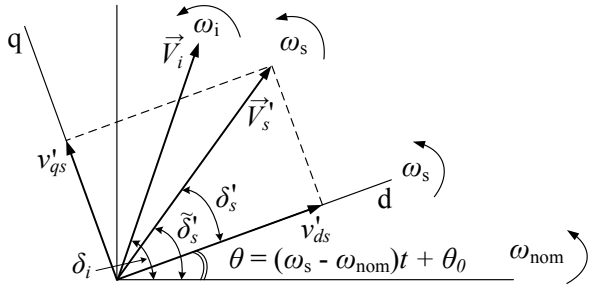

FIGURE 4.5: Relation between the two rotating reference frames.

It is seen in Figure 4.5 that $\tilde{\delta}'_s$ contains the angular difference θ between the two rotating reference frames. In addition, $\tilde{\delta}'_s$ is assumed to be calculated by the formula in (4.17). Thus, by using the COI principle, the angular difference θ is directly contained within the inverter phase angles δ_i, $i = 1,\ldots,n$.

A modification of the standard induction machine model.
It is seen in Figure 4.5 that:

$$v'_{ds} = V'_s \cos\delta'_s, \quad v'_{qs} = V'_s \sin\delta'_s. \tag{4.20}$$

For further analysis, it is assumed that $\cos\delta'_s \neq 0$ and $\sin\delta'_s \neq 0$. Then,

$$V'_s = \begin{cases} \dfrac{v'_{ds}}{\cos\delta'_s} & \text{if } \cos\delta'_s \neq 0, \\ \dfrac{v'_{qs}}{\sin\delta'_s} & \text{if } \sin\delta'_s \neq 0. \end{cases} \tag{4.21}$$

It is noteworthy that a modified induction machine model derived hereafter is only relevant for the case $(\cos\delta'_s \neq 0)$ and $(\sin\delta'_s \neq 0)$, where V'_s can be calculated as in (4.21).

In Figure 4.4, if $(R_s + jX'_s)$ is considered as a connecting power line to the induction machine S, the total electrical power $\vec{S}_s^{\text{cons.}}$ consumed by the induction machine can be computed by the voltage behind transient reactance $\vec{V}'_s$ and the stator current $\vec{I}_s$ as follows:

$$\vec{S}_s^{\text{cons.}} = \vec{V}'_s \cdot \vec{I}_s^{*} = (v'_{ds} + jv'_{qs})(i_{ds} - ji_{qs}) = \underbrace{v'_{ds}i_{ds} + v'_{qs}i_{qs}}_{=P_s^{\text{cons.}}} + j\underbrace{(v'_{qs}i_{ds} - v'_{ds}i_{qs})}_{=Q_s^{\text{cons.}}}, \tag{4.22}$$

where $P_s^{\text{cons.}}, Q_s^{\text{cons.}}$ denote the active and reactive power exchange at the voltage node $\vec{V}'_s$, $\vec{I}_s^{*}$ is the complex conjugate of the stator current $\vec{I}_s$, and "cons." is an abbreviation for *consumption*.

As mentioned above, an induction machine is considered as an active node in a microgrid. Moreover, positive power consumption can be reviewed as negative power generation [33, page 250]. Thus, it is considered that the induction machine S generates negative electrical power, injecting a negative current $-\vec{I}_s$ into the microgrid (see the direction of $\vec{I}_s$ in Figure 4.4). Thus, consider a network with n inverters and an induction machine, a Kron-reduced admittance matrix is derived similarly to (2.8) as follows:

$$\begin{bmatrix} \vec{I}_1 \\ \vec{I}_2 \\ \vdots \\ \vec{I}_n \\ -\vec{I}_s \end{bmatrix} = \begin{bmatrix} Y_{11} & Y_{12} & \dots & Y_{1n} & Y_{1s} \\ Y_{21} & Y_{22} & \dots & Y_{2n} & Y_{2s} \\ \vdots & \vdots & \ddots & \vdots & \vdots \\ Y_{n1} & Y_{n2} & \dots & Y_{nn} & Y_{ns} \\ Y_{s1} & Y_{s2} & \dots & Y_{sn} & Y_{ss} \end{bmatrix} \begin{bmatrix} \vec{V}_1 \\ \vec{V}_2 \\ \vdots \\ \vec{V}_n \\ \vec{V}'_s \end{bmatrix}. \tag{4.23}$$

Remark 4.2.3. It should be mentioned that elements of the admittance matrix in (4.23) are calculated with the nominal frequency ω_{nom}. The stator impedance $(R_s + jX'_s)$ (see Figure 4.4) is considered as part of a connecting power line to the induction machine, which is contained in elements of the admittance matrix in (4.23).

Hence, (negative) active and reactive power injection at node S is computed by the standard power flow equations (2.9) as follows:

$$P_s = -P_s^{\text{cons.}} = V_s'^2|Y_{ss}|\cos\phi_{ss} + \sum_{i=1}^{n} V'_s V_i |Y_{si}| \cos(\tilde{\delta}'_s - \delta_i - \phi_{si}) = -(v'_{ds}i_{ds} + v'_{qs}i_{qs}), \tag{4.24a}$$

$$Q_s = -Q_s^{\text{cons.}} = -V_s'^2|Y_{ss}|\sin\phi_{ss} + \sum_{i=1}^{n} V'_s V_i |Y_{si}| \sin(\tilde{\delta}'_s - \delta_i - \phi_{si}) = -(v'_{qs}i_{ds} - v'_{ds}i_{qs}), \tag{4.24b}$$

where ϕ_{si} and $|Y_{si}|$ are the angle and the absolute value of the mutual impedance Y_{si}, ϕ_{ss} and $|Y_{ss}|$ are associated to the self-admittance Y_{ss}.

As seen in (4.21) that V_s' in (4.24) can be expressed by v_{ds}', v_{qs}' and δ_s'. Therefore, with (4.21) and (4.24), i_{ds} and i_{qs} can be expressed by the following nonlinear functions:

$$i_{ds} = -v_{ds}'|Y_{ss}|\cos\phi_{ss} + v_{qs}'|Y_{ss}|\sin\phi_{ss} - \sum_{i=1}^{n} V_i|Y_{si}|\cos(\tilde{\delta}_s' - \delta_i - \phi_{si} - \delta_s'), \tag{4.25a}$$

$$i_{qs} = -v_{qs}'|Y_{ss}|\cos\phi_{ss} - v_{ds}'|Y_{ss}|\sin\phi_{ss} + \sum_{i=1}^{n} V_i|Y_{si}|\sin(\tilde{\delta}_s' - \delta_i - \phi_{si} - \delta_s'). \tag{4.25b}$$

In addition, the electrical torque $\mathcal{T}_s$ in (4.15) can be calculated as follows [33]:

$$\begin{aligned} \mathcal{T}_s &= \frac{P_s^{\text{cons.}}}{\omega_s} = \frac{v_{ds}' i_{ds} + v_{qs}' i_{qs}}{\omega_s} \\ &= \frac{1}{\omega_s}\left(-\left(v_{ds}'^2 + v_{qs}'^2\right)|Y_{ss}|\cos\phi_{ss} - \frac{v_{ds}'}{\cos\delta_s'}\sum_{i=1}^{n} V_i|Y_{si}|\cos(\tilde{\delta}_s' - \delta_i - \phi_{si})\right). \end{aligned} \tag{4.26}$$

As can be seen in (4.21), the phase angle δ_s' can be described as:

$$\delta_s' = \arctan\frac{v_{qs}'}{v_{ds}'}. \tag{4.27}$$

With the expressions (4.25) and (4.26), i_{ds}, i_{qs} and $\mathcal{T}_s$ in the induction machine model (4.15) are eliminated. With (4.27), δ_s' is replaced by v_{ds}' and v_{qs}'. With the COI principle presented in Equations (4.17) and (4.19), $\tilde{\delta}_s'$ and ω_s are replaced by δ_i and ω_i $(\Delta\omega_i)$, $i = 1, \ldots, n$. Thus, the derivatives of v_{ds}', v_{ds}' and ω_r in (4.15) can be described as the following nonlinear functions:

$$\begin{cases} \dot{v}_{ds}'(t) &= f_d(v_{ds}', v_{qs}', \omega_r, \Delta\omega_1, V_1, \delta_1, \ldots, \Delta\omega_n, V_n, \delta_n), \\ \dot{v}_{qs}'(t) &= f_q(v_{ds}', v_{qs}', \omega_r, \Delta\omega_1, V_1, \delta_1, \ldots, \Delta\omega_n, V_n, \delta_n), \\ \dot{\omega}_r(t) &= f_r(v_{ds}', v_{qs}', \omega_r, \Delta\omega_1, V_1, \delta_1, \ldots, \Delta\omega_n, V_n, \delta_n). \end{cases} \tag{4.28}$$

The differential equations above represent a modified induction machine model. Because of the complexity of the aforementioned variable replacements, the induction machine model (4.28) is not fully illustrated here.

Differences between the standard induction machine model (4.15) and the modified model (4.28) involve: the assumption on the COI principle in (4.17) and (4.19), the assumption of the phase angle δ_s' in (4.21), and the implementation of the power flow equations (4.24).

In the next section, the modified induction machine model (4.28) will be combined with the inverter model (3.3) to form an overall microgrid model, which is used for stability analysis and synthesis of inverter controllers.

4.3 State-space model of a microgrid with a dynamic load

In order to analyze the stability of a microgrid, including the feedback effect of load dynamics, a linearized state-space model of an overall microgrid is presented. This is done by combining the induction machine model (4.28) and an inverter model with state variables and control inputs defined in (3.4). The interesting equilibrium point of each inverter i is formerly defined in (3.5).

Based on the inverter model (3.3) derived in Chapter 3, the inverter model is extended with respect to the polynomial load model (4.2) as follows:

$$\begin{cases} \dot{\delta}_i &= \Delta\omega_i, \\ \dot{\tilde{P}}_i &= \dfrac{-\tilde{P}_i + P_i^p(V_1,\ldots,V_n,\delta_1,\ldots,\delta_n,v'_{ds},v'_{qs})}{\tau_i}, \\ \dot{\tilde{Q}}_i &= \dfrac{-\tilde{Q}_i + Q_i^p(V_1,\ldots,V_n,\delta_1,\ldots,\delta_n,v'_{ds},v'_{qs})}{\tau_i}, \end{cases} \tag{4.29}$$

where P_i^p, Q_i^p are given in (4.2) and v'_{ds}, v'_{qs} are $d-q$ components of the voltage behind transient reactance $\vec{V}'_s$ of the induction machine S.

The state variable $x_s(t)$ and the input $u(t)$ of the aggregate load S described by the model of an induction machine (4.28) can be chosen as follows:

$$x_s(t) = \begin{bmatrix} v'_{ds} - v'_{ds_0} \\ v'_{qs} - v'_{qs_0} \\ \omega_r - \omega_{r_0} \end{bmatrix}, \quad u(t) = \begin{bmatrix} u_1(t) \\ \vdots \\ u_n(t) \end{bmatrix}, \quad \text{with } u_i(t) = \begin{bmatrix} \Delta\omega_i \\ V_i - V_{i_0} \end{bmatrix}, \tag{4.30}$$

where the control input of S is chosen to be the same as the control input $u(t)$ of the inverters. A physical explanation is that the induction machine is fed by all inverters. As a result, the magnitude and frequency of the input voltage of S are influenced by the output frequency ω_i and voltage magnitude V_i of all inverters in the system, $i = 1,\ldots,n$.

The interesting equilibrium point of the aggregate load S is as follows:

$$\begin{aligned} x_{s_0} &= \begin{bmatrix} v'_{ds_0} & v'_{qs_0} & \omega_{r_0} \end{bmatrix}^T, \\ u_0 = \begin{bmatrix} 0 & V_{1_0} & \ldots & 0 & V_{n_0} \end{bmatrix}^T &= \begin{bmatrix} u_{1_0}^T & \ldots & u_{n_0}^T \end{bmatrix}^T. \end{aligned} \tag{4.31}$$

Hence, by linearizing the inverter model (4.29) and the induction machine model (4.28) (which is based on the induction machine model (4.15) and the variable replacements in (4.17), (4.19), (4.25), (4.26) and (4.27)) around the operating point (3.5) and (4.31), an LTI state-space model

of a microgrid with n inverters and an aggregate load S is obtained as follows:

$$\begin{cases} \dot{x}(t) &= Ax(t) + Bu(t) + Tx_s(t), \\ \dot{x}_s(t) &= A_s x_s(t) + B_s u(t) + T_s x(t), \end{cases} \tag{4.32}$$

where $x(t)$ is defined in (3.4), $A \in \mathbb{R}^{3n\times 3n}$, $B \in \mathbb{R}^{3n\times 2n}$ are the system matrices of inverters, $A_s \in \mathbb{R}^{3\times 3}$, $B_s \in \mathbb{R}^{3\times 2n}$ are the system matrices of the dynamic load S and $T \in \mathbb{R}^{3n\times 3}$, $T_s \in \mathbb{R}^{3\times 3n}$ are the interconnection matrices between inverters and the load S. The matrices are as follows:

$$\begin{aligned} A_s &= \begin{bmatrix} \frac{\partial \dot{f}_d}{\partial v'_{ds}}\Big|_0 & \frac{\partial \dot{f}_d}{\partial v'_{qs}}\Big|_0 & \frac{\partial \dot{f}_d}{\partial \omega_r}\Big|_0 \\ \frac{\partial \dot{f}_q}{\partial v'_{ds}}\Big|_0 & \frac{\partial \dot{f}_q}{\partial v'_{qs}}\Big|_0 & \frac{\partial \dot{f}_q}{\partial \omega_r}\Big|_0 \\ \frac{\partial \dot{f}_r}{\partial v'_{ds}}\Big|_0 & \frac{\partial \dot{f}_r}{\partial v'_{qs}}\Big|_0 & \frac{\partial \dot{f}_r}{\partial \omega_r}\Big|_0 \end{bmatrix}, B_s = \begin{bmatrix} \frac{\partial \dot{f}_d}{\partial \Delta\omega_1}\Big|_0 & \frac{\partial \dot{f}_d}{\partial V_1}\Big|_0 & \cdots & \frac{\partial \dot{f}_d}{\partial \Delta\omega_n}\Big|_0 & \frac{\partial \dot{f}_d}{\partial V_n}\Big|_0 \\ \frac{\partial \dot{f}_q}{\partial \Delta\omega_1}\Big|_0 & \frac{\partial \dot{f}_q}{\partial V_1}\Big|_0 & \cdots & \frac{\partial \dot{f}_q}{\partial \Delta\omega_n}\Big|_0 & \frac{\partial \dot{f}_q}{\partial V_n}\Big|_0 \\ \frac{\partial \dot{f}_r}{\partial \Delta\omega_1}\Big|_0 & \frac{\partial \dot{f}_r}{\partial V_1}\Big|_0 & \cdots & \frac{\partial \dot{f}_r}{\partial \Delta\omega_n}\Big|_0 & \frac{\partial \dot{f}_r}{\partial V_n}\Big|_0 \end{bmatrix}, \\ T_{s_i} &= \begin{bmatrix} \frac{\partial \dot{f}_d}{\partial \delta_i}\Big|_0 & 0 & 0 \\ \frac{\partial \dot{f}_q}{\partial \delta_i}\Big|_0 & 0 & 0 \\ \frac{\partial \dot{f}_r}{\partial \delta_i}\Big|_0 & 0 & 0 \end{bmatrix}, T_s = [T_{s_1} \ \dots \ T_{s_n}], \ T_i = \begin{bmatrix} 0 & 0 & 0 \\ \frac{\partial P_i^p}{\tau_i \partial v'_{ds}}\Big|_0 & \frac{\partial P_i^p}{\tau_i \partial v'_{qs}}\Big|_0 & 0 \\ \frac{\partial Q_i^p}{\tau_i \partial v'_{ds}}\Big|_0 & \frac{\partial Q_i^p}{\tau_i \partial v'_{qs}}\Big|_0 & 0 \end{bmatrix}, \ T = \begin{bmatrix} T_1 \\ \vdots \\ T_n \end{bmatrix}. \end{aligned} \tag{4.33}$$

Each inverter i, $i = 1,\dots,n$, corresponds to a subsystem with the following state-space model:

$$\dot{x}_i(t) = A_{ii}x_i(t) + B_{ii}u_i(t) + \sum_{k=1,\ k\neq i}^{n} \Big(A_{ik}x_k(t) + B_{ik}u_k(t)\Big) + T_i x_s(t), \tag{4.34}$$

where

$$A_{ii} = \begin{bmatrix} 0 & 0 & 0 \\ \frac{\partial P_i^p}{\tau_i \partial \delta_i}\Big|_0 & \frac{-1}{\tau_i} & 0 \\ \frac{\partial Q_i^p}{\tau_i \partial \delta_i}\Big|_0 & 0 & \frac{-1}{\tau_i} \end{bmatrix}, \ B_{ii} = \begin{bmatrix} 1 & 0 \\ 0 & \frac{\partial P_i^p}{\tau_i \partial V_i}\Big|_0 \\ 0 & \frac{\partial Q_i^p}{\tau_i \partial V_i}\Big|_0 \end{bmatrix}, \ A_{ik} = \begin{bmatrix} 0 & 0 & 0 \\ \frac{\partial P_i^p}{\tau_i \partial \delta_k}\Big|_0 & 0 & 0 \\ \frac{\partial Q_i^p}{\tau_i \partial \delta_k}\Big|_0 & 0 & 0 \end{bmatrix}, \ B_{ik} = \begin{bmatrix} 0 & 0 \\ 0 & \frac{\partial P_i^p}{\tau_i \partial V_k}\Big|_0 \\ 0 & \frac{\partial Q_i^p}{\tau_i \partial V_k}\Big|_0 \end{bmatrix}. \tag{4.35}$$

A slight abuse of notation in the system models above should be mentioned here. In (4.32) and (4.34), $A, B, A_{ii}, B_{ii}, A_{ik}$ and B_{ik} are still used in this chapter to denote the system matrices of the inverter part and the matrices of each inverter, respectively. This notation is similar to the notation in (3.6) and (3.7) in Chapter 3. The system matrices of inverters in (4.32) and (4.34) have the same structures as the system matrices in (3.6) and (3.7). However, with the polynomial load model (4.2) and the power flow equations (4.1), elements of matrices $A, B, A_{ii}, B_{ii}, A_{ik}$ and B_{ik} in (4.32) and (4.34) are different from the matrix elements in (3.6) and (3.7).

Remark 4.3.1. The linearization of the induction machine model (4.28) is algebraically difficult because of the complication of the model. This task can be simplified by using computer algebra

systems, such as Scilab or Matlab. In Appendix A.5, an example is provided that shows how to obtain the linearized model (4.32) for a microgrid with two inverters and an induction machine.

The system output is defined as follows:

$$y = x = \underline{C} \begin{bmatrix} x \\ x_s \end{bmatrix}, \tag{4.36}$$

where $\underline{C} = [I_{3n\times 3n} \;\; 0_{3n\times 3}]$.

The system model consisting of (4.32) and (4.36) can be compactly rewritten as follows:

$$\begin{cases} \dot{\underline{x}} &= \underline{A}\,\underline{x} + \underline{B}u, \\ y &= \underline{C}\,\underline{x}, \end{cases} \tag{4.37}$$

where $\underline{x} \in \mathbb{R}^{(3n+3)\times 1}$, $\underline{A} \in \mathbb{R}^{(3n+3)\times(3n+3)}$ and $\underline{B} \in \mathbb{R}^{(3n+3)\times 2n}$ as follows:

$$\underline{x} = \begin{bmatrix} x \\ x_s \end{bmatrix}, \; \underline{A} = \begin{bmatrix} A & T \\ T_s & A_s \end{bmatrix}, \; \underline{B} = \begin{bmatrix} B \\ B_s \end{bmatrix}. \tag{4.38}$$

Based on the microgrid model with a dynamic load (4.37), the control task is still the design of local state-feedback controllers K_i, $i = 1,\ldots,n$, for inverters as formulated in Problem 3.1.1. An additional requirement for the controller design in this chapter is taken so that inverter controllers should stabilize not only the inverters but also robustly stabilize the overall microgrid system (4.37), despite load dynamics. In the next section, two separate LMI stability conditions based on Lyapunov's stability theorem and the small-gain theorem are proposed. By solving the LMI problems, the resulting controllers will asymptotically stabilize the system (4.37).

Note that the inverter controllers described in Problem 3.1.1 concern only the inverter part of the system, no control action is performed for the dynamic load S.

Assumption: For the stability analysis in next section, it is assumed that the dynamic load S is asymptotically stable, i.e., all the eigenvalues of the matrix A_s obtain negative real parts. □

4.4 Stability of microgrids under load dynamics

4.4.1 Stability of the system based on Lyapunov's stability theorem

Consider the system (4.37). As in Chapter 3, the stabilizability of the system can be checked by the PBH rank test, whether matrix $[\underline{A} - \lambda I, \underline{B}]$ has full-row rank for all eigenvalues λ of $\underline{A}$ with $Re\lambda \geq 0$. By considering matrix $\underline{A}$ in (4.38), it is clear that the submatrix A possesses n zero

eigenvalues and $2n$ negative real eigenvalues determined by the time constants of the employed measuring low-pass filters (see Equation (3.10)). The submatrix A_s belongs to the linearized dynamic load. According to the assumption above, eigenvalues of A_s are in the open left-half plane. Thus, the PBH stabilizability test is reduced to checking the row rank of the matrix $[\underline{A}\ \ \underline{B}]$. Furthermore, it will be clear in the following part of this subsection that the inverter controllers formulated in Problem 3.1.1 will guarantee the asymptotic stability of the closed-loop system. Hence, the stabilizability of the system (4.37) is confirmed.

As the system is stabilizable, there exists a state-feedback controller $\underline{K}:\ u = \underline{K}\ \underline{x}$ so that the closed-loop system is asymptotically stable. Moreover, as there is no feedback control action for the dynamic load S, the controller $\underline{K}$ should be forced to obtain the following form:

$$\underline{K} = [K\ \ 0_{2n\times 3}], \tag{4.39}$$

where $K = \mathrm{diag}(K_1,\ldots,K_n)$ is the controller for the inverter part of the system as defined in Problem 3.1.1. The zero submatrix of $\underline{K}$ is associated to the states of the dynamic load S.

The controller $\underline{K}$ is actually an output-feedback controller as it does not feedback the states of the induction machine to inverter control inputs. It is shown as follows:

$$u(t) = \underline{K}\,\underline{x}(t) = [K\ \ 0]\begin{bmatrix} x(t) \\ x_s(t) \end{bmatrix} = K\underline{C}\,\underline{x}(t) = Kx(t) = Ky(t). \tag{4.40}$$

Therefore, in order to assure that every unstable mode is observable, it is necessary to check the *detectability* of the system (4.37).

Definition 4.1. [54] The system (4.37) is detectable if $(\underline{A} + L\underline{C})$ is asymptotically stable for some L. □

The system (4.37) is detectable if and only if the matrix $\begin{bmatrix} \underline{A} - \lambda I \\ \underline{C} \end{bmatrix}$ has full-column rank for all eigenvalues λ of $\underline{A}$ with $Re\lambda \geq 0$ [54].

It is assumed above that the induction machine is asymptotically stable with negative real eigenvalues. Moreover, it is mentioned in (3.10) that the inverter part obtains n zero eigenvalues, where the other $2n$ eigenvalues are negative real. Thus, the task to check the dectectability of the system (4.37) is reduced to checking, whether $\begin{bmatrix} \underline{A} \\ \underline{C} \end{bmatrix}$ has full-column rank.

By investigating the $(6n+3)\times(3n+3)$ matrix $\begin{bmatrix} \underline{A} \\ \underline{C} \end{bmatrix}$, it becomes apparent that its first $3n$ columns, each contains one nonzero element and one diagonal element of the identity matrix. All these nonzero elements appear in different positions of the respective columns, indicating

the linear independence of these columns. The last three columns of the matrix $\begin{bmatrix} \underline{A} \\ \underline{C} \end{bmatrix}$ contains the matrix A_s of the asymptotically stable induction machine. Hence, column rank of the matrix $\begin{bmatrix} \underline{A} \\ \underline{C} \end{bmatrix}$ is always $(3n+3)$, which implies the system detectability.

An overall closed-loop system consisting of the open-loop system (4.37) and the feedback control law $u(t) = \underline{K}\,\underline{x}(t)$ is as follows:

$$\dot{\underline{x}}(t) = (\underline{A} + \underline{B}\,\underline{K})\underline{x}(t). \tag{4.41}$$

Let $\underline{\mathcal{V}}(\underline{x}) = \underline{x}^T \underline{P}\,\underline{x} > 0$ be a Lyapunov function of the system (4.41), where $\underline{P} \in \mathbb{R}^{(3n+3)\times(3n+3)}$ is a symmetric positive definite matrix. According to Lyapunov's stability theorem 2.3, the asymptotic stability of the system (4.41) is guaranteed if $\dot{\underline{\mathcal{V}}}(\underline{x})$ is negative definite. $\dot{\underline{\mathcal{V}}}(\underline{x})$ is derived as follows:

$$\dot{\underline{\mathcal{V}}}(\underline{x}) = \dot{\underline{x}}^T \underline{P}\,\underline{x} + \underline{x}^T \underline{P}\,\dot{\underline{x}} = \underline{x}^T \big((\underline{A} + \underline{B}\,\underline{K})^T \underline{P} + \underline{P}(\underline{A} + \underline{B}\,\underline{K})\big)\underline{x}. \tag{4.42}$$

Forcing $\dot{\underline{\mathcal{V}}}(\underline{x})$ to be negative definite is equivalent to solving the following matrix inequality to design a controller $\underline{K}$. A resulting controller $\underline{K}$ guarantees the asymptotic stability of the system (4.41) if

$$\dot{\underline{\mathcal{V}}}(\underline{x}) < 0,\ \forall \underline{x} \neq 0 \quad \Leftrightarrow \quad (\underline{A} + \underline{B}\,\underline{K})^T \underline{P} + \underline{P}(\underline{A} + \underline{B}\,\underline{K}) < 0. \tag{4.43}$$

For an optimization purpose, an optimization objective $\underline{\gamma} > 0$ is introduced. With $\underline{\gamma} > 0$, the left-hand side matrix of the matrix inequality above can be forced to be "more" negative definite. This optimization procedure can be done as follows. Minimize $\underline{\gamma} > 0$ such that:

$$(\underline{A} + \underline{B}\,\underline{K})^T \underline{P} + \underline{P}(\underline{A} + \underline{B}\,\underline{K}) < -\frac{1}{\underline{\gamma}} I < 0 \tag{4.44a}$$

$$\Leftrightarrow \quad (\underline{A} + \underline{B}\,\underline{K})^T \underline{P} + \underline{P}(\underline{A} + \underline{B}\,\underline{K}) + \frac{1}{\underline{\gamma}} I < 0. \tag{4.44b}$$

According to the Schur complement (3.24), the matrix inequality above is equivalent to:

$$\begin{bmatrix} (\underline{A} + \underline{B}\,\underline{K})^T \underline{P} + \underline{P}(\underline{A} + \underline{B}\,\underline{K}) & I \\ I & -\underline{\gamma} I \end{bmatrix} < 0. \tag{4.45}$$

In order to design a controller $\underline{K}$ as defined in (4.39), the following variable transformation and variable constraints are taken:

$$\begin{aligned} \underline{\mathbf{X}} &= \underline{P}^{-1} = \mathrm{diag}(X_{11},\ldots,X_{nn},X_s) \in \mathbb{R}^{(3n+3)\times(3n+3)}, \\ \underline{\mathbf{Y}} &= \underline{K}\,\underline{P}^{-1} = [\mathrm{diag}(Y_{11},\ldots,Y_{nn}) \;\; 0_{2n\times 3}] \in \mathbb{R}^{2n\times(3n+3)}, \end{aligned} \tag{4.46}$$

where $X_s \in \mathbb{R}^{3\times 3}$, and $X_{ii} \in \mathbb{R}^{3\times 3}$, $Y_{ii} \in \mathbb{R}^{2\times 3}$, $i = 1,\ldots,n$. Note that because of the zero submatrix in the controller $\underline{K}$ in (4.39), $\underline{\mathbf{Y}}$ is defined to contain a zero submatrix.

By pre- and post-multiplying the left-hand side of the matrix inequality (4.45) with a symmetric positive definite matrix $\mathrm{diag}(\underline{P}^{-1},I)$, where $\underline{P}$ is block-diagonal, (4.45) can be equivalently transformed into the following LMI:

$$\begin{bmatrix} \underline{A}\,\underline{\mathbf{X}} + \underline{B}\,\underline{\mathbf{Y}} + (\underline{A}\,\underline{\mathbf{X}} + \underline{B}\,\underline{\mathbf{Y}})^T & \underline{\mathbf{X}} \\ \underline{\mathbf{X}} & -\underline{\gamma} I \end{bmatrix} < 0. \tag{4.47}$$

If the LMI above is feasible for $\underline{\mathbf{X}}$ and $\underline{\mathbf{Y}}$ with defined structures as in (4.46), there exists a positive definite matrix $\underline{P} = \underline{\mathbf{X}}^{-1} > 0$, which makes $\underline{\mathcal{V}}(\underline{x}) > 0$ and $\dot{\underline{\mathcal{V}}}(\underline{x}) < 0$. A resulting controller $\underline{K} = \underline{\mathbf{Y}}\,\underline{\mathbf{X}}^{-1}$ asymptotically stabilizes the overall microgrid (4.37). At the same time, as $\underline{\gamma} > 0$ is minimized, the controller $\underline{K}$ guarantees that the investigated upper bound of $\dot{\underline{\mathcal{V}}}(\underline{x})$ is the most negative. On the other hand, the LMI (4.47) also becomes more conservative as $\underline{\gamma}$ decreases.

With predefined structures of $\underline{\mathbf{X}}$ and $\underline{\mathbf{Y}}$ in (4.46), a resulting $\underline{K}$ obtains the defined structure in (4.39), where K is a block-diagonal controller for the inverter part. The constraints in (4.46) introduce conservatism to the LMI (4.47).

The LMI optimization problem can be summarized as follows:

$$\texttt{minimize } \underline{\gamma} \texttt{ such that } \begin{cases} \texttt{LMI } (4.47) \texttt{ is feasible over } \underline{\mathbf{X}} \texttt{ and } \underline{\mathbf{Y}}, \\ \underline{\mathbf{X}} \texttt{ and } \underline{\mathbf{Y}} \texttt{ are defined as in } (4.46), \\ \underline{\mathbf{X}} > 0, \\ 0 < \underline{\gamma}. \end{cases} \tag{4.48}$$

4.4.2 Robust stability with the small-gain theorem

The previous subsection considers the asymptotic stability of the microgrid, when parameters of the dynamic load are precisely known beforehand. As mentioned in Remark 4.2.2, it is nontrivial to determine parameters of the induction machine, as it does not concern a particular induction machine but an aggregated dynamic load. A controller design should take parametric uncertainties of the induction machine into consideration. This subsection presents a robust

controller design in the sense that for an *upper bound* of the dynamic load, a block-diagonal controller K should be designed to guarantee the asymptotic stability of the overall system.

The system (4.32) shows the interconnection between inverters and the dynamic load S. One useful tool in studying stability of interconnected systems is the small-gain theorem, see e.g., [54–57, 89]. A system gain allows to track how a norm of a signal increases or decreases as it passes through the system. In this section, based on the small-gain theorem, an LMI stability condition is derived to design state-feedback controllers for inverters, which asymptotically stabilize the inverter part despite influences of the dynamic load S.

In order to describe an amplifying gain between input and output vectors of a MIMO system, the definition of singular values is introduced.

Definition 4.2. [56] Consider a fixed frequency ω, where $G(j\omega)$ is a constant $(n \times m)$ complex matrix. The singular values of $G(j\omega)$ are denoted by $\sigma_i \geq 0$, $i = 1,\ldots,\min(n,m)$, which are computed as follows:

$$\sigma_i(G) = \sqrt{\gamma_i(G^H G)}, \tag{4.49}$$

where γ_i is an eigenvalue and G^H is the complex conjugate transpose of G. A maximum singular value is denoted by $\bar{\sigma}$ and a minimum singular value is denoted by $\underline{\sigma}$. □

In this subsection, the $\mathcal{H}_\infty$ norm will be implemented to specify a peak gain of a transfer function matrix. The definition of the $\mathcal{H}_\infty$ norm is given in the following.

Definition 4.3. [54–56] Consider a proper linear asymptotically stable system $G(s)$, whose frequency response is $G(j\omega)$. The $\mathcal{H}_\infty$ norm of $G(s)$ is equal to

$$\|G(s)\|_\infty = \max_\omega \bar{\sigma}(G(j\omega)), \tag{4.50}$$

where $\|\cdot\|_\infty$ denotes the $\mathcal{H}_\infty$ norm. □

A closed-loop system consisting of (4.32) and a feedback control law $u(t) = Kx(t)$ as defined in (3.11) is as follows:

$$\begin{cases} \dot{x}(t) &= (A+BK)x(t) + Tx_s(t), \\ \dot{x}_s(t) &= (B_sK + T_s)x(t) + A_s x_s(t). \end{cases} \tag{4.51}$$

Denote the Laplace transforms of $x(t)$ and $x_s(t)$ by $X(s)$ and $X_s(s)$, respectively. From the state-space model above, the transfer function matrices $G_{\text{inv}}(s)$ from $X_s(s)$ to $X(s)$ and $G_s(s)$

from $X(s)$ to $X_s(s)$ are derived as follows:

$$\begin{aligned} G_{\text{inv}}(s) &= (sI - A - BK)^{-1}T, \\ G_s(s) &= (sI - A_s)^{-1}(B_sK + T_s), \end{aligned} \tag{4.52}$$

where $G_{\text{inv}}(s)$ is a $3n \times 3$ transfer function matrix, and $G_s(s)$ is a $3 \times 3n$ transfer function matrix.

The interconnected system (4.51) can be considered as a feedback connection between inverters and the dynamic load S as shown in Figure 4.6.

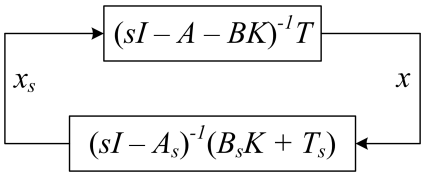

FIGURE 4.6: Feedback connection between inverters and a dynamic load S.

The feedback connection in Figure 4.6 can be rearranged as displayed in Figure 4.7.

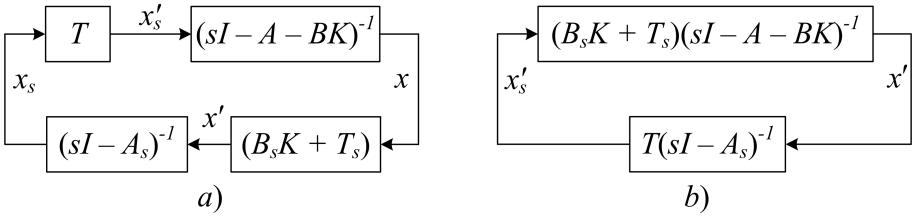

FIGURE 4.7: Rearranged feedback connection between inverters and a dynamic load S.

In Figure 4.7, the two states x' and x'_s are introduced only for the theory presentation. Let $X'(s)$ and $X'_s(s)$ be the Laplace transforms of x' and x'_s, respectively. Denote the transfer function matrices from $X'_s(s)$ to $X'(s)$ and from $X'(s)$ to $X'_s(s)$ by $G'_{\text{inv}}(s)$ and $G'_s(s)$, respectively. Then,

$$\begin{aligned} G'_{\text{inv}}(s) &= (B_sK + T_s)(sI - A - BK)^{-1}, \\ G'_s(s) &= T(sI - A_s)^{-1}. \end{aligned} \tag{4.53}$$

As the eigenvalues of matrix A_s are assumed to be in the open left-half plane. This indicates the asymptotic stability of the system $G'_s(s) = T(sI - A_s)^{-1}$, where T in (4.53) is a constant matrix. $\mathcal{H}_\infty$ norms of $(sI - A_s)^{-1}$ and $T(sI - A_s)^{-1}$ are defined.

According to the small-gain theorem, see e.g., [55, 57, 89], the feedback connection in Figure 4.7b is asymptotically stable if:

$$\begin{cases} G'_{\text{inv}}(s) \text{ and } G'_s(s) \text{ are asymptotically stable,} \\ \|G'_{\text{inv}}(s)G'_s(s)\|_\infty < 1. \end{cases} \tag{4.54}$$

Let $\gamma'_{\text{inv}} = \|G'_{\text{inv}}(s)\|_\infty$ and $\gamma'_s = \|G'_s(s)\|_\infty$. A more conservative version of the small-gain theorem (4.54) is inferred as follows:

$$\begin{cases} G'_{\text{inv}}(s) \text{ and } G'_s(s) \text{ are asymptotically stable,} \\ \|G'_{\text{inv}}(s)\|_\infty < \dfrac{1}{\|G'_s(s)\|_\infty} \;\Leftrightarrow\; \gamma'_{\text{inv}} < \dfrac{1}{\gamma'_s}. \end{cases} \tag{4.55}$$

Remark 4.4.1. The stability condition (4.54) concerns the frequency response of the overall system along the frequency axis, whereas the condition (4.55) involves the maximal gains γ'_{inv} and γ'_s of different separate parts of the system. Therefore, the stability condition (4.55) is a more conservative version of the small-gain theorem. $\mathcal{H}_\infty$ norm is submultiplicative, i.e. for asymptotically stable $G'_{\text{inv}}(s)$ and $G'_s(s)$, $\|G'_{\text{inv}}(s)G'_s(s)\|_\infty \leq \|G'_{\text{inv}}(s)\|_\infty \|G'_s(s)\|_\infty$. This leads to a more conservative result in the controller design presented hereafter.

With the assumption on the asymptotic stability of $G'_s(s)$, if the controller K asymptotically stabilizes $G'_{\text{inv}}(s)$ and decreases γ'_{inv} so that the condition (4.55) is satisfied, the feedback connection between inverters and the dynamic load S in Figure 4.7b will be asymptotically stable. Via the following theorem, an LMI-based controller design is proposed, which guarantees the asymptotic stability of $G'_{\text{inv}}(s)$, and simultaneously restricts the $\mathcal{H}_\infty$ norm $\gamma'_{\text{inv}} = \|G'_{\text{inv}}(s)\|_\infty$ so that $\gamma'_{\text{inv}} < \gamma_{\max} < \frac{1}{\gamma'_s}$.

Theorem 4.4. *Consider the transfer function matrix $G'_{inv}(s)$ in (4.53). Let $P_{ii} \in \mathbb{R}^{3\times 3}$, $i = 1,\ldots,n$, be symmetric positive definite matrices and $P = diag(P_{11},\ldots,P_{nn}) \in \mathbb{R}^{3n\times 3n}$, where n is the number of inverters in the microgrid. Define the variables $\mathbf{X}$ and $\mathbf{Y}$ as in (3.16). Then, a block-diagonal controller $K = \mathbf{Y}\mathbf{X}^{-1} \in \mathbb{R}^{2n\times 3n}$ guarantees the asymptotic stability of $G'_{inv}(s)$, and the $\mathcal{H}_\infty$ norm $\|G'_{inv}(s)\|_\infty = \gamma'_{inv}$ is less than an optimization objective $\gamma_{max} > 0$ if the following LMI is feasible:*

$$\begin{bmatrix} A\mathbf{X}+B\mathbf{Y}+(A\mathbf{X}+B\mathbf{Y})^T & I & (B_s\mathbf{Y}+T_s\mathbf{X})^T \\ I & -\gamma_{max}I & 0 \\ B_s\mathbf{Y}+T_s\mathbf{X} & 0 & -\gamma_{max}I \end{bmatrix} < 0. \tag{4.56}$$

Proof. The proof of Theorem 4.4 is based on the Bounded Real Lemma, see e.g., [54, 135], which implies that for a system represented by a quadruple of matrices (A,B,C,D), whose transfer function matrix is $G(s) = C(sI-A)^{-1}B+D$, the matrix A is Hurwitz and the $\mathcal{H}_\infty$ norm $\|G(s)\|_\infty$ is less than $\gamma_{\max}$ if and only if there exists a symmetric positive definite matrix P such that:

$$\begin{bmatrix} A^TP+PA & PB & C^T \\ B^TP & -\gamma_{\max}I & D^T \\ C & D & -\gamma_{\max}I \end{bmatrix} < 0. \tag{4.57}$$

If the matrix inequality above is satisfied with some symmetric $P > 0$, then $(A^T P + PA)$ is also negative definite, which indicates that all the eigenvalues of A obtain negative real parts, i.e., A is a Hurwitz matrix by Definition 2.6.

By applying the Bounded Real Lemma to the transfer function matrix $G'_{\text{inv}}(s)$ in (4.53), finding $\gamma_{\max} > 0$ such that $G'_{\text{inv}}(s)$ is asymptotically stable and $\|G'_{\text{inv}}(s)\|_\infty = \gamma'_{\text{inv}} < \gamma_{\max}$ is equivalent to checking the feasibility of the following matrix inequality:

$$\begin{bmatrix} (A+BK)^T P + P(A+BK) & P & (B_s K + T_s)^T \\ P & -\gamma_{\max} I & 0 \\ B_s K + T_s & 0 & -\gamma_{\max} I \end{bmatrix} < 0. \tag{4.58}$$

The matrix inequality (4.58) cannot be solved directly by available LMI tools because of the products of variables in $P(A+BK)$. By pre- and post-multiplying (4.58) by a symmetric positive definite matrix $\text{diag}(P^{-1}, I, I)$, where P is a block-diagonal matrix, the following is derived equivalently to (4.58):

$$\begin{bmatrix} P^{-1}(A+BK)^T + (A+BK)P^{-1} & I & P^{-1}(B_s K + T_s)^T \\ I & -\gamma_{\max} I & 0 \\ (B_s K + T_s)P^{-1} & 0 & -\gamma_{\max} I \end{bmatrix} < 0. \tag{4.59}$$

Then, by using the variable transformations $P^{-1} = \mathbf{X}$ and $KP^{-1} = \mathbf{Y}$ as defined in (3.16), the LMI (4.56) is derived equivalently to (4.59). Note that this change of variables does not introduce any conservatism to the LMI.

If the LMI (4.56) is feasible with $\mathbf{X} > 0$ and $\gamma_{\max} > 0$, the matrix inequality (4.58) is also feasible, which infers that $(A+BK)^T P + P(A+BK) < 0,\ P > 0$. This infers the asymptotic stability of the closed-loop inverter system.

Additionally, by virtue of the Bounded Real Lemma, if the LMI (4.56) is feasible, the $\mathcal{H}_\infty$ norm $\|G'_{\text{inv}}(s)\|_\infty = \gamma'_{\text{inv}}$ satisfies $0 \le \gamma'_{\text{inv}} < \gamma_{\max}$. The theorem is proved. □

In the feedback connection in Figure 4.7b, the $\mathcal{H}_\infty$ norm $\|G'_s(s)\|_\infty = \gamma'_s$ can be calculated in advance. By solving the LMI (4.56) with $\gamma_{\max}$ such that $0 < \gamma_{\max} < \frac{1}{\gamma'_s}$, a feasible controller will guarantee the asymptotic stability of the inverter closed-loop system and force the $\mathcal{H}_\infty$ norm γ'_{inv} to be less than $\gamma_{\max} < \frac{1}{\gamma'_s}$. According to the small-gain theorem (4.55), the asymptotic stability of the overall microgrid (4.51) is guaranteed as $\gamma'_{\text{inv}}\gamma'_s < \gamma_{\max}\gamma'_s < 1$.

The LMI optimization problem can be summarized as follows:

$$\texttt{minimize } \gamma_{\max} \texttt{ such that } \begin{cases} \texttt{LMI } (4.56) \texttt{ is feasible over } \mathbf{X} \texttt{ and } \mathbf{Y}, \\ \mathbf{X} \texttt{ and } \mathbf{Y} \texttt{ are defined as in } (3.16), \\ \mathbf{X} > 0, \\ 0 < \gamma_{\max} < \dfrac{1}{\gamma'_s} = \dfrac{1}{\|G'_s(s)\|_\infty}. \end{cases} \tag{4.60}$$

Remark 4.4.2. Because of the block-diagonal structure of $\mathbf{X}$ and $\mathbf{Y}$, the LMI (4.56) is a sufficient condition of the matrix inequality (4.58). Furthermore, the LMI condition (4.56) becomes more conservative if $\gamma_{\max}$ decreases.

4.5 Simulation study

In this section, an academic example is provided to validate the effectiveness of the proposed system modeling and the two LMI optimization problems to design inverter controllers. Consider the microgrid shown in Figure 4.8, which consists of two inverters, constant impedance loads and an induction machine S. Parameters of the test system are provided in Table 4.1. In the simulation, a large industrial induction machine is adopted with parameters recommended by the IEEE in [136].

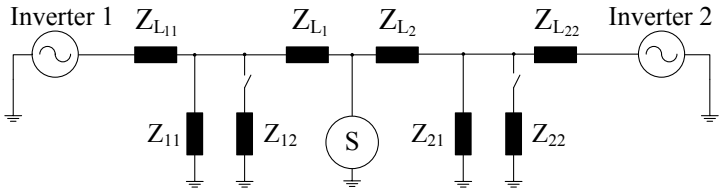

FIGURE 4.8: Test system with two inverters, impedance loads and an induction machine S.

The linearized model of the overall microgrid (4.32) is obtained (see Appendix A.5). After the linearization, the asymptotic stability of $G'_s(s)$ is verified by checking whether A_s is a Hurwitz matrix. For this particular example, A_s is Hurwitz with eigenvalues in the range $[-1.3814 \pm j6.2930, -0.008]$ and $G'_s(s)$ is asymptotically stable. The maximum singular value of $G'_s(j\omega)$ is calculated. In this example, the peak gain of $G'_s(j\omega)$ is $\gamma'_s = 8.75$ (see Figure 4.9), which is equal to the $\mathcal{H}_\infty$ norm of $G'_s(s)$ as $G'_s(s)$ is asymptotically stable.

For comparison purpose, inverter controllers will be designed by solving the two LMI optimization problems (4.48) and (4.60). The LMI problems are solved by using the Yalmip toolbox and SeDuMi solver in Matlab. By solving the LMI optimization problem (4.48), the following

TABLE 4.1: Test system parameters for simulation with dynamic loads

Voltages and phase angles	$V_{1_0} = 1029[\text{V}]$ $V_{2_0} = 1030 + 1.3i[\text{V}]$	$\delta_{1_0} = 0.005[\text{rad}]$ $\delta_{2_0} = 0.0035[\text{rad}]$
Active and reactive powers	$\tilde{P}_{1_0} = 16.7[\text{kW}]$ $\tilde{P}_{2_0} = 19.5[\text{kW}]$	$\tilde{Q}_{1_0} = 31.4[\text{kVar}]$ $\tilde{Q}_{2_0} = 34.8[\text{kVar}]$
Nominal frequency	$\omega_{\text{nom}} = 2\pi f_{\text{base}}[\text{rad/s}]$	$f_{\text{base}} = 50[Hz]$
Base values	$S_{\text{base}} = 10.8[\text{MVA}]$ $Z_{\text{base}} = 0.09823[\Omega]$ $\omega_{\text{base}} = \omega_{\text{nom}}$	$V_{\text{base}} = 1030[\text{V}]$ $\delta_{\text{base}} = 1[\text{rad}]$ $L_{\text{base}} = 0.00031[\text{H}]$
Load impedances	$Z_{11} = 58 + i10.8[\Omega]$ $Z_{12} = 25 + i25[\Omega]$	$Z_{21} = 45 + i28[\Omega]$ $Z_{22} = 28 + i23[\Omega]$
Line impedances	$Z_{L_1} = 0.3 + i0.3[\Omega]$ $Z_{L_{11}} = 0.3 + i0.3[\Omega]$	$Z_{L_2} = 0.3 + i0.3[\Omega]$ $Z_{L_{22}} = 0.3 + i0.3[\Omega]$
Inertia constants	$H_1 = 0.6$	$H_2 = 0.8$
Filter parameter	$\tau_1 = 0.0265[\text{s}]$	$\tau_2 = 0.0265[\text{s}]$
Polynomial model	$p_{1_1} = p_{1_2} = 0.4, p_{1_3} = 0.2$ $p_{2_1} = p_{2_2} = 0.3, p_{2_3} = 0.4$	$q_{1_1} = q_{1_2} = 0.4, q_{1_3} = 0.2$ $q_{2_1} = q_{2_2} = 0.3, q_{2_3} = 0.4$
Induction machine parameters	$R_s = 0.1277[\Omega]$ $R_r = 0.0884[\Omega]$ $H_s = 1.5[J(kg.m^2)]$ $\omega_{r_0} = 2\pi 49.8[\text{rad/s}]$ $\mathcal{T}_{m_0} = 200[N.m]$	$L_s = 0.0021[H]$ $L_r = 0.0053[H]$ $L_m = 0.1188[H]$ $a_r = 1, b_r = 0, c_r = 0$

inverter controllers are obtained with $\underline{\gamma} = 0.0001$:

$$K_1 = \begin{bmatrix} -41.0218 & 0.0806 & -6.3772 \\ 0.0381 & -0.0010 & -0.0001 \end{bmatrix}, \; K_2 = \begin{bmatrix} -41.3265 & 1.8712 & -4.5181 \\ -0.0342 & -0.0008 & -0.0001 \end{bmatrix}, \quad (4.61)$$

and their equivalences in actual quantities are as follows:

$$\begin{aligned} K_1 &= \begin{bmatrix} -41.02[\frac{1}{s}] & 0.74 \cdot 10^{-5}[\frac{\text{rad}}{\text{skW}}] & -6.38 \cdot 10^{-4}[\frac{\text{rad}}{\text{skVar}}] \\ 39.15[\frac{\text{V}}{\text{rad}}] & -10^{-4}[\frac{\text{V}}{\text{kW}}] & -10^{-5}[\frac{\text{V}}{\text{kVar}}] \end{bmatrix}, \\ K_2 &= \begin{bmatrix} -41.33[\frac{1}{s}] & 1.73 \cdot 10^{-4}[\frac{\text{rad}}{\text{skW}}] & -4.16 \cdot 10^{-4}[\frac{\text{rad}}{\text{skVar}}] \\ -35.22[\frac{\text{V}}{\text{rad}}] & -7.5 \cdot 10^{-5}[\frac{\text{V}}{\text{kW}}] & -10^{-5}[\frac{\text{V}}{\text{kVar}}] \end{bmatrix}. \end{aligned} \quad (4.62)$$

The maximum gain γ_s' of the transfer function matrix $G_s'(s)$ should be computed before solving the LMI problem (4.60). In this example, $\gamma_s' = 8.75$. By solving the LMI optimization problem (4.60), the following inverter controllers are derived with $\gamma_{\max} = 0.098$:

$$K_1 = \begin{bmatrix} -10.1229 & 2.1384 & -10.9608 \\ -0.0562 & 1.3916 & 0.2047 \end{bmatrix}, \; K_2 = \begin{bmatrix} -13.9681 & 1.3435 & -5.4928 \\ -0.0619 & 1.3386 & 0.2092 \end{bmatrix}, \quad (4.63)$$

and their equivalences in actual quantities are as follows:

$$K_1=\begin{bmatrix} -10.13[\frac{1}{s}] & 1.95\cdot 10^{-4}[\frac{\text{rad}}{\text{skW}}] & -10^{-3}[\frac{\text{rad}}{\text{skVar}}] \\ -57.9[\frac{\text{V}}{\text{rad}}] & 0.132[\frac{\text{V}}{\text{kW}}] & 0.0195[\frac{\text{V}}{\text{kVar}}] \end{bmatrix}, K_2=\begin{bmatrix} -14[\frac{1}{s}] & 1.2\cdot 10^{-4}[\frac{\text{rad}}{\text{skW}}] & -0.5\cdot 10^{-3}[\frac{\text{rad}}{\text{skVar}}] \\ -63.8[\frac{\text{V}}{\text{rad}}] & 0.128[\frac{\text{V}}{\text{kW}}] & 0.02[\frac{\text{V}}{\text{kVar}}] \end{bmatrix}. \tag{4.64}$$

The inverter controllers (4.64) force the $\mathcal{H}_\infty$ norm $\gamma'_{\text{inv}} = 0.061 < \gamma_{\max} < 0.1143 = \frac{1}{\gamma'_s}$. According to the small-gain theorem, K_1, K_2 in (4.64) guarantee the asymptotic stability of the closed-loop microgrid in Figure 4.7b. Maximum singular values of the frequency responses $G'_{\text{inv}}(j\omega)$ and $G'_s(j\omega)$, where $G'_{\text{inv}}(j\omega)$ is calculated with the controllers (4.64), are presented in Figure 4.9.

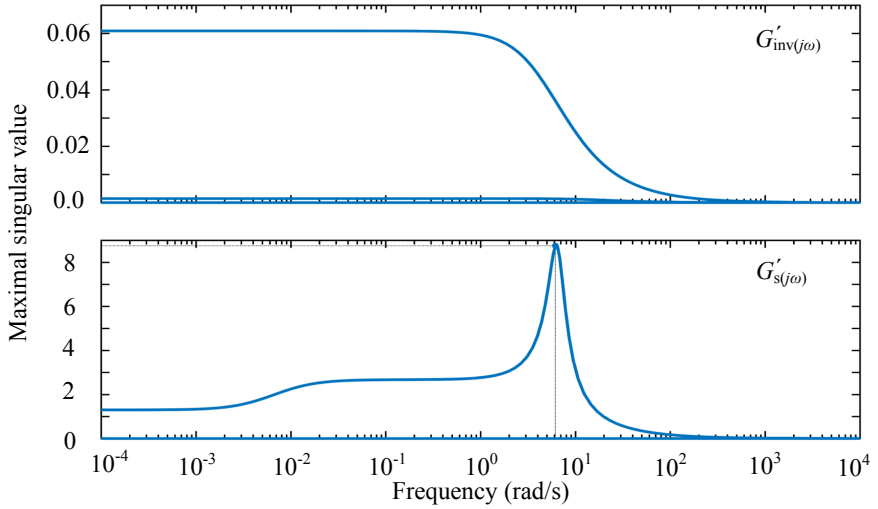

FIGURE 4.9: Maximum singular values of the frequency responses $G'_{\text{inv}}(j\omega)$ and $G'_s(j\omega)$.

Simulation is conducted in Matlab with the two controller pairs (4.62) and (4.64). A sequence of discrete events separated by time intervals is included in the simulation according to the following scenario: initially, Z_{11}, Z_{21} and the induction machine are connected to the system; at $t = 25[s]$, the mechanical torque of the induction machine is increased; at $t = 50[s]$ and $t = 75[s]$, Z_{12} and Z_{22} are successively connected to the system in the written order.

The simulation results with the controller pair (4.62) are presented in Figure 4.10. Figure 4.11 shows the simulation results of the system with the controller pair (4.64). It is seen that the microgrid is robustly stabilized under load uncertainties and load dynamics by both controller pairs.

At $t = 25[s]$, the mechanical torque $\mathcal{T}_m$ is changed, which indicates an increase of the power consumed by the induction machine. Consequently, the rotor speed is slightly changed and reaches a new equilibrium. Because of the change of the machine mechanical torque, there are transient oscillations of the rotor speed and the electrical torque. These oscillations cause slight oscillations of the inverter variables (voltage magnitudes and frequencies). This effect demonstrates the feedback influence of dynamic loads of the system stability.

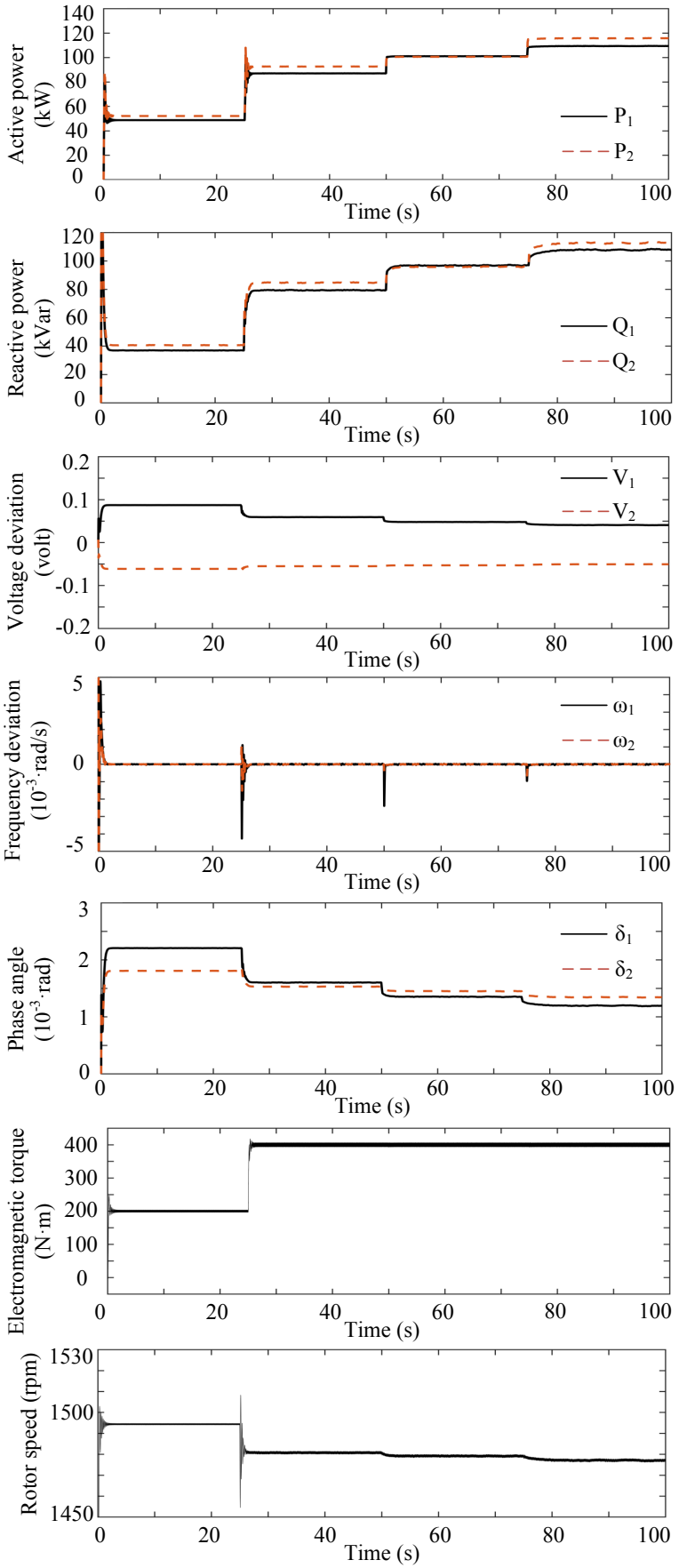

FIGURE 4.10: Transfer processes of the test system with the controller pair (4.62).

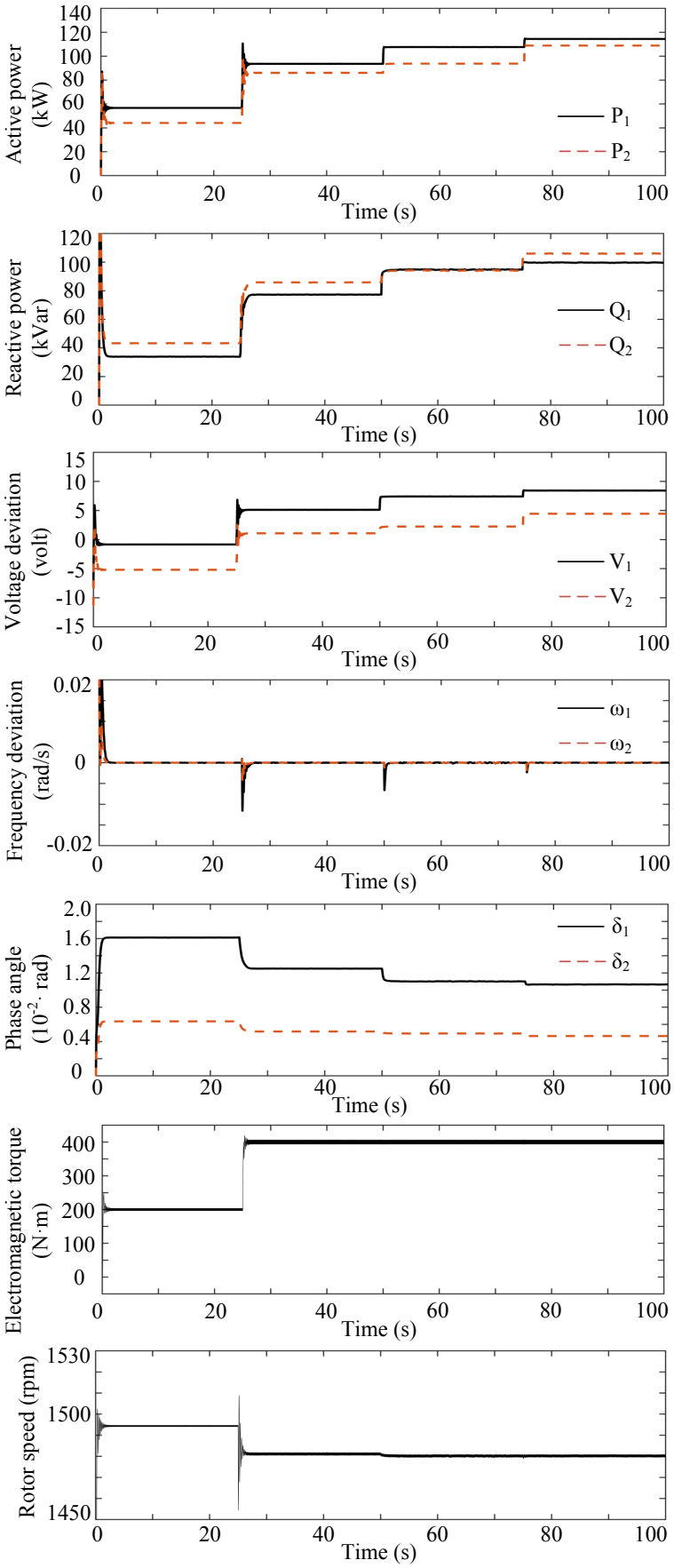

FIGURE 4.11: Transfer processes of the test system with the controller pair (4.64).

It is seen in Figures 4.10 and 4.11 that inverter output frequencies robustly converge to the nominal value, while voltage magnitudes vary around their nominal values. Because of load changes, steady-state deviations of voltage magnitudes are experienced. Steady-state deviations of voltage magnitudes caused by the controller pair (4.62) are relatively small. However, with the controller pair (4.64), the maximal steady-state magnitude deviation of voltages is approximately $8[V]$. Hence, voltage performance of the controller pair (4.64), designed by implementing the small-gain theorem (4.55), is worse compared to the controller pair (4.62), which is reflected by larger voltage magnitude deviations. Worse performance of the controller pair (4.64) can be explained by the conservatism of the small-gain theorem mentioned in Remark 4.4.1. Although magnitude deviation of $8[V]$ is still acceptable for most of conventional loads, there exists a possibility that (steady-state) magnitude deviations of voltages become even larger if larger load changes are applied to the system. Voltage performance will be considered in Chapter 5 to reduce steady-state magnitude deviations of voltages, which are caused by uncertainties. Steady-state magnitude deviations of voltages in the simulations illustrate the motivation for the use of the polynomial (voltage dependent) load model (4.2).

4.6 Summary

Load modeling has been investigated in the sense of voltage dependence and feedback influence of load dynamics. A combination of a polynomial load model and an induction machine model was chosen for load modeling in stability analysis of microgrids. A standard model of an induction machine was presented. An induction machine is considered as an active node in a microgrid. Based on the assumption on the Center of inertia and the implementation of several variable replacements, a modified model of an induction machine was proposed, which can be combined with the inverter model. A linearized state-space model of an overall microgrid was derived, which shows the interconnection between loads and inverters.

Two separate LMI stability conditions based on Lyapunov's stability theorem and the small-gain theorem were proposed to guarantee the asymptotic stability of the overall microgrid with dynamic loads. An academic example was presented to validate the system modeling and the effectiveness of the LMI stability conditions. The simulation results show that the overall system is robustly stabilized against load dynamics and load changes.

Thus far, the stability of microgrids against load dynamics and small load changes has been investigated. In the following, the control goal is extended so that microgrids must be stabilized, being subjected to larger load and line uncertainties. At the same time, inverters must still provide sufficient performance of voltages and frequencies to supply connected loads.

Chapter 5

Voltage performance control based on $\mathcal{H}_\infty$ control technique

In previous chapters, LMI stability conditions were proposed to design decentralized controllers of inverters in a microgrid, which asymptotically stabilize the inverters as well as compensate the feedback influence of dynamic loads on the overall system stability. The control approach guarantees zero steady-state frequency deviations. However, the voltage magnitude is defined as a control input of the power control loop of an inverter and should vary around a nominal value to modify the output power. Therefore, if a microgrid is subjected to load uncertainties during operation, these can negatively affect the stability of the system as well as the voltage performance in the sense of magnitude deviations and higher-frequency harmonics.

As reported in detail in literature [33, 70, 76, 137–141], voltages in power systems can contain higher-frequency harmonics, which are caused by the nonlinear nature of loads. Besides, it is seen in Equation (3.15) that load changes cause variations of voltage magnitudes. As stated in Chapter 2, according to grid-code requirements, see e.g., [59, 60], magnitude deviations of voltages as well as their total harmonic distortions (THD) should not exceed acceptable limits to sustain smooth and secure functionality of connected loads [142–144].

In this chapter, the robust stability of a microgrid and the robust performance of inverter output voltages are studied in the $\mathcal{H}_\infty$ control framework [54–56, 89]. First, a model of a microgrid with uncertainties is proposed. An additive model uncertainty caused by uncertain admittances in a microgrid is introduced. The $\mathcal{H}_\infty$ control technique used in this chapter requires that model uncertainty must be asymptotically stable [54, 56, 89]. In order to ensure that the considered model uncertainty is asymptotically stable, the inverter model (3.3) is slightly modified via a modification of the power control loop in Chapter 3 (see Figure 3.1). Accordingly, a modified inverter model is introduced and implemented in the $\mathcal{H}_\infty$ control in this chapter. Furthermore, a general control problem is formulated, where a generalized plant model of a microgrid with

possible uncertainties is presented. For robust controller design purpose, weight functions are introduced in the generalized plant model of a microgrid in order to specify requirements on the system robustness and the voltage performance. By using the $\mathcal{H}_\infty$ control technique, conditions for the robust stability and robust performance of a microgrid are introduced. Based on an $\mathcal{H}_\infty$ norm condition for robust performance, an LMI optimization problem is proposed. The LMI problem is relatively conservative. However, by solving a single LMI optimization problem, resulting decentralized inverter controllers simultaneously target several control goals: nominal stability, robust stability against model uncertainty, robust performance of voltage magnitudes against model uncertainty and changes of reference inputs (by a higher control level).

Remark 5.0.1. There exists a special $\mathcal{H}_\infty$ problem called the normalized left coprime factorization (NLCF), see e.g. [55] for more details. The NLCF design does not require asymptotically stable model uncertainties, which is an advantage over the standard $\mathcal{H}_\infty$ problem implemented in this chapter. A resulting controller $K(s)$ of the NLCF design has the following form [55]:

$$K(s) = W_e(s)K_w(s)W_a(s), \tag{5.1}$$

where $K_w(s)$ is a resulting transfer function matrix of a suboptimal $\mathcal{H}_\infty$ problem, $W_e(s)$ and $W_a(s)$ are weighting transfer function matrices. In general $K(s)$ in (5.1) is a dynamic controller, unless W_e, W_a are restricted to be constant real and a constant real K_w is derived. However, as a static controller with a predefined structure is designed in this chapter, the NLCF method is, therefore, not further investigated.

Regarding the voltage THD issue, by selecting suitable weight functions for voltages, resulting inverter controllers can reduce their higher-harmonic components. However, as the stability and performance analysis in this chapter is provided based on a linearized system model, no further statement can be made about the THD of inverter output voltages.

5.1 Modeling of microgrids with uncertainties

During operation microgrids can be perturbed by many factors, which may cause system instability and insufficient voltage performance. Thus, inverter controllers must compensate possible uncertainties. In order to include uncertainties in controller design, a model of microgrids with uncertainties is developed in this section. A derived system model allows to propose a controller design for robust stability and robust performance in the next section. The considered uncertainties are an *additive* uncertainty (a model uncertainty), which represents parametric uncertainties of loads and lines, and reference input changes by a higher control level (a disturbance input, i.e., signal uncertainty).

An additive model uncertainty represents an influence of impedance changes on stability of a microgrid. Load and line conditions of a microgrid can be arbitrarily changed during operation, which result in uncertain admittance matrices with elements $(Y_{ik} + \Delta Y_{ik})$, $i,k = 1,\ldots,n$. ΔY_{ik} physically represents variations of loads and lines from their initial values Y_{ik}. Accordingly, power flow equations with uncertain admittances can be derived similarly to the nominal power flow equations (2.9) by replacing Y_{ik} by $(Y_{ik} + \Delta Y_{ik})$, $i,k = 1\ldots,n$.

As will be shown later in this section, in order to derive a model uncertainty, which is caused by uncertain admittances ΔY_{ik}, $i,k = 1,\ldots,n$, power flow equations (2.9) will be linearized around a nominal equilibrium point. A resulting transfer function matrix is a matrix sum of a nominal transfer function matrix and an additive uncertainty. The asymptotic stability of an uncertain system under an additive uncertainty can be directly assessed if the transfer function matrices of both nominal and uncertain systems are asymptotically stable. For this purpose, a modification of the power control loop in Figure 3.1 is made. A new power control loop is presented in Figure 5.1.

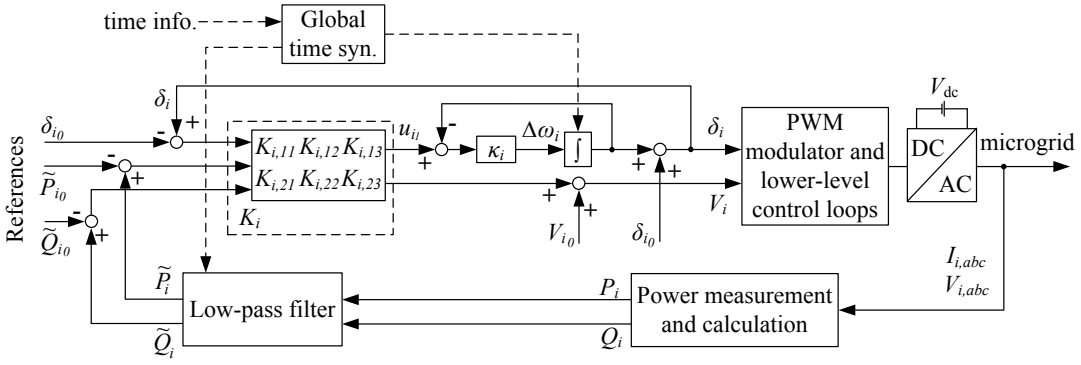

FIGURE 5.1: A modified power control loop of an inverter.

It is seen that the control loop in Figure 5.1 consists of an additional *subordinate* control loop for the first control input $u_{i_1}(t)$. This is also the only difference between the two control loops in Figure 3.1 and Figure 5.1. Based on the power control loop in Figure 5.1, the transfer function of the subordinate control loop is calculated as follows:

$$G_{\rm sub}(s) = \frac{\kappa_i}{s + \kappa_i}, \tag{5.2}$$

where $\kappa_i \in \mathbb{R}$, $\kappa_i > 0$. The constant κ_i is chosen to be positive so that the subordinate control loop $G_{\rm sub}(s)$ is asymptotically stable.

Hence, the subordinate control loop (5.2) replaces the integrator in (3.3), which causes zero eigenvalues of the open-loop microgrid (3.6). Based on the inverter model (3.3) and the subordi-

nate control loop (5.2), a modified inverter model is derived as follows:

$$\begin{cases} \dot{\delta}_i &= -\kappa_i(\delta_i - \delta_{i_0}) + \kappa_i u_{i_1}, \\ \dot{\tilde{P}}_i &= \dfrac{-\tilde{P}_i + P_i(V_1,\ldots,V_n,\delta_1,\ldots,\delta_n)}{\tau_i}, \\ \dot{\tilde{Q}}_i &= \dfrac{-\tilde{Q}_i + Q_i(V_1,\ldots,V_n,\delta_1,\ldots,\delta_n)}{\tau_i}. \end{cases} \tag{5.3}$$

A state variable $x_i(t)$ and an output $y_i(t)$ of the inverter model above are chosen as in (3.4), except the control inputs $u_i(t)$ and $u(t)$, which become as follows:

$$u_i(t) = [u_{i_1} \;\; V_i - V_{i_0}]^T, \quad u(t) = [u_1(t)^T \;\ldots\; u_n(t)^T]^T. \tag{5.4}$$

By linearizing the modified inverter model (5.3) around the equilibrium point (3.5), the following LTI state-space model of a microgrid is derived:

$$\begin{cases} \dot{x}(t) &= \tilde{A}x(t) + \tilde{B}u(t), \\ y(t) &= Cx(t) = x(t), \end{cases} \tag{5.5}$$

and an inverter i is associated to one subsystem of (5.5) with the following state-space model:

$$\dot{x}_i(t) = \tilde{A}_{ii}x_i(t) + \tilde{B}_{ii}u_i(t) + \sum_{\substack{k=1 \\ k\neq i}}^{n} \Big(A_{ik}x_k(t) + B_{ik}u_k(t)\Big), \quad i = 1,\ldots,n, \tag{5.6}$$

where $\tilde{A} \in \mathbb{R}^{3n\times 3n}, \tilde{B} \in \mathbb{R}^{3n\times 2n}, C = I_{3n\times 3n}$ is an identity matrix, and

$$\tilde{A}_{ii} = \begin{bmatrix} -\kappa_i & 0 & 0 \\ \left.\frac{\partial P_i}{\tau_i \partial \delta_i}\right|_0 & \frac{-1}{\tau_i} & 0 \\ \left.\frac{\partial Q_i}{\tau_i \partial \delta_i}\right|_0 & 0 & \frac{-1}{\tau_i} \end{bmatrix}, \tilde{B}_{ii} = \begin{bmatrix} \kappa_i & 0 \\ 0 & \left.\frac{\partial P_i}{\tau_i \partial V_i}\right|_0 \\ 0 & \left.\frac{\partial Q_i}{\tau_i \partial V_i}\right|_0 \end{bmatrix}, A_{ik} = \begin{bmatrix} 0 & 0 & 0 \\ \left.\frac{\partial P_i}{\tau_i \partial \delta_k}\right|_0 & 0 & 0 \\ \left.\frac{\partial Q_i}{\tau_i \partial \delta_k}\right|_0 & 0 & 0 \end{bmatrix}, B_{ik} = \begin{bmatrix} 0 & 0 \\ 0 & \left.\frac{\partial P_i}{\tau_i \partial V_k}\right|_0 \\ 0 & \left.\frac{\partial Q_i}{\tau_i \partial V_k}\right|_0 \end{bmatrix}. \tag{5.7}$$

It is seen in (5.7) that A_{ik} and B_{ik} remain unchanged, compared to (3.8). However, matrices $\tilde{A}_{ii}$ and $\tilde{B}_{ii}$ are different from A_{ii} and B_{ii} in (3.8). Moreover, $\tilde{A}$ and $\tilde{A}_{ii}$, $i = 1,\ldots,n$, are Hurwitz matrices (with $\kappa_i > 0$).

As mentioned above, in order to derive a model uncertainty, which is caused by uncertain admittances, Y_{ik} in the power flow equations (2.9) are replaced by $(Y_{ik} + \Delta Y_{ik})$, $i,k = 1\ldots,n$. By linearizing the inverter model (5.3) with the derived uncertain power flow equations around the nominal equilibrium (3.5), the following uncertain system is obtained:

$$\begin{cases} \dot{x}(t) &= (\tilde{A} + \Delta\tilde{A})x(t) + (\tilde{B} + \Delta\tilde{B})u(t), \\ y_d(t) &= x(t), \end{cases} \tag{5.8}$$

where $\Delta\tilde{A} \in \mathbb{R}^{3n\times 3n}$ and $\Delta\tilde{B} \in \mathbb{R}^{3n\times 2n}$ are caused by uncertain admittances, and $y_d(t)$ is the output of the uncertain system.

Denote the block-diagonal and block off-diagonal parts of $\Delta\tilde{A}, \Delta\tilde{B}$ by $\Delta\tilde{A}_{ii}, \Delta\tilde{B}_{ii}$ and $\Delta A_{ik}, \Delta B_{ik}$, $i \neq k$, respectively. It is seen in (5.7) that parameters of the power flow equations (2.9) only affect the matrix elements $\tilde{A}_{ii,21}$, $\tilde{A}_{ii,31}$, $\tilde{B}_{ii,22}$, $\tilde{B}_{ii,32}$, $A_{ik,21}$, $A_{ik,31}$, $B_{ik,22}$ and $B_{ik,32}$. Consequently, submatrices of $\Delta\tilde{A}$ and $\Delta\tilde{B}$ have the following structures:

$$\Delta\tilde{A}_{ii} = \begin{bmatrix} 0 & 0 & 0 \\ * & 0 & 0 \\ * & 0 & 0 \end{bmatrix}, \quad \Delta\tilde{B}_{ii} = \begin{bmatrix} 0 & 0 \\ 0 & * \\ 0 & * \end{bmatrix}, \quad \Delta A_{ik} = \begin{bmatrix} 0 & 0 & 0 \\ * & 0 & 0 \\ * & 0 & 0 \end{bmatrix}, \quad \Delta B_{ik} = \begin{bmatrix} 0 & 0 \\ 0 & * \\ 0 & * \end{bmatrix}, \tag{5.9}$$

where $i,k = 1,\ldots,n$, $i \neq k$ and $*$ denotes matrix elements, which can be zero or nonzero.

Based on the structures of $\tilde{A}$ and $\Delta\tilde{A}$, whose submatrices are presented in (5.7) and (5.9), respectively, it is seen that $(\tilde{A} + \Delta\tilde{A})$ is also a Hurwitz matrix, which implies the asymptotic stability of the uncertain system (5.8).

Remark 5.1.1. By considering the uncertain state-space model (5.8), the fact is neglected that with different load conditions, the system obtains different equilibrium points. However, the system variables $x(t)$, $u(t)$, $y_d(t)$ are defined relative to the nominal equilibrium point (3.5).

From (5.8) the following transfer function matrix of an uncertain microgrid is derived:

$$\tilde{G}_\Delta(s) = (sI - \tilde{A} - \Delta\tilde{A})^{-1}(\tilde{B} + \Delta\tilde{B}), \tag{5.10}$$

where $\tilde{G}_\Delta(s)$ is a $3n \times 2n$ transfer function matrix of the asymptotically stable uncertain system.

In order to separate $\tilde{G}_\Delta(s)$ into a nominal transfer function matrix and an uncertain part, the following lemma is implemented.

Lemma 5.1. *[54] Let $\mathcal{A}$ be a square matrix partitioned as follows:*

$$\mathcal{A} = \begin{bmatrix} \mathcal{A}_{11} & \mathcal{A}_{12} \\ \mathcal{A}_{21} & \mathcal{A}_{22} \end{bmatrix},$$

where $\mathcal{A}_{11}$ and $\mathcal{A}_{22}$ are also square matrices. Suppose $\mathcal{A}_{11}$ and $\mathcal{A}_{22}$ are both nonsingular matrices, then

$$(\mathcal{A}_{11} - \mathcal{A}_{12}\mathcal{A}_{22}^{-1}\mathcal{A}_{21})^{-1} = \mathcal{A}_{11}^{-1} + \mathcal{A}_{11}^{-1}\mathcal{A}_{12}(\mathcal{A}_{22} - \mathcal{A}_{21}\mathcal{A}_{11}^{-1}\mathcal{A}_{12})^{-1}\mathcal{A}_{21}\mathcal{A}_{11}^{-1}. \tag{5.11}$$

□

Apply Lemma 5.1 to $(sI-\tilde{A}-\Delta\tilde{A})^{-1}$, where

$$\mathcal{A}_{11}=sI-\tilde{A},\ \ \mathcal{A}_{12}=\Delta\tilde{A},\ \ \mathcal{A}_{21}=\mathcal{A}_{22}=I_{3n\times 3n}, \tag{5.12}$$

the following is derived:

$$(sI-\tilde{A}-\Delta\tilde{A})^{-1}=(sI-\tilde{A})^{-1}+(sI-\tilde{A})^{-1}\Delta\tilde{A}\left(I-(sI-\tilde{A})^{-1}\Delta\tilde{A}\right)^{-1}(sI-\tilde{A})^{-1}. \tag{5.13}$$

Plugging (5.13) into (5.10) yields the following:

$$\begin{aligned}
&\tilde{G}_\Delta(s)=(sI-\tilde{A}-\Delta\tilde{A})^{-1}(\tilde{B}+\Delta\tilde{B})\\
&=\left[(sI-\tilde{A})^{-1}+(sI-\tilde{A})^{-1}\Delta\tilde{A}\left(I-(sI-\tilde{A})^{-1}\Delta\tilde{A}\right)^{-1}(sI-\tilde{A})^{-1}\right](\tilde{B}+\Delta\tilde{B})\\
&=\underbrace{(sI-\tilde{A})^{-1}\tilde{B}}_{=\tilde{G}(s)}+\underbrace{(sI-\tilde{A})^{-1}\Delta\tilde{B}+(sI-\tilde{A})^{-1}\Delta\tilde{A}\left(I-(sI-\tilde{A})^{-1}\Delta\tilde{A}\right)^{-1}(sI-\tilde{A})^{-1}(\tilde{B}+\Delta\tilde{B})}_{:=\tilde{\Delta}(s)},
\end{aligned} \tag{5.14}$$

where $\tilde{G}(s)$ is the transfer function matrix of the nominal system (5.5), $\tilde{\Delta}(s)$ is an additive uncertainty. Note that with the defined structures of $\Delta\tilde{A}$ and $\Delta\tilde{B}$ in (5.9), $\tilde{\Delta}(s)$ is a structured uncertainty.

As $\tilde{\Delta}(s)=\tilde{G}_\Delta(s)-\tilde{G}(s)$, where $\tilde{G}_\Delta(s)$ and $\tilde{G}(s)$ are both asymptotically stable, $\tilde{\Delta}(s)$ is an asymptotically stable additive uncertainty. Note that an asymptotically stable uncertainty is a prerequisite for the implementation of the classical $\mathcal{H}_\infty$ control.

Consider the test microgrid in Figure 3.2. A nominal transfer function matrix $\tilde{G}(s)$ is derived with parameters in Table 3.1. Then, by varying load and line admittances, different cases of $\tilde{\Delta}(s)$ are derived. Accordingly, different singular values of $\tilde{\Delta}(j\omega)$ are obtained, some of which are presented in Figure 5.2. Remind that $\tilde{\Delta}(s)$ is a $3n\times 2n$ transfer function matrix, $\tilde{\Delta}(j\omega)$ has, therefore, $2n$ singular values. Maximum singular values of $\tilde{\Delta}(j\omega)$ associated to different load and line variations are denoted by the square symbols on the vertical axis of Figure 5.2.

A closed-loop microgrid with an additive uncertainty $\tilde{\Delta}(s)$ is shown in Figure 5.3, where $Y(s)$, $U(s)$, $Y_d(s)$, $R(s)$, $E(s)$ are the nominal system output, control input, perturbed system output, reference input and error, respectively.

At the power control level, inverters obtain reference inputs for their active and reactive power outputs. However, power references may not be equal to steady-state power outputs of inverters. The reason is, that with a static feedback controller K, an ideal reference tracking of output power is normally not achieved, unless the microgrid operates at an equilibrium point, where the power references are given. In addition, power reference inputs can be assigned on purpose by a higher control level, e.g., power management level, in order to accomplish an optimal

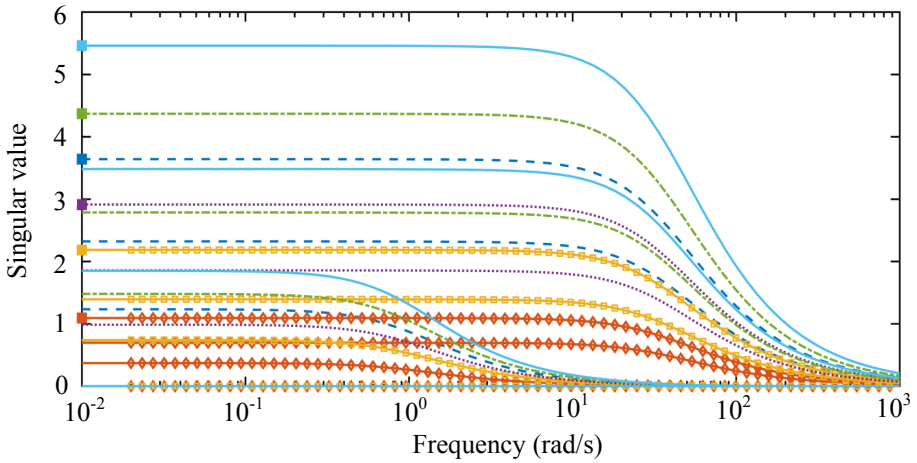

FIGURE 5.2: Singular values of $\tilde{\Delta}(j\omega)$ with different uncertain admittances.

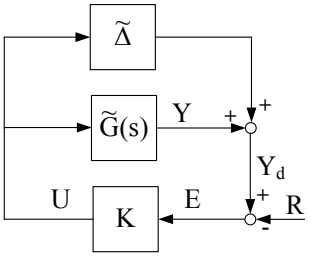

FIGURE 5.3: Closed-loop microgrid with an additive uncertainty.

system operation. For instance, power references are assigned to reduce mismatches between power references and output power. As a result, steady-state magnitude deviations of inverter output voltages from their nominal values can be decreased (see Equation (3.15)).

Thus, with a static controller K, power mismatches exist in most cases. The larger power mismatches are, the larger steady-state deviations of inverter output voltages become (see (3.15)). Reference changes (by a higher control level) and differences between power references and output power must be considered as a disturbance source on the performance of inverter output voltages. It should be mentioned that the system stability is only affected by $\tilde{\Delta}(s)$, while the performance of voltage magnitudes is affected by both $\tilde{\Delta}(s)$ and reference changes.

5.2 $\mathcal{H}_\infty$ control for microgrids with uncertainties

In the following, a system model with the aforementioned model uncertainty and disturbance input is proposed. Requirements on robustness and voltage performance are introduced in the framework by adding artificial weight functions to a generalized plant model of the system. Based on the $\mathcal{H}_\infty$ control technique, conditions for robust stability and robust performance are presented. The generalized plant model of the system with weight functions and disturbances will be given in Laplace domain, then a state-space realization is obtained. In the next section,

the derived state-space model allows to present a controller synthesis, which guarantees the robust stability of a microgrid and the robust performance of inverter output voltages.

It is noteworthy that the worst case scenario of the model uncertainty $\tilde{\Delta}(s)$ is considered, i.e. the structure of $\tilde{\Delta}(s)$ is neglected. It is consistent with the $\mathcal{H}_\infty$ control technique, which considers the system stability with respect to the worst case model uncertainty [145].

5.2.1 General control problem formulation

In $\mathcal{H}_\infty$ control it is preferable to reflect the knowledge of uncertainties and the system performance objectives by choosing appropriate weight functions. Thus, let $\tilde{\Delta}(s)$ defined in (5.14) be decomposed as:

$$\tilde{\Delta}(s) = \Delta(s)W_T(s), \quad \|\Delta\|_\infty < 1, \tag{5.15}$$

where $W_T(s)$ is a $2n \times 2n$ weight function matrix of load uncertainties, which are now represented by an uncertainty $\Delta(s)$. $\Delta(s)$ and $W_T(s)$ are selected to be asymptotically stable. Note that $\Delta(s)$ and $\tilde{\Delta}(s)$ are $3n \times 2n$ matrices as $\tilde{G}(s)$ and $\tilde{G}_\Delta(s)$.

Remark 5.2.1. There are different possibilities to weight $\tilde{\Delta}(s)$, such as $W_{T_1}(s)\Delta(s)W_{T_2}(s)$ or $W_T(s)\Delta(s)$ [56]. It is not straightforward to state which one suits best. However, the presented theory works for all cases.

A feedback system with possible uncertainties is displayed in Figure 5.4, where $\tilde{G}(s)$ consists of the interconnected inverters and K is the controller. The variables $U(s), Y(s), Y_d(s)$, and $E(s)$ are control input, nominal plant output, perturbed plant output, and error, respectively. $V_d(s)$ and $U_d(s)$ are the input and output of $\Delta(s)$, and $R(s)$ is a reference input. $W_U(s)$, $W_E(s)$ and $W_T(s)$ are weight functions, whose choice will be explained in the next subsection. Finally, $Z_1(s)$, $Z_2(s)$ are performance outputs.

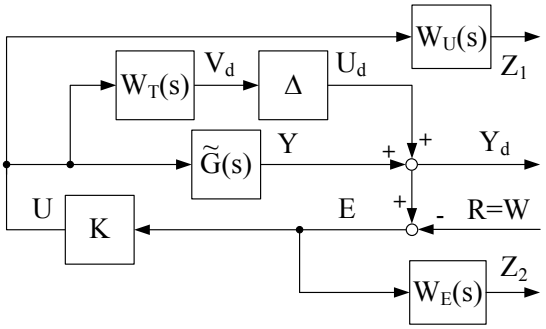

FIGURE 5.4: Feedback system with possible disturbances.

Concerning notation, capital and lower-case letters denote identical variables in the Laplace and time domain, respectively.

The reference input $W(s) = R(s)$ and the performance outputs $Z_1(s)$, $Z_2(s)$ are introduced for controller design purpose. It is seen from Figure 5.4 that $Z_1(s) = W_U(s)U(s)$ is a weighted control input, where the control input $U(s)$ consists of frequency and voltage deviations of all inverters (see (5.4)). Furthermore, $Z_2(s) = W_E(s)E(s)$ is a weighted control error, where $E(s)$ represents differences between system outputs, i.e. voltage phase angles and power outputs of inverters, and there reference inputs. Note that frequency deviations from a nominal value, e.g. $2\pi 50$ [rad/s], only happen during transients in the system, whereas steady-state voltage deviations can exist, depending on the control error $E(s)$. It will be clear later in this chapter that the objective of the $\mathcal{H}_\infty$ control is to minimize the $\mathcal{H}_\infty$ norm from the disturbance input $U_d(s)$ and the reference input $R(s)$ to the performance outputs $Z_1(s)$ and $Z_2(s)$.

The state variable $x(t)$ is defined as in (3.4), while the control input $u(t)$ of the inverters is defined in (5.4). The nominal output of the inverter plant $\tilde{G}(s)$ is defined as $y(t) = x(t)$. The variables $w(t)$, $u_d(t)$, $z_1(t)$ and $z_2(t)$ are defined in the time domain as follows:

$$\begin{aligned} w_i &= r_i \in \mathbb{R}^{3\times 1}, & w &= [w_1^T, \ldots, w_n^T]^T \in \mathbb{R}^{3n\times 1}, \\ u_{d_i} &\in \mathbb{R}^{3\times 1}, & u_d &= [u_{d_1}^T, \ldots, u_{d_n}^T]^T \in \mathbb{R}^{3n\times 1}, \\ z_{1_i} &\in \mathbb{R}^{2\times 1}, & z_1 &= [z_{1_1}^T, \ldots, z_{1_n}^T]^T \in \mathbb{R}^{2n\times 1}, \\ z_{2_i} &\in \mathbb{R}^{3\times 1}, & z_2 &= [z_{2_1}^T, \ldots, z_{2_n}^T]^T \in \mathbb{R}^{3n\times 1}, \end{aligned} \tag{5.16}$$

where the variables indicated by an index i are associated to an inverter i.

The system in Figure 5.4 can be displayed equivalently by a general control configuration for controller synthesis presented in Figure 5.5, where $P(s)$ itself includes the transfer function matrix $\tilde{G}(s)$ and the weight functions [56]. $P(s)$ is called a generalized plant model.

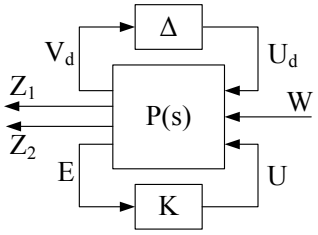

FIGURE 5.5: General control configuration.

The transfer function matrix $P(s)$ is derived from Figure 5.4 by the following relations:

$$\begin{aligned} V_d(s) &= W_T(s)U(s), \\ Z_1(s) &= W_U(s)U(s), \\ Z_2(s) = W_E(s)E(s) &= W_E(s)\big(-W(s) + U_d(s) + Y(s)\big), \\ E(s) &= -W(s) + U_d(s) + \tilde{G}(s)U(s), \end{aligned} \tag{5.17}$$

which infer the following:

$$\begin{bmatrix} V_d(s) \\ Z_1(s) \\ Z_2(s) \\ \hdashline E(s) \end{bmatrix} = \underbrace{\left[\begin{array}{cc:c} 0 & 0 & W_T(s) \\ 0 & 0 & W_U(s) \\ W_E(s) & -W_E(s) & W_E(s)\tilde{G}(s) \\ \hdashline I & -I & \tilde{G}(s) \end{array}\right]}_{:=P(s)} \begin{bmatrix} U_d(s) \\ W(s) \\ \hdashline U(s) \end{bmatrix} = \begin{bmatrix} P_{11}(s) & P_{12}(s) \\ P_{21}(s) & P_{22}(s) \end{bmatrix} \begin{bmatrix} U_d(s) \\ W(s) \\ \hdashline U(s) \end{bmatrix}. \tag{5.18}$$

Alternatively, the system in Figure 5.5 can be represented by the NΔ-structure in Figure 5.6, where $N(s)$ is related to $P(s)$ and K by a *lower linear fractional transformation* as follows:

$$\begin{aligned} F_l(P,K) = N(s) &= P_{11}(s) + P_{12}(s)K\big(I - P_{22}(s)K\big)^{-1}P_{21}(s) \\ &= \begin{bmatrix} W_T(s)KS(s) & -W_T(s)KS(s) \\ W_U(s)KS(s) & -W_U(s)KS(s) \\ W_E(s)S(s) & -W_E(s)S(s) \end{bmatrix}, \end{aligned} \tag{5.19}$$

where $S(s) = \big(I - \tilde{G}(s)K\big)^{-1}$ is the *sensitivity* of the system [56]. Note that the negative sign in $S(s)$ is caused by the fact that the feedback signal in Figure 5.4 is positive.

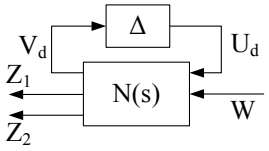

FIGURE 5.6: NΔ-structure for performance analysis.

The upper left block $N_{11}(s)$ of $N(s)$ in (5.19) is the transfer function matrix from $U_d(s)$ to $V_d(s)$. Hence, in order to analyze the robust stability of the system in Figure 5.4, the system is rearranged into the MΔ-structure presented in Figure 5.7 [56], where

$$M(s) = N_{11}(s) = W_T(s)KS(s). \tag{5.20}$$

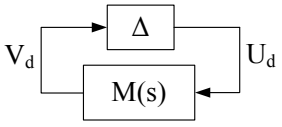

FIGURE 5.7: MΔ-structure for robust stability analysis.

According to the small-gain theorem (4.54), the system in Figure 5.7 is asymptotically stable if $M(s)$ and Δ are asymptotically stable and the system gain is less than 1, i.e., $\|M(s)\Delta\|_\infty < 1$.

With $\|\Delta\|_\infty < 1$, the system in Figure 5.7 is robustly stable if:

$$\|M(s)\|_\infty \leq 1. \tag{5.21}$$

It should be noted that the robust stability condition (5.21) includes some conservatism in the sense that the structure of the model uncertainty Δ is ignored.

For performance analysis, the NΔ-structure in Figure 5.6 is considered. In (5.19) the lower right blocks $N_{22}(s)$ and $N_{32}(s)$ of $N(s)$ are the transfer function matrices from $W(s)$ to $Z_1(s)$ and $Z_2(s)$, respectively. The system nominal performance (when $\Delta = 0$) is guaranteed if $N(s)$ is asymptotically stable and the $\mathcal{H}_\infty$ norm of the transfer function matrix from $W(s)$ to $Z_1(s)$ and $Z_2(s)$ is less than 1 [56]. The condition for nominal performance is as follows:

$$\begin{cases} N(s) \text{ is asymptotically stable,} \\ \left\| \begin{bmatrix} N_{22}(s) \\ N_{32}(s) \end{bmatrix} \right\|_\infty = \left\| \begin{bmatrix} -W_U(s)KS(s) \\ -W_E(s)S(s) \end{bmatrix} \right\|_\infty < 1. \end{cases} \tag{5.22}$$

Note that $W_U(s)$ and $W_E(s)$ are chosen, so that the condition (5.22) corresponds to desired performance goals.

Furthermore, in Figure 5.6, the uncertain closed-loop transfer function matrix from $W(s)$ to $Z_1(s)$ and $Z_2(s)$ is related to $N(s)$ and Δ by an *upper* linear fractional transformation as follows [56]:

$$F_u(N,\Delta) = \begin{bmatrix} N_{22}(s) \\ N_{32}(s) \end{bmatrix} + \begin{bmatrix} N_{21}(s) \\ N_{31}(s) \end{bmatrix} \Delta(I - N_{11}\Delta)^{-1} N_{12}. \tag{5.23}$$

The robust performance property of the system in Figure 5.6 is achieved if and only if $N(s)$ is asymptotically stable and the following condition is satisfied [56]:

$$\|F_u(N,\Delta)\|_\infty \leq 1, \ \ \forall \|\Delta\|_\infty < 1. \tag{5.24}$$

In [56] it is shown that the robust performance condition (5.24) is equivalent to a condition, which is related to a value called the structured singular value. Therefore, the definition of the structured singular value is given hereafter.

Definition 5.2. [56, 146] Let $\mathcal{M}$ be a given complex matrix. Let $\Delta = \text{diag}(\Delta_i), \ i = 1,\ldots,n$, denote a set of complex matrices with $\bar{\sigma}(\Delta) \leq 1$ and with a given block-diagonal structure (in which some of the blocks may be repeated and some may be restricted to be real). The real

non-negative function $\mu(\mathcal{M})$, called the *structured singular value*, is defined by:

$$\mu(\mathcal{M}) = \frac{1}{\min\{k_m | \det(I - k_m \mathcal{M}\Delta) = 0 \text{ for structured } \Delta, \bar{\sigma}(\Delta) \leq 1\}}. \tag{5.25}$$

If no such structured Δ exists then $\mu(\mathcal{M}) = 0$. □

The robust performance condition (5.24) is equivalent to the following condition [56]:

$$\mu_{\widehat{\Delta}}(N(j\omega)) \leq 1, \ \ \forall\omega, \tag{5.26}$$

where $\mu_{\widehat{\Delta}}(N(j\omega))$ is the structured singular value of $N(j\omega)$ with respect to $\widehat{\Delta}$, where

$$\widehat{\Delta} = \begin{bmatrix} \Delta & 0 \\ 0 & \Delta_P \end{bmatrix}, \tag{5.27}$$

and Δ_P is a full complex uncertainty with the same dimension as $F_u(N, \Delta)^T$.

The robust performance property is guaranteed if either the condition (5.24) or (5.26) is satisfied. However, from the conditions (5.24) and (5.26), it is a nontrivial task to formulate an LMI problem to design a controller K that guarantees the robust performance of the system in Figure 5.6. Nevertheless, as $\mu_{\widehat{\Delta}}(N(j\omega)) \leq \|N(s)\|_\infty, \forall\omega$ (see [56, page 338] for more detail), the following is a *sufficient* condition for (5.24) and (5.26) [56]:

$$\|N(s)\|_\infty \leq 1. \tag{5.28}$$

In the following subsection, for the robust performance of the system in Figure 5.6, a controller design is proposed by using the more conservative $\mathcal{H}_\infty$ norm condition (5.28). Since it is clear from (5.19) that $\|M(s)\|_\infty \leq \|N(s)\|_\infty$, the condition (5.28) is sufficient for (5.21).

The derived $N(s)$ in (5.19) recalls a standard stacked S/KS $\mathcal{H}_\infty$ problem. A small $\bar{\sigma}(S(j\omega))$ yields disturbance rejection of the system and a small $\bar{\sigma}(KS(j\omega))$ reduces control effort (see e.g., [56, 89]), where $\bar{\sigma}$ denotes a maximum singular value. $N(s)$ in (5.19) also presents a trade-off problem as $\bar{\sigma}(S(j\omega))$ and $\bar{\sigma}(KS(j\omega))$ cannot be simultaneously minimized. Therefore, the frequency-dependent weight functions are introduced so that by minimizing $\|N(s)\|_\infty$, the maximum singular value $\bar{\sigma}(S(j\omega))$ can be forced to be small in a range of frequency, where $\bar{\sigma}(KS(j\omega))$ can be large, and vice versa.

Remark 5.2.2. The feasibility of the conditions (5.21), (5.22) and (5.28) strongly depend on the choice of the weight functions, i.e., the required robustness and performance.

5.2.2 Choice of weight functions

The choice of weight functions for a particular control problem often involves ad hoc many iterations and fine tuning. There is no common form of weight functions that works in every case. Some guidelines on weight functions can be found in [54–56]. This thesis considers $W_U(s)$, $W_E(s)$ and $W_T(s)$ as illustrated in Figure 5.4, which should reflect the performance objectives and knowledge of the uncertainty, respectively. The weight functions $W_E(s)$, $W_T(s)$ and $W_U(s)$ must be chosen to be asymptotically stable to guarantee the asymptotic stability of $N(s)$ [55, 56].

As shown in (5.15), $\tilde{\Delta} = \Delta(s)W_T(s)$. Then, the (open-loop) transfer function matrix of the uncertain inverter system in Figure 5.4 is given by:

$$\tilde{G}_\Delta(s) = \tilde{G}(s) + \tilde{\Delta}(s) = \tilde{G}(s) + \Delta(s)W_T(s), \quad \|\Delta\|_\infty < 1, \tag{5.29}$$

where $\Delta(s)$ is an asymptotically stable model uncertainty.

From (5.29), the following lower bound of the $\mathcal{H}_\infty$ norm of $W_T(s)$ is achieved:

$$\|\tilde{G}_\Delta(s) - \tilde{G}(s)\|_\infty = \|\Delta W_T(s)\|_\infty \leq \|\Delta\|_\infty \|W_T(s)\|_\infty \leq \|W_T(s)\|_\infty. \tag{5.30}$$

Remark 5.2.3. If the robust stability condition (5.21) with the above defined $W_T(s)$ cannot be satisfied by any controller K, the robust stability condition (5.21) may be feasible with a smaller $\tilde{\Delta}(s)$ and a smaller maximum singular value of $W_T(s)$, respectively.

$W_T(s)$ should be chosen so that the $\mathcal{H}_\infty$ norm constraint in (5.30) is satisfied. Moreover, based on the frequency response technique, $W_T(s)$ is chosen so that the class of uncertainty

$$\{\tilde{\Delta}(s) \mid \tilde{\Delta}(s) = \Delta W_T(s),\ \|\Delta\|_\infty < 1,\ \Delta(s) \text{ is asymptotically stable}\} \tag{5.31}$$

covers all possible admittance uncertainties [1].

For simplicity of the theory presentation, $W_T(s)$ for a microgrid with n inverters is chosen to be a $2n \times 2n$ diagonal transfer function matrix with identical transfer functions, such as:

$$W_T(s) = W_t(s) I_{2n\times 2n}, \quad W_t(s) = \frac{\tau^t s + r_0^t}{(\tau^t / r_\infty^t)s + 1}, \tag{5.32}$$

[1] While designing robust inverter controllers, a range of possible admittance uncertainties should be determined beforehand. Based on the power flow equations (2.9) and the inverter model (5.3), a nominal and uncertain models of a microgrid can be obtained. Model uncertainties are subtractions of uncertain models from a nominal model (see Section 5.1). $W_T(s)$ can be defined as an upper bound for all considered admittance uncertainties (see Figure 5.8).

where r_0^t and r_∞^t are upper bounds for uncertainty $\tilde{\Delta}(s)$ at steady-state and at high-frequency, respectively. $1/\tau^t$ is the cutoff frequency, and the magnitude of the frequency response $W_t(j\omega)$ reaches r_∞^t at $\omega = \infty$.

For an uncertainty $\tilde{\Delta}(s)$, where the singular values of its corresponding frequency response matrix are shown in Figure 5.2, the choice of $W_t(s)$ is illustrated in Figure 5.8.

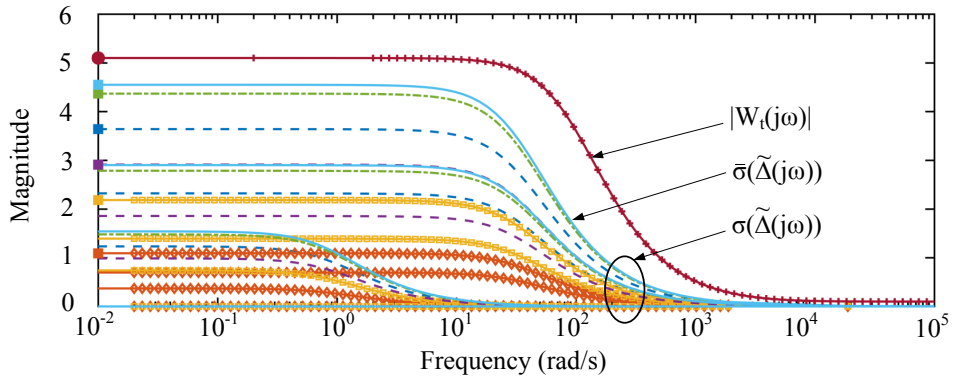

FIGURE 5.8: An example of $|W_t(j\omega)|$.

A weight function $W_E(s)$ is introduced for disturbance attenuation and reference tracking, i.e. reducing the control error $E(s)$. It is seen from Figure 5.4 that:

$$E(s) = -W(s) + U_d(s) + \tilde{G}(s)U(s) = -W(s) + U_d(s) + \tilde{G}(s)KE(s), \tag{5.33a}$$

$$\Leftrightarrow \quad \big(I - \tilde{G}(s)K\big)E(s) = -W(s) + U_d(s), \tag{5.33b}$$

$$\Rightarrow \quad E(s) = \big(I - \tilde{G}(s)K\big)^{-1}\big(-W(s) + U_d(s)\big) = S(s)\big(-W(s) + U_d(s)\big). \tag{5.33c}$$

The control error is weighted by $W_E(s)$ as follows:

$$Z_2(s) = W_E(s)E(s) = W_E(s)S(s)\big(-W(s) + U_d(s)\big). \tag{5.34}$$

From the equation above it is clear that amplifying gains of $W_E(j\omega)S(j\omega)$ (which are characterized by its singular values [55]) should be decreased to reduce influences of disturbance inputs on the performance output $Z_2(s)$ (weighted control error). Reference changes and output disturbances caused by model uncertainties typically happen at low frequencies and can therefore be successfully attenuated if the maximum singular value of $S(j\omega)$ is forced to be small at low frequencies. This can be done by selecting $W_E(s)$ so that the form of $W_E(j\omega)$ is similar to the frequency response of a low-pass filter, where the bandwidth of $W_E(s)$ is equal to the bandwidth of the mentioned disturbances.

Weight functions for each control error of an inverter i can be chosen as follows:

$$W_{e_{i1}}(s) = \frac{\tau_e^{\delta_i} s + r_{0_e}^{\delta_i}}{(\tau_e^{\delta_i}/r_{\infty_e}^{\delta_i})s+1}, \quad W_{e_{i2}}(s) = \frac{\tau_e^{\tilde{P}_i} s + r_{0_e}^{\tilde{P}_i}}{(\tau_e^{\tilde{P}_i}/r_{\infty_e}^{\tilde{P}_i})s+1}, \quad W_{e_{i3}}(s) = \frac{\tau_e^{\tilde{Q}_i} s + r_{0_e}^{\tilde{Q}_i}}{(\tau_e^{\tilde{Q}_i}/r_{\infty_e}^{\tilde{Q}_i})s+1}, \tag{5.35}$$

where $r_{0_e}^{\delta_i}$, $r_{0_e}^{\tilde{P}_i}$, $r_{0_e}^{\tilde{Q}_i}$ are low-frequency gains and $r_{\infty_e}^{\delta_i}$, $r_{\infty_e}^{\tilde{P}_i}$, $r_{\infty_e}^{\tilde{Q}_i}$ are high-frequency gains of the weight functions, respectively. $1/\tau_e^{\delta_i}$, $1/\tau_e^{\tilde{P}_i}$, $1/\tau_e^{\tilde{Q}_i}$ are cutoff frequencies.

A $3n \times 3n$ weight function matrix $W_E(s)$ for the overall system can be chosen as the following:

$$W_E(s) = \mathrm{diag}\big(W_{e_{11}}(s), W_{e_{12}}(s), W_{e_{13}}(s), \ldots, W_{e_{n1}}(s), W_{e_{n2}}(s), W_{e_{n3}}(s)\big). \tag{5.36}$$

An example of $W_{e_{ik}}(s)$, $i = 1,\ldots,n$, $k = 1,2,3$, is presented in Figure 5.9, where $\bar{\sigma}(S(j\omega)$ presents the maximum singular value of a desired sensitivity $S(j\omega)$.

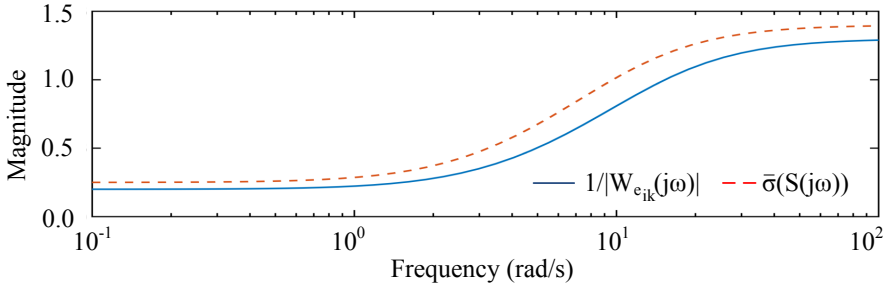

FIGURE 5.9: An example of $|W_{e_{ik}}(j\omega)|$.

Performance objectives of the control input $u = [u_1^T, \ldots, u_n^T]^T$, where $u_i = [u_{i_1}, V_i - V_{i_0}]^T$, are reflected by the weight function $W_U(s)$. As seen from Figure 5.4,

$$U(s) = KE(s) = K\big(-W(s) + U_d(s) + \tilde{G}(s)U(s)\big), \tag{5.37a}$$

$$\Leftrightarrow \quad \big(I - K\tilde{G}(s)\big)U(s) = K\big(-W(s) + U_d(s)\big), \tag{5.37b}$$

$$\begin{aligned} \Rightarrow \quad U(s) &= \big(I - K\tilde{G}(s)\big)^{-1} K\big(-W(s) + U_d(s)\big) \\ &= K\big(I - \tilde{G}(s)K\big)^{-1}\big(-W(s) + U_d(s)\big) \\ &= KS(s)\big(-W(s) + U_d(s)\big). \end{aligned} \tag{5.37c}$$

The control input is weighted as follows (see Figure 5.4):

$$Z_1(s) = W_U(s)U(s) = W_U(s)KS(s)\big(-W(s) + U_d(s)\big). \tag{5.38}$$

Amplifying gains of $W_U(j\omega)KS(j\omega)$ should be decreased to reduce influences of disturbance inputs on the performance input $Z_1(s)$. As stated in the beginning of this chapter, the reduction

of control effort is desired. That is, magnitude deviations of inverter output voltages should be reduced under uncertainties.

Moreover, by appropriately choosing $W_U(s)$, another performance objective for inverter output voltages can be additionally achieved, which is the attenuation of their higher-frequency harmonic components. Hence, the weight functions of the control inputs of an inverter i are selected as the following:

$$W_{u_{i1}}(s) = \frac{\tau_i^\omega s + r_{0_i}^\omega}{(\tau_i^\omega / r_{\infty_i}^\omega)s + 1}, \quad W_{u_{i2}}(s) = \frac{\tau_i^V s + r_{0_i}^V}{(\tau_i^V / r_{\infty_i}^V)s + 1}, \quad i = 1, \ldots, n, \tag{5.39}$$

where $r_{0_i}^\omega$, $r_{0_i}^V$ are low-frequency gains, $1/\tau_i^\omega, 1/\tau_i^V$ are the cutoff frequencies, and $W_{u_{i1}}(j\omega)$ and $W_{u_{i2}}(j\omega)$ reach high-frequency gains $r_{\infty_i}^\omega$, $r_{\infty_i}^V$ at $\omega = \infty$, respectively. Moreover, $r_{0_i}^\omega$, $r_{0_i}^V, r_{\infty_i}^\omega$, and $r_{\infty_i}^V$ in (5.39) are chosen to be greater than 1 in order to reduce magnitude deviations of the control inputs as well as magnitudes of their higher-frequency harmonics.

A $2n \times 2n$ weight function matrix $W_U(s)$ for the overall system is chosen as the following:

$$W_U(s) = \text{diag}\left(W_{u_{11}}(s), W_{u_{12}}(s), \ldots, W_{u_{n1}}(s), W_{u_{n2}}(s)\right). \tag{5.40}$$

An example of $W_{u_{ik}}(s)$, $i = 1, \ldots, n$, $k = 1, 2$, is presented in Figure 5.10, where $\bar{\sigma}(KS(j\omega))$ presents a maximum singular value of a desired frequency response $KS(j\omega)$.

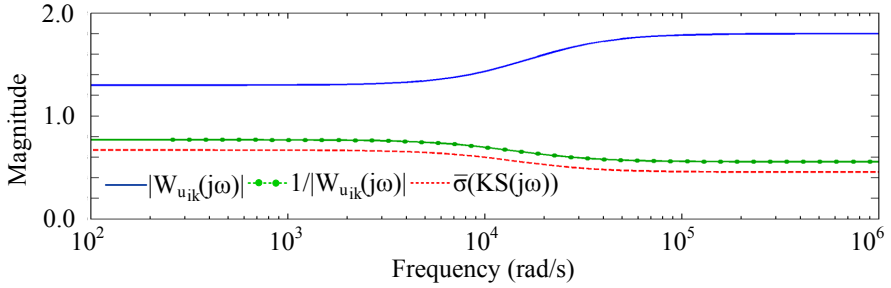

FIGURE 5.10: An example of $|W_{u_{ik}}(j\omega)|$.

Hence, if the robust performance condition (5.24) is satisfied with the above defined $W_U(s)$, $W_E(s)$ and $W_T(s)$, the robust performance of voltages specified by $W_U(s)$ is guaranteed despite the load uncertainty $\tilde{\Delta}(s)$ and changes of power references $R(s)$. It is expected that magnitude variations of voltages as well as their higher-frequency harmonic components are reduced as the gains of $W_U(s)$ are chosen to be greater than 1. Consequently, the THD of voltages also reduces.

Remark 5.2.4. Higher-frequency harmonics of voltages in power systems are caused by the nonlinearity of loads, generation units, etc. [33]. By investigating linearized models of microgrids, no further claim about higher-frequency harmonics of voltages could be made. It is a clear drawback of linear control methods, when linear system models are considered and it is hoped that the control approach will work for real nonlinear systems.

5.2.3 State-space realization of the overall system

In order to present an LMI optimization problem in the next section, which is based on the $\mathcal{H}_\infty$ norm condition (5.28), it is necessary to derive a state-space representation of $N(s)$. In this subsection, based on state-space realizations of each component of the system in Figure 5.4, a state-space representation of $N(s)$ is derived. The resulting state-space representation of $N(s)$ consists of the inverter model $\tilde{G}(s)$, the weight functions $W_T(s)$, $W_E(s)$ and $W_U(s)$, and the feedback control law $u(t) = Ke(t)$, where K needs to be designed.

It is noteworthy that based on the $\mathcal{H}_\infty$ control it is possible to design a dynamic feedback controller. However, in order to preserve the static controller structure introduced in Fig. 5.1, which also allows to synthesize droop-based power sharing controllers for inverters in the next chapter, the controller K is restricted to be static.

The inverter model $\tilde{G}(s)$ and the weight functions $W_T(s)$, $W_U(s)$ and $W_E(s)$ have, respectively, the following minimal state-space realizations:

$$\begin{aligned} \tilde{G}(s) &= \left[\begin{array}{c|c} \tilde{A} & \tilde{B} \\ \hline I & 0 \end{array}\right], \qquad W_T(s) = \left[\begin{array}{c|c} A_T & B_T \\ \hline C_T & D_T \end{array}\right], \\ W_U(s) &= \left[\begin{array}{c|c} A_U & B_U \\ \hline C_U & D_U \end{array}\right], \quad W_E(s) = \left[\begin{array}{c|c} A_E & B_E \\ \hline C_E & D_E \end{array}\right]. \end{aligned} \tag{5.41}$$

where $A_T, A_U, B_T, B_U, C_T, C_U, D_T, D_U \in \mathbb{R}^{2n\times 2n}$ as $W_T(s)$ and $W_U(s)$ are $2n \times 2n$ transfer function matrices, and $A_E, B_E, C_E, D_E \in \mathbb{R}^{3n\times 3n}$ as $W_E(s)$ is a $3n \times 3n$ transfer function matrix.

Note that no realization procedure is done for the inverter model $\tilde{G}(s)$. The state-space model of the inverters is already obtained in (5.5) by the linearization of the inverter model (5.3). Moreover, as the state-space realizations in (5.41) of the weight functions are minimal, (A_T, B_T), (A_U, B_U) and (A_E, B_E) are controllable, (A_T, C_T), (A_U, C_U) and (A_E, C_E) are observable (see, e.g. [54–56], for more details on controllability and observability of minimal state-space realizations).

Denote the states of $W_U(s), W_T(s), W_E(s)$ by $x_U \in \mathbb{R}^{2n\times 1}$, $x_T \in \mathbb{R}^{2n\times 1}$ and $x_E \in \mathbb{R}^{3n\times 1}$, respectively. The following state-space models are derived:

$$\begin{aligned} &\begin{cases} \dot{x} = \tilde{A}x + \tilde{B}u, \\ y = x, \end{cases} \qquad \begin{cases} \dot{x}_T = A_T x_T + B_T u, \\ v_d = C_T x_T + D_T u, \end{cases} \\ &\begin{cases} \dot{x}_U = A_U x_U + B_U u, \\ z_1 = C_U x_U + D_U u, \end{cases} \qquad \begin{cases} \dot{x}_E = A_E x_E + B_E e, \\ z_2 = C_E x_E + D_E e. \end{cases} \end{aligned} \tag{5.42}$$

In (5.42) $x(t)$, $u(t)$, $\tilde{A}$ and $\tilde{B}$ are the same state, control input vectors and system matrices as defined in (3.4), (5.4) and (5.5), respectively. As seen in Figure 5.4 and in the relations (5.17),

the error $e(t)$ is calculated in the time domain as follows:

$$e(t) = -r(t) + u_d(t) + y(t) = -w(t) + u_d(t) + x(t), \tag{5.43}$$

where $e(t)$ is the input of the controller K.

It is seen in Figure 5.6 that the input and output vectors of $N(s)$ are $[U_d(s)^T \ W(s)^T]^T$ and $[V_d(s)^T \ Z_1(s)^T \ Z_2(s)^T]^T$, respectively. Define in the time domain a state variable $\bar{x}(t)$, an input $\bar{w}(t)$ and an output $\bar{z}(t)$ of $N(s)$ in Figure 5.6 as the following:

$$\bar{x} = [x^T \ \ x_T^T \ \ x_U^T \ \ x_E^T]^T, \quad \bar{w} = [u_d^T \ \ w^T]^T, \quad \bar{z} = [v_d^T \ \ z_1^T \ \ z_2^T]^T, \tag{5.44}$$

where $\bar{x} \in \mathbb{R}^{10n\times 1}$, $\bar{w} \in \mathbb{R}^{6n\times 1}$, and $\bar{z} \in \mathbb{R}^{7n\times 1}$.

In the following, a state-space realization of $N(s)$ based on the state-space models in (5.42) and a feedback control law $u(t) = Ke(t)$ will be derived. The open-loop system equations (5.42) and (5.43) can be rearranged as follows:

$$\begin{cases} \begin{bmatrix} \dot{x} \\ \dot{x}_T \\ \dot{x}_U \\ \dot{x}_E \end{bmatrix} = \begin{bmatrix} \tilde{A} & 0 & 0 & 0 \\ 0 & A_T & 0 & 0 \\ 0 & 0 & A_U & 0 \\ B_E & 0 & 0 & A_E \end{bmatrix} \begin{bmatrix} x \\ x_T \\ x_U \\ x_E \end{bmatrix} + \begin{bmatrix} 0 & 0 \\ 0 & 0 \\ 0 & 0 \\ B_E & -B_E \end{bmatrix} \begin{bmatrix} u_d \\ w \end{bmatrix} + \begin{bmatrix} \tilde{B} \\ B_T \\ B_U \\ 0 \end{bmatrix} u, \\ \begin{bmatrix} v_d \\ z_1 \\ z_2 \end{bmatrix} = \begin{bmatrix} 0 & C_T & 0 & 0 \\ 0 & 0 & C_U & 0 \\ D_E & 0 & 0 & C_E \end{bmatrix} \begin{bmatrix} x \\ x_T \\ x_U \\ x_E \end{bmatrix} + \begin{bmatrix} 0 & 0 \\ 0 & 0 \\ D_E & -D_E \end{bmatrix} \begin{bmatrix} u_d \\ w \end{bmatrix} + \begin{bmatrix} D_T \\ D_U \\ 0 \end{bmatrix} u, \\ e = \begin{bmatrix} I & 0 & 0 & 0 \end{bmatrix} \begin{bmatrix} x \\ x_T \\ x_U \\ x_E \end{bmatrix} + \begin{bmatrix} I & -I \end{bmatrix} \begin{bmatrix} u_d \\ w \end{bmatrix}. \end{cases} \tag{5.45}$$

With the notations in (5.44), the open-loop system above can be rewritten as the following:

$$\begin{cases} \dot{\bar{x}}(t) = \bar{A}\bar{x}(t) + B_1\bar{w}(t) + \bar{B}u(t), \\ \bar{z}(t) = C_1\bar{x}(t) + D_{11}\bar{w}(t) + D_{12}u(t), \\ e(t) = \bar{C}\bar{x}(t) + D_{21}\bar{w}(t), \end{cases} \tag{5.46}$$

where the sizes of the system matrices are: $\bar{A} \in \mathbb{R}^{10n\times 10n}$, $B_1 \in \mathbb{R}^{10n\times 6n}$, $\bar{B} \in \mathbb{R}^{10n\times 2n}$, $C_1 \in \mathbb{R}^{7n\times 10n}$, $D_{11} \in \mathbb{R}^{7n\times 6n}$, $D_{12} \in \mathbb{R}^{7n\times 2n}$, $\bar{C} \in \mathbb{R}^{3n\times 10n}$, $D_{21} \in \mathbb{R}^{3n\times 6n}$. The system matrices possess the following forms:

$$\bar{A} = \begin{bmatrix} \tilde{A} & 0 & 0 & 0 \\ 0 & A_T & 0 & 0 \\ 0 & 0 & A_U & 0 \\ B_E & 0 & 0 & A_E \end{bmatrix}, B_1 = \begin{bmatrix} 0 & 0 \\ 0 & 0 \\ 0 & 0 \\ B_E & -B_E \end{bmatrix}, \bar{B} = \begin{bmatrix} \tilde{B} \\ B_T \\ B_U \\ 0 \end{bmatrix}, D_{11} = \begin{bmatrix} 0 & 0 \\ 0 & 0 \\ D_E & -D_E \end{bmatrix},$$
$$C_1 = \begin{bmatrix} 0 & C_T & 0 & 0 \\ 0 & 0 & C_U & 0 \\ D_E & 0 & 0 & C_E \end{bmatrix}, D_{12} = \begin{bmatrix} D_T \\ D_U \\ 0 \end{bmatrix}, \bar{C} = [I \ 0 \ 0 \ 0], \ D_{21} = [I \ -I]. \tag{5.47}$$

In order to formulate a convex LMI condition to design a state-feedback controller K for inverters in the following section, the open-loop system (5.46) is represented equivalently as follows:

$$\begin{cases} \dot{\bar{x}}(t) &= \bar{A}\bar{x}(t) + B_1\bar{w}(t) + \bar{B}u(t), \\ \bar{z}(t) &= C_1\bar{x}(t) + D_{11}\bar{w}(t) + D_{12}u(t), \\ e(t) &= \bar{C}\bar{x}(t) + \bar{C}\bar{D}_{21}\bar{w}(t), \end{cases} \tag{5.48}$$

with $D_{21} = \bar{C}\bar{D}_{21}$, where $\bar{D}_{21} \in \mathbb{R}^{10n\times 6n}$ is chosen as follows:

$$\bar{D}_{21} = \begin{bmatrix} I_{3n\times 3n} & 0 & 0 & 0 \\ -I_{3n\times 3n} & 0 & 0 & 0 \end{bmatrix}^T. \tag{5.49}$$

With the system representation (5.48), the following is derived:

$$u(t) = Ke(t) = K\big(\bar{C}\bar{x}(t) + \bar{C}\bar{D}_{21}\bar{w}(t)\big). \tag{5.50}$$

With $\bar{C}$ given in (5.47), define

$$\bar{K} = K\bar{C} = [K_{2n\times 3n} \ \ 0_{2n\times 2n} \ \ 0_{2n\times 2n} \ \ 0_{2n\times 3n}], \tag{5.51}$$

where $K = \mathrm{diag}(K_1, \ldots, K_n)$ is the state-feedback controller for the inverters. The control law in (5.50) is equivalent to the following:

$$u(t) = Ke(t) = K\big(\bar{C}\bar{x}(t) + \bar{C}\bar{D}_{21}\bar{w}(t)\big) = \bar{K}\bar{x}(t) + \bar{K}\bar{D}_{21}\bar{w}(t). \tag{5.52}$$

Consider the open-loop system (5.48). Close the control loop by applying the control law above, the following closed-loop system is obtained:

$$\begin{cases} \dot{\bar{x}}(t) &= \underbrace{(\bar{A} + \bar{B}\bar{K})}_{:=\breve{A}}\bar{x}(t) + \underbrace{(B_1 + \bar{B}\bar{K}\bar{D}_{21})}_{:=\breve{B}}\bar{w}(t), \\ \bar{z}(t) &= \underbrace{(C_1 + D_{12}\bar{K})}_{:=\breve{C}}\bar{x}(t) + \underbrace{(D_{11} + D_{12}\bar{K}\bar{D}_{21})}_{:=\breve{D}}\bar{w}(t), \end{cases} \tag{5.53}$$

where $\check{A} \in \mathbb{R}^{10n\times 10n}$, $\check{B} \in \mathbb{R}^{10n\times 6n}$, $\check{C} \in \mathbb{R}^{7n\times 10n}$, $\check{D} \in \mathbb{R}^{7n\times 6n}$ are as follows:

$$\check{A} = \begin{bmatrix} \tilde{A}+\tilde{B}K & 0 & 0 & 0 \\ B_T K & A_T & 0 & 0 \\ B_U K & 0 & A_U & 0 \\ B_E & 0 & 0 & A_E \end{bmatrix}, \quad \check{B} = \begin{bmatrix} \tilde{B}K & -\tilde{B}K \\ B_T K & -B_T K \\ B_U K & -B_U K \\ B_E & -B_E \end{bmatrix},$$
$$\check{C} = \begin{bmatrix} D_T K & C_T & 0 & 0 \\ D_U K & 0 & C_U & 0 \\ D_E & 0 & 0 & C_E \end{bmatrix}, \quad \check{D} = \begin{bmatrix} D_T K & -D_T K \\ D_U K & -D_U K \\ D_E & -D_E \end{bmatrix}. \tag{5.54}$$

With the input $\bar{w}(t)$ and output $\bar{z}(t)$ defined in (5.44), the state-space model above is a state-space representation of the transfer function matrix $N(s)$ in Figure 5.6. On the other hand, the transfer function matrix $N(s)$ of the closed-loop system is derived from (5.53) as follows:

$$N(s) = \check{C}(sI - \check{A})^{-1}\check{B} + \check{D}. \tag{5.55}$$

Problem 5.2.1. *Design the state-feedback controller $u(t) = Ke(t)$ as defined in (5.52) so that the system (5.53) is asymptotically stable, while its $\mathcal{H}_\infty$ norm satisfies $\|N(s)\|_\infty \leq 1$. At the same time, K must obtain a block-diagonal structure $K = diag(K_1, \ldots, K_n)$, where K_i is a state-feedback controller of an inverter i.*

5.3 $\mathcal{H}_\infty$ performance controller design based on LMI optimization

In this section, based on the $\mathcal{H}_\infty$ norm condition (5.28) and the state-space representation of $N(s)$ derived above, an LMI optimization problem is proposed. By solving the LMI problem, resulting inverter controllers will guarantee the robust stability of the system and the robust performance of inverter output voltages.

For the proof of the theorem derived in this section, the following lemma is provided.

Lemma 5.3. *For any $\mu > 0$ and any symmetric positive definite matrix* $\mathbf{X}$*,*

$$-\frac{1}{\mu}\mathbf{X}\mathbf{X} \leq I - \frac{2\mathbf{X}}{\sqrt{\mu}}. \tag{5.56}$$

Proof. A product of a matrix with its transpose is a positive semidefinite matrix. Hence,

$$\left(\frac{\mathbf{X}}{\sqrt{\mu}} - I\right)^T \left(\frac{\mathbf{X}}{\sqrt{\mu}} - I\right) \geq 0, \tag{5.57}$$

which immediately leads to (5.56). □

Recall the following relation between inverse matrices of positive definite matrices.

Lemma 5.4. *[147, Corollary 7.7.4] If $\mathcal{A}$, $\mathcal{B} \in \mathbb{R}^{n\times n}$ are symmetric positive definite matrices, then $\mathcal{A} \geq \mathcal{B}$ if and only if $\mathcal{B}^{-1} \geq \mathcal{A}^{-1}$.*

The proof of Lemma 5.4 can be found in [147]. Based on the two lemmas above, the following lemma is introduced and proved, whose result will be used in the proof of the main theorem.

Lemma 5.5. *Let $\mathcal{A}$, $\mathcal{B}$, $\mathcal{D}_1$, $\mathcal{D}_2$ be matrices with appropriate sizes, which satisfy the following:*

$$\begin{bmatrix} \mathcal{A} & \mathcal{B} \\ \mathcal{B}^T & \mathcal{D}_2 \end{bmatrix} < 0, \quad \textit{and} \quad \mathcal{D}_1 \leq \mathcal{D}_2 < 0, \tag{5.58}$$

where $\mathcal{D}_1$ and $\mathcal{D}_2$ are symmetric negative definite matrices with the same size. Then, the following holds:

$$\begin{bmatrix} \mathcal{A} & \mathcal{B} \\ \mathcal{B}^T & \mathcal{D}_1 \end{bmatrix} < 0. \tag{5.59}$$

Proof. According to Lemma 5.4, the following is inferred:

$$\mathcal{D}_1 \leq \mathcal{D}_2 < 0, \tag{5.60a}$$
$$\Leftrightarrow \quad -\mathcal{D}_1 \geq -\mathcal{D}_2 > 0, \tag{5.60b}$$
$$\Leftrightarrow \quad (-\mathcal{D}_2)^{-1} \geq (-\mathcal{D}_1)^{-1} > 0. \tag{5.60c}$$

By pre- and post-multiplying both sides of the last inequality by a matrix $\mathcal{B}$ with an appropriate size, the following is inferred:

$$\mathcal{B}(-\mathcal{D}_2)^{-1}\mathcal{B}^T \geq \mathcal{B}(-\mathcal{D}_1)^{-1}\mathcal{B}^T, \tag{5.61a}$$
$$\Leftrightarrow \quad -\mathcal{B}(\mathcal{D}_2)^{-1}\mathcal{B}^T \geq -\mathcal{B}(\mathcal{D}_1)^{-1}\mathcal{B}^T, \tag{5.61b}$$
$$\Leftrightarrow \quad \mathcal{A} - \mathcal{B}(\mathcal{D}_2)^{-1}\mathcal{B}^T \geq \mathcal{A} - \mathcal{B}(\mathcal{D}_1)^{-1}\mathcal{B}^T. \tag{5.61c}$$

According to the Schur complement in (3.24), the following conditions are equivalent:

$$\begin{bmatrix} \mathcal{A} & \mathcal{B} \\ \mathcal{B}^T & \mathcal{D}_2 \end{bmatrix} < 0 \;\Leftrightarrow\; \begin{cases} \mathcal{D}_2 < 0, \\ \mathcal{A} - \mathcal{B}(\mathcal{D}_2)^{-1}\mathcal{B}^T < 0. \end{cases} \tag{5.62}$$

The right-hand side of (5.62) and (5.61c) imply that $\mathcal{A} - \mathcal{B}(\mathcal{D}_1)^{-1}\mathcal{B}^T < 0$, where $\mathcal{D}_1 < 0$. According to the Schur complement in (3.24), this is equivalent to

$$\begin{bmatrix} \mathcal{A} & \mathcal{B} \\ \mathcal{B}^T & \mathcal{D}_1 \end{bmatrix} < 0. \tag{5.63}$$

□

The following theorem gives a *sufficient* stability condition to design the controller K as formulated in Problem 5.2.1. By restricting $\|N(s)\|_\infty \leq 1$, i.e., the robust performance condition (5.28) is satisfied, the robust stability and robust performance of the system in Figure 5.6 are guaranteed for all $\|\Delta\|_\infty < 1$.

Theorem 5.6. *Consider the system (5.53) with the transfer function matrix (5.55). Let $P_{ii} \in \mathbb{R}^{3\times 3}$, $i = 1,\ldots,n$, and $P_W \in \mathbb{R}^{7n\times 7n}$ be symmetric positive definite matrices, where n is the number of inverters in the system. Define $\bar{P} = diag(P_{11},\ldots,P_{nn},P_W) \in \mathbb{R}^{10n\times 10n}$. Let $\gamma_P > 0$ be an optimization variable. Define the following LMI variables:*

$$\begin{aligned} \bar{\mathbf{X}} &= diag(\mathbf{X}_{11},\ldots,\mathbf{X}_{nn},\mathbf{X}_W) = \bar{P}^{-1}, \\ \bar{\mathbf{Y}} &= [\mathbf{Y}\ \ 0_{2n\times 2n}\ \ 0_{2n\times 2n}\ \ 0_{2n\times 3n}] = \bar{K}\bar{P}^{-1},\ \mathbf{Y} = diag(\mathbf{Y}_{11},\ldots,\mathbf{Y}_{nn}), \end{aligned} \tag{5.64}$$

where $\mathbf{X}_W \in \mathbb{R}^{7n\times 7n}$, $\bar{\mathbf{Y}} \in \mathbb{R}^{2n\times 10n}$, and $\mathbf{X}_{ii} \in \mathbb{R}^{3\times 3}$, $\mathbf{Y}_{ii} \in \mathbb{R}^{2\times 3}$, $i = 1,\ldots,n$.
Then $||N(s)||_\infty < \gamma_P$ and $\check{A} = (\bar{A} + \bar{B}\bar{K})$ is Hurwitz if the following LMI optimization problem is feasible:

$$\begin{bmatrix} \bar{\mathcal{F}} & \bar{\mathcal{L}}_1 & \bar{\mathcal{L}}_2 & \bar{\mathcal{L}}_3 \\ \bar{\mathcal{L}}_1^T & -\mu_1 I & 0 & 0 \\ \bar{\mathcal{L}}_2^T & 0 & -\mu_2 I & 0 \\ \bar{\mathcal{L}}_3^T & 0 & 0 & I - \frac{2\bar{\mathbf{X}}}{\sqrt{\mu_1+\mu_2}} \end{bmatrix} < 0, \tag{5.65}$$

where $\mu_1 > 0, \mu_2 > 0$ are design parameters, and $\bar{\mathcal{L}}_1, \bar{\mathcal{L}}_2, \bar{\mathcal{L}}_3, \bar{\mathcal{F}}$ are defined as follows:

$$\bar{\mathcal{F}} = \begin{bmatrix} \bar{A}\bar{\mathbf{X}} + \bar{B}\bar{\mathbf{Y}} + (\bar{A}\bar{\mathbf{X}} + \bar{B}\bar{\mathbf{Y}})^T & B_1 & (C_1\bar{\mathbf{X}} + D_{12}\bar{\mathbf{Y}})^T \\ B_1^T & -\gamma_P I & D_{11}^T \\ C_1\bar{\mathbf{X}} + D_{12}\bar{\mathbf{Y}} & D_{11} & -\gamma_P I \end{bmatrix}, \bar{\mathcal{L}}_1 = \begin{bmatrix} \bar{B}\bar{\mathbf{Y}} \\ 0 \\ 0 \end{bmatrix}, \bar{\mathcal{L}}_2 = \begin{bmatrix} 0 \\ 0 \\ D_{12}\bar{\mathbf{Y}} \end{bmatrix}, \bar{\mathcal{L}}_3 = \begin{bmatrix} 0 \\ \bar{D}_{21}^T \\ 0 \end{bmatrix}. \tag{5.66}$$

Proof. The proof of Theorem 5.6 is based on the Bounded Real Lemma (4.57). By applying the Bounded Real Lemma to the transfer function matrix $N(s)$ in (5.55), $||N(s)||_\infty < \gamma_P$ and $\check{A} = (\bar{A} + \bar{B}\bar{K})$ is Hurwitz if there exists a solution $\bar{P} = \bar{P}^T > 0$ to the following matrix inequality:

$$\begin{bmatrix} \check{A}^T\bar{P} + \bar{P}\check{A} & \bar{P}\check{B} & \check{C}^T \\ \check{B}^T\bar{P} & -\gamma_P I & \check{D}^T \\ \check{C} & \check{D} & -\gamma_P I \end{bmatrix} < 0. \tag{5.67}$$

Note that because $\bar{P}$ is defined to be block-diagonal, (5.67) is a sufficient condition.

Define the variables $\bar{\mathbf{X}} = \bar{P}^{-1}, \bar{\mathbf{Y}} = \bar{K}\bar{P}^{-1}$ as in (5.64). By pre- and post-multiplying (5.67) by a symmetric positive definite matrix $\text{diag}(\bar{P}^{-1}, I, I)$, where $\bar{P}$ is a block-diagonal matrix, the

following equivalent matrix inequality is derived:

$$\begin{bmatrix} \bar{A}\bar{\mathbf{X}}+\bar{B}\bar{\mathbf{Y}}+(\bar{A}\bar{\mathbf{X}}+\bar{B}\bar{\mathbf{Y}})^T & B_1+\bar{B}\bar{K}\bar{D}_{21} & (C_1\bar{\mathbf{X}}+D_{12}\bar{\mathbf{Y}})^T \\ (B_1+\bar{B}\bar{K}\bar{D}_{21})^T & -\gamma_P I & (D_{11}+D_{12}\bar{K}\bar{D}_{21})^T \\ C_1\bar{\mathbf{X}}+D_{12}\bar{\mathbf{Y}} & D_{11}+D_{12}\bar{K}\bar{D}_{21} & -\gamma_P I \end{bmatrix} < 0. \tag{5.68}$$

With the notations in (5.66), the matrix inequality (5.68) can be decomposed as follows:

$$\begin{aligned} &\underbrace{\begin{bmatrix} \bar{A}\bar{\mathbf{X}}+\bar{B}\bar{\mathbf{Y}}+(\bar{A}\bar{\mathbf{X}}+\bar{B}\bar{\mathbf{Y}})^T & B_1 & (C_1\bar{\mathbf{X}}+D_{12}\bar{\mathbf{Y}})^T \\ B_1^T & -\gamma_P I & D_{11}^T \\ C_1\bar{\mathbf{X}}+D_{12}\bar{\mathbf{Y}} & D_{11} & -\gamma_P I \end{bmatrix}}_{=\bar{\mathcal{F}}} + \underbrace{\begin{bmatrix} 0 & \bar{B}\bar{\mathbf{Y}}\bar{\mathbf{X}}^{-1}\bar{D}_{21} & 0 \\ 0 & 0 & 0 \\ 0 & 0 & 0 \end{bmatrix}}_{=\bar{\mathcal{L}}_1\bar{\mathbf{X}}^{-1}\bar{\mathcal{L}}_3^T} \\ &+ \underbrace{\begin{bmatrix} 0 & 0 & 0 \\ (\bar{B}\bar{\mathbf{Y}}\bar{\mathbf{X}}^{-1}\bar{D}_{21})^T & 0 & 0 \\ 0 & 0 & 0 \end{bmatrix}}_{=\bar{\mathcal{L}}_3\bar{\mathbf{X}}^{-1}\bar{\mathcal{L}}_1^T} + \underbrace{\begin{bmatrix} 0 & 0 & 0 \\ 0 & 0 & 0 \\ 0 & D_{12}\bar{\mathbf{Y}}\bar{\mathbf{X}}^{-1}\bar{D}_{21} & 0 \end{bmatrix}}_{=\bar{\mathcal{L}}_2\bar{\mathbf{X}}^{-1}\bar{\mathcal{L}}_3^T} + \underbrace{\begin{bmatrix} 0 & 0 & 0 \\ 0 & 0 & (D_{12}\bar{\mathbf{Y}}\bar{\mathbf{X}}^{-1}\bar{D}_{21})^T \\ 0 & 0 & 0 \end{bmatrix}}_{=\bar{\mathcal{L}}_3\bar{\mathbf{X}}^{-1}\bar{\mathcal{L}}_2^T} \\ &= \quad \bar{\mathcal{F}}+\bar{\mathcal{L}}_1\bar{\mathbf{X}}^{-1}\bar{\mathcal{L}}_3^T+\bar{\mathcal{L}}_3\bar{\mathbf{X}}^{-1}\bar{\mathcal{L}}_1^T+\bar{\mathcal{L}}_2\bar{\mathbf{X}}^{-1}\bar{\mathcal{L}}_3^T+\bar{\mathcal{L}}_3\bar{\mathbf{X}}^{-1}\bar{\mathcal{L}}_2^T \ < \ 0. \end{aligned} \tag{5.69}$$

A product of a matrix with its transpose is a positive semidefinite matrix, thus

$$\begin{aligned} &\left(\frac{1}{\sqrt{\mu_1}}\bar{\mathcal{L}}_1-\sqrt{\mu_1}\bar{\mathcal{L}}_3\bar{\mathbf{X}}^{-1}\right)\left(\frac{1}{\sqrt{\mu_1}}\bar{\mathcal{L}}_1-\sqrt{\mu_1}\bar{\mathcal{L}}_3\bar{\mathbf{X}}^{-1}\right)^T \geq 0 \\ \Leftrightarrow \ &\frac{1}{\mu_1}\bar{\mathcal{L}}_1\bar{\mathcal{L}}_1^T+\mu_1\bar{\mathcal{L}}_3\bar{\mathbf{X}}^{-1}\bar{\mathbf{X}}^{-1}\bar{\mathcal{L}}_3^T-\bar{\mathcal{L}}_1\bar{\mathbf{X}}^{-1}\bar{\mathcal{L}}_3^T-\bar{\mathcal{L}}_3\bar{\mathbf{X}}^{-1}\bar{\mathcal{L}}_1^T \geq 0 \\ \Leftrightarrow \ &\frac{1}{\mu_1}\bar{\mathcal{L}}_1\bar{\mathcal{L}}_1^T+\mu_1\bar{\mathcal{L}}_3\bar{\mathbf{X}}^{-1}\bar{\mathbf{X}}^{-1}\bar{\mathcal{L}}_3^T \ \geq \ \bar{\mathcal{L}}_1\bar{\mathbf{X}}^{-1}\bar{\mathcal{L}}_3^T+\bar{\mathcal{L}}_3\bar{\mathbf{X}}^{-1}\bar{\mathcal{L}}_1^T. \end{aligned} \tag{5.70}$$

Similarly, the following can be achieved:

$$\frac{1}{\mu_2}\bar{\mathcal{L}}_2\bar{\mathcal{L}}_2^T+\mu_2\bar{\mathcal{L}}_3\bar{\mathbf{X}}^{-1}\bar{\mathbf{X}}^{-1}\bar{\mathcal{L}}_3^T \ \geq \ \bar{\mathcal{L}}_2\bar{\mathbf{X}}^{-1}\bar{\mathcal{L}}_3^T+\bar{\mathcal{L}}_3\bar{\mathbf{X}}^{-1}\bar{\mathcal{L}}_2^T. \tag{5.71}$$

By using the inequalities (5.70) and (5.71), the following upper bound of the matrix inequality (5.69) is derived:

$$\begin{aligned} &\bar{\mathcal{F}} \ +\bar{\mathcal{L}}_1\bar{\mathbf{X}}^{-1}\bar{\mathcal{L}}_3^T+\bar{\mathcal{L}}_3\bar{\mathbf{X}}^{-1}\bar{\mathcal{L}}_1^T+\bar{\mathcal{L}}_2\bar{\mathbf{X}}^{-1}\bar{\mathcal{L}}_3^T+\bar{\mathcal{L}}_3\bar{\mathbf{X}}^{-1}\bar{\mathcal{L}}_2^T \\ &\quad \leq \ \bar{\mathcal{F}}+\frac{1}{\mu_1}\bar{\mathcal{L}}_1\bar{\mathcal{L}}_1^T+\mu_1\bar{\mathcal{L}}_3\bar{\mathbf{X}}^{-1}\bar{\mathbf{X}}^{-1}\bar{\mathcal{L}}_3^T+\frac{1}{\mu_2}\bar{\mathcal{L}}_2\bar{\mathcal{L}}_2^T+\mu_2\bar{\mathcal{L}}_3\bar{\mathbf{X}}^{-1}\bar{\mathbf{X}}^{-1}\bar{\mathcal{L}}_3^T. \end{aligned} \tag{5.72}$$

Hence, by forcing the above upper bound of (5.69) to be negative definite, a sufficient condition for (5.69) is derived as follows:

$$\bar{\mathcal{F}}+\frac{1}{\mu_1}\bar{\mathcal{L}}_1\bar{\mathcal{L}}_1^T+\mu_1\bar{\mathcal{L}}_3\bar{\mathbf{X}}^{-1}\bar{\mathbf{X}}^{-1}\bar{\mathcal{L}}_3^T+\frac{1}{\mu_2}\bar{\mathcal{L}}_2\bar{\mathcal{L}}_2^T+\mu_2\bar{\mathcal{L}}_3\bar{\mathbf{X}}^{-1}\bar{\mathbf{X}}^{-1}\bar{\mathcal{L}}_3^T<0. \tag{5.73}$$

According to the Schur complement (3.24), the following is derived equivalently from (5.73):

$$\begin{bmatrix} \bar{\mathcal{F}} & \bar{\mathcal{L}}_1 & \bar{\mathcal{L}}_2 & \bar{\mathcal{L}}_3 \\ \bar{\mathcal{L}}_1^T & -\mu_1 I & 0 & 0 \\ \bar{\mathcal{L}}_2^T & 0 & -\mu_2 I & 0 \\ \bar{\mathcal{L}}_3^T & 0 & 0 & -\frac{1}{\mu_1+\mu_2}\bar{\mathbf{X}}\bar{\mathbf{X}} \end{bmatrix}<0. \tag{5.74}$$

Based on the inequality (5.56), it holds that:

$$-\frac{1}{\mu_1+\mu_2}\bar{\mathbf{X}}\bar{\mathbf{X}}\leq I-\frac{2\bar{\mathbf{X}}}{\sqrt{\mu_1+\mu_2}}. \tag{5.75}$$

According to Lemma 5.5, where $\mathcal{D}_1=-\frac{1}{\mu_1+\mu_2}\bar{\mathbf{X}}\bar{\mathbf{X}}$, $\mathcal{D}_2=I-\frac{2\bar{\mathbf{X}}}{\sqrt{\mu_1+\mu_2}}$, the matrix inequality (5.74) and the relation (5.75) yield the following sufficient condition for (5.74):

$$\begin{bmatrix} \bar{\mathcal{F}} & \bar{\mathcal{L}}_1 & \bar{\mathcal{L}}_2 & \bar{\mathcal{L}}_3 & \\ \bar{\mathcal{L}}_1^T & -\mu_1 I & 0 & 0 & \\ \bar{\mathcal{L}}_2^T & 0 & -\mu_2 I & 0 & 0 \\ \bar{\mathcal{L}}_3^T & 0 & 0 & I-\frac{2\bar{\mathbf{X}}}{\sqrt{\mu_1+\mu_2}} & \end{bmatrix}<0. \tag{5.76}$$

Note that by the virtue of the Schur complement, the feasibility of the LMI (5.65) simultaneously implies that the matrix $\left(I-\frac{2\bar{\mathbf{X}}}{\sqrt{\mu_1+\mu_2}}\right)$ in (5.75) is negative definite. This completes the proof. □

The asymptotic stability of the inverters should be noted here. If the LMI (5.65) is feasible, $\check{A}=(\bar{A}+\bar{B}\bar{K})$ is Hurwitz. Thus,

$$\check{A}=\bar{A}+\bar{B}\bar{K}=\begin{bmatrix} \tilde{A} & 0 & 0 & 0 \\ 0 & A_T & 0 & 0 \\ 0 & 0 & A_U & 0 \\ B_E & 0 & 0 & A_E \end{bmatrix}+\begin{bmatrix} \tilde{B} \\ B_T \\ B_U \\ 0 \end{bmatrix}\begin{bmatrix} K & 0 & 0 & 0 \end{bmatrix}=\left[\begin{array}{c|ccc} \tilde{A}+\tilde{B}K & 0 & 0 & 0 \\ \hline B_TK & A_T & 0 & 0 \\ B_UK & 0 & A_U & 0 \\ B_E & 0 & 0 & A_E \end{array}\right]. \tag{5.77}$$

It is inferred from (5.77) that eigenvalues of $(\tilde{A}+\tilde{B}K)$ are also the eigenvalues of matrix $\check{A}$. If $\check{A}$ is a Hurwitz matrix, $(\tilde{A}+\tilde{B}K)$ is also a Hurwitz matrix. Hence, the feasibility of the LMI (5.65) guarantees the asymptotic stability of the nominal closed-loop inverter part.

Moreover, if the LMI (5.65) is feasible with $\gamma_P \leq 1$, $\|N(s)\|_\infty < \gamma_P \leq 1$ and the condition (5.28) is satisfied. Consequently, the robust stability and robust performance of the system are assured with $\|\Delta\|_\infty \leq 1$. The LMI optimization problem for robust stability and robust performance is formulated as follows:

$$\texttt{minimize } \gamma_P \texttt{ such that } \begin{cases} \texttt{LMI } (5.65) \texttt{ is feasible over } \bar{\mathbf{X}} \texttt{ and } \bar{\mathbf{Y}}, \\ \bar{\mathbf{X}} \texttt{ and } \bar{\mathbf{Y}} \texttt{ are defined as in } (5.64), \\ \bar{\mathbf{X}} > 0, \\ \mu_1, \mu_2 > 0, \\ 0 < \gamma_P \leq 1. \end{cases} \tag{5.78}$$

Remark 5.3.1. $\mu_1, \mu_2 > 0$ are introduced to add two more degrees of freedom to solve the LMI problem (5.78). $\mu_1, \mu_2 > 0$ are set in advance. If the LMI problem is infeasible for some μ_1, μ_2, different values for μ_1, μ_2 can be taken. Thus, $\mu_1, \mu_2 > 0$ allow to create an iterative algorithm to solve the LMI problem (5.78) until a feasible result is derived. However, this issue is not further investigated in the thesis. For the simulation example in this chapter, constant $\mu_1, \mu_2 > 0$ are set in advance.

Remark 5.3.2. By implementing the $\mathcal{H}_\infty$ control technique, a system model includes additional weight functions in itself. Therefore, when designing optimal output feedback controllers, resulting controllers generally obtain a higher order. In this case, the system model (5.48) has a higher order than the model (5.5) of inverters. However, by defining in advance the structures of the LMI variables as in (5.64), resulting controller $\bar{K}$ obtains a defined structure $\bar{K} = [K \;\; 0 \;\; 0 \;\; 0]$, where $K = \text{diag}(K_1, \ldots, K_n)$ is the controller for the inverters. No high-order controller is synthesized.

Depending on particular cases, the LMI optimization problem (5.78) can be conservative and even infeasible with $\gamma_P \leq 1$. In case of infeasibility, the constraint on γ_P can be modified as the following with $\gamma_P^{\max} > 1$:

$$0 < \gamma_P < \gamma_P^{\max}, \tag{5.79}$$

so that the LMI optimization problem (5.78) obtains feasible solutions. In this case, the nominal asymptotic stability is still guaranteed as shown in (5.77). However, performance specifications are violated as $\|N(s)\|_\infty < 1$ is not guaranteed. Nevertheless, as the feasibility of the LMI (5.65) guarantees that $\|N(s)\|_\infty < \gamma_P$, by minimizing γ_P while solving the LMI problem (5.78) (even with $\gamma_P^{\max} > \gamma_P > 1$), $\|N(s)\|_\infty$ is still decreased. Smaller $\|N(s)\|_\infty$ implies smaller amplification of the disturbance inputs $U_d(s)$ and $W(s)$, when they pass through the system.

Furthermore, with resulting controllers (where $\gamma_P > 1$), robust stability and robust performance properties can still be checked by the norm conditions (5.21) and (5.24), respectively. That is:

- If $\|M(s)\|_\infty \leq 1$, the robust stability of the closed-loop system is guaranteed.
- If $\|F_u(N,\Delta)\|_\infty \leq 1$ and $\|M(s)\|_\infty \leq 1$, the robust stability and the robust performance of the system are guaranteed.

5.4 Simulation study

In this section, a simulation study is provided to show the effectiveness of the system modeling and the controller design technique based on the LMI problem (5.78). The test system in the simulation study of Chapter 3 is considered once again with two additional impedances Z_{12} and Z_{22} as shown in Figure 5.11. Z_{12} and Z_{22} are added to illustrate larger load changes (model uncertainty). Parameters of the test system with additional details are provided in Table 5.1.

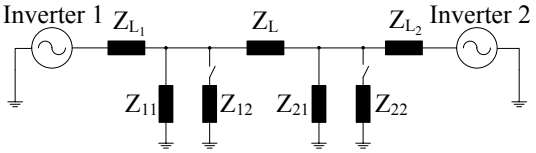

FIGURE 5.11: Test system with two inverters and impedance loads.

TABLE 5.1: Test system parameters and chosen weight functions

Voltages and phase angles	$V_{1_0} = 1029[\text{V}]$ $V_{2_0} = 1030 + 1.3i[\text{V}]$	$\delta_{1_0} = 0.000[\text{rad}]$ $\delta_{2_0} = 0.0013[\text{rad}]$
Active and reactive powers	$\tilde{P}_{1_0} = 10.75[\text{kW}]$ $\tilde{Q}_{1_0} = 3.56[\text{kVar}]$	$\tilde{P}_{2_0} = 15.62[\text{kW}]$ $\tilde{Q}_{2_0} = 8.06[\text{kVar}]$
Base values	$S_{\text{base}} = 108[\text{kVA}]$ $Z_{\text{base}} = 9.823[\Omega]$	$V_{\text{base}} = 1030[\text{V}]$ $\delta_{\text{base}} = 1[\text{rad}]$
Load impedances	$Z_{11} = 108 + i10.8[\Omega]$ $Z_{12} = 69 + i15[\Omega]$	$Z_{21} = 45 + i28[\Omega]$ $Z_{22} = 60 + i19[\Omega]$
Line impedances	$Z_{\text{L}_1} = 0.4 + i0.4[\Omega]$ $Z_{\text{L}_2} = 0.4 + i0.3[\Omega]$	$Z_{\text{L}} = 0.8 + i0.42[\Omega]$
Nominal frequency	$\omega_{\text{nom}} = 2\pi 50[\text{rad/s}]$	
Filter parameter	$\tau_1 = 0.0265[\text{s}]$	$\tau_2 = 0.0265[\text{s}]$
Reference changes	$\tilde{P}^{\text{r}}_{1_0} = 10[\text{kW}]$ $\tilde{P}^{\text{r}}_{2_0} = 5[\text{kW}]$	$\tilde{Q}^{\text{r}}_{1_0} = 5[\text{kVar}]$ $\tilde{Q}^{\text{r}}_{2_0} = 8[\text{kVar}]$
$W_{u_{i1}}(s) = W_{u_{i2}}(s)$ $i = 1,2$	$r^{\omega}_{0_i} = r^{V}_{0_i} = 2.3$ $r^{\omega}_{\infty_i} = r^{V}_{\infty_i} = 5.9$	$\tau^{\omega}_i = \tau^{V}_i = 1e-2[\text{s}]$
$W_t(s)$	$r^t_0 = 5.1,\ r^t_\infty = 0.1$	$\tau^t = 1e-3[\text{s}]$
$W_e(s)$	$r^e_0 = 0.2,\ r^e_\infty = 0.02$	$\tau^t = 1e-2[\text{s}]$

The system model (5.48) and the LMI problem (5.78) are constructed with the parameters in Table 5.1. Nominal load and line impedances are Z_{11}, Z_{21}, Z_{L_1} and Z_{L_2}, respectively. In order to include admittance uncertainties, load impedances are changed down to 50% of their nominal values. Line impedances are slightly varied around nominal values. Accordingly, different

model uncertainties and a matching $W_T(s)$ are derived as shown in Figure 5.8. Note that for this example, $\kappa_1 = \kappa_2 = 1$ are chosen in advance. By solving the LMI optimization problem (5.78) with $\mu_1 = \mu_2 = 1e-7$, the following performance controllers are obtained with $\gamma_P = 0.319$:

$$K_1^p = \begin{bmatrix} -1.5 \cdot 10^{-5} & 10^{-8} & -10^{-8} \\ -10^{-9} & 0 & 0 \end{bmatrix}, \tag{5.80}$$

$$K_2^p = \begin{bmatrix} -1.5 \cdot 10^{-5} & 10^{-8} & -10^{-8} \\ -2.2 \cdot 10^{-8} & 0 & 0 \end{bmatrix}, \tag{5.81}$$

where their equivalences in actual quantities are:

$$\begin{aligned} K_1^p &= \begin{bmatrix} -1.5 \cdot 10^{-5}[\frac{1}{s}] & 10^{-10}[\frac{\text{rad}}{\text{skW}}] & -10^{-10}[\frac{\text{rad}}{\text{skVar}}] \\ -10^{-6}[\frac{\text{V}}{\text{rad}}] & 0[\frac{\text{V}}{\text{kW}}] & 0[\frac{\text{V}}{\text{kVar}}] \end{bmatrix}, \\ K_2^p &= \begin{bmatrix} -1.5 \cdot 10^{-5}[\frac{1}{s}] & 10^{-10}[\frac{\text{rad}}{\text{skW}}] & -10^{-10}[\frac{\text{rad}}{\text{skVar}}] \\ -2.2 \cdot 10^{-5}[\frac{\text{V}}{\text{rad}}] & 0[\frac{\text{V}}{\text{kW}}] & 0[\frac{\text{V}}{\text{kVar}}] \end{bmatrix}. \end{aligned} \tag{5.82}$$

The performance controllers K_1^p and K_2^p return $\|N(s)\|_\infty = 0.283$. Hence, with $\|N(s)\|_\infty = 0.283 < 1$, the robust performance condition (5.28) is satisfied. Therefore, the robust stability of the system as well as the robust performance of the control input are guaranteed with respect to the chosen weight functions $W_U(s)$, $W_E(s)$ and $W_T(s)$. The maximum singular value of the frequency response $N(j\omega)$ with the performance controllers K_1^p and K_2^p is shown in Figure 5.12.

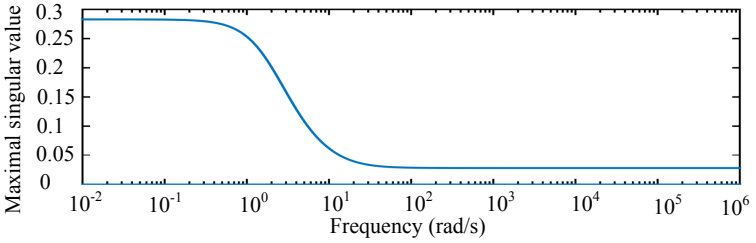

FIGURE 5.12: $\bar{\sigma}(N(j\omega))$ of the test system with the performance controllers (5.82).

For comparison purpose, a simulation of the test system in Figure 5.11 is conducted in Matlab with two pairs of controllers:

- Robust performance controllers (5.82) with the power control loop in Figure 5.1,
- Nominal controllers (3.31) with the power control loop in Figure 3.1, which are designed in Chapter 3.

It should be mentioned that the nominal inverter controllers (3.31) do not guarantee the robust stability of the system and the robust performance of voltages. However, it will be shown via this particular simulation that the controllers (3.31) with the power control loop in Figure 3.1 still coincidentally stabilize the system despite uncertainties.

A sequence of discrete events separated by ten-second intervals is included in the simulation according to the following scenario: initially, Z_{11} and Z_{21} are connected to the system, then Z_{12} and Z_{22} are successively added in the written order; finally, reference changes (by applying $\tilde{P}_{i_0} := \tilde{P}_{i_0} + \tilde{P}^{\mathrm{r}}_{i_0}$, $\tilde{Q}_{i_0} := \tilde{Q}_{i_0} + \tilde{Q}^{\mathrm{r}}_{i_0}$ to the power control loops in Figure 3.1 and Figure 5.1) are included in the simulation. The simulation results are presented in Figure 5.13. The graphs denoted by "p" are achieved by the performance controllers K_1^p and K_2^p, while the other graphs are obtained by the nominal controllers K_1 and K_2 in (3.31).

It is seen in Figure 5.13 that the system is robustly stabilized by both pairs of controllers despite load changes. With both controller pairs, inverter output frequencies converge to the nominal value and inverter output voltages vary around their nominal values to modify output power. When a load is connected, both inverters react and generate more power to supply the load demand. After load changes, new equilibrium points are reached, which are different from previous equilibrium points.

Regarding the voltage performance, it should be mentioned that the magnitude deviations of voltages derived in the simulation are relatively small and can be unrealistic. This is because of the simplicity of the test microgrid as well as ideal conditions of the simulation. With the nominal controllers, it is seen that the additional loads Z_{12} and Z_{22} cause steady-state magnitude deviations of voltages. The purpose of the power reference changes at $t = 30[s]$ and $t = 40[s]$ is to reduce power mismatches between generated output power and their references. Consequently, deviations of V_1 and V_2 from their nominal values are reduced.

It is also seen in Figure 5.13 that with the robust performance controllers K_1^p and K_2^p, magnitude deviations of voltages are significantly reduced, compared to the case with the nominal controllers. Steady-state magnitude deviations of voltages caused by K_1^p and K_2^p are too small to be noticed in Figure 5.13. Moreover, it is seen from the simulation results that the performance controllers reduce frequency deviations during transients, compared to the case with the nominal controllers.

Regarding the higher-frequency components in voltages, it is noteworthy that the simulation above is performed with ideal voltage sources with controllable voltage magnitude and phase angle, but not with VSIs. Therefore, voltages obtain ideal sinusoidal form and no claim could be made about the THD of voltages. If the same simulation is accomplished with VSIs with the three-level control hierarchy presented in Figure 2.4, it is expected that inverter output voltages will obtain higher-frequency components (because of inverter switching, nonlinear loads, etc.).

Remark 5.4.1. It is seen in the simulation above that there is a sort of power sharing between inverters as both inverters react to load changes and inject power to supply load demand. It will be shown in the next chapter that the power sharing performance can be improved by adjusting

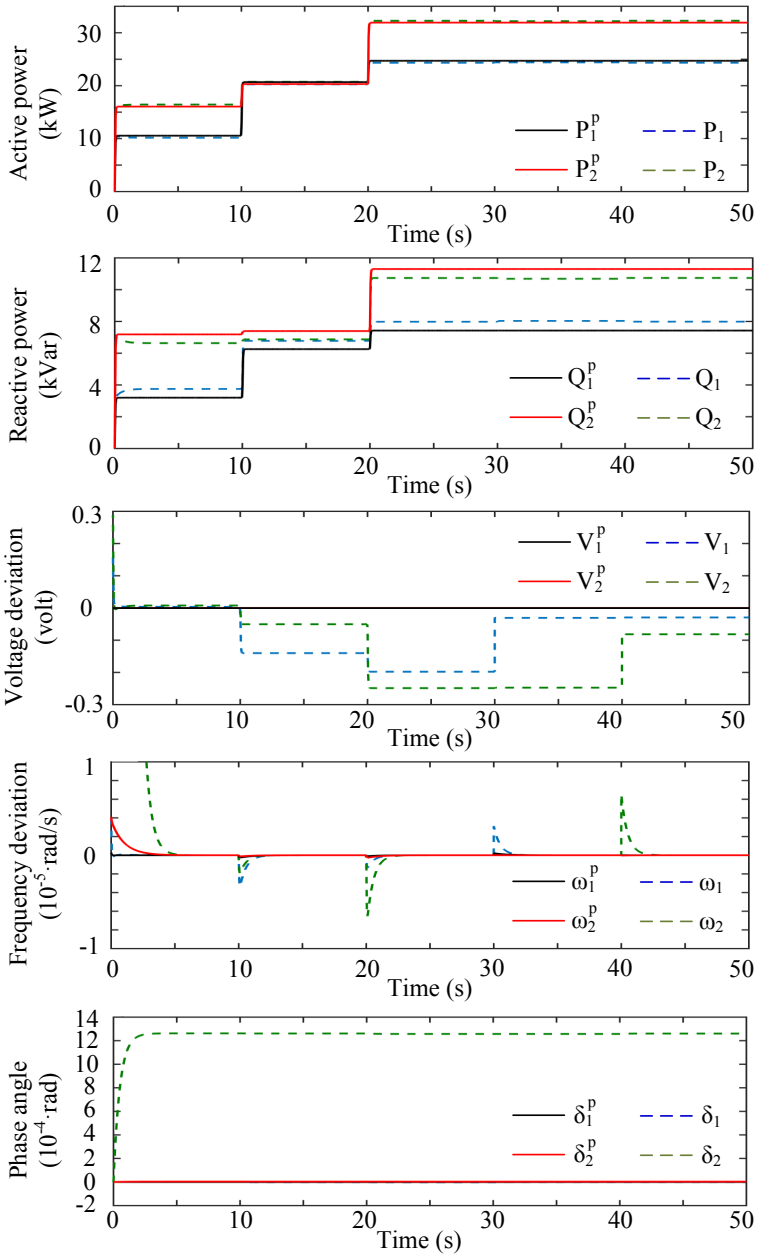

FIGURE 5.13: Transfer processes of the test system with both controller pairs.

the controller gains appropriately. This procedure is done without causing system instability and performance problem to voltages.

5.5 Summary

Using the $\mathcal{H}_\infty$ control technique, robust stability and robust performance of voltages against uncertainties in a microgrid were studied. As the considered $\mathcal{H}_\infty$ control framework requires asymptotically stable model uncertainties for robust stability analysis, a modification of the inverter power control loop was proposed. With the modification, the integrator in Figure 3.1

was replaced by an asymptotically stable subordinate control loop (see Figure 5.1). With the modified power control loop, the resulting additive model uncertainty of a microgrid (caused by uncertain admittances) is asymptotically stable. Then, a generalized plant model of an inverter-based microgrid with possible uncertainties and weight functions was introduced. Based on an $\mathcal{H}_\infty$ norm condition for robust performance, an LMI optimization problem was proposed to design inverter controllers. Resulting controllers guarantee the robust stability of a microgrid, zero steady-state frequency deviations as well as the robust performance of voltages against uncertainties.

As the $\mathcal{H}_\infty$ norm condition (5.24) for robust performance property is a sufficient condition, the proposed LMI problem (5.78) based on this $\mathcal{H}_\infty$ norm condition can be conservative. In addition, inappropriate choices of weight functions can drastically increase the conservatism of the LMI problem.

In order to validate the effectiveness of the proposed robust controller design method, a Matlab simulation of a simple microgrid was provided. Simulation results have shown that the robust stability of the system and the robust performance of inverter output voltages with respect to uncertainties are achieved.

A particular strength of $\mathcal{H}_\infty$ control is that it allows to design dynamic controllers, e.g. proportional-integral controllers. In case some renewable source inverters should maximally inject their available power into a microgrid to increase system operating efficiency, proportional-integral controllers will allow these inverters to track their maximal power references. Thus, it is possible with the $\mathcal{H}_\infty$ framework to simultaneously design proportional-integral controllers for several inverters and proportional controllers for remaining inverters, which then collectively guarantee the system robust performance.

Another key strength of $\mathcal{H}_\infty$ control is that extra model uncertainties and disturbance inputs, e.g., measurement noise, output disturbances, multiplicative uncertainties, can be additionally included in the proposed robust stability and robust performance analysis of microgrids. For instance, if there exist measurement noise or output disturbances to the nominal plant output $Y(s)$ in Figure 5.4, these signal uncertainties can be included in the presented framework for robust stability and robust performance analysis without any difficulty. $\mathcal{H}_\infty$ control allows to simultaneously consider different uncertain sources within a single control problem.

In the next chapter, based on the power control loop in Figure 5.1 and Theorem 5.6, a design of droop-based power sharing controllers for inverters is proposed. This is done by introducing particular structures to the LMI variables of the LMI problem (5.65). Thereby, an advantage of the proposed control approach in this chapter becomes clear. Power sharing controllers must be designed so that, on one hand power sharing performance is improved, and on the other hand, the system robust stability and robust voltage performance are guaranteed.

Chapter 6

Power sharing between inverters

Due to environmental and economic factors amongst others, it is preferable that inverters are able to form a desired power flow within a microgrid. Considering power flows within a microgrid, the interconnection between inverter nodes is directly addressed, which is a disturbance source for the stability of inverters (see Remark 3.1.2). In general, power flow strategies should be accomplished by decentralized power controllers of inverters [11, 19, 20, 22, 38]. Although being the main goal at the power control level of a microgrid, power flow strategies can be pursued only when the system stability is assured.

Power flow strategy in inverter-based microgrids will be discussed in the sense of power sharing. Power sharing is commonly understood as an ability of generation units in a power system, in which all generation units share an increase of system load by predefined ratios [5, 20]. For inverter-based microgrids, power sharing plays an important role since by sharing total system load between inverters, overload of particular inverters is avoided. It should be noted that small overcurrent over several cycles (due to, e.g., connecting a load) can lead to total damage of such power electronic devices like IGBT inverters.

The simulation in Chapter 5 has shown that with the power control loop in Figure 5.1, all inverters react to load changes at different system nodes, i.e., power sharing between inverters is accomplished. In this chapter, it will be shown that by integrating the idea of the droop control to the power control loop in Figure 5.1, power sharing performance can be improved. Note that unlike the classical droop control in (2.20), an *angle droop control* for active power sharing will be investigated together with the well-known voltage droop control for reactive power sharing.

Droop gains in inverter controllers will be defined. Inverter controllers will be designed by solving the LMI optimization problem (5.65) with additional variable constraints. By forcing particular structures to the LMI variables, phase angle and voltage droop controllers for inverters will be derived as results of the LMI problem. Moreover, power sharing ratios between inverters

can also be set by adding a constraint to the LMI variables. Inverter controllers will then obtain desired ratios between droop gains to share the system load without causing stability and voltage performance problems. Nevertheless, additional constraints on LMI variables will add conservatism to the LMI problem (5.65). It is noteworthy that an improvement of power sharing performance will be shown by a simulation. However, an exactly as desired power sharing is neither proved nor obtained in the simulation.

6.1 Power sharing gains in a decentralized controller

Power sharing is usually understood as an ability of inverters to share any increase in system load. In this chapter, power sharing control is investigated for the control loop proposed in Figure 5.1. The reason is that load changes lead to model uncertainty of a microgrid, which is discussed in chapter 5. Thus, power sharing controllers will be designed by implementing the LMI problem (5.65).

The design of power sharing controllers presented hereafter can be similarly applied to the control loop in Figure 3.1, where inverter controllers can be computed by solving the LMI problem (3.27). However, it should be noted that the LMI problem (3.27) does not robustly guarantee the system stability under load changes, which actually should be shared among inverters. This is the main reason for choosing the control loop in Figure 5.1 for the power sharing purpose.

A controller of an overall microgrid with the control loop proposed in Figure 5.1 has a form $K = \mathrm{diag}(K_1, \ldots, K_n)$, where $K_i \in \mathbb{R}^{2\times 3}$ is a controller of an inverter i, $i = 1, \ldots, n$. In order to include the power sharing capability in inverter controllers, the idea of the droop control is implemented. That is, by modifying phase angles and magnitudes of inverter output voltages, output active and reactive power is modified [33]. As mentioned above, an angle droop control is implemented for active power sharing and a voltage droop control is responsible for reactive power sharing. Consider a controller K_i in Figure 5.1, the control law is expressed as follows:

$$u_i(t) = K_i x_i(t) \quad \Leftrightarrow \quad \begin{bmatrix} u_{i_1} \\ V_i - V_{i_0} \end{bmatrix} = \begin{bmatrix} K_{i,11} & K_{i,12} & K_{i,13} \\ K_{i,21} & K_{i,22} & K_{i,23} \end{bmatrix} \begin{bmatrix} \delta_i - \delta_{i_0} \\ \tilde{P}_i - \tilde{P}_{i_0} \\ \tilde{Q}_i - \tilde{Q}_{i_0} \end{bmatrix}. \tag{6.1}$$

As droop controllers for inverters will be designed, particular matrix elements of a controller $K_i \in \mathbb{R}^{2\times 3}$ are forced to be zero. It will be shown later that by solving the LMI problem (5.65), the following structure of $K_i \in \mathbb{R}^{2\times 3}$ can be derived, if the LMI variables are forced to obtain

particular structures:

$$u_i(t) = K_i x_i(t) \quad \Leftrightarrow \quad \begin{bmatrix} u_{i_1} \\ V_i - V_{i_0} \end{bmatrix} = \begin{bmatrix} 0 & K_{i,12} & 0 \\ 0 & 0 & K_{i,23} \end{bmatrix} \begin{bmatrix} \delta_i - \delta_{i_0} \\ \tilde{P}_i - \tilde{P}_{i_0} \\ \tilde{Q}_i - \tilde{Q}_{i_0} \end{bmatrix}. \tag{6.2}$$

where $K_{i,12}$ and $K_{i,23}$ are active and reactive power droop gains of K_i, respectively.

Moreover, from the inverter model (5.3) the following is obtained:

$$\Delta\omega_i = \dot{\delta}_i = -\kappa_i(\delta_i - \delta_{i_0}) + \kappa_i u_{i_1}, \;\; \kappa_i \in \mathbb{R}, \; \kappa_i > 0. \tag{6.3}$$

Substituting (6.3) into (6.2) yields the following:

$$\Delta\omega_i = -\kappa_i \underbrace{(\delta_i - \delta_{i_0})}_{\Delta\delta_i} + \kappa_i \cdot K_{i,12} \underbrace{(\tilde{P}_i - \tilde{P}_{i_0})}_{\Delta\tilde{P}_i}, \tag{6.4a}$$

$$\underbrace{V_i - V_{i_0}}_{\Delta V_i} = K_{i,23} \underbrace{(\tilde{Q}_i - \tilde{Q}_{i_0})}_{\Delta\tilde{Q}_i}. \tag{6.4b}$$

Without loss of generality, it is assumed that $\kappa_i = 1$, $i = 1,\ldots,n$, in the following part of this chapter. For the active power sharing mechanism, an assumption of the classical droop control is adopted, (see e.g., [17, 21, 33, 42, 148]). Suppose that frequency deviations at different inverter nodes are identical. Accordingly, the following is derived from (6.4a):

$$\Delta\omega_i = -\Delta\delta_i + K_{i,12}\Delta\tilde{P}_i = \Delta\omega_k = -\Delta\delta_k + K_{k,12}\Delta\tilde{P}_k, \quad i,k = 1,\ldots,n. \tag{6.5}$$

Note that at steady-state, $\lim_{t\to\infty}\Delta\omega_i(t) = \lim_{t\to\infty}\Delta\omega_k(t) = 0$, $i,k = 1,\ldots,n$. Hence, the above equation becomes as follows in steady-state:

$$-\Delta\delta_i + K_{i,12}\Delta\tilde{P}_i = -\Delta\delta_k + K_{k,12}\Delta\tilde{P}_k = 0, \quad i,k = 1,\ldots,n. \tag{6.6}$$

According to the phase angle calculation in (3.2) together with the assumption of identical network frequency, the following can be inferred from (6.6):

$$\Delta\delta_i = \Delta\delta_k = K_{i,12}\Delta\tilde{P}_i = K_{k,12}\Delta\tilde{P}_k, \quad i,k = 1,\ldots,n. \tag{6.7}$$

Equation (6.7) indicates that the amount of active power picked up by each inverter depends on relations between droop gains $K_{i,12}$, $i = 1,\ldots,n$.

Remark 6.1.1. It is commonly assumed that frequency deviation is identical at different buses and nodes in a power system [33]. Thus, Equation (6.5) is relatively accurate and widely accepted in microgrid communities. This in turn implies the accuracy of Equation (6.7) as well as good active power sharing performance.

For the case of reactive power sharing, it is assumed that voltage deviations at different nodes of a microgrids are identical. Thus, the following is derived from (6.4b):

$$\Delta V_i = K_{i,23}\Delta\tilde{Q}_i = \Delta V_k = K_{k,23}\Delta\tilde{Q}_k, \qquad i,k = 1,\dots,n. \tag{6.8}$$

Similarly, the amount of reactive power generated by each inverter depends on relations between droop gains $K_{i,23}$, $i = 1,\dots,n$.

Remark 6.1.2. It is noteworthy that the reactive power sharing law (6.8) serves as a mimic of the active power sharing in (6.7). This approach is often used by microgrid researchers and can be found in number of publications, e.g. [8, 15, 26, 38, 39, 42, 72, 74]. However, because of voltage drops over power lines (because of line impedances)[1], deviations of voltage magnitudes at different points in a power system are, in essence, not equal to each other. Thus, the voltage relation in (6.8) is less accurate. Accordingly, it is expected that performance of the reactive power sharing is relatively modest (see [85, 149] for more details on the relation between voltage deviations and reactive power sharing performance in microgrids).

Remark 6.1.3. Note that in this chapter a straightforward method is proposed to improve the power sharing performance. In general, a desired power sharing performance is not derived. To the best of my knowledge there still does not exist any analytical solution to precisely obtain a desired power sharing in communicationless inverter-based microgrids with arbitrary R/X ratios of connecting lines.

Remark 6.1.4. Ratios between droop gains of different inverters specify power portions injected by inverters. For instance, ratios between droop gains can be chosen depending on capacities of generation units so that DERs with larger capacities inject more power than DERs with smaller capacities. That is [27],

$$K_{1,12}\cdot P_1^{\text{rated}} = K_{2,12}\cdot P_2^{\text{rated}} = \cdots = K_{n,12}\cdot P_n^{\text{rated}}, \tag{6.9a}$$

$$K_{1,23}\cdot Q_1^{\text{rated}} = K_{2,23}\cdot Q_2^{\text{rated}} = \cdots = K_{n,23}\cdot Q_n^{\text{rated}}. \tag{6.9b}$$

where P_i^{rated} and Q_i^{rated}, $i = 1,\dots,n$, are rated active and reactive power of an inverter i, which are known beforehand.

[1] Steady-state voltage drop over a power line is a product of the line impedance and the current flow over it [33, 36].

In the next section, additional constraints are introduced for LMI variables, so that by solving the LMI problem (5.65), resulting inverter controllers obtain the form as presented in (6.2). Simultaneously, it will be shown that desired power sharing ratios described by the relations in (6.7) and (6.8) can also be set by a constraint on the LMI variables.

6.2 Design of power sharing controllers

An additive uncertainty $\tilde{\Delta}(s)$ caused by load changes can be obtained as in Section 5.1. Suppose $\tilde{\Delta}(s)$ can be rewritten as $\Delta(s)W_T(s)$, $\|\Delta\|_\infty < 1$ as in (5.15). The power sharing is considered for load changes within this bound so that the robust stability of the system and the robust performance of voltages are always guaranteed.

In this section, additional constraints on LMI variables are introduced to the LMI problem (5.65) in Theorem 5.6 so that resulting inverter controllers obtain the form presented in (6.2). Moreover, by adding a constraint on LMI variables, desired power sharing ratios between inverters can also be set.

Consider the LMI optimization problem (5.65) in Theorem 5.6. According to the variable definition in (5.64), a controller K_i of an inverter i can be calculated as follows:

$$K_i = \mathbf{Y}_{ii}\mathbf{X}_{ii}^{-1}, \;\; i = 1,\ldots,n. \tag{6.10}$$

For K_i to obtain the form in (6.2), the following structure constraints for LMI variables are introduced:

$$\mathbf{Y}_{ii} = \begin{bmatrix} 0 & \mathbf{Y}_{ii,12} & 0 \\ 0 & 0 & \mathbf{Y}_{ii,23} \end{bmatrix}, \quad \mathbf{X}_{ii} = \begin{bmatrix} \mathbf{X}_{ii,11} & 0 & 0 \\ 0 & \mathbf{X}_{ii,22} & 0 \\ 0 & 0 & \mathbf{X}_{ii,33} \end{bmatrix}, \quad i = 1,\ldots,n. \tag{6.11}$$

If the LMI optimization problem (5.65) is feasible with the variable constraint above, a resulting $\bar{\mathbf{X}} = \mathrm{diag}(\mathbf{X}_{11},\ldots,\mathbf{X}_{nn},\mathbf{X}_W)$ is symmetric positive definite. Thus, $\mathbf{X}_{ii}$, $i = 1\ldots,n$, is also positive definite and there exists an inverse matrix of $\mathbf{X}_{ii}$. A resulting inverter controller can be calculated as follows:

$$K_i = \mathbf{Y}_{ii}\mathbf{X}_{ii}^{-1} = \begin{bmatrix} 0 & \mathbf{Y}_{ii,12} & 0 \\ 0 & 0 & \mathbf{Y}_{ii,23} \end{bmatrix} \underbrace{\begin{bmatrix} \frac{1}{\mathbf{X}_{ii,11}} & 0 & 0 \\ 0 & \frac{1}{\mathbf{X}_{ii,22}} & 0 \\ 0 & 0 & \frac{1}{\mathbf{X}_{ii,33}} \end{bmatrix}}_{=\mathbf{X}_{ii}^{-1}} = \begin{bmatrix} 0 & \frac{\mathbf{Y}_{ii,12}}{\mathbf{X}_{ii,22}} & 0 \\ 0 & 0 & \frac{\mathbf{Y}_{ii,23}}{\mathbf{X}_{ii,33}} \end{bmatrix}. \tag{6.12}$$

The droop gains defined in (6.2) are computed as follows:

$$K_{i,12} = \frac{\mathbf{Y}_{ii,12}}{\mathbf{X}_{ii,22}}, \quad K_{i,23} = \frac{\mathbf{Y}_{ii,23}}{\mathbf{X}_{ii,33}}, \quad i = 1,\dots,n. \tag{6.13}$$

In order to set power sharing ratios between inverters as described in (6.7), the following constraints are introduced to the LMI variables:

$$\begin{cases} \mathbf{X}_{ii,22} = \mathbf{X}_{kk,22}, \\ \mathbf{X}_{ii,33} = \mathbf{X}_{kk,33}, \\ \dfrac{\mathbf{Y}_{kk,12}}{\mathbf{Y}_{ii,12}} = \dfrac{K_{k,12}}{K_{i,12}} = \dfrac{\Delta P_i}{\Delta P_k}, \\ \dfrac{\mathbf{Y}_{kk,23}}{\mathbf{Y}_{ii,23}} = \dfrac{K_{k,23}}{K_{i,23}} = \dfrac{\Delta Q_i}{\Delta Q_k}, \end{cases} \quad i,k = 1,\dots,n. \tag{6.14}$$

The first two constraints in (6.14) indicate that ratios between droop gains can be set by adjusting ratios between $\mathbf{Y}_{ii,12}$ and $\mathbf{Y}_{kk,12}$ as well as between $\mathbf{Y}_{ii,23}$ and $\mathbf{Y}_{kk,23}$, respectively, where $i,k = 1,\dots,n$. Consequently, based on the power sharing control laws (6.7), (6.8) and (6.13), the latter two constraints for power sharing ratio are obtained.

Remark 6.2.1. While using Yalmip toolbox [97] and SeDuMi solver [98] in Matlab to solve the LMI problem (5.65), the constraints (6.11) and (6.14) can be easily added in advance to the LMI variables.

The constraints (6.11) and (6.14) make the LMI problem (5.65) more conservative. It is comprehensible as resulting inverter controllers are required to simultaneously satisfy several control goals: robust stability, robust performance of a microgrid and a desired power sharing between inverters. In the next section, a simulation is provided to exhibit these specifications of inverter controllers.

Remark 6.2.2. The power sharing mechanism is based on the assumptions on frequency and voltage deviations in (6.7) and (6.8). Thus, the power sharing performance depends on the accuracy of these assumptions, which is mentioned in Remarks 6.1.1 and 6.1.2. From the other hand, the power sharing performance can be improved by increasing droop gains as suggested by [1, 150]. In fact, an increase of the controller gains $K_{i,12}$ and $K_{i,23}$, $i = 1,\dots,n$, can improve the accuracy of the assumptions (6.7) and (6.8). An explanation is given as follows. By considering Equation (6.7), it is apparent that with a small controller gain $K_{i,12}$, a deviation of active power ΔP_i at node i yields small $\Delta\delta_k$ as it is assumed that $\Delta\delta_k = \Delta\delta_i = K_{i,12}\Delta P_i$. As a result, a small control gain $K_{k,12}$ and a small phase angle deviation $\Delta\delta_k$ lead to small deviation ΔP_k at node k, i.e. poor performance of active power sharing. This explanation can also be applied for the case of reactive power sharing with a voltage droop control in (6.8). Hence, small controller gains $K_{i,12}$ and $K_{i,23}$, $i = 1,\dots,n$, lead to poor power sharing performance. Therefore, in order

to improve the performance of the presented power sharing approach, it is necessary to increase the controller gains $K_{i,12}$ and $K_{i,23}$, $i = 1,\ldots,n$.

As seen in (6.13), an increase of the droop gains $K_{i,12}$ and $K_{i,23}$ can be realized by reducing $\mathbf{X}_{ii,22} > 0$ and $\mathbf{X}_{ii,33} > 0$, respectively. As most LMI solvers only accept one minimization objective, the reduction of $\mathbf{X}_{ii,22}$, $\mathbf{X}_{ii,33} > 0$ should be formulated as one minimization objective. There are two direct options as follows. The first option supposes a constraint $\mathbf{X}_{ii,22} = \mathbf{X}_{ii,33} > 0$, where $\mathbf{X}_{ii,22} = \mathbf{X}_{kk,22}$ and $\mathbf{X}_{ii,33} = \mathbf{X}_{kk,33}$, $i,k = 1,\ldots,n$, as introduced in (6.14). Then, by minimizing $\mathbf{X}_{ii,22} > 0$ while solving the LMI problem (5.65), an increase of the droop gains can be achieved. However, this option adds more conservatism to the LMI problem, which is already conservative. In order to avoid an extra constraint on LMI variables, the second option is proposed, which is the minimization of the sum $(\mathbf{X}_{ii,22} + \mathbf{X}_{ii,33}) > 0$. This minimization objective can be implemented to increase the controller gains $K_{i,12}$ and $K_{i,23}$.

Hence, the first minimization objective mentioned above increases the droop gains at the cost of additional conservatism of the LMI optimization problem. The second option does not suppose any additional variable constraint. However, with the second minimization objective, one cannot be sure that a resulting $\mathbf{X}_{ii,22}$ or $\mathbf{X}_{ii,33}$ gets the smallest possible value. In the following LMI problem the second option will be employed as additional conservatism is not desired.

The LMI optimization problem to design power sharing controllers for inverters is recast as follows:

$$\texttt{minimize } (\mathbf{X}_{ii,22} + \mathbf{X}_{ii,33}) \texttt{ such that } \begin{cases} \texttt{LMI } (5.65) \texttt{ is feasible over } \bar{\mathbf{X}} \texttt{ and } \bar{\mathbf{Y}}, \\ \bar{\mathbf{X}} \texttt{ and } \bar{\mathbf{Y}} \texttt{ are defined as in } (5.64), \\ \texttt{where submatrices } \mathbf{X}_{ii} \texttt{ and } \mathbf{Y}_{ii},\ i = 1,\ldots,n, \\ \texttt{have the structures as in } (6.11), \\ \mathbf{X}_{ii} \texttt{ and } \mathbf{Y}_{ii},\ i = 1,\ldots,n, \texttt{ satisfy the} \\ \texttt{constraint } (6.14), \\ \bar{\mathbf{X}} > 0, \\ \mu_1, \mu_2 > 0, \\ 0 < \gamma_P \leq 1. \end{cases} \tag{6.15}$$

6.3 Simulation study

In this section, a simulation is provided to demonstrate the power sharing capability of inverters with controllers designed by the LMI problem (6.15). The test system in Chapter 5 presented in Figure 5.11 is repeated. Parameters of the test system can be found in Table 5.1. By solving the LMI problem (6.15) with an intention to obtain an *equal* power sharing between inverters, the

droop gains $K_{1,12} = K_{2,12} = -1.9 \cdot 10^{-3}[\frac{\text{rad}}{\text{skW}}]$ and $K_{1,23} = K_{2,23} = -3.1[\frac{\text{V}}{\text{kVar}}]$ are derived. The simulation results showing the power sharing effect are displayed in Figure 6.1. Simulation results of the microgrid with the power sharing controllers are presented, compared to the simulation with the performance controllers K_1^p and K_2^p given in (5.82). The graphs denoted by "*share*" are derived by the power sharing controllers, while the index "p" is associated to the performance controllers.

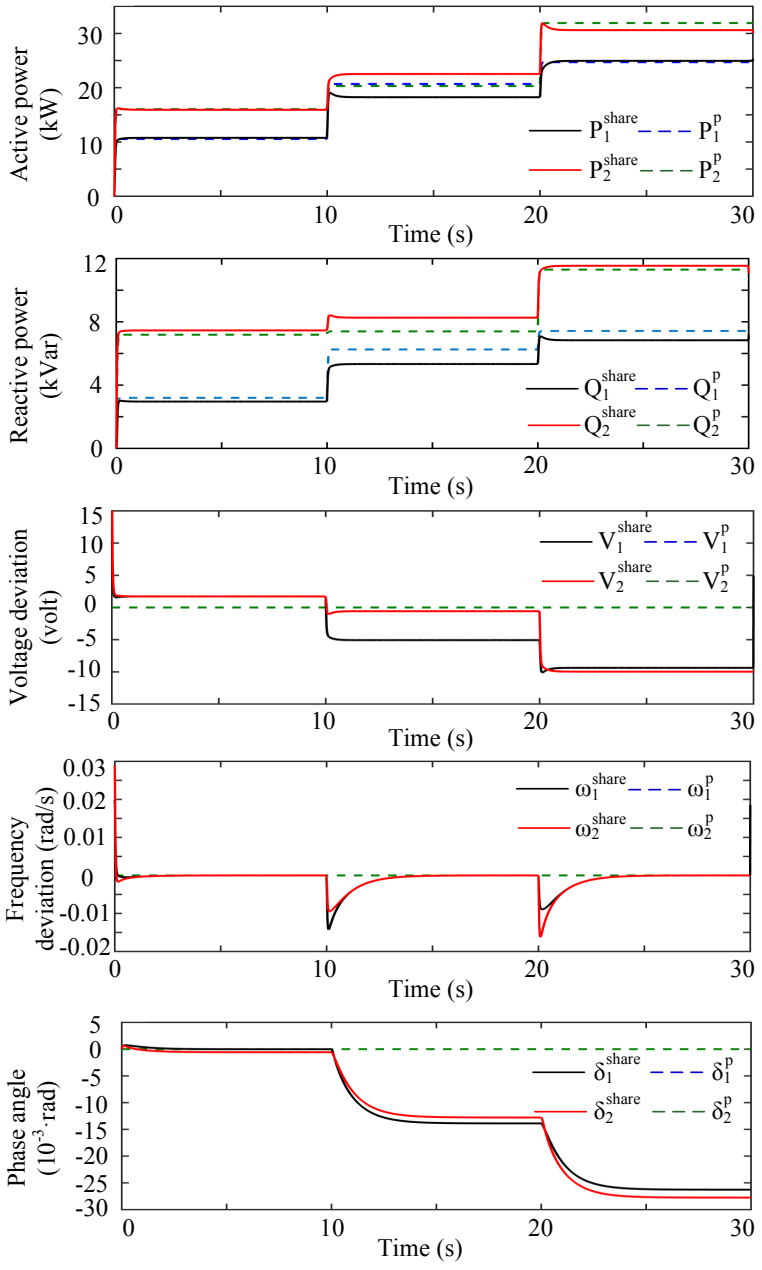

FIGURE 6.1: Power sharing simulation - equal power sharing.

As seen in Figure 6.1, the robust stability of the system against the considered load changes is achieved with the power sharing controllers. Variations of frequencies and phase angles of the two inverters are much alike and yield a good performance of active power sharing. At

$t = 10[s]$, an additional load is connected to node 1 and each inverter injects approximately the same amount of active power ($\Delta\tilde{P}_1 \cong 6.6[\text{kW}],\ \Delta\tilde{P}_2 \cong 7.5[\text{kW}]$) to supply the load change. The same power sharing mechanism is seen at $t = 20[s]$, when a load is connected to node 2 ($\Delta\tilde{P}_1 \cong 8.1[\text{kW}],\ \Delta\tilde{P}_2 \cong 6.7[\text{kW}]$). However, an intended exact equal active power sharing is not derived.

Opposed to that, the simulation shows a local behaviour of voltages, which leads to a poor performance of reactive power sharing as well as unequal magnitude deviations of inverter output voltages. Power sharing controllers result in larger variations of voltage magnitudes, compared to K_1^p and K_2^p. Based on Equation (6.8), it is seen that a larger droop gain $K_{i,23}$ causes larger steady-state deviation of voltage magnitude. Fortunately, $K_{i,12}$ and $K_{i,23}$ are designed by the LMI optimization problem (6.15), where voltage performance is considered. Therefore, the voltage magnitudes deviate within an acceptable limit ($< 1\%$ of the nominal value).

Remark 6.3.1. It is well-known and documented in a number of publications, see e.g. [41, 150], that if droop gains are increased, good power sharing performance can be achieved at the expense of degrading voltage performance (in the sense of both magnitude and frequency deviations). For the case of frequency and voltage droop control, a limit of circa 2% is usually set for frequency and voltage deviations. In the power sharing approach investigated here, instead of a frequency droop control an angle droop control is employed, where inverter output frequencies always converge to a nominal value. Thus, it is only necessary to set a limit for voltage magnitude deviations.

In order to demonstrate another power sharing ratio between the two inverters, the LMI problem (6.15) is solved with an intention to derive a $(1:2)$ power sharing ratio between the two inverters. The droop gains in actual quantities $K_{1,12} = -3.5 \cdot 10^{-3}[\frac{\text{rad}}{\text{skW}}]$, $K_{1,23} = -2.1[\frac{\text{V}}{\text{kVar}}]$ and $K_{2,12} = -1.76 \cdot 10^{-3}[\frac{\text{rad}}{\text{skW}}]$, $K_{2,23} = -1.02[\frac{\text{V}}{\text{kVar}}]$ are derived for the two inverters, respectively.

The same simulation scenario as above is repeated. The simulation results are presented in Figure 6.2, which show a sufficient performance of voltages and frequencies. Deviations of phase angles of the two inverters are similar and yield a good performance of active power sharing. With the load change at $t = 10[s]$, $\Delta\tilde{P}_2 = 8.6[\text{kW}] = 1.54\Delta\tilde{P}_1$. With the load change at $t = 20[s]$, $\Delta\tilde{P}_2 = 9.7[\text{kW}] = 1.98\Delta\tilde{P}_1$. Although an exact $(1:2)$ power sharing ratio is not derived, the simulation indicates that the actual power sharing ratio corresponds to the predefined ratio. Opposed to that, voltage deviations (caused by load changes) at outputs of the two inverters are not equal. Consequently, a poor performance of reactive power sharing is derived.

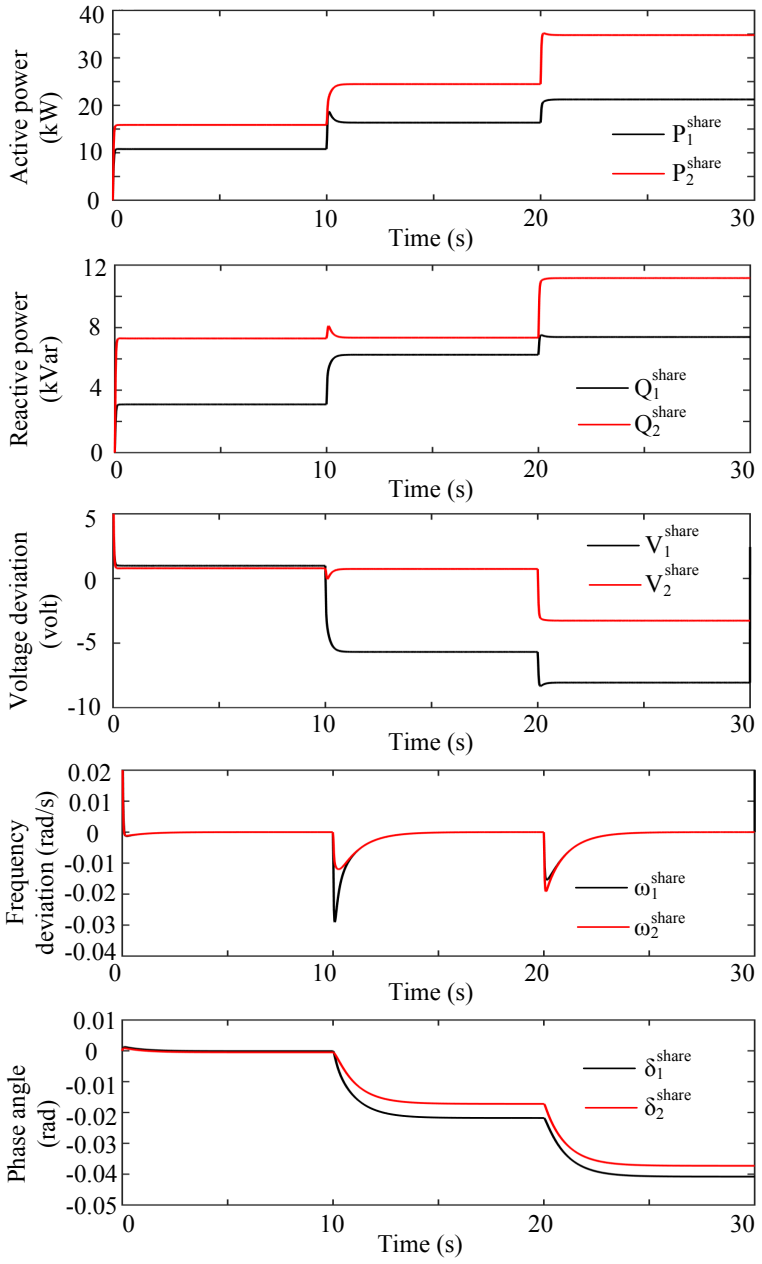

FIGURE 6.2: Power sharing simulation - (1:2) power sharing ratio.

6.4 Summary

In this chapter, the power sharing between inverters in a microgrid has been considered. An angle droop control was proposed for active power sharing between inverters. A classical voltage droop control was implemented for reactive power sharing. Several variable constraints were introduced to the LMI optimization problem in Theorem 5.6 so that droop controllers are derived for the active and reactive power sharing mechanism. Power sharing performance can be improved by increasing droop gains. The increase of droop gains in inverter controllers was formulated as an optimization objective for the LMI problem.

Although a desired power sharing is not analytically proved, resulting droop controllers in fact increase power exchange between system nodes as illustrated in a simulation. The simulation also showed that the active power sharing is better than the case of reactive power sharing. With arbitrary R/X ratios of connecting lines between inverters, power sharing is accomplished without causing stability and voltage performance problems to microgrids.

Chapter 7

Conclusion and outlook

7.1 Conclusion

The thesis has investigated several key control challenges associated to a stable, reliable and beneficial operation of inverter-based microgrids. The control of power flows within a microgrid was defined as the main control goal at the power control level. However, since a control loop is introduced, the closed-loop stability as well as the performance of voltages and frequencies were defined as the essential requirements for a normal operation of microgrids. Accordingly, for studying the robust stability and robust performance (in the sense of voltage and frequency deviations) of microgrids, several LTI state-space models have been proposed, which include interconnected inverters, load dynamics and different uncertainties. A decentralized power control loop for each inverter was presented. The (robust) stabilizing control approach is decentralized as there is no communication and control interconnection between inverters. A global time signal is required for the clock synchronization between inverters, but no other communication link between inverters is needed. With respect to different system models and different control goals, e.g. nominal stability, robust stability and robust performance of inverter output voltages, different LMI optimization problems were formulated to achieve the related control goals. Regarding the power sharing, based on the idea of the classical droop control, additional constraints on LMI variables were introduced so that by solving a single LMI problem, resulting droop controllers for inverters are derived, which simultaneously satisfy several control goals: robust stability, robust performance and power sharing. As shown in a simulation, resulting controllers noticeably improve the active power sharing performance.

All the presented theories were validated via simulations, which showed that the control goals: the robust stability of microgrids against load dynamics or a model uncertainty as well as the robust performance of voltages and frequencies under a model uncertainty and reference changes (by a higher control level) and the power sharing between inverters were achieved.

7.2 Outlook

As validated by simulations, the intended control goals were achieved by the proposed power control loops and the associated LMI stability conditions, respectively. However, as linear models of naturally nonlinear microgrids were considered, dynamics caused by system nonlinearities were therefore neglected. This leads to the fact that the proposed system models may be inaccurate for particular cases. Accordingly, for future work it is necessary to consider nonlinear models of microgrids for the stability and performance analysis.

Regarding the weight functions in Chapter 5, without knowledge and experience working with real microgrids, it is nontrivial to state how to select the most appropriate weight functions for particular microgrid cases. This lack of knowledge may create problems for the robust controller design procedure, while solving the proposed LMI problem. Therefore, the issue with weight functions must be thoroughly studied in future work. Additionally, the robust controller design presented in Chapter 5 neglects structure of model uncertainties. This structural aspect of uncertainties should be investigated in future work to reduce conservatism of the controller design.

Another interesting question is the reactive power sharing. As shown via the simulation in Chapter 6, the performance of reactive power sharing is modest. So far, droop-based control approaches may not be suitable for reactive power sharing, or the proposed modeling of microgrids is not accurate enough for this purpose. For this control goal, a novel control approach and a novel system modeling must be investigated.

For a realistic plug-and-play operation of microgrids, a synchronization procedure for inverters should be investigated. Regarding the synchronization problem, an inverter can be connected to a microgrid only in the case the inverter output voltage is exactly the same as the voltage of the connection point on the microgrid side (the same magnitude, phase angle, frequency, phase sequence). This condition is required so that when an inverter is connected to a microgrid, the inverter does not inject any power into the system. A smooth connection of an inverter to a microgrid does not result in large oscillations of system variables. Furthermore, due to the plug-and-play operation, a microgrid is inherently a switched system. A microgrid should be modelled as a switched system and its robust stability against switching events must be studied.

Last but not least, inverter control algorithms are usually run on microcontrollers or programmable logic controllers (PLC), whose sample time is not infinitely small to be considered as continuous. Therefore, a discretized version of inverter controllers should be studied.

As stated in the beginning of the thesis, the most important question is: How to make microgrids work? It is hoped that the thesis has brought several useful contributions into the microgrid research field. The proposed theories should be verified for real microgrids.

Appendix A

A.1 Power flow equations

From the admittance matrix (2.8), $\vec{I}_i$ is obtained as follows:

$$\vec{I}_i = \sum_{k=1}^{n} \vec{V}_k Y_{ik}. \tag{A.1}$$

Moreover, the total power injection at node i is calculated as follows [33]:

$$\vec{S}_i = \vec{V}_i \vec{I}_i^*, \tag{A.2}$$

where $\vec{I}_i^*$ denotes the complex conjugate of $\vec{I}_i$.

$\vec{V}_k$ can be presented in phasor form as $\vec{V}_k = V_k e^{j\delta_k}$. Similarly, $Y_{ik} = |Y_{ik}|(\cos\phi_{ik} + j\sin\phi_{ik}) = |Y_{ik}|e^{j\phi_{ik}}$. By plugging the above expression of $\vec{I}_i$ into the expression of $\vec{S}_i$, the following is derived:

$$\begin{aligned}
\vec{S}_i &= \vec{V}_i \cdot \vec{I}_i^* = \vec{V}_i \cdot \sum_{k=1}^{n} \vec{V}_k^* Y_{ik}^* = \sum_{k=1}^{n} V_i e^{j\delta_i} \cdot V_k e^{-j\delta_k} \cdot Y_{ik}^* \\
&= \sum_{k=1}^{n} V_i V_k e^{j(\delta_i - \delta_k)} Y_{ik}^* = \sum_{i=1}^{n} V_i V_k e^{j(\delta_i - \delta_k)} |Y_{ik}| e^{-j\phi_{ik}} \\
&= \sum_{i=1}^{n} V_i V_k |Y_{ik}| e^{j(\delta_i - \delta_k - \phi_{ik})} = \sum_{i=1}^{n} V_i V_k |Y_{ik}| \left(\cos(\delta_i - \delta_k - \phi_{ik}) + j\sin(\delta_i - \delta_k - \phi_{ik})\right).
\end{aligned} \tag{A.3}$$

By separating the right-hand side of the equation above in real and imaginary parts, P_i and Q_i in (2.9) are obtained.

A.2 Active and reactive power control loops

Recall that:

$$|Y_{ik}| = \frac{1}{\sqrt{R_{ik}^2 + X_{ik}^2}},\ \cos\phi_{ik} = \frac{R_{ik}}{\sqrt{R_{ik}^2 + X_{ik}^2}},\ \sin\phi_{ik} = \frac{X_{ik}}{\sqrt{R_{ik}^2 + X_{ik}^2}}. \tag{A.4}$$

$$\begin{aligned}
P_i &= \sum_{k=1}^{n} V_i V_k |Y_{ik}| \cos(\delta_i - \delta_k - \phi_{ik}) = V_i^2 |Y_{ii}| \cos\phi_{ii} + \sum_{k=1, k\neq i}^{n} V_i V_k |Y_{ik}| \cos(\delta_i - \delta_k - \phi_{ik}) \\
&= V_i^2 \frac{R_{ii}}{R_{ii}^2 + X_{ii}^2} + \sum_{k=1, k\neq i}^{n} V_i V_k \frac{1}{\sqrt{R_{ik}^2 + X_{ik}^2}} \big(\cos(\delta_i - \delta_k)\cos\phi_{ik} + \sin(\delta_i - \delta_k)\sin\phi_{ik}\big) \\
&= V_i^2 \frac{R_{ii}}{R_{ii}^2 + X_{ii}^2} + \sum_{k=1, k\neq i}^{n} V_i V_k \big(\cos(\delta_i - \delta_k)\frac{R_{ik}}{R_{ik}^2 + X_{ik}^2} + \sin(\delta_i - \delta_k)\frac{X_{ik}}{R_{ik}^2 + X_{ik}^2}\big) \\
&= V_i^2 G_{ii} + \sum_{k=1, k\neq i}^{n} V_i V_k \big(\cos(\delta_i - \delta_k) G_{ik} - \sin(\delta_i - \delta_k) B_{ik}\big).
\end{aligned} \tag{A.5}$$

$$\begin{aligned}
Q_i &= \sum_{k=1}^{n} V_i V_k |Y_{ik}| \sin(\delta_i - \delta_k - \phi_{ik}) = -V_i^2 |Y_{ii}| \sin\phi_{ii} + \sum_{k=1, k\neq i}^{n} V_i V_k |Y_{ik}| \sin(\delta_i - \delta_k - \phi_{ik}) \\
&= -V_i^2 \frac{X_{ii}}{R_{ii}^2 + X_{ii}^2} + \sum_{k=1, k\neq i}^{n} V_i V_k \frac{1}{\sqrt{R_{ik}^2 + X_{ik}^2}} \big(\sin(\delta_i - \delta_k)\cos\phi_{ik} - \cos(\delta_i - \delta_k)\sin\phi_{ik}\big) \\
&= -V_i^2 \frac{R_{ii}}{R_{ii}^2 + X_{ii}^2} + \sum_{k=1, k\neq i}^{n} V_i V_k \big(\sin(\delta_i - \delta_k)\frac{R_{ik}}{R_{ik}^2 + X_{ik}^2} - \cos(\delta_i - \delta_k)\frac{X_{ik}}{R_{ik}^2 + X_{ik}^2}\big) \\
&= V_i^2 B_{ii} + \sum_{k=1, k\neq i}^{n} V_i V_k \big(\sin(\delta_i - \delta_k) G_{ik} + \cos(\delta_i - \delta_k) B_{ik}\big).
\end{aligned} \tag{A.6}$$

A.3 Linearization of the power flow equations

Recall the power flow equations of each inverter i:

$$\begin{aligned}
P_i &= \sum_{k=1}^{n} V_i V_k |Y_{ik}| \cos(\delta_i - \delta_k - \phi_{ik}), \\
Q_i &= \sum_{k=1}^{n} V_i V_k |Y_{ik}| \sin(\delta_i - \delta_k - \phi_{ik}),
\end{aligned} \tag{A.7}$$

and the equilibrium point:

$$x_{i_0} = [\delta_{i_0}, \tilde{P}_{i_0}, \tilde{Q}_{i_0}]^T,\ u_{i1_0} = 0,\ u_{i2_0} = V_{i_0}. \tag{A.8}$$

$$\left.\frac{\partial P_i}{\partial \delta_i}\right|_0 = -\sum_{k=1}^{n} V_{i_0} V_{k_0} |Y_{ik}| \sin(\delta_{i_0} - \delta_{k_0} - \phi_{ik}). \tag{A.9}$$

$$\left.\frac{\partial P_i}{\partial V_i}\right|_0 = 2V_{i_0}|Y_{ii}|\cos(\phi_{ii}) + \sum_{k=1,k\neq i}^{n} V_{k_0}|Y_{ik}|\cos(\delta_{i_0} - \delta_{k_0} - \phi_{ik}). \tag{A.10}$$

$$\left.\frac{\partial P_i}{\partial \delta_k}\right|_0 = \sum_{k=1}^{n} V_{i_0} V_{k_0} |Y_{ik}| \sin(\delta_{i_0} - \delta_{k_0} - \phi_{ik}),\ \text{where } k \neq i. \tag{A.11}$$

$$\left.\frac{\partial P_i}{\partial V_k}\right|_0 = \sum_{k=1,k\neq i}^{n} V_{i_0}|Y_{ik}|\cos(\delta_{i_0} - \delta_{k_0} - \phi_{ik}),\ \text{where } k \neq i. \tag{A.12}$$

$$\left.\frac{\partial Q_i}{\partial \delta_i}\right|_0 = \sum_{k=1}^{n} V_{i_0} V_{k_0} |Y_{ik}| \cos(\delta_{i_0} - \delta_{k_0} - \phi_{ik}). \tag{A.13}$$

$$\left.\frac{\partial Q_i}{\partial V_i}\right|_0 = -2V_{i_0}|Y_{ii}|\sin(\phi_{ii}) + \sum_{k=1,k\neq i}^{n} V_{k_0}|Y_{ik}|\sin(\delta_{i_0} - \delta_{k_0} - \phi_{ik}). \tag{A.14}$$

$$\left.\frac{\partial Q_i}{\partial \delta_k}\right|_0 = -\sum_{k=1}^{n} V_{i_0} V_{k_0} |Y_{ik}| \cos(\delta_{i_0} - \delta_{k_0} - \phi_{ik}),\ \text{where } k \neq i. \tag{A.15}$$

$$\left.\frac{\partial Q_i}{\partial V_k}\right|_0 = \sum_{k=1}^{n} V_{i_0}|Y_{ik}|\sin(\delta_{i_0} - \delta_{k_0} - \phi_{ik}),\ \text{where } k \neq i. \tag{A.16}$$

A.4 Linearization of a microgrid using Matlab Simulink

Create an m-file in Matlab *microgrid_sfcn.m*, where the states and control inputs of the inverters are renamed as follows:

$$\begin{gathered} \delta_1 - \delta_{1_0} = x_1, \quad \tilde{P}_1 - \tilde{P}_{1_0} = x_2, \quad \tilde{Q}_1 - \tilde{Q}_{1_0} = x_3, \\ \delta_2 - \delta_{2_0} = x_4, \quad \tilde{P}_2 - \tilde{P}_{2_0} = x_5, \quad \tilde{Q}_2 - \tilde{Q}_{2_0} = x_6, \\ \Delta\omega_1 = u_1, \quad V_1 - V_{1_0} = u_2, \quad \Delta\omega_2 = u_3, \quad V_2 - V_{2_0} = u4. \end{gathered} \tag{A.17}$$

```
function [sys,x0] = microgrid_sfcn(t,x,u,flag)
if abs(flag) == 1
    % inputs
    u1 = u(1);
    u2 = u(2);
```

```
    u3 = u(3);
    u4 = u(4);
    % states
    x1 = x(1);
    x2 = x(2);
    x3 = x(3);
    x4 = x(4);
    x5 = x(5);
    x6 = x(6);
    % parameters
    Y_11=0.1696 - 0.2309i;
    Y_12=0.0988 - 0.1365i;
    Y_21=-0.0988 - 0.1365i;
    Y_22= 0.2612 - 0.2338i;
    phi_11=-0.9374;
    phi_12=-0.9442;
    phi_21=-0.9442;
    phi_22=-0.7301;
    tau_1=1/37.7;
    tau_2=1/37.7;
    % math model
    P_1=u2*u2*abs(Y_11)*cos(phi_11) + u2*u4*abs(Y_12)*cos(x1-x4-phi_12);
    Q_1=-u2*u2*abs(Y_11)*sin(phi_11) + u2*u4*abs(Y_12)*sin(x1-x4-phi_12);
    P_2=u4*u4*abs(Y_22)*cos(phi_22) + u2*u4*abs(Y_21)*cos(x4-x1-phi_21);
    Q_2=-u4*u4*abs(Y_22)*sin(phi_11) + u2*u4*abs(Y_21)*sin(x4-x1-phi_21);

    dx1=u1;
    dx2=(-x2 + P_1)/tau_1;
    dx3=(-x3 + Q_1)/tau_1;
    dx4=u3;
    dx5=(-x5 + P_2)/tau_2;
    dx6=(-x6 + Q_2)/tau_2;

    sys = [dx1 dx2 dx3 dx4 dx5 dx6];
elseif flag == 3
    sys = [x(1) x(2) x(3) x(4) x(5) x(6)];
elseif flag == 0
    % initial condition
    S_base = 40e+6;
```

```
    delta_10 = 0 ;
    P_10     = 10750/S_base;
    Q_10     = 3560/S_base;
    delta_20 = 0.0013;
    P_20     = 15620/S_base;
    Q_20     = 8060/S_base;

    sys = [6 0 6 4 0 0];
    x0 =  [delta_10 P_10 Q_10 delta_20 P_20 Q_20];
elseif flag == 9
    sys =[];
end
```

Create a simulink model *microgrid_sys.mdl* as presented in Figure A.1.

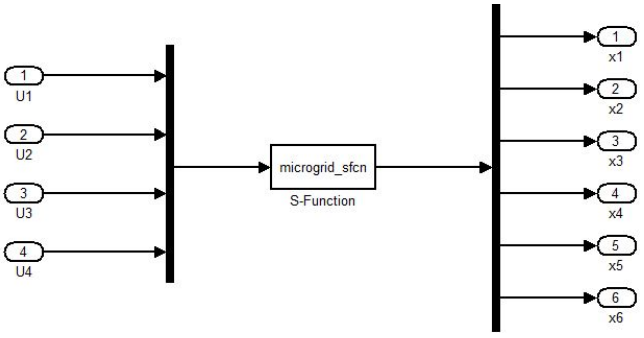

FIGURE A.1: Simulink model for linearization of a microgrid.

A run file *run_microgrid.m* is constructed as follows:

```
clear all; clc;
    S_base = 40e+6;
    V_base = 1030;
    delta_10 = 0 ;
    P_10     = 10750/S_base;
    Q_10     = 3560/S_base;
    delta_20 = 0.0013;
    P_20     = 15620/S_base;
    Q_20     = 8060/S_base;
    u1 = 0;
    u2 = 1029/V_base;
    u3 = 0;
    u4 = abs(1030+1.3i)/V_base;
```

```
    u = [u1; u2; u3; u4];
    x = [delta_10 P_10 Q_10 delta_20 P_20 Q_20];

[A,B,C,D] = linmod('microgrid_sys', x,u)
```

A.5 Linearization of an overall microgrid with dynamic loads

Similar to the linearization in Appendix A.4, three matlab files were created for the linearization of a microgrid with a dynamic load (an induction machine):

- Simulink file *microgrid_sysload.mdl*.
- Matlab file *microgrid_sfcnload.m*, which is a S-function in the Simulink model *microgrid_sysload.mdl*.
- Matlab executing file *run_microgridload.m*, which specifies the operating point, where the system is linearized.

The Simulink file *microgrid_sysload.mdl* is presented in Figure A.2.

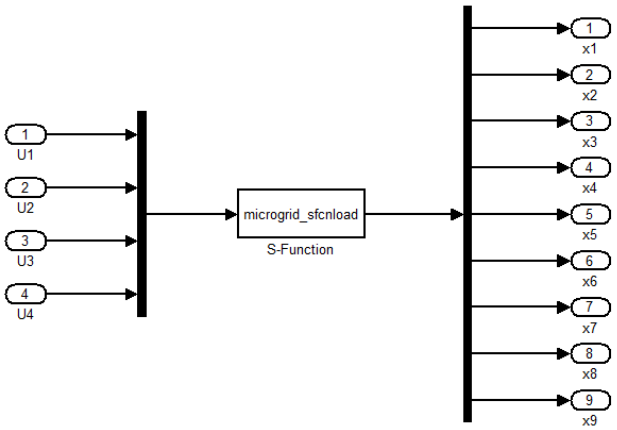

FIGURE A.2: Simulink model for linearization of a microgrid with a dynamic load.

The matlab file *microgrid_sfcnload.m* is as follows:

```
function [sys,x0] = microgrid_sfcn(t,x,u,flag)

if abs(flag) == 1
    % inputs
    u1 = u(1);
```

```
u2 = u(2);
u3 = u(3);
u4 = u(4);
% states
x1 = x(1);
x2 = x(2);
x3 = x(3);
x4 = x(4);
x5 = x(5);
x6 = x(6);
x7 = x(7);
x8 = x(8);
x9 = x(9);

% enter parameters of the test system
% calculate admittance matrix
Y1=[1/Z_L11, -(1/Z_L11 + 1/Z_L1 + 1/Z_L2 + 1/Z_L22),
   -(1/Z_L11 + 1/Z_11), -(1/Z_L11 + 1/Z_L1 + 1/Z_L2 + 1/Z_21),
   -(1/Z_L11 + 1/Z_L1 + 1/Z_s);
    0, 1/Z_L22, -(1/Z_L22 + 1/Z_L2 + 1/Z_L1 + 1/Z_11),
   -(1/Z_L22 + 1/Z_21), -(1/Z_L22 + 1/Z_L2 + 1/Z_s);
    0, 0, 1/Z_11, -(1/Z_11 + 1/Z_L1 + 1/Z_L2 + 1/Z_21),
   -(1/Z_11 + 1/Z_L1 + 1/Z_L2 + 1/Z_s);
    0, 0, 0 ,1/Z_21, -(1/Z_21 + 1/Z_L2 + 1/Z_s);
    0, 0, 0, 0, 1/Z_s];

Y1(2,1)=Y1(1,2);
Y1(3,1)=Y1(1,3);
Y1(3,2)=Y1(2,3);
Y1(4,1)=Y1(1,4);
Y1(4,2)=Y1(2,4);
Y1(4,3)=Y1(3,4);
Y1(5,1)=Y1(1,5);
Y1(5,2)=Y1(2,5);
Y1(5,3)=Y1(3,5);
Y1(5,4)=Y1(4,5);

Y3=zeros(4,4);
Y3(1,1)=Y1(1,1) - Y1(1,5)*Y1(5,1)/Y1(5,5);
```

```
Y3(1,2)=Y1(1,2) - Y1(1,5)*Y1(5,2)/Y1(5,5);
Y3(1,3)=Y1(1,3) - Y1(1,5)*Y1(5,3)/Y1(5,5);
Y3(1,4)=Y1(1,4) - Y1(1,5)*Y1(5,4)/Y1(5,5);

Y3(2,1)=Y1(2,1) - Y1(2,5)*Y1(5,1)/Y1(5,5);
Y3(2,2)=Y1(2,2) - Y1(2,5)*Y1(5,2)/Y1(5,5);
Y3(2,3)=Y1(2,3) - Y1(2,5)*Y1(5,3)/Y1(5,5);
Y3(2,4)=Y1(2,4) - Y1(2,5)*Y1(5,4)/Y1(5,5);

Y3(3,1)=Y1(3,1) - Y1(3,5)*Y1(5,1)/Y1(5,5);
Y3(3,2)=Y1(3,2) - Y1(3,5)*Y1(5,2)/Y1(5,5);
Y3(3,3)=Y1(3,3) - Y1(3,5)*Y1(5,3)/Y1(5,5);
Y3(3,4)=Y1(3,4) - Y1(3,5)*Y1(5,4)/Y1(5,5);

Y3(4,1)=Y1(4,1) - Y1(4,5)*Y1(5,1)/Y1(5,5);
Y3(4,2)=Y1(4,2) - Y1(4,5)*Y1(5,2)/Y1(5,5);
Y3(4,3)=Y1(4,3) - Y1(4,5)*Y1(5,3)/Y1(5,5);
Y3(4,4)=Y1(4,4) - Y1(4,5)*Y1(5,4)/Y1(5,5);

Y4=zeros(3,3);
Y4(1,1)=Y3(1,1) - Y3(1,4)*Y3(4,1)/Y3(4,4);
Y4(1,2)=Y3(1,2) - Y3(1,4)*Y3(4,2)/Y3(4,4);
Y4(1,3)=Y3(1,3) - Y3(1,4)*Y3(4,3)/Y3(4,4);

Y4(2,1)=Y3(2,1) - Y3(2,4)*Y3(4,1)/Y3(4,4);
Y4(2,2)=Y3(2,2) - Y3(2,4)*Y3(4,2)/Y3(4,4);
Y4(2,3)=Y3(2,3) - Y3(2,4)*Y3(4,3)/Y3(4,4);

Y4(3,1)=Y3(3,1) - Y3(3,4)*Y3(4,1)/Y3(4,4);
Y4(3,2)=Y3(3,2) - Y3(3,4)*Y3(4,2)/Y3(4,4);
Y4(3,3)=Y3(3,3) - Y3(3,4)*Y3(4,3)/Y3(4,4);

Y_admittance=Y4;
Y_11=Y_admittance(1,1);
Y_12=Y_admittance(1,2);
Y_13=Y_admittance(1,3);
Y_21=Y_admittance(2,1);
Y_22=Y_admittance(2,2);
Y_23=Y_admittance(2,3);
```

```
Y_31=Y_admittance(3,1);
Y_32=Y_admittance(3,2);
Y_33=Y_admittance(3,3);

phi_11=atan(imag(Y_11)/real(Y_11));
phi_12=atan(imag(Y_12)/real(Y_12));
phi_13=atan(imag(Y_13)/real(Y_13));
phi_21=atan(imag(Y_21)/real(Y_21));
phi_22=atan(imag(Y_22)/real(Y_22));
phi_23=atan(imag(Y_23)/real(Y_23));
phi_31=atan(imag(Y_31)/real(Y_31));
phi_32=atan(imag(Y_32)/real(Y_32));
phi_33=atan(imag(Y_33)/real(Y_33));

% math model
delta_s_prime_tilde = (x1*H1 + x4*H2)/(H1+H2);
ws=(u3*H2 + u1*H1)/(H1+H2);
Vs=sqrt(x7*x7 + x8*x8);
delta_s_prime=atan(x8/x7);

i_ds=-x7*abs(Y_33)*cos(phi_33) + x8*abs(Y_33)*sin(phi_33)
     - u2*abs(Y_31)*cos(delta_s_prime_tilde-x1-phi_31-delta_s_prime)
     - u4*abs(Y_32)*cos(delta_s_prime_tilde-x4-phi_32-delta_s_prime);
i_qs=-x8*abs(Y_33)*cos(phi_33) - x7*abs(Y_33)*sin(phi_33)
     + u2*abs(Y_31)*sin(delta_s_prime_tilde-x1-phi_31-delta_s_prime)
     + u4*abs(Y_32)*sin(delta_s_prime_tilde-x4-phi_32-delta_s_prime);
Ts=(x7*i_ds + x8*i_qs)/ws;
Tm=Tm0*(ar*(x9*x9)/(ws*ws) + br*x9/ws + cr);

P_1=u2*u2*abs(Y_11)*cos(phi_11) + u2*u4*abs(Y_12)*cos(x1-x4-phi_12) +
   u2*Vs*abs(Y_13)*cos(x1-delta_s_prime_tilde-phi_13);
Q_1=-u2*u2*abs(Y_11)*sin(phi_11) + u2*u4*abs(Y_12)*sin(x1-x4-phi_12) +
   u2*Vs*abs(Y_13)*sin(x1-delta_s_prime_tilde-phi_13);
P_2=u4*u4*abs(Y_22)*cos(phi_22) + u2*u4*abs(Y_21)*cos(x4-x1-phi_21) +
   u4*Vs*abs(Y_23)*cos(x4-delta_s_prime_tilde-phi_23);
Q_2=-u4*u4*abs(Y_22)*sin(phi_11) + u2*u4*abs(Y_21)*sin(x4-x1-phi_21) +
   u4*Vs*abs(Y_23)*sin(x4-delta_s_prime_tilde-phi_23);

dx1=u1;
```

```
    dx2=(-x2 + P_1)/tau_1;
    dx3=(-x3 + Q_1)/tau_1;

    dx4=u3;
    dx5=(-x5 + P_2)/tau_2;
    dx6=(-x6 + Q_2)/tau_2;

    dx7=(-1/T0)*x7 + (-1/T0)*(Xs-Xs_prime)*i_qs + (ws-x9)/ws;
    dx8=(-1/T0)*x8 + (1/T0)*(Xs-Xs_prime)*i_ds - (ws-x9)/ws;
    dx9=(ws/(2*Hs))*(Ts-Tm);

    sys = [dx1 dx2 dx3 dx4 dx5 dx6 dx7 dx8 dx9];

elseif flag == 3
    sys = [x(1) x(2) x(3) x(4) x(5) x(6) x(7) x(8) x(9)];

elseif flag == 0
    % enter initial condition
    sys = [9 0 9 4 0 0];
    x0 =  [delta_10 P_10 Q_10 delta_20 P_20 Q_20 v_ds_0 v_qs_0 omega_r_0];

elseif flag == 9
    sys =[];

end
```

The executing file *run_microgridload.m* is as follows:

```
u = [u1; u2; u3; u4];
x = [delta_10 P_10 Q_10 delta_20 P_20 Q_20 v_ds_0 v_qs_0 omega_r_0];

[A,B,C,D] = linmod('microgrid_sysload.mdl', x, u);
As = A([7 8 9], [7 8 9]);
Bs = B([7 8 9], [1 2 3 4]);
Cs = eye(3);
Ainv = A([1 2 3 4 5 6], [1 2 3 4 5 6]);
Binv = B([1 2 3 4 5 6], [1 2 3 4]);
T=A([1 2 3 4 5 6],[7 8 9]);
Ts=A([7 8 9],[1 2 3 4 5 6]);
```

Bibliography

[1] Ritwik Majumder. Some aspects of stability in microgrids. *IEEE Transactions on Power Systems*, 28(3):3243–3252, 2013.

[2] D.J. Hill. Nonlinear dynamic load models with recovery for voltage stability studies. *IEEE Transactions on Power Systems*, 8(1):166–176, Feb. 1993.

[3] *Kyoto protocol to the united nations framework convention on climate change*. United Nations, 1998.

[4] P. Piagi and R. H. Lasseter. Autonomous control of microgrids. In *2006 IEEE Power Engineering Society General Meeting*, pages 8 pp.–, 2006.

[5] R. H. Lasseter and P. Paigi. Microgrid: A conceptual solution. In *2004 IEEE 35th Annual Power Electronics Specialists Conference (IEEE Cat. No.04CH37551)*, volume 6, pages 4285–4290, June 2004.

[6] R. H. Lasseter. Microgrids. In *2002 IEEE Power Engineering Society Winter Meeting. Conference Proceedings (Cat. No.02CH37309)*, volume 1, pages 305–308, 2002.

[7] IEEE. Guide for design, operation, and integration of distributed resource island systems with electric power systems. *IEEE Std 1547.4-2011*, pages 1–54, July 2011.

[8] N. Pogaku, M. Prodanovic, and T.C. Green. Modeling, analysis and testing of autonomous operation of an inverter-based microgrid. *IEEE Transactions on Power Electronics*, 22(2), March 2007.

[9] Nagaraju Pogaku, Milan Prodanovic, and Timothy C Green. Inverter-based microgrids: Small-signal modelling and testing. *The 3rd IET International Conference on Power Electronics, Machines and Drives*, pages 499–504, 2006.

[10] K. De Brabandere, B. Bolsens, J. Van den Keybus, A. Woyte, J. Driesen, and R. Belmans. A voltage and frequency droop control method for parallel inverters. *IEEE Transactions on Power Electronics*, 22(4):1107–1115, July 2007.

[11] H. Nikkhajoei and R.H. Lasseter. Distributed generation interface to the CERTS microgrid. *IEEE Transactions on Power Delivery*, 24(3):1598–1608, July 2009.

[12] CERTS program. Integration of distributed energy resources - The CERTS MicroGrid Concept. *Consultant report*, October 2003.

[13] Robert H Lasseter, Joseph H Eto, B Schenkman, J Stevens, H Vollkommer, D Klapp, E Linton, Hector Hurtado, and J Roy. CERTS microgrid laboratory testbed. *IEEE Transactions on Power Delivery*, 26(1):325–332, 2011.

[14] Johannes Schiffer, Daniele Zonetti, Romeo Ortega, Aleksandar M. Stankovic, Tevfik Sezi, and Jörg Raisch. A survey on modeling of microgrids - From fundamental physics to phasors and voltage sources. *Automatica*, 74:135–150, 2016.

[15] F. Katiraei, R. Iravani, N. D. Hatziargyriou, and A. Dimeas. Microgrids management. *IEEE power & energy magazine*, June 2008.

[16] JA Peças Lopes, CL Moreira, FO Resende, et al. Microgrids black start and islanded operation. In *15th Power systems computation conference (PSCC), Liege*, August 2005.

[17] K. De Brabandere. *Voltage and frequency droop control in low voltage grids by distributed generators with inverter front-end.* PhD thesis, Katholieke Universiteit Leuven, Leuven, Belgium, October 2006.

[18] B. Kroposki, T. Basso, and R. DeBlasio. Microgrid standards and technologies. In *IEEE Power and Energy Society General Meeting - Conversion and Delivery of Electrical Energy in the 21st Century*, pages 1–4, July 2008.

[19] Johannes Schiffer, Adolfo Anta, Truong Duc Trung, Joerg Raisch, and Tevfik Sezi. On power sharing and stability in autonomous inverter-based microgrids. In *IEEE 51st Annual Conference on Decision and Control*, December 2012.

[20] Truong Duc Trung. A robust decentralized controller design for inverter-based microgrids with dynamic loads. In *IECON 2013-39th Annual Conference of the IEEE Industrial Electronics Society*, pages 1507–1512, 2013.

[21] J.M. Guerrero, J. Matas, L.G. de Vicuna, M. Castilla, and J. Miret. Wireless-control strategy for parallel operation of distributed-generation inverters. *IEEE Transactions on Industrial Electronics*, October 2006.

[22] Robert H. Lasseter. Extended CERTS microgrid. In *IEEE Power and Energy Society General Meeting - Conversion and Delivery of Electrical Energy in the 21st Century*, pages 1–5, 2008.

[23] Ritwik Majumder, Arindam Ghosh, Gerard Ledwich, and Firuz Zare. Power sharing and stability enhancement of an autonomous microgrid with inertial and non-inertial DGs with DSTATCOM. In *IEEE International Conference on Power Systems, (ICPS'09)*, pages 1–6, 2009.

[24] Josep M Guerrero, Néstor Berbel, José Matas, Luis García de Vicuña, and Jaume Miret. Decentralized control for parallel operation of distributed generation inverters in microgrids using resistive output impedance. In *IECON 2006 - 32nd Annual IEEE Conference on Industrial Electronics*, pages 5149–5154, 2006.

[25] Y.A.-R.I. Mohamed and E.F. El-Saadany. Adaptive decentralized droop controller to preserve power sharing stability of paralleled inverters in distributed generation microgrids. *IEEE Transactions on Power Electronics*, 23(6):2806–2816, November 2008.

[26] John W. Simpson-Porco, Florian Doerfler, and Francesco Bullo. Synchronization and power sharing for droop-controlled inverters in islanded microgrids. *Automatica*, 49(9): 2603 – 2611, 2013.

[27] M.C. Chandorkar, D.M. Divan, and R. Adapa. Control of parallel connected inverters in standalone AC supply systems. *IEEE Transactions on industry applications*, 29(1), Feb. 1993.

[28] R. M. S. Filho, P. F. Seixas, P. C. Cortizo, and G. Gateau. Small-signal stability enhancement of communicationless parallel connected inverters. In *the 35th Annual Conference of IEEE Industrial Electronics*, pages 863–870, November 2009.

[29] Azrik M Roslan, Khaled H Ahmed, Stephen J Finney, and Barry W Williams. Improved instantaneous average current-sharing control scheme for parallel-connected inverter considering line impedance impact in microgrid networks. *IEEE Transactions on Power Electronics*, 26(3):702–716, 2011.

[30] M. Barnes, J. Kondoh, H. Asano, J. Oyarzabal, G. Ventakaramanan, Robert Lasseter, N. Hatziargyriou, and Tim Green. Real-world microgrids - An overview. In *IEEE International Conference on System of Systems Engineering, (SoSE '07)*, pages 1–8, April 2007.

[31] P. Moylan. Implications of passivity in a class of nonlinear systems. *IEEE Transactions on Automatic Control*, 19(4):373–381, August 1974.

[32] F. Doerfler and F. Bullo. Spectral analysis of synchronization in a lossless structure-preserving power network model. In *First IEEE International Conference on Smart Grid Communications (SmartGridComm)*, pages 179–184, october 2010.

[33] Prabha Kundur, Neal J Balu, and Mark G Lauby. *Power system stability and control*, volume 7. McGraw-hill New York, 1994.

[34] G. Kron. *Equivalent Circuits of Electric Machinery*. General Electric series. J. Wiley & Sons, 1951.

[35] J. Rocabert, A. Luna, F. Blaabjerg, and P. Rodriguez. Control of power converters in AC microgrids. *IEEE Transactions on Power Electronics*, 27(11):4734–4749, November 2012.

[36] Johannes Schiffer. *Stability and Power Sharing in Microgrids*. PhD Thesis, Technische Universität Berlin, Germany, 2015.

[37] C. T. Lee, C. C. Chu, and P. T. Cheng. A new droop control method for the autonomous operation of distributed energy resource interface converters. *IEEE Transactions on Power Electronics*, 28(4):1980–1993, April 2013.

[38] J.M. Guerrero, J.C. Vasquez, J. Matas, L.G. de Vicuna, and M. Castilla. Hierarchical control of droop-controlled AC and DC microgrids; A general approach toward standardization. *IEEE Transactions on Industrial Electronics*, 58(1):158–172, Jan. 2011.

[39] E. A. A. Coelho, P. C. Cortizo, and P. F. D. Garcia. Small signal stability for single phase inverter connected to stiff AC system. In *Conference Record of the 1999 IEEE Industry Applications Conference. Thirty-Forth IAS Annual Meeting (Cat. No.99CH36370)*, volume 4, pages 2180–2187, 1999.

[40] W. Yao, M. Chen, J. Matas, J. M. Guerrero, and Z. M. Qian. Design and analysis of the droop control method for parallel inverters considering the impact of the complex impedance on the power sharing. *IEEE Transactions on Industrial Electronics*, 58(2): 576–588, Feb 2011. ISSN 0278-0046.

[41] A. Tuladhar, H. Jin, T. Unger, and K. Mauch. Parallel operation of single phase inverter modules with no control interconnections. In *Proceedings of APEC 97 - Applied Power Electronics Conference*, volume 1, pages 94–100 vol.1, Feb 1997.

[42] E.A.A. Coelho, P.C. Cortizo, and P.F.D. Garcia. Small-signal stability for parallel-connected inverters in stand-alone AC supply systems. *IEEE Transactions on Industry Applications*, 38(2), April 2002.

[43] J. Schiffer, E. Fridman, and R. Ortega. Stability of a class of delayed port-Hamiltonian systems with application to droop-controlled microgrids. In *54th IEEE Conference on Decision and Control (CDC)*, pages 6391–6396, December 2015.

[44] Yixin Zhu, Fang Zhuo, and Liansong Xiong. Communication platform for energy management system in a master-slave control structure microgrid. In *IEEE 7th International Power Electronics and Motion Control Conference (IPEMC 2012)*, volume 1, pages 141–145, 2012.

[45] F Katiraei and MR Iravani. Power management strategies for a microgrid with multiple distributed generation units. *IEEE Transactions on Power Systems*, 21(4):1821–1831, 2006.

[46] T. Dragicevic, J.M. Guerrero, J.C. Vasquez, and D. Skrlec. Supervisory control of an adaptive-droop regulated DC microgrid with battery management capability. *IEEE Transactions on Power Electronics*, 29(2):695–706, Feb. 2014.

[47] Paul Krause, Oleg Wasynczuk, Scott D Sudhoff, and Steven Pekarek. *Analysis of electric machinery and drive systems*, volume 75. John Wiley & Sons, 2013.

[48] J. Morren, S. W H De Haan, and J.A. Ferreira. Contribution of DG units to primary frequency control. In *2005 International Conference on Future Power Systems*, page 6 pp., November 2005.

[49] Walter Kuehn. Control and stability of power inverters feeding renewable power to weak AC grids with no or low mechanical inertia. In *IEEE Power Systems Conference and Exposition, PSCE'09. IEEE/PES*, pages 1–8, 2009.

[50] Q. C. Zhong and G. Weiss. Synchronverters: Inverters that mimic synchronous generators. *IEEE Transactions on Industrial Electronics*, 58(4):1259–1267, April 2011.

[51] J. Driesen and K. Visscher. Virtual synchronous generators. In *IEEE Power and Energy Society General Meeting - Conversion and Delivery of Electrical Energy in the 21st Century*, pages 1–3, July 2008.

[52] K. Visscher and S.W.H. de Haan. Virtual synchronous machines for frequency stabilisation in future grids with a significant share of decentralized generation. In *SmartGrids for Distribution. IET-CIRED. CIRED Seminar*, pages 1–4, June 2008.

[53] Prabha Kundur, John Paserba, Venkat Ajjarapu, Göran Andersson, Anjan Bose, Claudio Canizares, Nikos Hatziargyriou, David Hill, Alex Stankovic, Carson Taylor, et al. Definition and classification of power system stability IEEE/CIGRE joint task force on stability terms and definitions. *IEEE Transactions on Power Systems*, 19(3):1387–1401, 2004.

[54] K. Zhou and J.C. Doyle. *Essentials of Robust Control*. Prentice Hall, 1998. ISBN 9780135258330.

[55] J. Raisch. *Mehrgrößenregelung im Frequenzbereich*. Methoden der Regelungs- und Automatisierungstechnik. Oldenbourg, 1994. ISBN 9783486217964.

[56] S. Skogestad and I. Postlethwaite. *Multivariable feedback control: analysis and design*. John Wiley, 2005. ISBN 9780470011676.

[57] H.K. Khalil. *Nonlinear Systems*. Prentice Hall PTR, 2002. ISBN 9780130673893.

[58] F Katiraei, MR Iravani, and PW Lehn. Small-signal dynamic model of a micro-grid including conventional and electronically interfaced distributed resources. *IET generation, transmission & distribution*, 1(3):369–378, 2007.

[59] Energinet. Grid connection of wind turbines to networks with voltages below 100 kV, regulation tf 3.2.6. May 2004.

[60] M. Tsili and S. Papathanassiou. A review of grid code technical requirements for wind farms. *Renewable Power Generation, IET*, 3(3):308–332, September 2009.

[61] National Grid Electricity Transmission. The grid code. March 2014.

[62] Sung-Il Jang and Kwang-Ho Kim. An islanding detection method for distributed generations using voltage unbalance and total harmonic distortion of current. *IEEE Transactions on Power Delivery*, 19(2):745–752, 2004.

[63] Cenelec standard voltages (iec 60038:2009, modified); german version en 60038:2011. April 2012.

[64] Ieee recommended practice and requirements for harmonic control in electric power systems. *IEEE Std 519-2014 (Revision of IEEE Std 519-1992)*, pages 1–29, June 2014. doi: 10.1109/IEEESTD.2014.6826459.

[65] Ewald Fuchs and Mohammad AS Masoum. *Power quality in power systems and electrical machines*. Academic press, 2011.

[66] R. Arnold. Solutions to the power quality problem. *Power Engineering Journal*, 15(2): 65–73, April 2001.

[67] A. M. Gaouda, M. M. A. Salama, M. R. Sultan, and A. Y. Chikhani. Power quality detection and classification using wavelet-multiresolution signal decomposition. *IEEE Transactions on Power Delivery*, 14(4):1469–1476, Oct 1999.

[68] M. Prodanovic and T.C. Green. High-quality power generation through distributed control of a power park microgrid. *IEEE Transactions on Industrial Electronics*, 53(5): 1471–1482, October 2006.

[69] JFG Cobben, WL Kling, and JMA Myrzik. Power quality aspects of a future microgrid. In *2005 IEEE International Conference on Future Power Systems*, pages 5–pp, 2005.

[70] S. Chowdhury and P. Crossley. *Microgrids and Active Distribution Networks*. IET renewable energy series. Institution of Engineering and Technology, 2009. ISBN 9781849190145.

[71] João Abel Peças Lopes, André Guimarães Madureira, and Carlos Coelho Leal Monteiro Moreira. A view of microgrids. *Wiley Interdisciplinary Reviews: Energy and Environment*, 2(1):86–103, 2013.

[72] F. Doerfler, J. W. Simpson-Porco, and F. Bullo. Breaking the Hierarchy: Distributed Control & Economic Optimality in Microgrids. *IEEE Transactions on Control of Network Systems*, 2014.

[73] JA Peas Lopes, CL Moreira, and AG Madureira. Defining control strategies for microgrids islanded operation. *IEEE Transactions on Power Systems*, 21(2):916–924, 2006.

[74] J. W. Simpson-Porco, Shafiee Q., F. Doerfler, J. M. Vasquez, J. M. Guerrero, and F. Bullo. Distributed averaging controllers for secondary frequency and voltage control in microgrids. *IEEE Transactions on Industrial Electronics*, 2014.

[75] J. Schiffer, R. Ortega, A. Astolfi, J. Raisch, and T. Sezi. Conditions for stability of droop-controlled inverter-based microgrids. *Automatica*, 50(10):2457–2469, 2014.

[76] Tine Vandoorn, Bart Meersman, Jeroen De Kooning, and Lieven Vandevelde. Controllable harmonic current sharing in islanded microgrids: DG units with programmable resistive behavior toward harmonics. *IEEE Transactions on Power Delivery*, 27(2):831–841, 2012.

[77] J. Schiffer, D. Goldin, J. Raisch, and T. Sezi. Synchronization of droop-controlled microgrids with distributed rotational and electronic generation. In *IEEE 52nd Annual Conference on Decision and Control (CDC)*, pages 2334–2339, December 2013.

[78] S. Dasgupta, S. N. Mohan, S. K. Sahoo, and S. K. Panda. A plug and play operational approach for implementation of an autonomous-micro-grid system. *IEEE Transactions on Industrial Informatics*, 8(3):615–629, August 2012.

[79] MJ Yang, F Zhuo, XW Wang, HP Guo, and YJ Zhou. Research of seamless transfer control strategy of microgrid system. In *IEEE 8th International Conference on Power Electronics and ECCE Asia (ICPE & ECCE 2011)*, pages 2059–2066. IEEE, 2011.

[80] G. M. S. Azevedo, F. Bradaschia, M. C. Cavalcanti, F. A. S. Neves, J. Rocabert, and P. Rodriguez. Safe transient operation of microgrids based on master-slave configuration. In *2011 IEEE Energy Conversion Congress and Exposition*, pages 2191–2195, September 2011.

[81] Hans-Peter Beck and Ralf Hesse. Virtual synchronous machine. In *9th IEEE International Conference on Electrical Power Quality and Utilisation, (EPQU 2007)*, pages 1–6, 2007.

[82] Ralf Hesse, Dirk Turschner, and Hans-Peter Beck. Micro grid stabilization using the virtual synchronous machine (VISMA). In *Proceedings of the International Conference*

on Renewable Energies and Power Quality (ICREPQŠ09), Valencia, Spain, pages 15–17, 2009.

[83] Qing-Chang Zhong, Phi-Long Nguyen, Zhenyu Ma, and Wanxing Sheng. Self-synchronized synchronverters: Inverters without a dedicated synchronization unit. *IEEE Transactions on Power Electronics*, 29(2):617–630, Feb. 2014.

[84] F. Doerfler, J. W. Simpson-Porco, and F. Bullo. Plug-and-play control and optimization in microgrids. In *IEEE Conf. on Decision and Control*, Los Angeles, CA, USA, December 2014.

[85] J. Schiffer, T. Seel, J. Raisch, and T. Sezi. Voltage stability and reactive power sharing in inverter-based microgrids with consensus-based distributed voltage control. *IEEE Transactions on Control Systems Technology*, 2015.

[86] J. Schiffer., T. Seel, J. Raisch, and T. Sezi. A consensus-based distributed voltage control for reactive power sharing in microgrids. In *13th European Control Conference (ECC)*, pages 1299–1305, June 2014.

[87] PWC. The future of microgrids their promise and challenges. July 2012.

[88] T.L. Vandoorn, J.D.M. De Kooning, B. Meersman, J.M. Guerrero, and L. Vandevelde. Automatic power-sharing modification of P/V droop controllers in low-voltage resistive microgrids. *IEEE Transactions on Power Delivery*, 27(4):2318–2325, October 2012.

[89] J.M. Maciejowski. *Multivariable feedback design*. Electronic systems engineering series. Addison-Wesley, 1989. ISBN 9780201182439.

[90] A.G. Phadke. Synchronized phasor measurements in power systems. *Computer Applications in Power, IEEE*, 6(2):10–15, April 1993.

[91] Jaime De La Ree, Virgilio Centeno, James S Thorp, and Arun G Phadke. Synchronized phasor measurement applications in power systems. *IEEE Transactions on Smart Grid*, 1(1):20–27, 2010.

[92] R. Majumder, B. Chaudhuri, A. Ghosh, R. Majumder, G. Ledwich, and F. Zare. Improvement of stability and load sharing in an autonomous microgrid using supplementary droop control loop. *IEEE Transactions on Power Systems*, 25(2):796–808, May 2010.

[93] T. Kailath. *Linear systems*. Prentice-Hall information and system sciences series. Prentice-Hall, 1980. ISBN 9780135369616.

[94] B. Labibi, H.J. Marquez, and T. Chen. LMI optimization approach to robust decentralized controller design. *International Journal of Robust and Nonlinear Control*, 21(8): 904–924, 2011.

[95] C. Scherer, P. Gahinet, and M. Chilali. Multiobjective output-feedback control via LMI optimization. *IEEE Transactions on Automatic Control*, 42(7):896–911, July 1997.

[96] R. H. Lasseter. Smart Distribution: Coupled Microgrids. *Proceedings of the IEEE*, 99 (6):1074–1082, June 2011.

[97] J. Lofberg. YALMIP : a toolbox for modeling and optimization in matlab. In *2004 IEEE International Symposium on Computer Aided Control Systems Design*, pages 284–289, September 2004.

[98] J.F. Sturm. Using SeDuMi 1.02, a MATLAB toolbox for optimization over symmetric cones. *Optimization Methods and Software*, 11–12:625–653, 1999. Version 1.05 available from `http://fewcal.kub.nl/sturm`.

[99] R. Majumder, A. Ghosh, G. Ledwich, and F. Zare. Angle droop versus frequency droop in a voltage source converter based autonomous microgrid. In *Power Energy Society General Meeting, 2009. PES '09. IEEE*, pages 1–8, July 2009.

[100] Petter Lundström, Sigurd Skogestad, and Zi-Qin Wang. Performance weight selection for H-infinity and μ-control methods. *Transactions of the Institute of Measurement and Control*, 13(5):241–252, 1991.

[101] B. Pal and B. Chaudhuri. *Robust Control in Power Systems*. Power Electronics and Power Systems. Springer, 2005. ISBN 9780387259499.

[102] IEEE. Standard for a precision clock synchronization protocol for networked measurement and control systems. *IEEE Std 1588-2008 (Revision of IEEE Std 1588-2002)*.

[103] M. Shahidehpour and Y. Wang. *Communication and Control in Electric Power Systems: Applications of Parallel and Distributed Processing*. IEEE Press series on power engineering. Wiley, 2004. ISBN 9780471462910.

[104] Josep M Guerrero, Poh Chiang Loh, Mukul Chandorkar, and Tzung-Lin Lee. Advanced control architectures for intelligent microgrids, Part I: Decentralized and hierarchical controladvanced control architectures for intelligent microgrids. *IEEE Transactions on Industrial Electronics*, 60(4):1254–1262, 2013.

[105] G.J. Geier, T.M. King, H.L. Kennedy, R.D. Thomas, and B.R. McNamara. Prediction of the time accuracy and integrity of GPS timing. In *Proceedings of the 49th IEEE International Frequency Control Symposium*, pages 266–274, May 1995.

[106] J. Dellas and M. Schwartz. The use of GPS (Global Positioning System) for synchronizing frequency converters. In *Proceedings of the 2001 IEEE/ASME Joint Railroad Conference*, pages 93–98, 2001.

[107] Wilsun Xu and Y. Mansour. Voltage stability analysis using generic dynamic load models. *IEEE Transactions on Power Systems*, 9(1):479–493, Feb. 1994.

[108] I.A. Hiskens and J.V. Milanovic. Load modelling in studies of power system damping. *IEEE Transactions on Power Systems*, 10(4):1781–1788, November 1995.

[109] Jovica V Milanovic and IA Hiskens. Effects of load dynamics on power system damping. *IEEE Transactions on Power Systems*, 10(2):1022–1028, 1995.

[110] D. Popovic, I.A. Hiskens, and D.J. Hill. Investigations of load-tap changer interaction. *International Journal of Electrical Power and Energy Systems*, 18(2):81 – 97, 1996.

[111] Y.V. Makarov, V.A. Maslennikov, and D.J. Hill. Revealing loads having the biggest influence on power system small disturbance stability. *IEEE Transactions on Power Systems*, 11(4):2018–2023, November 1996.

[112] N Jayawarna, X Wu, Y Zhang, N Jenkins, and M Barnes. Stability of a microgrid. 2006.

[113] P. Ju, E. Handschin, and D. Karlsson. Nonlinear dynamic load modelling: Model and parameter estimation. *IEEE Transactions on Power Systems*, 11(4):1689–1697, November 1996.

[114] Arthur R Bergen and David J Hill. A structure preserving model for power system stability analysis. *IEEE Transactions on Power Apparatus and Systems*, (1):25–35, 1981.

[115] JV Milanovic and IA Hiskens. The effects of dynamic load on steady state stability of synchronous generator. *Proceedings of the international conference on Electrical Machines. ICEM*, 94:722–727, 1994.

[116] F.T. Dai, J.V. Milanovic, N. Jenkins, and V. Roberts. The influence of voltage variations on estimated load parameters. In *16th International Conference and Exhibition on Electricity Distribution. Part 1: Contributions. CIRED. (IEE Conf. Publ No. 482)*, volume 2, page 6 pp., 2001.

[117] A.R. Bergen and D.J. Hill. A structure preserving model for power system stability analysis. *IEEE Transactions on Power Apparatus and Systems*, PAS-100(1):25–35, Jan. 1981.

[118] He Renmu, Ma Jin, and David J Hill. Composite load modeling via measurement approach. *IEEE Transactions on Power Systems*, 21(2):663–672, 2006.

[119] G.W. Stagg and A.H. El-Abiad. *Computer methods in power system analysis*. McGraw-Hill Education - Europe, 1968.

[120] MA Pai, Peter W Sauer, and Bernard C Lesieutre. Static and dynamic nonlinear loads and structural stability in power systems. *Proceedings of the IEEE*, 83(11):1562–1572, 1995.

[121] DH Popovic, IA Hiskens, and DJ Hill. Stability analysis of induction motor networks. *International Journal of Electrical Power and Energy Systems*, 20(7):475–487, 1998.

[122] Jin-Cheng Wang, Hsiao-Dong Chiang, Chung-Liang Chang, Ah-Hsing Liu, C-H Huang, and Chiung-Yi Huang. Development of a frequency-dependent composite load model using the measurement approach. *IEEE Transactions on Power Systems*, 9(3):1546–1556, 1994.

[123] L. Ljung. *System Identification: Theory for the User*. Pearson Education, 1998. ISBN 9780132440530.

[124] William W Price, Kim A Wirgau, Alexander Murdoch, James V Mitsche, Ebrahim Vaahedi, and M El-Kady. Load modeling for power flow and transient stability computer studies. *IEEE Transactions on Power Systems*, 3(1):180–187, 1988.

[125] Ebrahim Vaahedi, HM Zein El-Din, and William W Price. Dynamic load modeling in large scale stability studies. *IEEE Transactions on Power Systems*, 3(3):1039–1045, 1988.

[126] D-Q Ma and Ping Ju. A novel approach to dynamic load modelling. *IEEE Transactions on Power Systems*, 4(2):396–402, 1989.

[127] D.N. Kosterev, A. Meklin, J. Undrill, B. Lesieutre, W. Price, D. Chassin, R. Bravo, and S. Yang. Load modeling in power system studies: WECC progress update. In *IEEE Power and Energy Society General Meeting - Conversion and Delivery of Electrical Energy in the 21st Century*, pages 1–8, July 2008.

[128] Chia-Jen Lin, Yung-Tien Chen, C-Y Chiou, C-H Huang, H-D Chiang, Jin-Cheng Wang, and Lazhar Fekih-Ahmed. Dynamic load models in power systems using the measurement approach. *IEEE Transactions on Power Systems*, 8(1):309–315, 1993.

[129] Ma Jin, He Renmu, and D.J. Hill. Load modeling by finding support vectors of load data from field measurements. *IEEE Transactions on Power Systems*, 21(2):726–735, May 2006.

[130] J.D. Glover, M. Sarma, and T. Overbye. *Power Systems Analysis and Design*. Cengage Learning, 2007. ISBN 9780534548841.

[131] George K Stefopoulos and AP Meliopoulos. Induction motor load dynamics: Impact on voltage recovery phenomena. In *IEEE Transmission and Distribution Conference and Exhibition, 2005/2006 IEEE PES*, pages 752–759, 2006.

[132] D. S. Brereton, D. G. Lewis, and C. C. Young. Representation of induction-motor loads during power-system stability studies. *Transactions of the American Institute of Electrical Engineers. Part III: Power Apparatus and Systems*, 76(3):451–460, April 1957.

[133] T Athay, R Podmore, and S Virmani. A practical method for the direct analysis of transient stability. *IEEE Transactions on Power Apparatus and Systems*, (2):573–584, 1979.

[134] A. Pai. *Energy Function Analysis for Power System Stability*. Kluwer international series in engineering and computer science. Springer, 1989. ISBN 9780792390350.

[135] Carsten Scherer and Siep Weiland. Linear matrix inequalities in control. Lecture notes, 2003.

[136] WW Price, CW Taylor, and GJ Rogers. Standard load models for power flow and dynamic performance simulation. *IEEE Transactions on power systems*, vol. 10, 1995.

[137] Ambrish Chandra, Bhim Singh, BN Singh, and Kamal Al-Haddad. An improved control algorithm of shunt active filter for voltage regulation, harmonic elimination, power-factor correction, and balancing of nonlinear loads. *IEEE Transactions on Power Electronics*, 15(3):495–507, 2000.

[138] George Weiss, Qing-Chang Zhong, Tim C Green, and Jun Liang. H-infinity repetitive control of DC-AC converters in microgrids. *IEEE Transactions on Power Electronics*, 19 (1):219–230, 2004.

[139] Savita Soma and Nagabhushan. Reduction of harmonics in a power system through series compensation. *World journal of science and technology*, (1(8):140-143), 2011.

[140] F.Z. Peng. Harmonic sources and filtering approaches. *Industry Applications Magazine, IEEE*, 7(4):18–25, July 2001.

[141] U. Borup, F. Blaabjerg, and P.N. Enjeti. Sharing of nonlinear load in parallel-connected three-phase converters. *IEEE Transactions on Industry Applications*, 37(6):1817–1823, November 2001.

[142] Takaharu Takeshita and Nobuyuki Matsui. Current waveform control of PWM converter system for harmonic suppression on distribution system. *IEEE transactions on industrial electronics*, 50(6):1134–1139, 2003.

[143] José Matas, Miguel Castilla, Luis Garcia de Vicuna, Jaume Miret, and Juan Carlos Vasquez. Virtual impedance loop for droop-controlled single-phase parallel inverters using a second-order general-integrator scheme. *IEEE Transactions on Power Electronics*, 25(12):2993–3002, 2010.

[144] H. Laaksonen and K. Kauhaniemi. Voltage and current THD in microgrid with different DG unit and load configurations. In *CIRED Seminar 2008: SmartGrids for Distribution*, pages 1–4, June 2008.

[145] B. Pal and B. Chaudhuri. *Robust Control in Power Systems*. Power Electronics and Power Systems. Springer, 2006. ISBN 9780387259505.

[146] J. Doyle. Analysis of feedback systems with structured uncertainties. *IEE Proceedings D - Control Theory and Applications*, 129(6):242–250, November 1982. ISSN 0143-7054. doi: 10.1049/ip-d.1982.0053.

[147] Roger A. Horn and Charles R. Johnson. *Matrix Analysis*. Cambridge University Press, New York, NY, USA, 1986. ISBN 0-521-30586-1.

[148] S.V. Iyer, M.N. Belur, and M.C. Chandorkar. A generalized computational method to determine stability of a multi-inverter microgrid. *IEEE Transactions on Power Electronics*, 25(9), Sept. 2010.

[149] Y. W. Li and C. N. Kao. An accurate power control strategy for power-electronics-interfaced distributed generation units operating in a low-voltage multibus microgrid. *IEEE Transactions on Power Electronics*, 24(12):2977–2988, Dec 2009. ISSN 0885-8993.

[150] J. M. Guerrero, L. G. de Vicuna, J. Matas, M. Castilla, and J. Miret. A wireless controller to enhance dynamic performance of parallel inverters in distributed generation systems. *IEEE Transactions on Power Electronics*, 19(5):1205–1213, Sept 2004. ISSN 0885-8993. doi: 10.1109/TPEL.2004.833451.